A process-oriented biogeochemical model for marine ecosystems: Development, numerical study, and application

Marcos Duarte Mateus

January 2006

Contents

Abstract

Over the last two decades, biogeochemical modelling in marine environments underwent considerable advances. The MOHID system has followed this trend, reflecting now the state-of-the-art in circulation models. As such, the driving force beyond the present work was to equip the MOHID system with a model that also reflects the state-of-the-art in biogeochemical modelling. To achieve this purpose, mohid.Life.1.0 was developed, a model for marine systems that is able to describe biogeochemical processes with greater detail than the NPZ approach already implemented in MOHID. This work not only contains the description of the model with its process-oriented baseline philosophy, but it also addresses its behaviour when subject to standard tests. The model is also tested in a real case scenario with an application to the Tagus Estuary, Portugal. The model performance shows that the model has the ability to respond to different conditions in a realistic way. Results also show that the model reproduces the basic functioning of water-column food webs and nutrient dynamics in marine systems. In the Tagus application, the model helped to address uncertainties in knowledge of the functioning of this particular system, and also to reinforce some assumptions made in other experimental and numerical studies.

Keywords: Ecological models; process-oriented; biogeochemical cycles; water-quality; MOHID system; Tagus estuary.

Resumo

Durante as últimas décadas, a modelação biogeoquímica dos ambientes marinhos tem experimentado avanços significativos. O sistema MOHID tem seguido esta tendência e reflecte actualmente o estado da arte na modelação da circulação oceânica. A principal força motriz deste trabalho foi equipar o sistema MOHID com um modelo que reflectisse o estado da arte da modelação biogeoquímica. Para alcançar este objectivo foi desenvolvido o modelo mohid.Life.1.0, mais detalhado do que a aproximação Nutrientes – Fitoplâncton – Zooplâncton anteriormente implementada no sistema MOHID. Para além de uma descrição do algoritmo do modelo e da sua filosofia de base, este trabalho contém uma análise do comportamento do modelo quando sujeito a diferentes testes. O modelo foi também testado numa aplicação a um cenário real, nomeadamente ao Estuário do Tejo, Portugal. O comportamento do modelo mostrou a sua capacidade para responder de uma forma realista a diferentes condições. Os resultados mostraram também que o modelo reproduz o funcionamento básico das teias alimentares na coluna de água e da dinâmica de nutrientes dos sistemas marinhos. Na aplicação ao Estuário do Tejo, o modelo permitiu abordar algumas incertezas em relação ao funcionamento do sistema e reproduziu correctamente os mecanismos geralmente assumidos, tanto em estudos numéricos como em estudos experimentais, como controlo do sistema.

Palavras-chave: Modelos ecológicos; orientado por processos; ciclos biogeoquímicos; qualidade da água; sistema MOHID; Estuário do Tejo.

Acknowledgments

First of all, I must express my gratitude to Prof. Ramiro Neves. Among many things, I am grateful for his invitation to join the MARETEC "gang" and to pursue my PhD Thesis under his supervision, for putting up with me for so long, for keeping my mind in a constant struggle, and for widening my vision on so many things. I am also thankful to Prof. Helena Galvão for agreeing to co-supervise my work and for the assistance that kept me on the right tracks in the early days of my work.

Then there is a myriad of friends and colleagues that somehow, and in so many different ways, have given a decisive contribution to improve the quality of this work and to keep me focused: Prof. Henrique Coelho, a colleague and a friend, responsible for what can be called my "academic career"; Ana Barbosa for the contagious enthusiasm and some really valuable lessons on "phytoplankton ecology"; Job Baretta for the priceless lessons, for the thorough corrections of early versions of this manuscript and spirited comments, and above all for taking me serious; Luis Fernandes for the assistance in the first steps of this project and especially for naming the model "Life"; Rui Caldeira and Hernani Theias for or all the comments and suggestions, especially for helping me overcome the initial shock of using LaTeXas the text editor for this work; Pedro Galvão for all the fruitful philosophical discussion on the role of models in science and anywhere else (especially those at 8 a.m.); Rosa for helping me out with the "units" problems; Guillaume Riflet for making his work my own with no strings attached; Sofia Saraiva for the valuable data and help; José Chambel and Francisco Campuzano for the support in the right moment; João Robert for the "smash!" attitude; Paulo Chambel for proof reading this work and for walking with me the extra (and final) mile; Ricardo Lemos for the absolute commitment to reading as much of this work as was humanly possible in such a short time and for the valuable corrections; all the friends in the BMP Class of 93 (Universidade do Algarve) for the inspiration and support.

Finally, I'm especially indebted to my family, particularly to my parents and grandparents, for believing that I am making a man of myself. Also, to my friends at *A Rocha* for the support, for teaching me excellence in science and its ultimate goal in the benefit of all creation and as a praise to the Creator.

Words are insufficient to express my appreciation and gratitude to my wife Sandra and to my son Misael, who love me above anything and keep me in balance, with or without a degree. To them I show my gratitude in love...

This work was supported by a Doctoral Grant, reference SFRH/BD/1235/2000, from the Fundação para a Ciência e Tecnologia.

To Prof. Martin Sprung,
a teacher who devoted much of his life to
unveil the mysteries of life in the oceans
and to share them with his students

Overview

This introductory section contains an outline of the thesis structure. A detailed description of each chapter is out of the scope of this overview. Instead only the main topics in each chapter content are mentioned.

Chapter 1

A general introduction to the thesis framework is presented here. A brief revision is made to recent developments in ecological models, along with a description of the current state-of-the-art. Major changes in paradigms in the development of ecological models are also highlighted and current trends in marine systems modelling strategies are discussed.

Chapter 2

A background to the adopted modelling philosophy is addressed in this chapter, the main assumptions of the model are listed, as well as the theoretical fundament behind them. The link between the ecological model developed here and the MOHID modelling system is also mentioned. This section also describes the formulation of the model components.

Chapter 3

Some numerical tests on the model performance are presented in this chapter. This section comprises an analysis of the implemented functions, as well as some checks on formulation coherence. A schematic application to a virtual mesocosm is used in the assessment of model behaviour. A sensitivity analysis is performed to the model and the results are discussed. A modeled mean state, defined as the "standard" run, is used as a base for a series of parameter sensitivity analysis by parameter perturbation ($\pm 10\%$). The results of the sensitivity analysis are qualitatively classified by distinguishing parameters with different degrees of influence on model results.

Chapter 4

This chapter deals with an application to a real system, the Tagus Estuary (Portugal). Here, the model's capability to reproduce known biogeochemical patterns of real systems is assessed.

Chapter 5

Based on the model development, tests and applications, this chapter contains a general discussion of the work in the previous chapters.

Chapter 6

Brief section with the concluding remarks about the work, naming the main achievements, limitations and future developments.

Chapter 1

Introduction

Water quality modelling has evolved dramatically since its beginning in the early decades of the 20th century. However, it was not a linear development, but followed the concerns of the time and, after the 1960s, the available computational capabilities. In the pre-computer era, the range of problems that could be addressed with models was constrained by the lack of computational tools. Model solutions were in closed form, making its applications limited and confined to cases with linear kinetics, simple geometries and steady-state receiving waters. In this context, the first study cases using models go back to 1925 [1], and were related with the amount of dissolved oxygen in lakes and rivers as a function of sewage discharge.

The first mathematical models developed for marine systems did not appear until the 1940s in the form of planktonic ecosystem models. They were formulated to explain the seasonal variation in the standing stock of phytoplankton and zooplankton observed on Georges Bank, USA [2, 3]. These first models had a simple design with time-dependent equations describing the variations in zooplankton and phytoplankton populations over time. Their structure was constrained by the data sets available at the time, as well as by the level of understanding of marine systems. Hence, there was not sufficient information to achieve a complex formulation for the model components.

The emergence of the digital computer era in the 1960s, followed almost immediately by its wide dissemination, led to major advances in modelling techniques and in the ways in which they could be applied. The computational capacity allowed researchers to address more complex systems characterized by intricate geometries and complicated kinetics. And all this in time-variable simulations. For the first time models were used in the study of two-dimensional systems such as wide estuaries and bays. It was also during this decade that models start to be used as tools in more comprehensive studies of water-quality problems.

With the growing concern over environmental issues during the 1970s,

numerical ecological models begun to be used in the study of several different systems. Unlike the oxygen fate in the water and the urban point sources that were the major focus of all models applications during the previous decade, eutrophication problems became the water-quality problem of the day. And to achieve models with the capacity to study this complex process with all its implications, mechanistic representations of biological processes were included. As a result, the use of nutrient/food-chain models became widespread. By then, the existing computational capabilities had made it possible to address feedback processes and nonlinear kinetics.

It was also during the 1970s that one of the first attempts to combine a marine food-web model with a circulation model was implemented to study the controlling processes of primary production in the upwelling region off the coast of Oregon [4]. This model had five coupled equations to assess space and time distribution of each component (phytoplankton, zooplankton, nitrate, ammonium, and detritus) induced by horizontal and vertical circulation velocities. These, in turn, were affected by wind forcing, bottom topography, incident solar radiation, and surface, inter-layers and bottom stress.

Over the last two decades, modelling efforts aimed at describing nutrient cycling of the microbial food webs underwent considerable advances. These advances have addressed processes from simple bacteria-algae interactions to complex microbial systems. In the process, the last two decades have witnessed an explosion of both numerical models development and utilization by groups devoted to the study of natural systems (universities, research centres, etc.), decision making entities (e.g., governments, local authorities), and environmental protection and conservation agencies.

Among several reasons explaining this phenomena, the most obvious can be highlighted: (1) the huge increase in computation capacity together with (2) the advances in knowledge about natural systems; (3) the awareness of the limitation of experimental techniques, especially when it comes to sampling limitations and material availability and costs; and finally (4) the lack of proper tools to address multi-disciplinary problems and to study multi-compartment systems and their inter-connectivity.

The trend has been to increase the degree of sophistication in models. Ecological models addressing single processes or just a few processes in aquatic systems are still widely used. But with time, models have evolved from a few processes simulations or simple food chains to ecosystem scale models (hence the term ecological models), and at the same time increasing the parameterization detail of the process. This opening in the scope of models has merged biological, physical and chemical processes to study large scale areas into what is know known as biogeochemical models.

The latest developments in the use of mathematical models is without doubt linked with the emergence of operational oceanography. Operational oceanography embraces hindcasting, nowcasting and forecasting of parame-

ters, from physics to ecology, on scales from global to coastal [5]. At least when it comes to forecasting, models play a leading role. And in this setup, a new kind of modelling approach has emerged, namely, operational modelling. Beginning with simple models in the early 20th century, the evolution in the use of numerical models has led to operational systems developed to address the needs of specific coastal, marine and estuarine environments, taking into account relevant processes and dynamics, and employing technologies such as data assimilation whenever data is available.

Numerical models stand as a way to look at real systems and to translate then into compartments, identifying the connection between them. They are versatile tools that enable an in-depth look at natural systems incapable to be achieved by the simple combination of analytical methods. The use of models makes it possible to explain causes and effects in environmental processes, the distinction between anthropogenic and natural contamination sources and their respective impact, etc. Modelling results are also important to complement data from traditional experimental research methods. By coupling these models with hydrodynamic models it is possible to relate information from different fields and to establish causal relations among them. Because models have the capability to bridge the gap between small scale and large scale processes, they become an essential tool for understanding complex processes like nutrient regeneration or sequestering in the vast context of the major biogeochemical cycles [6].

With time, models have become indispensable tools in environmental studies and management decisions. It is obvious that no model will ever address all problems and answer all questions at the same time. For this reason there are so many water quality model classes or types. Some of them with broad application versatility, while others with limited applicability given their specificity in some particular processes. That is the reason why it is so difficult to define the state-of-the-art in modelling at a given time. The wide spectrum of available models is the simple reflex of their importance in the study of natural systems and the final proof of their importance as a research tools [7].

1.1 A glance at the state-of-the-art

Mathematical models are increasingly being used to study aquatic ecosystem as a whole and to study the dynamics of some compartments of these systems like marine microbial ecosystems (see revision made by Fasham [8]). Usually, models of whole ecosystems result from joining sub-models representing particular processes, trophic levels or particular species/functional groups within the food web. Based on that, the understanding of processes is an important prerequisite for the development of enhanced ecosystem models.

In the last decades there has been an exponential increase in knowledge about the innumerous components of aquatic systems and their relations. Side by side with this progress, and also with the increase of computer power, the development of ecological and biogeochemical models for these systems is experiencing a major impulse forward. Since the early 1960s, considerable emphasis has been placed on nitrogen following the general accepted view of nitrogen as the limiting nutrient in water. But the availability of improved methods for analysis of transient components in the nutrient cycles has led to a greater knowledge of complex processes of uptake and cycling of the various chemical species. In the process, early models with just a few compartments have been replaced with models considering a wide range of state variables, for both biological and chemical entities. Likewise, the explicit parameterization of just one element, usually nitrogen for being assumed as the limiting nutrient, gave way to multi-element models where carbon is explicitly addressed and carbon to nutrient ratios are no longer static but dynamic. As a result of this evolution, numerical modelling of biologic systems is improving as a tool for the study of these complex and dynamic systems. Therefore, they are becoming an aid to understand those systems.

Because there have been numerous efforts to summarize the diversity of ecological models produced in the last decade or so, only a brief mention will be presented here. Model application to aquatic environments has become widespread and has been used to study large-scale phenomena as well as micro-scale processes. So, the production and adaptation of models in the last decades has been explosive and, as a consequence, hard to follow and to keep a detailed knowledge about each developed model. However, a simplistic description of the available degrees of complexity in biogeochemical models can be briefly resumed here. According to a recent article [9], the most simple type of these models are the NPZ models, followed by the medium complexity models with the same baseline philosophy (N as the currency, etc.) but with additional key processes like the microbial loop as an important pathway of remineralising organic matter, and reaching high complexity in models like ERSEM.

Of all the processes related with aquatic ecological models, primary production has been probably the most modeled process. Some detailed reviews on this models have been produced (e.g. [10]), but they soon become out of date due to the volume of models developed each year. The modelling of primary producers has departed from simple considerations of the major limiting factors (light, temperature and nutrients) to abridge detailed physiological control on the growth and environmental forcing as well. A few examples of these developments can be highlighted, ranging from the development of general mechanistic models of population dynamics [11], down to processes like the modelling of phytoplankton blooms triggering and shaping factors [12, 13], their sinking dynamics [14, 15] and the interaction effects of

the usual limiting factors on phytoplankton growth [16].

Regarding microbial food webs models, Davidson [17] presents a detailed review on the several models available, their main characteristics and applications. The increased awareness on the importance of microbial communities on aquatic food webs since the development of the "microbial loop" concept [18] has favoured modelling efforts to study processes like the several control factors on bacterial growth rates [19]. Even the interaction between phytoplankton and bacteria has received considerable modelling effort (e.g. [20, 21, 22]).

Finally, new studies on the dynamic of nutrients in water, especially their recycling trough mineralization, has revealed a complexity way beyond the limited and over-simplified approach of using rates for this process in models. And it was probably this advance in our knowledge about the food webs, more than any other, that was responsible for the development of variable stoichiometric models, with special emphasis on the recycling of organic nutrient through mineralization by bacteria and excretion by zooplankton [23, 24].

There has also been observed a prolific use of coupled biological-physical models with a considerable degree of complexity, but even here the models vary widely. Despite the high number of parameters and processes considered, some only have carbon and nitrogen dynamics with fixed stoichiometry (e.g. [25]) while others have a multi-parameters approach with variable stoichiometry (a typical example is the ERSEM II model [26, 27, 28, 29]). Because of its complexity describing the main processes within the complex food web of the North Sea ecosystem (including physical processes, nutrient cycles, and, pelagic and benthic organisms), ERSEM has been pointed out as defining the state-of-the-art in ecosystem modelling [30].

The scale of ecological models applications varies also, ranging from small water bodies and lakes to the global oceanic scale. So, while some ecological models are used to study regions like the Benguela upwelling system [25] or the North Sea (ERSEM), others are used to study the global ocean [31, 32]. But despite the high complexity in the parameterization of some of these models (some [31, 32] even consider micronutrient limitation by iron), they are used mainly in 1D applications.

With this background, the actual state-ot-the-art in ecological models applied to aquatic systems is not so much on the degree of complexity of the biogeochemical or water quality module, or the type of water circulation (1D, 2D or 3D) and spatial resolution alone, but rather on the combinations of all these aspects [33, 34, 35]. To have a 3D setting with a fine mesh or with nested models able to simulate small scale hydrodynamic phenomena coupled with a basic NPZ (Nutrient-Phytoplankton-Zooplankton) does not reflect the state-of-the-art, nor does the use of detailed multi-parameter, multi-compartments and decoupled stoichiometry ecological models coupled with box models or a 1D simulation. Only when the actual paradigms of

both ecological and physical models meet, one can have a state-of-the-art model.

1.2 A changing paradigm

More than to address every single model and its specific parameterization, it is important to highlight the main features of recent models, and to put them in perspective with older ones. The change in ecological modelling paradigm is a clear consequence of the increasing knowledge of planktonic systems in all water environments (coastal, estuarine, neritic, etc.).

The effort to understand the complex dynamics of natural systems has produced a vast amount of data which in turn has helped researchers to understand forcing mechanisms and abiotic controls of natural assemblages of planktonic communities. Thus, model complexity has been pushed along by newly available information and data. Consequently, older sets of approaches and techniques to model natural systems have been continuously evolving.

1.2.1 Variable internal composition

The coupling of population dynamics to fluxes of nutrient elements has led to the development of stoichiometric models. Until recently, most of these ecological models have frequently rested on the assumption of constant proportions of elements in organisms biomass. This homeostasis in composition has been assumed for both prey and predators. Even for autotrophic organisms like algae, constant elemental composition is still used despite well-documented variations showing otherwise. Recent modelling approaches, however, rest on the fact that the crucial elements cycles in marine systems (i.e. carbon and nitrogen) are explicitly addressed. So, variable stoichiometry presupposes that nutrient content variation is in part controlled by processes controlling the carbon dynamic.

Despite being a falling paradigm with all its potential limitations, the static elemental composition approach has shed some light on the relation between population dynamics and nutrient recycling. And it was the awareness of its limitation that led to its abandon and to the adoption of multi-element / variable stoichiometry paradigm in ecological models. In this new approach, it is possible to have a clearer understanding of the controlling mechanisms of predator nutrient recycling impact on the availability of limiting nutrients for prey, and also on the possible outcome of prey competition for those nutrients. Among other hot topics in ecology, this approach can clarify the relation dynamics between heterotrophic bacteria and autotrophic organisms in aquatic systems.

1.2.2 Structured based models

With the advances in the study of aquatic ecosystems, models have evolved from initial bulk-approach strategies to multi-structure components. This change led to the gradual replacement of general groups like "phytoplankton" or "zooplankton" by size class organisms or functional classes within these groups. This improvement has made models more realistic and has pushed model parameterization to reflect the continuous increase in knowledge of aquatic systems components [36].

1.2.3 Chlorophyll to Carbon ratio

As water-quality models increase in complexity, another process that has receive particular attention in the modelling effort has been the explicit parameterization of intracellular chlorophyll production and quotas. Chlorophyll *a* has been adopted as a measure of algal biomass for some time now, specially for its measurement simplicity when compared to other elements. However, the knowledge that the chlorophyll-to-carbon ratio is not constant (usually varying between 0.01 and 0.1 mg$Chla$ mgC^{-1}), but varies is response to light levels and cell physiological state, has paved the way to the incorporation of acclimation mechanisms into the modeled processes of phytoplankton dynamics. This acclimation (i.e. the variability of Chl$a$:N and Chl$a$:C) of the photosynthetic apparatus is a physiological response to external conditions, namely the variations in irradiance and nutrient availability. In response to the growing awareness of photo adaptation importance, over the past decade a number of models have been developed to account for variable chlorophyll content in algae. Light history is reflected in changes of Chl$a$:C in these models, which in turn affects the instantaneous photosynthesis-light response. Two reasons have been pointed out to explain the growing importance of this variability in models [37]: (a) the shifting in the focus of models from the habitual nutrient/food-chain interaction to an organic carbon cycle characterization, as a consequence of the application of water-quality models beyond eutrophication studies; (b) water-quality models are being increasingly used to analyze cleaner systems than those studied in the past, and these systems typically exhibit more variable light levels with light penetrating beyond well-mixed surface layers.

1.2.4 Multi-element models

Another basic improvement in ecological models has been the abandonment of the simplistic NPZ (nutrient-phytoplankton-zooplankton) model structure, now decades-old. Starting from below, models with only one nutrient (usually nitrogen) or two (nitrogen and phosphorus) impose several limitations because primary producers groups rely differently on different nutrients. The huge range of species or functional groups cannot be addressed

with a single nutrient, at the risk of making an oversimplification of producer's role in the system. As an example, diatoms which can be considered as an important group in coastal and estuarine systems cannot be properly modelled without considering silica as a nutrient in the model. Otherwise it will respond to nitrogen and phosphorus external concentration in the same way as any other phytoplankton group.

Nutrients like nitrogen or phosphorus frequently limits phytoplankton production and for that reason are generally employed as a model currency. Sometimes only one nutrient is used, usually nitrogen because it is widely assumed as the limiting nutrient in the ocean. However, taking nutrients like nitrogen or phosphorus as a model currency can be a problem when one tries to accommodate a bacterioplankton compartment into the model. The reason lies in the fact that the growth of heterotrophic bacteria may be carbon or energy limited. So, a multielement model with a decoupled carbon, nitrogen, and phosphorus stoichiometry is best suited to study the role of heterotrophic bacteria in the food web. Some authors [24] have shown that when applied to microbial ecosystems, models with variable stoichiometry may predict the reduction of efficiency or organic carbon mineralization when the supply of mineral nutrients is low and when equilibria are unstable.

Besides, an explicit description of the nutrient flow (or multiple nutrient flow) through the microbial food web, in addition to the carbon flow, enables the study of the relative importance of nutrient recycling by the microbial food web versus its role as a link to higher trophic levels. In multielement models the flow of carbon is usually calculated assuming fixed C:N ratios for state variables. Elemental ratios in zooplankton and bacteria, and to a lesser extent phytoplankton, are relatively constant, whereas ratios in DOM are more variable, for example having highest C:N ratios during accumulation in spring. In addition, ratios in zooplankton and bacteria are commonly different (lower) than those in phytoplankton and DOM. Taking bacterioplankton as an example, it is necessary to balance the stoichiometry of nitrogen cycling with DOC uptake and respiration.

Considering each nutrient cycle explicitly enables nutrient ratios in each compartment to be dynamic, as it is in natural systems. Looking at phytoplankton N:P ratios one can find this non-static nutrient cell content stoichiometry. Nutrient ratios are used to characterize the physiological state of plankton crops and the state of annual succession of plankton development in the sea. Competition for nitrogen occurs because bacterial C:N ratio is lower than phytoplankton, and so they have a higher demand for nitrogen per biomass unit than phytoplankton. Competition for phosphorus is particularly relevant because bacteria with a C_{50}:N_{10}:P_1 ratio need relatively more phosphorus than phytoplankton with a C_{106}:N_{16}:P_1 ratio. Kirchman [38] points out that bacteria should have low C:P ratios because most of the phosphorus is in the phospholipids in the cell membrane and in nucleic acids, and small cells have high surface area to volume ratios. In contrast,

DNA content of bacteria is much higher than phytoplankton, reaching as much as 20% of cellular C. Altogether, the amount of P needed for cell membrane and DNA implies that this element requirements is in proportion much higher than N needs. Over vast areas of the open ocean, both phytoplankton primary production and bacterioplankton activity is then phosphorus limited, and this limitation of bacterial activity in particular might lead to an accumulation of DOC.

Similar reasons explain the need for different functional phytoplanktonic groups in the parameterization of producers. A single group of producers is not enough to account for spatial and temporal variability that characterize such biological systems. Processes like mixotrophy and competition between groups are way too much important to be disregarded by modelers. Finally, there is the zooplankton that just like phytoplankton has considerable differences among groups that must be reflected in separated state variable by models.

As a consequence of the increasing parameterization and state variables addressed in recent models, the degree of difficulty to calibrate and sometimes to explain the results has also increased. But such demanding conditions are no longer an excuse to go back to simplistic models. Nevertheless, NPZ models are still used when a compromise between results and running time must be attained or when users knowledge about planktonic systems is somehow reduced.

1.3 Model complexity

Over the last decades, ecological models have been constructed with different levels of detail. The diversity in the degree of complexity of ecological models reflects to some extent that there is less consensus about the basic equations describing it than for the physical system [39]. No single growth model has been preferred by the modelling or experimental community, and the variety of available phytoplankton growth models partly reflects their different uses. Models tend to be chosen to address specific questions or problems, but also based on their computational requirements. For example, models based on extracellular concentrations are preferred for ecosystem-scale models with computational constraints [40], while intracellular models are preferred by experimentalists who wish to test their understanding of underlying processes [41]. Nonetheless, the range of phytoplankton growth models contrasts with the universal agreement over the governing equations of many physical systems, such as fluid motions. Furthermore, the governing equations of many physical systems typically have tightly constrained parameter values.

It is unlikely that a rigorous derivation of a single set of equations describing the observed range of phytoplankton growth behaviours will be found in

the near future. Even so, a set of equations that takes advantage of easily quantified physical laws, and specifically designed to approximate phytoplankton growth behaviour for a range of potentially limiting factors (such as nutrients, light and temperature), may capture a broader range of *in situ* growth behaviour than empirical models based on laboratory experiments or field data alone [16].

The simple traditional pelagic structure adopted in conceptual models and transposed to mathematical ecological models has now been expanded to include more trophic levels in which microorganisms play a very substantial role. In a revision made on microbial food web models, Davidson [17] mentions that the explicit inclusion of bacterioplankton is often necessary to simulate the observed dynamics of aquatic systems. So, the choice of excluding such compartments of the microbial loop impair model results and disregards current developments in aquatic ecological studies.

While increasing the capacity and applicability of model, adding increasing levels of complexity within ecosystem components has its own disadvantages. Probably the main disadvantage comes from the need to set the appropriate parameters for the model processes and the lack of detailed data to validate results. In addition, the large number of species-specific parameters makes it difficult to use such complex models for phytoplankton communities in natural water bodies. Another drawback is the potential decrease in use of this type of models as management tools, given their dependency on a high number of highly uncertain parameters [42].

At present, the number of uncertainties and the imprecision of a large number of parameters used in this kind of models limit their use as a tool to predict biomass of production of the functional groups represented in them [43, 44]. In this context, the model should be viewed as hypothesis to explain the gross features of system dynamics which can be evaluated as additional become available, refined as knowledge improves or simply dismissed if found to be false.

The relevance of any particular model can be judged by its performance, which might be its ability to derive fundamental properties from a minimum set of assumptions [44, 43]. Simple models usually depend on fewer assumptions and have a limited range of unknown parameters. But simple models can also be found to be too simplistic because they do not consider some of the fundamental processes of the systems they try to simulate.

But our ability to understand the link between assumptions and model output decreases rapidly with model complexity. Therefore, each modelling application must start by identifying the relevant processes of a given system before dismissing options that are *a priori* excluded, such as silica limitation, bacterioplankton activity, etc.

Nevertheless, the ongoing evolution of ecological models complexity means necessarily that complexity must increase following the increase in knowledge, and also computer power, even if to a minor extent. All simulation

models aim to represent system behaviour with a limited set of knowledge. As knowledge on the functioning components of a given system increases, so must the detail of representation of that system by a model. On the other hand, the continuous increase in computational power experienced over the last decades seems likely to continue in the future. So, while being limited to the constraints of present computer power, any model development effort must consider the ongoing growing capacity of computers.

Finally, complex models may provide a theoretical basis for the development of even more complex marine ecological models as understanding, laboratory techniques, and field data collection advances [36].

1.4 The *MOHID* modelling system

Starting in 1985 with a 2D hydrodynamic semi-implict model with finite differences [45], the *MOHID* system has been developed throughout the years by a team of researchers and students to become a 3D hydrodynamic model [46] with a finite volume discretization [47]. In time, the simulated physical processes have increased dramatically, and as a direct result of this progress, the scope of *MOHID* applications has become wider, both in detail and in scale (from estuaries to ocean basins). Among several possible examples of *MOHID* use as a numerical tool in the study of marine systems there is the study of internal tides [48] and of different aspects of the dynamics of estuaries, from a general circulation 3D modelling [49] to more specific physical processes like mixing [50]. Coastal and oceanic-scale simulations have also been studied. Just to name a few, the slope current along the Western European Margin [51], the circulation off the Iberian coast [52] and in a broader scale, the circulation in the European ocean margin [53]. The wide spectrum of applications reveals *MOHID* versatility and utility, and the gain in experience has contributed to test and improve it. A detailed description about the development of *MOHID* structure and modelling philosophy has been recently thoroughly addressed elsewhere [54], and so, only a brief synthesis is presented here.

MOHID code, developed in *FORTRAN 95* programming language, is adapted around the concept of object-oriented programming. This kind of code architecture makes possible the use of classes (i.e. a set of variables and subroutines) to define a process or a set of processes. In its basic arrangement, *MOHID* is divided into several classes (i.e. the "objects"), each class being responsible for the management of one or more processes represented and all the associated variables (table. 1.1). All the simulated processes by *MOHID* in the water column can be subdivided in some major groups: time-evolution of both turbulent and non-turbulent flow properties, time-evolution of the water properties in Eulerian and Lagrangian referential, water quality processes, and vertical movements independent from flow.

Each one of this groups can use one or several classes. In the code, a class is defined as a module and in this sense, *MOHID* is arranged as number of modules. A module can depend on other modules or it can stand by its own. So, any improvements in the *MOHID* model can be achieved by adding a new module or just by updating an existing one.

To achieve versatility, *MOHID* has been written in a modular way, allowing an easy inclusion of new biogeochemical models. The first attempt to incorporate a water quality module in the *MOHID* system took place in 1995 with the coupling of the hydrodynamic model with an Eulerian transport model to simulate nitrogen and phosphorus cycles and primary production in Tagus estuary [55]. The emergence of new challenges in model simulations allied with demanding problems to study has led to the awareness that the water quality module had to become 0D, enabling its use independently of the adopted transport model dimension and referential (1D, 2D or 3D). This philosophy in the model structure means that any adopted or developed model can address all the biological or chemical processes without any dependence on the hydrodynamic processes. For its versatility, the actual version of *MOHID* retains this philosophy.

In the last years the *MOHID* system have incorporated in its code two basic water quality models, each one with its own level of detail and best suited to specific aquatic systems. The first model adopted, labeled *WaterQuality*, was initially developed using the US Environmental Protection Agency model [56]. Despite successful improvements made in this code, the baseline philosophy has been rather untouched when it comes to nutrient cycles and biological/chemical processes. This model is best suited to applications in estuaries and coastal systems. The other adopted model was the CE-QUAL-W2 River Basin Model developed by the US Army Corps of Engineers [57, 58, 59, 60]. It is characterized by a detailed parameterization for both biological and chemical processes and it has been developed to simulate freshwater systems like rivers, branches, lakes, dams and reservoirs.

Table 1.1: Some examples of major classes (or modules) responsible for the management of some processes and related properties in the *MOHID* system. (adapted from [54])

Class or Module	**Controlled Processes**	**Related Properties**
AdvectionDiffusion	Advection & diffusion	-
Benthos	Erosion & deposition Organic matter degradation	Some water quality properties Bottom stress Rugosity
FreeVerticalMovement	Particulate material sinking velocity	-
Geometry	Vertical discretization evolution	Volume Area Height
HorizontalGrid	Coordinate conversion	Grid coordinates Horizontal step
Hydrodynamic	Continuity Force balance	Non-turbulent flow properties
Lagrangian	Tracer's trajectory	Water properties in a Lagrangian referential
Surface	Stress calculation from wind speed	Radiation / heat fluxes Wind stress Water/atmosphere gas exchange
Turbulence	Turbulent processes	Turbulent flow properties
WaterProperties	-	Water properties in an Eularian referential
WaterQuality	All water quality properties (depending on the WQ model)	Chemical and biological processes affecting water quality properties

1.5 Becoming operational

Operational oceanography includes making, disseminating, and interpreting measurements of different parameters from seas and oceans in order to provide forecasts of future conditions. The implementation of operational systems is expanding rapidly to embrace dynamically coupled atmosphere–ocean–coastal models or modules involving simulations over a range of time scales. Likewise, the scope is extending from essentially physical parameters (e.g. tides, surges, waves and temperature) and chemical parameters related to water quality, to biological/ecological parameters indicative of ecosystem variability [5].

The rapid advances in monitoring techniques systems, scientific understanding, computational power and numerical methods (for both modelling and assimilation), have been pointed out as presenting new exciting opportunities in the study and monitoring of many aquatic systems [61]. Nevertheless, the strong investment and associated progress of implementing an operational modelling system will ultimately depend on demonstrable benefits for end users. But when it comes to water quality problems, the enormous challenges that coastal and estuarine systems face today may well justify all the effort.

The actual challenge in the *MOHID* system continuous development and application lies in its integration into operational systems. In a sense it can be said that achieving an operational model is the great next step in the *MOHID* evolution. This change will undoubtedly bring along real-time data assimilation modules into *MOHID* system, widening its capacity as a modelling tool. Recent advances of operational oceanography are pushing *MOHID* system towards an operational framework, and the implications of such high demand requires a full operational model for physical process as well as water quality related processes. In a recent review paper on water quality models in coastal systems [39], a brief description on the history of both hydrodynamic and ecological models is presented showing that nowadays there are already some successful 3D circulation models working in an operational platform. The same, however, is not true for ecological models. The state-of-the-art in this field will soon be defined by linking fine-grid 3D hydrodynamic models with ecological models with many variables (ERSEM as a reference). Operational modelling in this area is programmed to occur in the end of the present decade.

1.6 Rationale

In view of the advances in knowledge on aquatic systems over the last two decades, it becomes clear that marine biogeochemical models must take into account the key elements (processes, elements, biological groups, etc.) of

the systems they try to study. Probably the more relevant are the crucial role of the microbial loop, the interactions of different primary and secondary groups of producers, variable Chla:C ratios in producers, and the variable elemental composition (stoichiometry) within each biological group and organic matter compartments.

The driving force beyond the present work was to develop such a model, the *mohid.Life.1.0*. The model here presented was built inside a modelling platform that already captures what can be described as the state-of-the-art in circulation models, namely, the MOHID model. This work marks a shift from a modelling approach based on the linear NPZ modelling approach [56], previously incorporated in the MOHID, to a more sophisticated and complex modelling approach based on the ERSEM model.

Some numerical analyses and tests are performed to assess model performance and results quality. These tests consist in the implementation of the model to an idealized scenario (mesocosm) and finally in an implementation to a real system. The Tagus estuary was chose as the study site to profit from previous modelling applications with a simpler ecological model and the experience and knowledge gained with it. Another intention of this implementation is to realize in what way the developed model enables the advance in the knowledge of the controlling mechanism for production, when compared to an implementation with a simpler model.

The development of *mohid.Life.1.0* inside the MOHID model will generate a numerical tool able to address a much larger set of processes in marine systems. This, in turn, will enable the study of a wider range of problems and the potential broadening in the comprehension of the systems where the model will be applied. Besides, the effort carried out here represents an update for MOHID to the actual state in ecological modelling of marine systems, as well as, an essential step towards an operational platform.

Chapter 2

Model *mohid.Life.1.0* structure

2.1 Introduction

Several characteristics have to be considered when choosing a water quality / ecological model or when developing one from scratch. Aspects like the water body type, temporal and spatial scales, and the physical/chemical/biological processes that one wants to address must be defined prior to any choice of models and/or modelling approaches.

Water bodies are usually classified into four major classes: (a) lakes and reservoirs, (b) rivers and channels, (c) estuaries and coastal systems, and (d) oceanic basins. Each one of these classes has its own particular set of characteristics (physical, chemical and biological). In lakes and reservoirs the surface extension is usually quite bigger than the depth, flow velocities are extremely low and the residence time is usually high. Relatively high flow velocities and variable residence times characterize rivers and channels. Also, the surface extension and depth vary significantly. Estuaries and coastal systems can have different geometries with different length scales, and can combine different flow regimes and residence times. Finally, oceanic basins are so complex that cannot be defined by some major characteristics of geometry, flow regime and residence times. In conclusion, each class presents its own challenges when it comes to produce a model to study them.

There are also some differences in model's capacity to represent spatial scales. The selection of a spatial scale in a model is not so much a function of the scale of the study area, but rather a function of its physical properties, the processes in study and the available computing capacity. Some models can be used in cases with a single volume of water assuming a complete mixture (0D). This type of models is best suited to a less detailed level of analysis. The next level of spatial representation is achieved when it is assumed that there is a gradient in at least one direction (1D). This approach

can be used when processes like the vertical variation in deep lakes or the horizontal flow in rivers play an important role in the system. By adding a gradient in another direction (2D), whether vertical or horizontal, it is possible to study systems with a two-dimensional hydrodynamic regime.

More detailed models are able to represent gradients in all three directions or dimensions (3D). This type of approach is generally used in estuarine, coastal and oceanic systems. The complexity of the model does not follow necessarily the complexity of the system in study. So, it is possible to apply an 1D model in the study of a coastal system, in the same way as it is possible to use a 3D approach when modelling a river or reservoir.

Different approaches are also adopted in the way models represent time scales. Some models can only address stationary conditions without any variation or evolution over time. Other models can in turn account for the temporal variation of each property with the evolution of the simulation being calculated over small time intervals or time steps, usually ranging from minutes to a few days.

2.1.1 Major guidelines

As already mentioned in the previous chapter, the code architecture of *MOHID* allows an easy incorporation of new modules. *mohid.Life.1.0* is, in that sense, a new addition to the *MOHID* system. All ecological modules in the *MOHID* system are models *per se*. So when the "*module*" nomenclature is used, it addresses the model as a component of the *MOHID* system. When incorporated into *MOHID* it becomes a module of the vast *MOHID* model. Therefore, any water quality/ecological model can benefit from all transport modules and be potentially used in every class of water bodies. Like any new addition to the code, this was designed to address specific water quality processes. The parameterization of biological and chemical processes in this water quality model were developed having in mind applications to saltwater or brackish water systems (estuary, coastal, oceanic systems, etc.), irrespective of their physical conditions (size, geometry, residence time, etc.).

In its basic setup, the model presented here is a twelve-component water column ecological model comprising three classes of standard organisms (producers, consumers, decomposers), organic matter (particulate, dissolved labile and semi-labile), nitrate, ammonium, phosphate, silicate acid, biogenic silica and oxygen. Producers and consumers, can have several functional groups that can be added to the model. This capacity was developed in the code to render it more versatile using a generic constituent approach. As an example, inside the producer component, the model user can define a group for diatoms, other for picoalgae, etc. The same can be done for consumers.

The model assumes that all living organisms and all forms of organic matter have variable contents of the elements C, N and P. In addition, all forms of producers have a chlorophyll cell content and, as an option, a

silica fraction too. Hence, a particular producer group can be defined by up to 5 state-variables (carbon, nitrogen, phosphorus, chlorophyll, and silica content). In all, the model accounts for several dozens of state variables, depending on the settings defined by the user.

Altogether, the model accounts for the biogeochemical cycles of carbon, nitrogen, phosphorus, silica and oxygen. Some of these elements only have a partial cycle (oxygen), while others (nitrogen and phosphorus) have a more detailed cycle parameterization. Many of the biotic and detritus compartments contain multiple elemental pools, and so it is possible to track carbon, nitrogen, phosphorous and silica through the ecosystem. A schematic of the model is shown in Figure 2.1.

For simplicity, the code is divided into four sections or compartments: producers, consumers, decomposers and biogeochemical processes. The first three sections comprise biological processes specific for each group in question, while the last deals only with processes involving organic matter and nutrient dynamics without any dependence on biological groups of the model (e.g. nitrification rate, biogenic silica dissolution, etc.). The next chapters will present a detailed description of each one of these sections. Process-oriented models on which *mohid.Life.1.0* is based are appropriate for modelling stoichiometric and element cycling in ecosystems because they allow explicit consideration of mass-balance constraints for each element and provide explicit information on the relationships between physiological functions and recycling processes [22].

The ecosystem model has been developed to be incorporated into the *MOHID* framework. For this reason, all processes and state variables are calculated for a control volume (figure 2.2), regardless of any transport scheme. If not coupled to an hydrodynamic model, the ecological model becomes non-dimensional (or 0D). Since all water quality related processes are managed by an independent class (or module in the *MOHID* code), the ecological model can easily be linked with Lagrangian or Eulerian transport (1D, 2D or 3D) schemes in which all state variables are expressed as concentrations, no matter whether they are dissolved (nutrients, oxygen, etc.) or particles (POM, producers, etc.). For each control volume, a system of linear equations is solved resolving the interdependence of different properties. The model was constructed using a Euler forward scheme (explicit method) as the integration method, chosen for being relatively easy to code.

The control-volume approach consists of dividing the water body into finite segments or "*control volumes*" [37]. As it can be inferred from figure 2.2, there are n unknowns that need to be determined for each control volume. Consequently, n equations must be solved simultaneously. The mass balance for each property must take into account the transport in the interfaces between volumes as well as sources and sinks within each control volume. In 1D applications only the concentrations at the interfaces between the segment and its upstream and downstream neighbours are considered

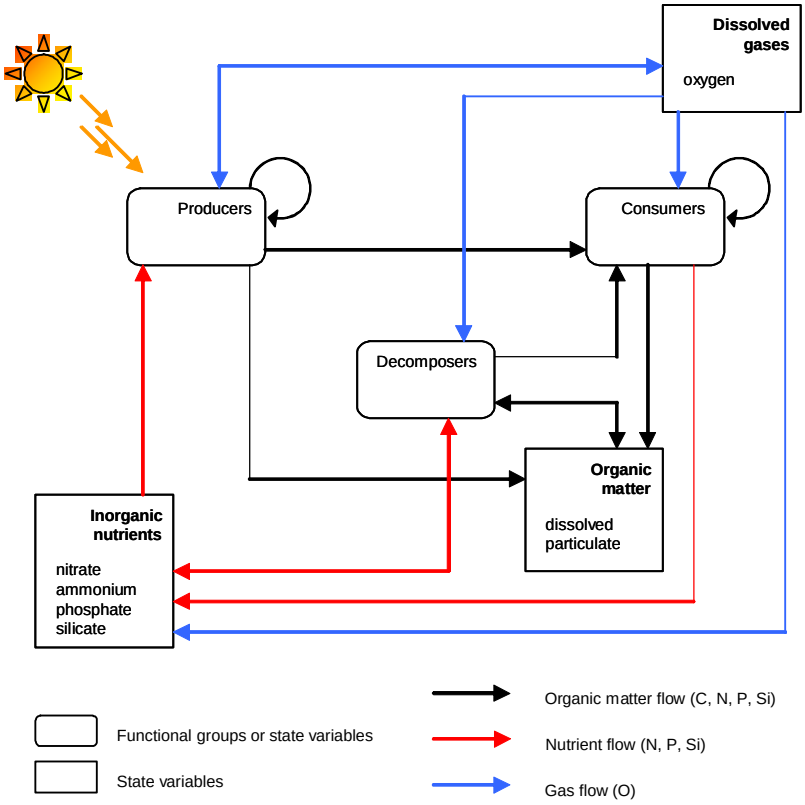

Figure 2.1: Diagram of *mohid.Life.1.0* model showing the relation between state variables and the flux of elements.

(in a 1D horizontal case) or between top and down neighbours (in a 1D vertical case, where each control-volume is usually addressed as a layer). In 2D applications neighbour segments can be upstream and downstream and top and down, or else upstream and downstream and longitudinal. In the last type of application, 3D, the segment is surrounded by all sides by other segments (except in boundary segments).

With this methodology, the application of this biogeochemical model into a complex 3D advection-diffusion model under the present *MOHID* structure is a relatively easy and straightforward task. The transport model has to store all space dependent variables and calculate their advection with the mean flow and horizontal diffusion, and their vertical diffusion (even if this process is a physiological response). All destruction and production processes (sinks and sources) are calculated by the biogeochemical module which in turn is called by means of a loop over all horizontal grid nodes of the 3D model.

2.1.2 Basic equations

The choice of a particular mathematical model to simulate water quality conditions of any aquatic system depends on the characteristics of the system, the level of accuracy needed in face of the objectives, available data about the system, and available methodologies to correctly represent the processes involved. Of special importance is the representation of the dynamic conditions of the system, because they influence the transport conditions and consequently the evolution in time of the chemical and biological constituents. Together with chemical and biological processes, physical processes must be addressed to account for the transport of each property over time. So, the property concentration (C) depends on physical, chemical, and biological characteristics of the environment:

$$C = f(physics,\ chemistry,\ biology). \tag{2.1}$$

The evolution over time of each model compartment or state-variable can be described by an equation with the following form:

$$\left.\frac{\partial C_i}{\partial t}\right|_{i=1,2,\ldots,n} = Physics\,(C_i) + Biology\,(C_i) \tag{2.2}$$

where C_i stands for each modeled property or state-variable (ammonium, phosphate, etc.). For each compartment, the term $Physics$ represents changes to the property concentration caused by physical processes like vertical and horizontal advection and diffusive effects.

The transport of any given property in the model is usually resolved by the advection - diffusion equation (eq. 2.3). It does not change the identity of the property being transported because it only moves matter from one

position in space to another. Diffusion can be defined as the variation of the property concentration in relation to its own gradient. So, it refers to the movement of mass due to random water motion or mixing. The *Physics* term parameterization encompasses this gain/loss of the property by advection and diffusion processes and can be described as:

$$\frac{\partial C}{\partial t} = \frac{\partial}{\partial x}\left(D_x \frac{\partial C}{\partial x} - u_x C\right) + \frac{\partial}{\partial y}\left(D_y \frac{\partial C}{\partial y} - u_y C\right) + \frac{\partial}{\partial z}\left(D_z \frac{\partial C}{\partial z} - u_z C\right) + F\left(C, t\right) \tag{2.3}$$

where C is the property concentration, $D_{x,y,z}$ the diffusion coefficients in each direction, $u_{x,y,z}$ the velocity in each direction. This calculation is made outside the water quality module by the hydrodynamic module of *MOHID*. Finally, $F(C,t)$ represents the loss/gain term of the property calculated by the water quality model.

The terms *Biology* and *Chemistry* represent biological and chemical sources and sinks of the same compartment. They are usually lumped into the same category (usually named *Biology*) given that both are addressed inside the biogeochemical model. Biological and physical processes are two distinctive factors affecting the concentration of each property in a control volume but they are not fully independent of each other. Probably the best way to illustrate the relation between them is the sinking velocity calculation for producers. The sinking velocity implies a lost of mass from the control volume and can be considered as a physical process. But this velocity can also be a function of nutrient stress of each group. This dependence of a physical parameter on biological conditions shows that it is difficult to have fully independent physical and biological modules.

Biological constituents of the pelagic model are grouped in functional groups. These functional groups are modeled according to the concept of "*standard organism*" [26], considering universal biological processes such as food uptake, assimilation, excretion, respiration, mortality, predation and related carbon and nutrient flux dynamics (figure 2.3). According to this concept, the fundamental equation describing the net growth of a standard organism can be expressed as:

$$\frac{\partial X_c}{\partial t} = \left[up - (res + mort + exc)\right].X_c - G \tag{2.4}$$

in which the carbon biomass of the standard organism (X_c) depends on the specific uptake rate (up), specific total respiration rate (res), specific mortality rate ($mort$), specific total excretion rate (exc), and on the grazing rate (G). Uptake and predation are usually defined as a linear function response to substrate or prey density. A simple encounter mechanism is

assumed to govern prey consumption kinetics. Except for predation on prey and unless indicated otherwise, mortality rate is density independent.

Three major classes of standard organisms are outlined: producers, consumers and decomposers. Together with biogeochemical functions, they form the core blocks (i.e., modules) of the model. So, the structure of the biogeochemical model is in fact composed by a set of interlinked modules. Except for the biogeochemical module, every other major class or module can contain several groups or species (e.g., diatoms, flagellates, etc.). Depending on the application setup (type of ecosystem and biological processes to study) it is possible to remove some of these groups or add some new.

Non-biological state variables used in the model are inorganic nutrients (nitrogen, phosphorus and silicate acid), oxygen and organic matter. In the basic setup of the model, carbon and chlorophyll are expressed in mg m^{-3}, nutrients in mmol Nut m^{-3} and oxygen in mg O_2 l^{-1}. However, the model deals with any unit system, provided that all initial values, parameters, and conversion factors show coherence. In this way, the unit system used is user-defined, meaning that there is no unit conversion inside the model.

Within the code structure of each module, none of the processes has explicitly received priority over others. Thus, processes take place in a sequential order according to the programmed structure. The only obvious priority imposition in the processes inside each group is related with nutrient excretion and mineralization; these processes only take place after the model upgrades the variable matrix with new values resulting from all other processes (discussed in the next chapters).

For simplicity in the notation used to describe the model, some conventions are used to address processes affecting carbon and nutrient dynamics inside each group:

- Unless indicated otherwise, all descriptions are the same for producer groups and so P denotes phytoplankton biomass. An upper index following P denotes an individual group (e.g. P^1 for diatoms). By itself, P is used when primary producers are being addressed as a whole. The same procedure is used to consumers or zooplankton (Z) and decomposers or bacteria (B).
- When describing a process or addressing a rate, a lower index may be used to denote the standing stock or biomass density in question (c, n, p and s for C, N, P and Si, respectively). In that sense, P_c stands for phytoplankton carbon biomass and P_n, P_p, and P_{si} for nutrient content.
- An upper index can be used sometimes for other insightful information. In parameters this notation is frequently used to refer to the process.

2.1.3 Generic units system

Ecological models projected for neritic or pelagic zones in marine systems tend to express bulk quantities in mg m^{-3}, while freshwater ecological mod-

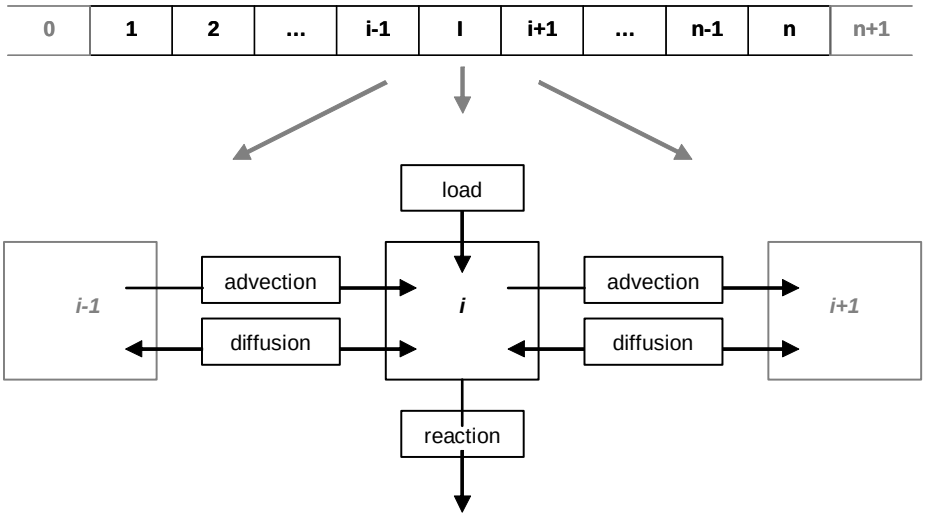

Figure 2.2: Mass balance around a control volume (Adapted from Chapra [37]). Segments 0 and n+1 represent boundary segments.

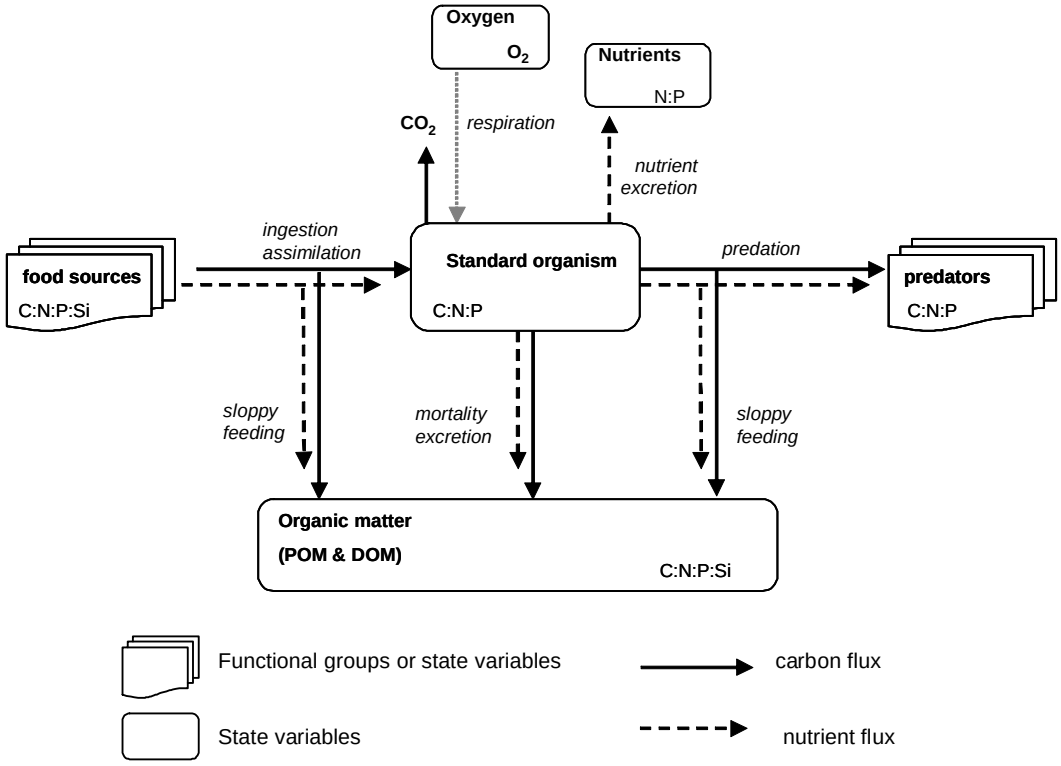

Figure 2.3: The concept of standard organism applied to a consumer or secondary producer (SP), with several processes and element fluxes illustrated.

els in mg l^{-1}. In addition, some variables like dissolved oxygen that are usually expressed in mg l^{-1}, have their own standard units (or at least most frequently used) irrespective of the unit system used in all or part of the variables. Frequently models are developed for a particular area and set of conditions. As a consequence, units often are determined by the unit system of the available data sets that will be used to calibrate or test the model.

To achieve greater versatility in use and function, *mohid.Life.1.0* is prepared to work with any unit system. This means that the model was not developed around any particular unit system. Therefore use is not restricted to any predefined unit convention. Another additional advantage of this code arrangement strategy is to allow the use of different unit systems for different variables. To achieve this versatility, all conversion factors, ratios and other unit dependent constants must be defined by the user. In this system, coherence in units is user dependent. So, the user must bear in mind that the model does not check consistency or possible unit incoherence in fluxes. As the model setup grows in complexity (additional producers and consumers groups, and increasing complexity in trophic relations), some minor changes in the model output are expected. This change is a result of possible rounding errors that might occur with some unit systems, accumulated at each time step.

2.1.4 Baseline philosophy

Every model development, and adaptations to a lesser extent, have a baseline philosophy that defines the modelling strategy when it comes to choosing the variables to be considered and processes to be addressed. Likewise, any modelling approach to a biological system must rely on some assumptions that can be to a lesser or greater extent based on current knowledge of the dynamics of those systems. The following list presents the major assumptions in *mohid.Life.1.0*.

Assumption 1. All living organisms have variable cellular nutrient content (or elemental stoichiometry) of elements N, and P (also Si when considered). So, they are considered as non-homeostatic, i.e., they do not have fixed biochemical ratios in their biomass.

Assumption 2. Although individuals within each population at any time are assumed to have identical nutrient content, these contents vary over time, depending on nutrient availability.

Assumption 3. Among producers, chlorophyll synthesis and cell content varies in response to light conditions and nitrogen uptake in an explicit way through an acclimation process.

Assumption 4. Mineralization occurs via decomposers and consumers, whenever the substrate carbon:nutrient ratios are higher than the maximum ratio defined for each group.

Assumption 5. The carbon cycle is open, meaning that respired carbon is not considered in the carbon balance, and the inorganic carbon source is never limiting.

Assumption 6. Decomposers (or bacteria), can use nutrients in their mineral form (a process known as immobilization) along with nutrients in the organic form consumed together with carbon in organic matter substrates. There is no preference factor in the uptake kinetics.

2.1.5 Dependence on other *MOHID* modules

As stated before, each module inside the *MOHID* system addresses different processes and manages its related variables. This approach makes water-quality/ecologic modules independent from other modules to some extent, and that is the reason why it can be used in any setting, from 0D to 3D (i.e., independently from the transport processes). Nonetheless, the object-oriented programming philosophy of *MOHID* allows transmission of information between modules. More than an option, this transmission is crucial to model some processes because it conveys forcing like light and temperature to the ecological model. This exchange on information can work in both directions; the ecologic model can import and export information.

Probably the simplest example can be found in the temperature forcing for biology rates and limitations. Because temperature is a property whose variation in time and in space (both the horizontal and vertical fields) is managed outside the ecologic module, its importance in the control of several physiologic processes makes it necessary to have temperature values in each control volume over time. So, in each time step the ecologic module gets a temperature value calculated somewhere else. Temperature is therefore a typical case of information import by the water quality module.

The last process of information exchange between modules comprises both the export and import of information, involving the impact of some properties in the absorption of light in water. In order to respond to the light regime, the water quality module has to receive the available radiation value in the water from outside. The radiation levels are, in turn, affected by the chlorophyll, DOM and POM concentration in the water and by the absorption of light by the water molecules. In order to address this feedback mechanism, the water quality module exports the mentioned concentration values to the *LightExtinctionModule*, which then uses them to calculate the light extinction in water. Finally the available radiation is send back to the water quality module to be used in processes like chlorophyll synthesis.

2.1.6 Light climate

Given its particular relevance in primary production, the parameterization of light extinction in the water column is presented here. Light energy available

at the water surface I_0 $\left(\mathrm{W\,m^{-2}}\right)$ or incident short wave radiance can be calculated for a given latitude and longitude or else a set of measurements can be used to force the model. To calculate the specific amount of solar radiation available for a control volume, first the model has to estimate the absorption of light in the water column above (layers) and within the control volume itself. This is obtained knowing the total absorption coefficient and the height of the water column above. If the control volume is on the surface, then the incident radiation is considered.

Photons are absorbed by water, clay particles, chlorophyll content in phytoplankton, and other light-absorbing particles. The net extinction coefficient for PAR (k_{par}) is defined as the sum of each individual contribution of water molecules, chlorophyll, DOM and POM absorption:

$$k_{par} = \epsilon_w + \left(\epsilon_{chl}.\sum_{i=1}^{n} P_{chl}^{i}\right) + \epsilon_{doc}.DOC + \epsilon_{poc}.POC \tag{2.5}$$

To estimate the contribution of chlorophyll the absorption, all the contributions within the producers group have to be considered, hence, the sum $\sum_{i=1}^{n} P_{chl}^{i}$, where i is a particular group and n the total number of producer groups. Here, it is assumed that the light gradient follows the Lambert-Beer's law, which states that the light intensity at depth z and time t is:

$$I_{(z,t)} = I_0\ e^{-k_{par}.z} \tag{2.6}$$

A short description of each parameter and variable and their units can be found in table 2.1.

Given that all water quality related processes are accounted for in a control volume approach, they are independent of the number of layers considered. So, each time ambient radiation is addressed it will be in the form of the incident radiation (I_0), which for all matter is the radiance in a specific control volume, whether this volume is on the surface or somewhere in the water column.

2.2 Producers module

2.2.1 Background review

Photosynthesis is a process that takes place in chlorophyll-containing tissues of plants exposed to light. It is responsible for the formation of carbohydrates from carbon dioxide and a source of hydrogen. Even though the photosynthetic process as a whole is composed of numerous single reactions, the fundamental relationship governing the photosynthetic process of algae can be expressed in the basic equation:

$$nCO_2 + nH_2O \xrightarrow{light} n\,(CH_2O) + nO_2 + nH_2O \tag{2.7}$$

Table 2.1: List of parameters and variables used to calculate light attenuation in the water column.

Symbol	Parameters	Units
I_0	Incident short wave radiance	$\mathrm{W\,m^{-2}}$
ϵ_w	Absorption coefficient for water	$\mathrm{m^{-1}}$
ϵ_{chl}	Absorption coefficient for chlorophyll	$\mathrm{m^{-1}/\left(mg\,m^{-3}\right)}$
ϵ_{doc}	Absorption coefficient for DOC	$\mathrm{m^{-1}/\left(mg\,m^{-3}\right)}$
ϵ_{poc}	Absorption coefficient for POC	$\mathrm{m^{-1}/\left(mg\,m^{-3}\right)}$
	Variables	
k_{par}	Absorption coefficient for PAR	$\mathrm{W\,m^{-2}}$
I_z	Average PAR in the control volume	$\mathrm{W\,m^{-2}}$

Based on the Redfield[1]-Richards ratio, the formation of an average molecule of phytoplanktonic organic matter by the process of photosynthesis is:

$$106CO_2+122H_2O+16HNO_3+H_3PO_4 \xrightarrow{light} \underbrace{(CH_2O)_{106}\,(NH_3)_{16}\,(H_3PO_4)}_{\text{empirical formula}}+138O_2 \tag{2.8}$$

According to this equation it is possible to see that besides carbon dioxide and water, dissolved inorganic nitrogen and phosphorus are also required by phytoplankton. For that reason the availability of these elements is sometimes a limiting factor for phytoplankton growth given their relatively low concentration in seawater.

Growth models are usually based on extracellular concentrations of nutrients and take the form:

$$\mu = \mu^{max}.f\,(\text{limiting factors}) \tag{2.9}$$

where μ is the growth rate, μ^{max} the maximum growth rate and f (limiting factors) is a function describing the effect of any potential limiting factors on growth. These factors include ambient nutrient concentrations, but also consider temperature and light limitations.

Primary production modelling is generally summarized as relationship between carbon assimilation (or oxygen production) and incident light intensity. These relationships are mainly derived empirically, although some may

[1] The 'Redfield ratio' or 'Redfield stoichiometry' refers to the molar ratio of carbon (C), nitrogen (N) and phosphorus (P) in phytoplankton (principally diatoms) when nutrients are not limiting.

have a physiological background [62, 63]. In their model of plankton population dynamics, Baird and Emsley [11] modeled phytoplankton by analogy to chemical kinetics as a function of intracellular nutrient and energy reserves. In a detailed review, Behrenfeld and Falkowski [10] present a wide spectrum of productivity models developed in the last four decades. They range from simple relationships between surface chlorophyll concentrations and daily carbon fixation in the euphotic zone, to wavelength resolved models, where the absorbed radiation is converted into net photosynthesis.

Physical (and some times chemical) processes govern light until it reaches the producers cell. Only then, biological processes become important. In most water quality models the rate of photosynthesis $P(t)$ is assumed to be directly proportional to the available light energy $I(t)$, $P(t) \propto I(t)$. In coupled biological-physical models, irradiance or light availability is determined by known laws of physics. So, the underwater light regime and light extinction in depth depend on the model parameterization of processes like light absorption, refraction, etc. In other models (e.g. [64, 65, 41]), light drives photosynthesis which, when balanced by respiration, changes the storing process of carbon within the cell. This modelling approach also considers adaptation like the production of pigments under low light regimes.

Nutrient uptake

While photosynthesis supplies the phytoplankton with energy and $C-H-O$ compounds, algal cells have to take up other elements from the surrounding water, like dissolved nutritional compounds, to build up new biomass. This process is defined as nutrient uptake.

Elements may be divided according to the quantity needed by the organisms. Nutrients that make up more than 0.1 % of organic material (Ca, K, Mg, N, P, S, Cl, Si) are referred as macronutrients, whereas those needed only in small amounts (e.g. Fe, Mn, Cu, Zn, Mo, Co, B, V, Se) are labeled micronutrients. In most cases, nutrient uptake takes place against a concentration gradient requiring an active ion transport systems, a process that requires energy provided by photosynthesis or respiration.

Early models typically considered the uptake of one macronutrient, nitrogen usually. As modelling techniques advanced and the knowledge of phytoplankton physiology increased, production models started to incorporate at least one more macronutrient, phosphorus. With the vast array of available ecological models in the present, not only macronutrients are considered but also some models considered one micronutrient, namely iron, to study specific cases where it is known this element to be a decisive factor in production (e.g. [66]).

Even though Michaelis-Menten kinetics (Monod equation, referred as MMM from now on) is frequently used, it is only valid in constant external nutrient concentrations scenarios (e.g. in chemostat culture) and if nutri-

ent are not stored internally in significant amounts. When this is not the case, the cell quota model of Droop [67] is more realistic. The use of the Monod equation is frequent in most water quality models because of their assumption of a fixed stoichiometry, whereas the Droop cell quota approach is characteristic in models where stoichiometry varies.

The basic growth limitation term according to Droop is:

$$\Omega_{nut} = 1 - \frac{q_0}{q} \tag{2.10}$$

where q is the internal nutrient concentration and q_0 the minimum internal concentration.

Growth rate in the Droop model is completely independent of the external nutrient concentrations and depends exclusively on the internal cell quota. Replenishment of storage after nutrient addition will lead to very high uptake rates (luxury consumption) uncoupled from growth rate. This separation of the mechanisms of uptake and growth reflects the principle that growth only occurs after the internal nutrient concentration reaches a given quota. So, high population growth rates require high cellular content of limiting nutrients, and low growth rates occur when one or more nutrients have reduced content.

In most cases, phytoplankton growth models consider only a one nutrient limiting rate approach, often the nutrient that limits the cell yield. In natural conditions, however, cells will be under stress caused by transient changes in the concentrations of several extracellular and intracellular nutrients [68]. Besides, dual nutrient limitation can occur. Considering these needs, recent approaches to model phytoplankton growth have developed the capacity to represent the behaviour of a population under multiple nutrient stresses.

Respiration

Respiration is the set of processes by which oxygen is introduced into the cell system, and carbon dioxide is removed. Due to difficulties in discriminating algal and non-algal respiration, it is common practice to assume that respiration is a fixed proportion of the light saturated gross photosynthetic rate [69]. The respiration process can be divided in photorespiration and dark respiration. Photorespiration is the light-dependent uptake of oxygen and the oxidation of reduced substances. Dark respiration is the controlled oxidation of organic compounds, which occurs in the mitochondria and cytoplasm. Dark respiration can be divided into two components: (1) the basal or maintenance respiration, and (2) a growth-rate-dependent component [70].

In ecosystem models, parameterization of phytoplankton respiration is largely based on correlation as opposed to the mechanistic understanding of

the process. Taking ERSEM I [71] as an example, phytoplankton respiration is composed of three distinct processes: activity respiration, nutrient stress respiration and resting (maintenance) respiration. The specific activity respiration is proportional to the specific growth rate, whereas the nutrient stress respiration is proportional to the difference between the specific maximal potential growth rate and the specific actual gross growth rate. The specific rest respiration rate is a function of seawater temperature and day length. In ERSEM II [28] this parameterization is changed in the way that the nutrient stress respiration is left out, so that the basal (rest) respiration is no longer dependent on the day length. Also, the activity respiration is dependent on the incorporated assimilation (and not on growth, therefore being decoupled from the nutrient situation).

Exudation

Exudation, also known as cell leakage or extracellular release, is a broader term used to abridge different processes of dissolved matter release by algal cell as a result of several factors. It differs from excretion because it manly covers the diffuse loss of unspecific organic matter by living cells.

Exudation is the result of several processes: (a) Photorespiration, which is the light-dependent uptake of oxygen (and so tightly coupled with photosynthesis) and the oxidation of reduced substances; (b) Persistent passive permeation of small organic molecules through the cell membrane; (c) Active release of excess photosynthates that accumulate when fixation exceeds incorporation into new cell material.

There is no clear explanation for the factors involved in the exudation of dissolved organic matter by phytoplankton. Ambient concentration of dissolved inorganic nitrogen has been shown to have a negative correlation with the release of DOM, implying that nutrient stress stimulates this release.

Models usually calculate exudation as a fixed percentage of total carbon fixation. In ERSEM, exudation is composed of "activity excretion" (function of assimilation) and "nutrient-stress-dependent excretion" (function of internal nutrient quota).

Rates of production and exudation may be different for carbon and nitrogen. Several compounds containing C and N, like simple sugars and aminoacids may be leaked from cells, but exudation due to an overflow of photosynthate might be expected to be dominated by non-nitrogenous compounds. Some models make a distinction between leakage, which occurred in the phytoplankton's C:N ratio, and exudation that was only carbon (e.g. [72]). Other models have an exudation term that only considers DOC.

Carbohydrates exudation

Along with lipids, carbohydrates are the most important cellular reservoirs of chemical energy, and are usually found in the seawater as free saccharides, with only a negligible part as their derivatives (e.g., amino sugars). The biosynthesis of carbohydrates is directly coupled with photosynthesis and is, therefore, light dependent. Besides diurnal variations of intracellular carbohydrate pools, vertical gradients of biosynthesis indicate that the highest contribution to the carbohydrate pool is near the surface. At night, carbohydrates are used as chemical energy and converted to other chemical compounds such as proteins, and as a consequence the cell reservoirs decrease. Between 15 and 90% of photoassimilated carbon may be released as carbohydrates by algae during growth periods [73].

The release of dissolved carbohydrates is affected by the physiological state and nutrient ratios [74, 75]. Intracellular carbohydrate pools increase during nutrient limitation [76], and this nutrient stagnation accelerates not only the production but also the release of carbohydrates to the surrounding waters, especially during daytime. This release will have an impact on the food chain because even at low concentrations sugars provide a substantial food source for heterotrophic bacteria [77].

Phytoplankton grazing

Ecosystem food web studies and models tend to address photosynthetic and heterotrophic organisms separately. But in the microbial world this division may not be necessarily adequate because some protists can combine both abilities. Phytoplankton grazing is usually termed as mixotrophy. Mixotrophy is defined as the capacity of combining photosynthesis and phagotrophy in the same individual [78]. Mixotrophic predation influences prey population dynamics and size distribution, as well as nutrient turnover in the pelagic zone. Recent studies [79, 80] have show that mixotrophic flagellates are abundant and quantitatively important as bacterivores in a number of different marine environments.

In mixotrophs, the relative importance of both photo and phagotrophic modes of nutrition is species-specific and varies as a function of environmental parameters like particle density, light and pH [81], inorganic nutrient concentrations [82], and perhaps dissolved organic carbon [83]. Some mixotrophs can switch from photoautotrophy to phagotrophy and vice versa. Based on the large variation among species, some authors [81] introduced the concept of a "mixotrophic gradient"; the gradient ranges from almost purely photoautotrophic to almost purely phagotrophic nutrition. Mixotrophs near the photoautotrophic extreme are pigmented flagellates that only occasionally have been observed with ingested particles and growth is primarily due to photosynthesis. Near the heterotrophic extreme, phagotrophy can

be the primary mechanism supporting growth, whereas photosynthesis improves the survival during times of low food particle concentrations. In low-light environments or environments in which inorganic nutrients have been consumed, phagotrophy provides a means of survival and growth for mixotrophic species in competition with other phytoplankton.

Little modelling effort has been focused on the mixotrophs, at least in part due to the lack of quantitative information on the abundance and information on their physiology [17]. Thingstad *et al.* [84] presented a detailed mathematical analysis of algal mixotrophy in "chemostat scenarios" with mixotrophs in different trophic positions. Recently, an improved model version of ERSEM [29] has included mixotrophic flagellates, defined as protists of a size between 2-20 μm that are able to photosynthesize and feed heterotrophically at the same time. Nutrient availability and food concentrations determine the degree to which they behave autotrophically or heterotrophically.

Lysis

Lysis can be defined as the pathological, age-dependent or post-mortem hydrolytic degradation of protoplasm. The results is a release of dissolved or particulate material as a consequence of death or cell destruction. Several factors can induce cell lysis:

A. Phytoplankton cells can be destroyed and lyse is caused by the interaction with other organisms. This can occur in the following ways: (i) As the result of virus infection [85]; (ii) due to interaction with bacteria, either caused by dissolved organic substances excreted by the bacteria or by direct contact [86]; (iii) induced by certain species of heterotrophic flagellates [87]; (iv) mechanical destruction by the feeding action of zooplankton [88]. In this last process, known as "sloppy feeding", phytoplankton cells are not entirely ingested.

B. Phytoplankton cell lysis may be caused by environmental factors. Because phytoplankton cell lysis events apparently occur after blooms, when growth conditions become suboptimal [89], environmental stress like nutrient or light limitation [90] might trigger cell death.

Parameterization of phytoplankton cell lysis in ecological models is largely based on empirical findings. In ERSEM formulation, for instance, lysis products are partly particulate and partly dissolved, being the particulate fraction dependent on the actual nutrient cell quota [28].

Sedimentation

The passive settlement due to gravity, usually referred as sedimentation, is one of the major loss processes of phytoplankton. It depends mainly on the sinking or settling velocity and on all the processes affecting it. The sinking

Table 2.2: Some random examples of sinking velocities of different organic particles in aquatic environments. (from [37])

Particle type	**Diameter** (μm)	**Sinking velocity** $\left(\mathrm{m\,d^{-1}}\right)$
Phytoplankton	2	0.08
	25	0.2
	50	1.9
	84	1.1
POC	1-10	0.2
	10-64	1.5
	>64	2.3

velocity of a particle $\left(v_s,\ \mathrm{m\,d^{-1}}\right)$ is described by Stoke's law by:

$$v_s = \alpha . \frac{g}{18} . \left(\frac{\rho_s - \rho_w}{\mu} \right) . d^2 \tag{2.11}$$

where α is a dimensionless factor to account for the effect of the particle's shape on the sinking velocity (1.0 for a sphere), g the acceleration due to gravity $\left(= 981\,\mathrm{cm\,s^{-2}}\right)$, ρ_s and ρ_w the densities of the particle and water, respectively $\left(\mathrm{g\,cm^{-3}}\right)$, μ the dynamic viscosity $\left(\mathrm{g\,cm^{-1}\,s^{-1}}\right)$, and d the effective particle diameter (μm). According to this law, the sinking velocity is linearly dependent on particle density and quadratically dependent on diameter. Nevertheless, particles in natural systems have complex shapes (leading to $\alpha < 1$), implying that diameter is not the only decisive aspect in settling velocities in water, as it can be seen in table 2.2.

The sinking rate in diatoms changes with growth stage and can be under physiological control. This control has been shown to vary with the energy status of cells, with sinking rates increasing when energy is decreasing by nutrient limitation, prolonged darkness, or metabolic inhibitors [91]. A detailed study [92] about the influence of nutrient depletion on the sinking rate of four marine diatoms showed that silicate depletion caused the greatest increase in sinking rate for all four species. However, nitrogen and phosphorus depletion caused lower sinking rates in 3 species. This observation demands a re-evaluation of the axiom that nutrient depletion necessarily causes increased sinking rates.

In field investigations, observed density and size distribution of phytoplankton are frequently insufficient to account for observed vertical fluxes. The main reason for this discrepancy is that suspended particles may aggregate into large (ranging from mm to cm in size), rapidly sinking "marine snow" particles, which typically consist of a mixture of inorganic particles, detrital organic material as well as microorganisms. These aggregates are fragile and normally disintegrate when sampled by traditional means (net, pumps, water samplers).

Aggregates of suspended particles can also be formed by physical coagulation, a process by which suspended particles collide due to fluid shear or different settling velocities and stick together upon collision. The coagulation rate depends on the collision rate between particles and on their stickiness, i.e., the probability of adhesion upon collision. Most pelagic diatoms are sticky at times [93] and therefore form aggregates by physical coagulation [94].

Most ecosystem models account for sedimentation (or sinking of algae) as a major loss process of phytoplankton from the euphotic zone. Sinking velocity is to a large extent physiologically determined but it is often parameterized as a purely physical process. Recent models consider a biological control in sedimentation velocity by the implementation of a sinking velocity that is dependent on the nutrient status of cells.

2.2.2 Basic module outline

Using ERSEM as a reference, primary producers are divided in four functional groups or size classes as a basic setup of the model: diatoms (20-200 μm), autotrophic flagellates (2-20 μm), picoalgae (0.2-2 μm), and mixotrophic flagellates (20-200 μm). The major difference between diatoms and other phytoplankton groups in the model is that diatoms are dependent on silicate. So, the parameterization is extended to account for this extra nutrient requirement and limitation. The mixotrophy process is another major difference within the parameterization of producers (described below). A generic description of the processes involved in the parameterization of producers is portrayed in figure 2.4.

Besides these parameterization differences, all other processes are modeled in the same way for all groups, so that several producers can be defined only by using different parameter values. Although the basic setup of the model considers these four functional groups, the model code is prepared to work with generic constituents for producers, consumers and decomposers. This versatility in the code allows to add n groups or species of producers. In addition, it is possible to define if a producer needs silica (in the case of having more than one diatom species or a group of silicoflagellates) and if it can become mixotrophic.

Phytoplankton growth rates are determined by available light and nutrients using a modified form of the growth model of Geider *et al.* [64, 65, 41]. Ratios between all of the phytoplankton pools vary dynamically as phytoplankton adapt to changing light levels and nutrient availability. Maximum and minimum cell quotas for each nutrient are input parameters to the model. If phytoplankton is unable to attain their maximum cell quota through uptake, carbon fixation (growth rate) is reduced proportionately. Whichever nutrient is currently most limiting (expressed by the lowest cell quota relative to the maximum quotas) modifies the carbon fixation rates.

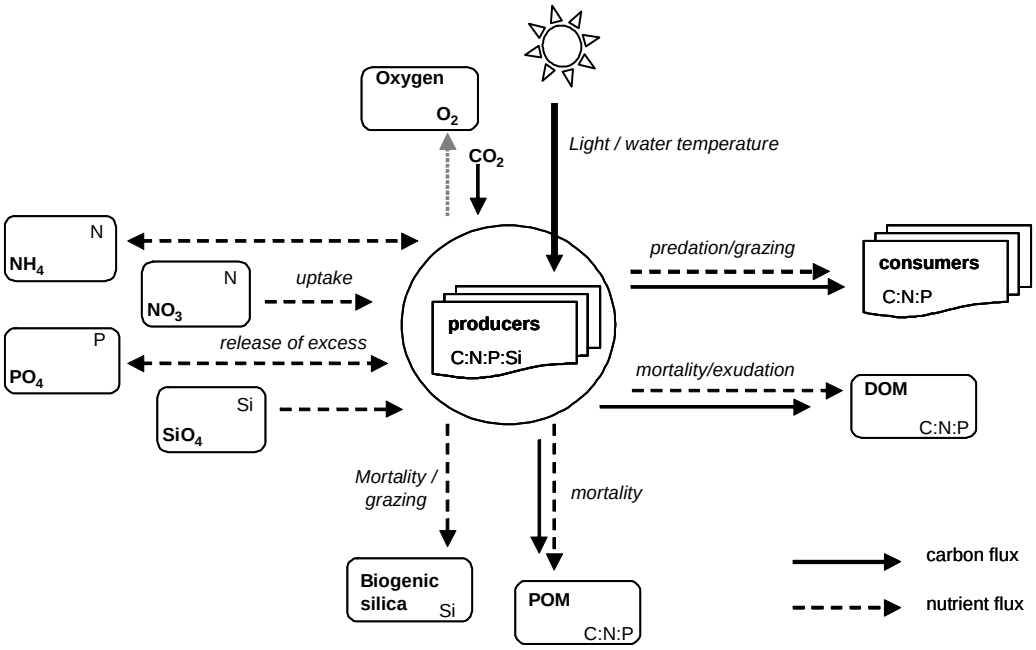

Figure 2.4: Carbon and nutrients mass fluxes related with primary producers activity. Phytoplankton groups (1 to 4) are: diatoms (20-200μm), mixotrophic flagellates (2-20μm), picoalgae (0.2-2μm), and flagellates (20-200μm). Diatoms differ from all other phytoplankton groups in their silica dependence (see text for details).

The model parameterization includes the following regulatory features from the Geider *et al.* [41] model: (1) the carbon-specific, light-saturated photosynthetic rate depends on the internal nitrogen status of the cell; (2) the carbon-specific, light-limited photosynthetic rate depends on the Chl*a*:C ratio; (3) Chl*a* synthesis requires N assimilation; (4) Chl*a* synthesis is downregulated when the rate of light absorption exceeds the rate of utilization of photons for carbon fixation, with the extent of downregulation being governed by the imbalance between rates of light absorption and photosynthesis; (5) the maximum rate of nutrient assimilation is regulated by the internal nutrient status/quota of the cells.

Most of the modelling of primary producers follows the scheme presented by Baretta-Bekker *et al.* [28], in which phytoplankton population depends on internal nutrient concentration. For that reason, the intracellular quotas of nitrogen and phosphorus are calculated (also silica when needed). Three values are used for each nutrient in order to regulate the cell nutrient:carbon stoichiometry. The first sets a minimum value for the nutrient:carbon ratio $\left(\chi_{n,p}^{min}\right)$, characterizing a situation with no internal nutrient storage. As such, it corresponds only to the nutrient content of the structural parts of the cell. The second value refers to the average stoichiometric C_{106}:N_{16}:P_1 ratio in phytoplankton $\left(\chi_{n,p}^{R}\right)$, usually known as Redfield ratio [95]. Finally, the third value specifies the maximum nutrient quota $\left(\chi_{n,p}^{min}\right)$, which is the maximum nutrient storage capacity of a cell.

The adopted reference values can be the same used in most models with variable C, N and P stoichiometry, corresponding to half and twice the Redfield ratio for the minimum and maximum nutrient quotas, respectively. However, other values can be chosen. For N and P these parameters are defined as:

$$\chi_n^R = (N/C)_{redfield} \quad ; \quad \chi_p^R = (P/C)_{redfield} \tag{2.12}$$

$$\chi_n^{min} = (N/C)_{min} \quad ; \quad \chi_p^{min} = (P/C)_{min} \tag{2.13}$$

$$\chi_n^{max} = (N/C)_{max} \quad ; \quad \chi_p^{max} = (P/C)_{max} \tag{2.14}$$

According to this concept, the threshold between limiting and non-limiting nutrient situation is defined by the Redfield ratio (χ_n^R and χ_p^R). Every time one of the nutrient quotas (given by the nut:C ratio) falls below the Redfield ratio, reflecting a nutrient limitation situation, loss terms due to excretion and lysis begin to increase.

The intracellular nutrient pool status is characterized by a minimum limiting dimensionless factor (Ω_{np}) with a value between 0 and 1. This factor is given by:

$$\Omega = \min\left(\Omega_n, \Omega_p\right) \tag{2.15}$$

with,

$$\Omega_j = ramp\left[0, \left(\chi_j - \chi_j^{min}\right) / \left(\chi_j^R - \chi_j^{min}\right), 1\right] \quad with\ j = n, p \tag{2.16}$$

hence,

$$\Omega_j = 1 \quad if \quad \chi_j \geqslant \chi_j^R$$

$$\Omega_j = 0 \quad if \quad \chi_j = \chi_j^{min}$$

$$0 < \Omega_j < 1 \quad if \quad \chi_j^{min} < \chi_j < \chi_j^R$$

As a general rule, regulating or limiting factors are 1 under optimum or non-limiting conditions and tend towards 0 in strong limiting situations. This value depends on the actual nitrogen and phosphorus quota, χ_n and χ_p respectively. The value of each quota (the actual quota) is easily attained by dividing the organism nutrient content by the carbon content.

Instead of the ramp function, $ramp(a, x, b) = \min(b, \max(a, x))$, other functions can be used to describe the intracellular nutrient pool status. The function defined in the model is the same used by Baretta-Bekker *et al.* [28] who also propose other functions. An additional factor, χ_s, is used for diatoms to address the external silicate limitation.

2.2.3 Carbon dynamics

Carbon biomass is affected by assimilation, excretion and respiration processes. Every time these processes are addressed they only concern carbon components. The rate of each one of these processes is controlled by several regulation factors (commonly known as limiting factors): light limitation (Ω_L), temperature dependence (Ω_T), and combined N and P limitation (Ω_{np}). For diatoms or any other producer depending on silica for growth, another factor is used to express the external Si limitation (Ω_{si}). The temperature dependence factor can be calculated in two different ways by the model:

$$\Omega_T = (Q_{10})^{\frac{temp}{10^o - 1}} \tag{2.17}$$

or

$$\Omega_T = \exp\left[-4000. \left(\frac{1}{temp + 273.15} - \frac{1}{temp_{ref} + 273.15}\right)\right] \tag{2.18}$$

In the first method, Q_{10} is the characteristic temperature coefficient for each functional group. For a reference temperature, assuming 10 °C, the factor has the vale 1 and for all other temperatures the values is determined by the value of Q_{10}. The second method consists in an exponential dependence or an Arrhenius equation where -4000 is the slope in the Arrhenius plot. Two parameters are used in this function: ambient temperature and a reference temperature value, $temp_{ref}$. In both methods $temp$ is the water temperature around the cell.

Considering the temperature dependence and silica limitation (whenever used by the producer), the maximum rate of C-specific photosynthesis is achieved by:

$$P_c^{max} = r^{ass}.\Omega_T \tag{2.19}$$

where r^{ass} is the maximum specific daily assimilation rate at a reference temperature. The potential assimilation rate is not dependent on nutrient limitation, whether this might be induced by the internal nutrient pool or the external ambient concentration. In silica depending organisms the silica limitation factor (Ω_s) is also multiplied in equation 2.19. In this case, the relation between the different limitation factors is multiplicative.

The light control over production is parameterized according to a slightly modified approach to the growth model of Geider *et al.* [41]. The actual specific assimilation/photosynthesis rate is described by:

$$P_c^{phot} = P_c^{max}\left[1 - \exp\left(\frac{-\alpha^{chl}.\chi_{chl}.I_0}{P_c^{max}}\right)\right] \tag{2.20}$$

where α^{chl} is the chlorophyll light absorption coefficient, χ_{chl} the chlorophyll cell quota or Chl$a$:C ratio, and I_0 the incident irradiance. With this approach, considering phytoplankton acclimation to light and nutrients, the light history is reflected on growth by the variation of the Chl$a$:C. As it will be seen below, this ratio is in turn affected by nitrogen limitation and the variability of the N:C cell ratio.

Exudation

Assuming that some assimilated products are not used and exuded as DOC, the exuded fraction (exu) of assimilation becomes:

$$exu = P_c^{phot}.\left[\phi^{ex} + (1 - \phi^{ex}).(1 - \Omega_{np})\right] \tag{2.21}$$

This is modeled considering an activity excretion $\left(P_c^{phot}.\phi^{ex}\right)$ that is directly influenced by nutrient-stress-dependent excretion given by $(1 - \Omega_{np})$. So, activity and nutrient-stress excretion are linked together. In the equation, ϕ^{ex} is a dimensionless factor representing the fraction of assimilated carbon that is exuded under nutrient-rich conditions.

Considering two extreme scenarios, no nutrient limitation ($\Omega_{np} = 1$) and total limitation ($\Omega_{np} = 0$), exu becomes:

$$\begin{aligned} P_c^{phot}.\phi^{ex} \quad if \quad \Omega_{np} &= 1 \\ P_c^{phot} \quad if \quad \Omega_{np} &= 0 \end{aligned}$$

In the second case, where $exu = P_c^{phot}$, all the assimilation products are exuded as DOC and no biomass growth takes place.

Assimilation and respiration

By subtracting the exuded fraction to the assimilated, the incorporated carbon $\left(ass^{inc}\right)$ is attained:

$$ass^{inc} = P_c^{phot} - exu \tag{2.22}$$

From here it is possible to calculate the net primary production $\left(ass^{net}\right)$ just by calculating the difference between incorporated $\left(ass^{inc}\right)$ and respired carbon:

$$ass^{net} = ass^{inc} - res \tag{2.23}$$

with,

$$res = \left(r^{bas}.\Omega_T\right) + \left(q^{res}.ass^{inc}\right) \tag{2.24}$$

Total respiration (res) is the sum of the contribution of two different processes represented by each term in equation 2.24: the first term accounts for the basal respiration, while the second for the activity respiration. Basal respiration depends on a basal respiration rate $\left(r^{bas}\right)$ and temperature. It affects only the biomass because it is independent of the uptake. Under severe light or nutrient limitation, net primary production may become negative due to basal respiration. The activity respiration is a fraction (q^{res}) of the incorporated carbon $\left(ass^{inc}\right)$.

Mortality

Grazing, mortality (lysis) and sinking are also included as loss terms. Mortality caused by cell burst (or lysis) is assumed in the model as a way to implicitly represent the effect of several mortality processes attributed to different causes (viruses, bacteria, mechanical causes, etc.). The lysis rate (lys) is not assumed to be constant nor temperature dependent. Because it can be enhanced by nutrient-limited conditions, the average lysis rate increases with nutrient stress (low Ω_{np}). The lysis rate is formulated as:

$$lys = r^{lys}\left(\frac{1}{\Omega_{np} + 0.1}\right) \tag{2.25}$$

where r^{lys} is the specific background lysis rate under conditions with no nutrient limitation. Products resulting from phytoplankton death can be divided into particulate and dissolved. The division is determined by a calculated fraction $\left(q^{POM}\right)$, quantifying the amount that goes to POM, and depends on the actual and minimal intracellular nutrient quotas:

$$q^{POM} = \min\left(\frac{\chi_p^{min}}{\chi_p}, \frac{\chi_n^{min}}{\chi_n}\right) \tag{2.26}$$

With the distinction made regarding the final lysis products it is possible

to assume that nutrients in the structural parts of the cell are diverted to POM while those in cytoplasm are routed to the DOM pool. Phytoplankton mortality products are thus calculated:

$$\begin{aligned} P_m^{POM} &= lys.q^{POM} \\ P_m^{DOM} &= lys.\left(1 - q^{POM}\right) \end{aligned} \tag{2.27}$$

The same procedure is used to calculate the fraction of exuded carbon that goes to each organic carbon pool:

$$\begin{aligned} P_e^{POM} &= exu.q^{POM} \\ P_e^{DOM} &= exu.\left(1 - q^{POM}\right) \end{aligned} \tag{2.28}$$

Finally, part $\left(\varphi_P^{sl}\right)$ of DOM that is exuded and released as mortality products is diverted to a semi-labile pool, while the rest $\left(\varphi_P^{l}\right)$ goes to a labile pool.

Sedimentation

The final loss process, the loss of producers by vertical movements (i.e. sedimentation or sinking), is dependent on the intracellular nutrient quota. The calculation scheme adopted in this model follows the formulation proposed by Varela *et al.* [71] with the alterations made by Baretta-Bekker *et al.* [28] to account for internal nutrient limitation instead of the external one.

Sinking velocity is calculated based on a minimal reference sedimentation rate (σ_P^m) or background sedimentation velocity, a nutrient stress sedimentation rate $\left(\sigma_P^{str}\right)$ representing the sinking velocity under total nutrient limitation, a nutrient stress threshold $\left(\Omega_{nut}^{sed}\right)$ below which increased sedimentation occurs, and on the actual total nutrient limitations (Ω_{nut}). Sinking velocity is formulated as:

$$\sigma_p = \sigma_P^{str}.\max\left(0, \Omega_{nut}^{sed} - \Omega_{nut}\right) + \sigma_P^m \tag{2.29}$$

Whenever silica is used, the total nutrient limitation is obtained from:

$$\Omega_{nut} = \min\left(\Omega_s, \Omega_{np}\right) \tag{2.30}$$

This parameterization is applied for all silica-dependent organisms because of the external silicate limitation (Ω_s). For other groups where there is no uptake of silica, only N and P limitation is considered.

Table 2.3: Parameter list for the producers module

Symbol	Parameter	Reference Units
χ_n^R	Redfield N:C ratio	$\mathrm{mmol}N\,(\,\mathrm{mg}C)^{-1}$
χ_n^{min}	Minimum N:C ratio	$\mathrm{mmol}N\,(\,\mathrm{mg}C)^{-1}$
χ_n^{max}	Maximum N:C ratio	$\mathrm{mmol}N\,(\,\mathrm{mg}C)^{-1}$
χ_p^R	Redfield P:C ratio	$\mathrm{mmol}P\,(\,\mathrm{mg}C)^{-1}$
χ_p^{min}	Minimum P:C ratio	$\mathrm{mmol}P\,(\,\mathrm{mg}C)^{-1}$
χ_p^{max}	Maximum P:C ratio	$\mathrm{mmol}P\,(\,\mathrm{mg}C)^{-1}$
χ_s^R	Standard Si:C ratio	$\mathrm{mmol}Si\,(\,\mathrm{mg}C)^{-1}$
$\chi_{chl:c}$	Chl$a$:C ratio	$\mathrm{mg}Chl\,(\,\mathrm{mg}C)^{-1}$
α^{chl}	Initial slope of the photosynthesis-light curve	$\mathrm{mg}C\,\mathrm{m}^2(\,\mathrm{mg}Chl\,\mathrm{W\,d})^{-1}$
$\chi_{chl:n}^{max}$	Maximum Chl:N ratio	$\mathrm{mg}Chl\,(\,\mathrm{mmol}N)^{-1}$
I_0	Incident irradiance	$\mathrm{W\,m}^{-2}$
Q_{10}	Q_{10} value	Dimensionless
$temp_{ref}$	Reference temperature	°C
r^{ass}	Maximum assimilation rate	d^{-1}
ϕ^{ex}	Exudation under nutrient stress	Dimensionless
r^{bas}	Basal respiration rate	d^{-1}
q^{res}	Respired fraction of production	Dimensionless
r^{lys}	Minimum lysis rate	d^{-1}
σ_P^{str}	Nutrient stress sedimentation rate	$\mathrm{m\,d}^{-1}$
σ_P^m	Minimum sedimentation rate	$\mathrm{m\,d}^{-1}$
Ω_{nut}^{sed}	Nutrient stress threshold	Dimensionless
Q_{max}	Maximum rate of storage filling	d^{-1}
k^{n1}	Affinity for NO_3 (uptake rate)	$(\,\mathrm{mg}C)^{-1}\ \mathrm{m}^{-3}\,\mathrm{d}^{-1}$
k^{n2}	Affinity for NH_4 (uptake rate)	$(\,\mathrm{mg}C)^{-1}\ \mathrm{m}^{-3}\,\mathrm{d}^{-1}$
k^p	Affinity for PO_4 (uptake rate)	$(\,\mathrm{mg}C)^{-1}\ \mathrm{m}^{-3}\,\mathrm{d}^{-1}$
r^s	Release rate of excess silicate	d^{-1}
k_s	Silicate uptake Michaelis constant	$\mathrm{mmol}Si\,\mathrm{m}^{-3}$
φ_P^{sl}	DOM fraction diverted to semi-labile pool	Dimensionless

2.2.4 Nitrogen and phosphorus dynamics

Primary producers in the model can uptake two forms of nitrogen, namely nitrate $\left(NO_3^-\right)$ and ammonium $\left(NH_4^+\right)$. The main form of dissolved phosphorus in marine systems is inorganic orthophosphate, usually designated as phosphate. In the pH range characteristic of seawater, orthophosphate $\left(PO_4^{3-}\right)$ ions are largely associated as HPO_4^{2-}. The model assumes no difference in these ionic forms. Hence, primary producers can uptake phosphorus as phosphate. The uptake rate is dependent on both the external concentration of each of these elements and on the degree of filled storage capacity. From this, the potential uptake in the model depends upon on several conditions: internal nutrient storage, external nutrient concentration, and the affinity of each phytoplankton group for a specific nutrient. All nutrient uptake processes are detached from carbon assimilation processes. Nevertheless, to assure a stoichiometric balance, nutrient uptake is dependent on the carbon uptake to some extent.

Several processes that affect carbon biomass (e.g., mortality, sedimentation, etc.) also affect cell nutrient content, P_n and P_p. The model accounts for this influence on nutrients by multiplying rates controlling P_c with instantaneous C:nut ratios. This procedure is used for all processes that influence organisms as a whole, and is also adopted in the parameterization of consumers and decomposers.

Uptake

The model assumes that nutrient uptake is dependent on both external and internal nutrient concentrations. For each nutrient, the uptake is defined as the amount needed to replenish its intracellular storage or reserves, plus the amount to form new biomass. This amount is given by:

$$\upsilon_j^{int} = \left[\left(ass^{net}.\chi_j^{max}\right) + \left(\chi_j^{max} - \chi_j\right).\chi_{max}\right] \quad , \; j = n, p \tag{2.31}$$

The filling rate of nutrient reserves will depend on the maximal rate of storage filling (χ_{max}). Because nutrient uptake also depends on the external concentration, at actual phosphate external concentration $[PO_4]$, the amount that phytoplankton is able to uptake depends on the affinity, k^p, for this element and is calculated as:

$$\upsilon_p^{ext} = k^p.\left[PO_4\right] \tag{2.32}$$

The existence of two nitrogen sources affects the amount of nitrogen that phytoplankton can uptake $\left(\upsilon_n^{ext}\right)$ because of their unequal availability and different affinities for each one of them $\left(k^{n1} \text{ and } k^{n2}\right)$. This process is formulated as:

$$\upsilon_{n1}^{ext} = k^{n1}.\left[NO_3\right] \tag{2.33}$$

$$\upsilon_{n2}^{ext} = k^{n2}.\left[NH_4\right] \tag{2.34}$$

Total nitrogen uptake is simply achieved by the sum of both sources:

$$\upsilon_n^{ext} = \upsilon_{n1}^{ext} + \upsilon_{n2}^{ext} \tag{2.35}$$

The uptake becomes the minimum between the potential uptake rate dependent on internal conditions and on the external factors:

$$\upsilon_j = \min\left(\upsilon_j^{int}, \upsilon_j^{ext}\right) \quad , \; j = n, p \tag{2.36}$$

In nitrogen the flux is divided in two parts, one for each nitrogen source:

$$\text{if } \upsilon_n > 0, \left\{ \begin{array}{ll} \upsilon_{n1}^{phy} = \left(\frac{\upsilon_{n1}^{ext}}{\upsilon_n^{ext}}\right).\upsilon_n.P_c & \text{for } NO_3 \\ \\ \upsilon_{n2}^{phy} = \left(\frac{\upsilon_{n2}^{ext}}{\upsilon_n^{ext}}\right).\upsilon_n.P_c & \text{for } NH_4 \end{array} \right\} \tag{2.37}$$

Regarding phosphate uptake, assuming this as the only P source, the realized uptake equals the result of the minimum expressed in equation 2.36 multiplied by the carbon quota concentration (P_c):

$$\upsilon_p^{phy} = \upsilon_p.P_c \tag{2.38}$$

Excretion

In periods without primary production, respiration may cause the realized uptake (υ_n or υ_p) to become negative, leading to excretion of nutrient in their inorganic form. In the case of phosphorus, the surplus is excreted as phosphate. As for nitrogen, excretion caused by surplus only occurs in the form of ammonium. For both nutrients, the excreted excess $\left(\phi_j^{phy}\right)$ is calculated according to:

$$\phi_j^{phy} = \left(\chi_j - \chi_j^{max}\right).P_c \qquad \text{if} \quad \chi_j > \chi_j^{max} \qquad , \; j = n, p \tag{2.39}$$

Nutrient loss by mortality only occurs in organic forms. For each nutrient, the dissolved and particulate fraction resulting from mortality is calculated in the same way as carbon (equation 2.27), the only difference being the fact that for each nutrient it is the phytoplankton group nitrogen or phosphorus content considered (P_n and P_p instead of P_c).

Silica dynamics

Silicate parameterization in primary producers is only valid for functional groups that need this nutrient. In the model, Si to elements (C, N, P) ratios may change over time. This variation is supported by recent studies [96] suggesting that depending on iron concentration in the water, the Si:N uptake ratio can vary by about a factor of 4.

Table 2.4: Variables used in the producers module (carbon dynamics).

Symbol	Variables	Reference Units
P_c	Producers carbon	$\mathrm{mg}C\,\mathrm{m}^{-3}$
P_n	Producers nitrogen	$\mathrm{mmol}N\,\mathrm{m}^{-3}$
P_p	Producers phosphorus	$\mathrm{mmol}P\,\mathrm{m}^{-3}$
P_{si}	Producers silica	$\mathrm{mmol}Si\,\mathrm{m}^{-3}$
P_{chl}	Producers chlorophyll	$\mathrm{mg}Chl\,\mathrm{m}^{-3}$
Ω_{np}	Intracellular nutrient pool status	Dimensionless
Ω_n	Intracellular nitrogen limitation	Dimensionless
Ω_p	Intracellular phosphorus limitation	Dimensionless
Ω_{si}	External silicate limitation	Dimensionless
Ω_{nut}	Nutrient limitation (when considering silica)	Dimensionless
Ω_T	Temperature limitation	Dimensionless
P_c^{max}	Maximum value of P_c^{phot}	d^{-1}
P_c^{phot}	C-specific photosynthesis rate	d^{-1}
exu	Exudation rate	d^{-1}
ass^{inc}	Total carbon assimilation rate	d^{-1}
ass^{net}	Net primary production	d^{-1}
res	Total respiration rate	d^{-1}
lys	Lysis rate	d^{-1}
q^{POM}	Fraction of mortality products to POM	Dimensionless
P_m^{DOM}	Mortality products to labile DOM (rate)	d^{-1}
P_m^{POM}	Mortality products to semi-labile DOM (rate)	d^{-1}
P_e^{DOM}	Exuded products to labile DOM (rate)	d^{-1}
P_e^{POM}	Exuded products to semi-labile DOM (rate)	d^{-1}
σ_p	Sinking velocity	$\mathrm{m}\,\mathrm{d}^{-1}$

Table 2.5: Variables used in the producers module (nutrient and chlorophyll dynamics).

Symbol	Variables	Reference Units
υ_n^{int}	Nitrogen uptake intracellular demand	$\mathrm{mmol}N\,(\,\mathrm{mg}C)^{-1}\,\mathrm{d}^{-1}$
υ_p^{int}	Phosphorus uptake intracellular demand	$\mathrm{mmol}P\,(\,\mathrm{mg}C)^{-1}\,\mathrm{d}^{-1}$
υ_{n1}^{ext}	Potential nitrate uptake	$\mathrm{mmol}N\,(\,\mathrm{mg}C)^{-1}\,\mathrm{d}^{-1}$
υ_{n2}^{ext}	Potential ammonium uptake	$\mathrm{mmol}N\,(\,\mathrm{mg}C)^{-1}\,\mathrm{d}^{-1}$
υ_p^{ext}	Potential Phosphate uptake	$\mathrm{mmol}P\,(\,\mathrm{mg}C)^{-1}\,\mathrm{d}^{-1}$
υ_n^{ext}	Total potential nitrogen uptake	$\mathrm{mmol}N\,(\,\mathrm{mg}C)^{-1}\,\mathrm{d}^{-1}$
υ_n	Realized total nitrogen uptake	$\mathrm{mmol}N\,(\,\mathrm{mg}C)^{-1}\,\mathrm{d}^{-1}$
υ_p	Realized total phosphorus uptake	$\mathrm{mmol}P\,(\,\mathrm{mg}C)^{-1}\,\mathrm{d}^{-1}$
υ_{n1}^{phy}	Realized nitrate uptake	$\mathrm{mmol}N\,\mathrm{m}^{-3}\,\mathrm{d}^{-1}$
υ_{n1}^{phy}	Realized ammonium uptake	$\mathrm{mmol}N\,\mathrm{m}^{-3}\,\mathrm{d}^{-1}$
υ_p^{phy}	Realized phosphate uptake	$\mathrm{mmol}P\,\mathrm{m}^{-3}\,\mathrm{d}^{-1}$
ϕ_n^b	Excreted NH_4	$\mathrm{mmol}N\,\mathrm{m}^{-3}$
ϕ_p^b	Excreted PO_4	$\mathrm{mmol}P\,\mathrm{m}^{-3}$
υ_s	Silica uptake flux	$\mathrm{mmol}Si\,\mathrm{m}^{-3}\,\mathrm{d}^{-1}$
ρ_{chl}	Chlorophyll synthesis regulation term	$\mathrm{mg}Chl\,(\,\mathrm{mmol}N)^{-1}$
P_{ac}	Chlorophyll synthesis rate (photoacclimation)	d^{-1}

Contrary to nitrogen and phosphorus, silica is not stored internally and so, silicate dynamics differs from other nutrients. Here, the cell quota $\left(\chi_s^R\right)$ is equal to a fixed standard value, assuming that silicate uptake flux is proportional to carbon net production $\left(ass^{net}\right)$. The uptake is expressed as:

$$\upsilon_s^{phy} = \left[\max\left(0, ass^{net}.\chi_s^R\right) - \max\left(0, \chi_s - \chi_s^R\right).r^s\right].P_c \tag{2.40}$$

The uptake and release of excess silica are separated in the uptake equation. The uptake is addressed in the first term and the condition $ass^{net} > 0$ must be verified. The release of excess silica (second term in the equation) is determined by a release rate, r^s. However, it must be stressed that silica excretion is not an active mechanism in diatoms because this element is a crystalline structural element in the cell. Eventually, silica excretion will take place if by any reason (e.g., DOC excretion) the C:Si ratio drops below the defined value.

Because concentration in the water can be zero, a limiting factor for silica uptake must be considered. The silica limiting function (Ω_s) that prevents uptake to occur if there is no silicate in the water is formulated using a MMM function:

$$\Omega_s = \frac{[SiO_4]}{[SiO_4] + k_s} \tag{2.41}$$

This limiting factor is added in equation 2.19 for the maximal specific pri-

mary production in diatoms or any other silica-depending organisms considered.

Chlorophyll dynamics

The model of phytoplankton growth and physiological acclimation (to irradiance, nutrient concentration and temperature) treats nutrient uptake and photosynthesis rates as functions of both environmental factors and cellular chemical compositions (Chl$a$:C and N:C).

As already mentioned, photoadaptation is modelled according to the models proposed by other authors [64, 41]. Chlorophyll synthesis (P_{ac}) is regulated by the balance between photosynthetic carbon fixation and light absorption (the ratio of energy assimilated to energy absorbed). This regulation term (ρ_{chl}) is formulated as:

$$\rho_{chl} = \chi_{chl:n}^{max} . \frac{P_c^{phot}}{\alpha^{chl} . \chi_{chl:c} . I_0} \tag{2.42}$$

where $\chi_{chl:n}^{max}$ is the maximum value of Chal:N ratio. The remaining variables have already been defined for equation 2.20. The chlorophyll synthesis parameterization is then:

$$P_{ac} = \frac{\rho_{chl} . up_n}{\chi_{chl:c}} - \phi_{chl} \tag{2.43}$$

Chlorophyll synthesis is assumed to be proportional to nitrogen uptake (up_n), reflecting the need for the synthesis of proteins used in light harvesting complexes and elsewhere in the photosynthetic system. A chlorophyll degradation rate is also considered in the formulation (ϕ_{chl}). Besides this potential loss term, chlorophyll can also be lost by phytoplankton mortality and so this has to be considered in the mass balance equation (equation 2.48).

According to this parameterization the instantaneous rates of light utilization, carbon assimilation, chlorophyll a synthesis, and nutrient assimilation are determined by environmental variables. This way the instantaneous rates can change in time due to the effects of past environmental conditions by including intracellular variables Chl$a$:C and N:C.

2.2.5 Myxotrophy

Organisms capable of performing mixotrophy (like mixotrophic flagellates) differ from other groups because they are able to alternate between autotrophy and heterotrophy, depending on nutrient availability. Theoretically they can photosynthesize and feed on other organisms at the same time.

The parameterization of this group is achieved with a combination of code from producers and consumers. The degree of its autotrophic or heterotrophic behaviour is determined by food and nutrient availability. The

prey on which these organisms feed upon in their heterotrophic regime can be defined by the user. Since it is assumed that these organisms can feed on both ways, nutrient uptake is conditioned by the feeding strategy, osmotrophically when performing autotrophy (producer behaviour) and phagotrophically when performing heterotrophy (consumer behaviour). Nutrient excretion (mineralization) is assumed to be the same as for other producers.

2.2.6 Mass balance equations

For each phytoplankton group the mass balance for carbon, nitrogen, phosphorus, silica (diatoms or other silica-dependent organisms only), and chlorophyll is:

$$\frac{\partial P_c}{\partial t} = \left(P_c^{phot} - res - exu - mort\right).P_c - G_{P_c}^{Z_c} \tag{2.44}$$

$$\frac{\partial P_n}{\partial t} = \upsilon_{n1}^{phy} + \upsilon_{n2}^{phy} - \phi_n^{phy} - mort.P_n - G_{P_n}^{Z_c} \tag{2.45}$$

$$\frac{\partial P_p}{\partial t} = \upsilon_p^{phy} - \phi_p^{phy} - mort.P_p - G_{P_p}^{Z_c} \tag{2.46}$$

$$\frac{\partial P_s}{\partial t} = \upsilon_s^{phy} - \phi_s^{phy} - mort.P_s - G_{P_s}^{Z_c} \tag{2.47}$$

$$\frac{\partial P_{chl}}{\partial t} = P_{ac}.P_{chl} - mort.\chi_{chl:c} \tag{2.48}$$

2.3 Consumers module

2.3.1 Background review

Closing the food web

Some models have only one zooplankton compartment, which grazes on the large detrital pool and on phytoplankton (e.g. [97]). The single grazer approach, merging microzooplankton and larger zooplankton in the same group, has been considered more stable than one with multiple classes of zooplankton [97, 98]. Nevertheless, this stability sometimes files to represent the actual complexity of the simulated systems. The inclusion of all consumers into one zooplankton group represents a compromise between faster running simulations and the need of a relevant tool to address consumers role in a particular system.

Taking a different approach, some models go as far as to incorporate 4 different groups with macrozooplankton included [25]. Taking the ERSEMII as a reference to what might be considered the sate-of-the-art in ecological

models [39], the multiple zooplankton group approach is the way to go. ERSEMII includes microzooplankton, heterotrophic flagellates and mesozooplankton. The first two groups have the same code differing only on parameters values, while the last has a distinct parameterization to account for different physiology and ecology.

The role of consumers in marine system is very complex. Microzooplankton refers to all heterotrophic planktonic organisms ranging between 20 μm and 200 μm in size, mainly filter-feeding ciliates, except heterotrophic flagellates and all larval stages of larger zooplankton and benthic organisms. They feed upon several phytoplankton groups (diatoms, flagellate phytoplankton and picoalgae) and also on other zooplankton like heterotrophic flagellates. Heterotrophic flagellates, on the other hand, feed upon bacteria and phytoplankton groups (flagellate phytoplankton, picoalgae and mixotrophic flagellates). The last group, omnivorous zooplankton, is a component of mesozooplankton and can feed upon diatoms, autotrophic flagellates, and on the other two consumer groups. Because of their diversity, all consumers groups also feed upon themselves.

Heterotrophic nanoflagellates are considered to be the principal consumers of picoplankton in many oceanic systems. They are typically the most important herbivores in oligotrophic open ocean where photosynthetic picoplankton usually dominates total autotrophic carbon fixation. In costal ecosystems, where the picophytoplankton importance decreases relatively to larger forms, small flagellates play a decisive role in determining if heterotrophic bacteria production is transferred to higher trophic levels or if it is remineralized back to primary producers.

Larger-size groups of zooplankton (like copepods) are considered to be the closure of the microbial food web in aquatic systems. Their grazing control and nutrient regeneration through excretion has an important role in shaping trophic dynamics. But despite their importance, they are usually not considered in ecological models. Some recent models, however, have incorporated a group of omnivorous zooplankton to accommodate the notion of a group of mesozooplankton with a distinct dynamic from other groups like microzooplankton or heterotrophic flagellates [29]. In ERSEMII, the modelling effort of mesozooplankton goes as far as to include a structured population model of the copepod *Calanus* sp. [99].

Grazing

Unlike commonly assumed, assimilation of a prey by any predator is not a one step process. It can be divided into a series of events, such as searching, encounter, attack, capture, and finally ingestion [100]. Digested food is used for growth and also respiration to provide the energy required to maintain basal metabolism. Most models, however, only consider the final steps in their parameterization (capture and ingestion) by assuming a clearance rate

with a fraction of prey lost by sloppy feeding. Some efforts have been made to address at least some of this processes in models (e.g. [11]). Some model applications are highly parameterized when it comes to grazing preferences of predators upon prey [32], while others have a more straightforward approach with predefined values of prey availability. The parameterization of grazing rates can also vary from linear relations between predator and prey abundance to equations with a quadratic density dependent term. The main difference between these approaches is that in the first case the rate is proportional to predator and prey density, while in the last grazing rates decline at low prey biomass.

Nutrient recycling

The designation "recycling" has been used to distinguish the process usually labeled as exudation from remineralization. Nutrient regeneration or remineralization consists in the breakdown of organic material [101], followed by the release of nutrients in their inorganic form. So, nutrients released by this process are termed mineralized or regenerated nutrients. Recycled nutrients, on the other hand, are better described as nutrients that are taken into the cell, but then leak or are actively excreted as a result of inefficiencies in growth or when nutrient quotas are exceeded.

Nutrient recycling by zooplankton is the direct result of prey ingestion with higher nutrient:carbon ratios than the consumer needs [24]. The nutrient excess ends up being excreted in the inorganic form, hence the application of the term remineralization also to zooplankton activity. The recycling of organic nutrients is a direct consequence of grazing. Part of the ingested prey is incorporated into new zooplankton biomass (carbon and nutrients), and the remaining grazed material is lost by sloppy feeding, remineralization or excretion. After being recycled through grazing, nutrients enter directly the appropriate nutrient pool.

2.3.2 Basic module outline

Secondary producers, or consumers, are defined in the basic model setup as three distinct groups: microzooplankton, heterotrophic flagellates, and omnivorous zooplankton. To confer versatility to the model, the code is prepared to let this number be increased or decreased by the user. In addition, the predator/prey relation is also defined by the user. Ultimately, the complexity of the food web can be adjusted by the model user to different conditions. But despite the number of consumer groups added to the simulations, the parameterization is the same for all. Contrary to models like ERSEMII,. a different set of equations is not used to control larger zooplankton groups.

2.3.3 Carbon dynamics

As with other organisms, several factors have a direct influence in the carbon dynamics, namely, respiration, excretion, mortality and grazing.

Grazing

Ingestion of prey by predators is handled with a linear functional response to prey density, assuming a simple encounter mechanism governing prey consumption. The grazing process is in fact considered to be the uptake process. The specific grazing rate of any consumer group depends on the availability of food or prey $\left(\beta_x^{Z^i}\right)$ to each predator and on prey abundance $\left(X_c^i\right)$, according to:

$$\Phi_z = \sum_{i=1}^{n} \beta_x^{Z^i} . X_c^i \tag{2.49}$$

As an example, the total grazing of one consumer group (Φ_z) will be the sum of singular grazing processes on each individual prey class. Considering the first group of producers as a prey, the grazing will be determined by $\beta_{P^1}^{Z^1} . P_c^1$.

The specific uptake rate of consumers or grazing follows a MMM formulation and so it depends on a maximum specific uptake rate (V_z^{max}), on a half saturation value (k_z) and on the amount of available food (Φ_z). The uptake process is also temperature dependent (with the temperature limitation according to equation 2.17 or 2.18). The uptake rate in then:

$$G_z = V_z^{max} . \frac{\Phi_z}{\Phi_z + k_z} . \Omega_T \tag{2.50}$$

Respiration and excretion

In the model the respiration process ($resp_z$) is divided in two terms, activity respiration ($resp_z^a$) and standing stock respiration ($resp_z^{ss}$). While the standing stock respiration depends on temperature, the activity respiration depends on the uptake rate or grazing (G_z), on the assimilation efficiency $\left(ass_z^{ef}\right)$, and on activity excretion or excreted fraction of non-assimilated uptake (ϕ_z^{na}). According to this, the respiration process is defined by:

$$resp_z^{ss} = \left(r_z^{10} . \Omega_T\right) \tag{2.51}$$

$$resp_z^a = \left[G_z . \left(1 - ass_z^{ef}\right) . \left(1 - \phi_z^{na}\right)\right] \tag{2.52}$$

$$resp_z = resp_z^{ss} + resp_z^a \tag{2.53}$$

with r_z^{10} as the rest respiration at a reference temperature. In a fashion

similar to the activity respiration, the specific excretion (exc_z) is a fraction $\left(1 - ass_z^{ef}\right)$ of the specific uptake or grazing (G_z). Overall, the excretion rate depends on the grazing rate, the assimilation efficiency $\left(ass_z^{ef}\right)$ and on the excreted fraction of non-assimilated uptake (ϕ_z^{na}) according to the following equation:

$$exc_z = G_z.\left(1 - ass_z^{ef}\right).\phi_z^{na} \tag{2.54}$$

From this it is clear that the partitioning between respiration and excretion is determined by activity excretion (ϕ_z^{na}).

Mortality

Zooplankton mortality usually closes ecosystem models at the upper end of the food chain. Zooplankton mortality consists of a linear biomass-dependent mortality loss, which parameterizes zooplankton losses due to respiration and predation by higher trophic levels [102]. Upon mortality, zooplankton biomass is partitioned between the sinking (POM) and the non-sinking (DOM) detrital pools.

Mortality is another process where carbon and nutrients are lost, i.e., transferred from biomass to organic matter. The calculation of the specific mortality rate ($mort_z$) takes into account a temperature-independent term $\left(m_z^{ti}\right)$ and a term to describe the dependency on the relative water oxygen saturation:

$$mort_z = \left(1 - \Omega_o\right).m_z^o + m_z^{ti} \tag{2.55}$$

where m_z^o is the oxygen-dependent mortality rate and the limitation imposed by the oxygen levels in water calculated by:

$$\Omega_o = \frac{[O_2]}{[O_2] + k_z^o} \tag{2.56}$$

with k_z^o as a half oxygen saturation.

Products resulting from excretion and mortality are divided in dissolved and particulate organic matter pools, with the fraction that ends up in the particulate organic matter pool defined by a constant parameter, q_z^{POM}. The resulting fraction for each organic matter pool is calculated according to:

$$\text{mortality products} \left[\begin{array}{l} Z_m^{POM} = mort_z.q_z^{POM} \\ \\ Z_m^{DOM} = mort_z.\left(1 - q_z^{POM}\right) \end{array} \right] \tag{2.57}$$

$$\text{excretion products} \left[\begin{array}{l} Z_e^{POM} = exc_z.q_z^{POM} \\ \\ Z_e^{DOM} = exc_z.\left(1 - q_z^{POM}\right) \end{array} \right] \tag{2.58}$$

Table 2.6: List of parameters used in the consumers module.

Symbol	Parameter	Reference Units
χ_n^{max}	Maximum N:C ratio	$\mathrm{mmol}N\,(\,\mathrm{mg}C)^{-1}$
χ_n^{min}	Minimum N:C ratio	$\mathrm{mmol}N\,(\,\mathrm{mg}C)^{-1}$
χ_p^{max}	Maximum P:C ratio	$\mathrm{mmol}P\,(\,\mathrm{mg}C)^{-1}$
χ_p^{min}	Minimum P:C ratio	$\mathrm{mmol}P\,(\,\mathrm{mg}C)^{-1}$
r_z^{10}	Rest respiration	d^{-1}
ass_z^{ef}	Assimilation efficiency	Dimensionless
ϕ_z^{na}	Excreted fraction of uptake	Dimensionless
Q_{10}	Q_{10} value	Dimensionless
q_z^{POM}	Fraction of excretion to POM	Dimensionless
m_z^o	Oxygen-dependent mortality rate	d^{-1}
m_z^{ti}	Temperature-independent mortality rate	d^{-1}
k_z^o	Oxygen half saturation constant	$\mathrm{mg}O_2\,\mathrm{l}^{-1}$
V_z^{max}	Maximum specific uptake	d^{-1}
k_z	Half saturation value for uptake	$\mathrm{mg}C\,\mathrm{m}^{-3}$
β_x^{Zi}	Availability of prey (x)	Dimensionless

2.3.4 Nutrient dynamics

Except for the inorganic nutrient excretion process, all nutrient dynamics are dependent on carbon dynamics. Predators obtain nutrients by ingesting prey according to the linear function mentioned above (eq. 2.50). Because predator and prey have distinct C:N:P ratios, it is expected that the ratios on the predator vary in function of prey nutrient content. Predator's nutrient quotas increase as a result of prey ingestion and respiration (where only carbon is released), and decrease due to excretion of nutrient excess.

Assimilation and recycling

The grazed amount of nutrient content is not fully incorporated or fixated by predators. Total ingested prey is divided in two fluxes: the assimilated flux and the recycled flux. Depending on the actual nutrient quotas, a fraction of it is assimilated and the other is directly released as inorganic nutrients. This second fraction can be considered as recycled nutrients resulting from respiration.

Following a scheme close to the one presented by Grover [24], originally proposed by Thingstad [103], it is assumed that when a nutrient becomes severely limiting for predators (i.e., when quota approaches its minimum value, χ^{min}) the proportion of assimilated nutrients from the ingested flux will be maximum. Conversely, when a nutrient is not limiting (when quota approaches its maximum value, χ^{max}), the assimilated proportion of ingested nutrient flux will approach 0. When assimilation is high, recycling is

low, and vice-versa. The proportion of nutrient that is assimilated $\left(\rho_j^z\right)$ is calculated as:

$$\rho_j^z = \max\left(\frac{\chi_j^{max} - \chi_j}{\chi_j^{max} - \chi_j^{min}}, 0\right) \quad , \; j = n, p \tag{2.59}$$

Following these assumptions for nutrient assimilation and recycling by predators, the assimilated flux of nitrogen and phosphorus intake (G_j^{ass}, with $j = n, p$) as a consequence of the grazing process, is dependent on the predator concentration (Z_c), on specific grazing rate (G_z) and on the prey actual nutrient quota $\left(\chi_j^{prey}\right)$. It is given by:

$$G_j^{ass} = G_z.\rho_j^z.\chi_j^{prey}.Z_c \quad , \; j = n, p \tag{2.60}$$

The recycled nutrient flux is then:

$$G_j^{rec} = G_z.\left(1 - \rho_j^z\right).\chi_j^{prey}.Z_c \quad , \; j = n, p \tag{2.61}$$

Consumers feeding upon diatoms do not assimilate silica and so it is assumed that during grazing, the silica quota reverts directly to the biogenic silica pool. The grazed silica fraction is obtained by:

$$G_s^z = G_z.\chi_s^{prey}.Z_c \tag{2.62}$$

Nutrient ratios $\left(\chi_n,\ \chi_p\right)$ might go above the imposed maximum $\left(\chi_n^{max},\ \chi_p^{max}\right)$ and whenever that occurs, nutrients will be excreted to maintain the ratios below or equal the maximum value. Nitrogen excess (φ_n) is released as ammonium while phosphorus is expelled as phosphate. Nutrient excretion for a standard organism is calculated according to equation 2.39. If the difference between actual and maximum nutrient quota becomes negative there is no excretion of inorganic nutrients until the maximum value is re-attained.

2.3.5 Mass balance equations

For consumers, the mass balance for carbon, nitrogen, and phosphorus is expressed by:

$$\frac{\partial Z_c}{\partial t} = \left(G_z - resp_z - exc_z - mort_z\right).Z_c - G \tag{2.63}$$

$$\frac{\partial Z_j}{\partial t} = G_j^{ass} - \left(exc_z + mort_z\right).Z_j - \varphi_j - G \quad , \; j = n, p \tag{2.64}$$

Table 2.7: List of definitions of variables used in the consumers module.

Symbol	Variables	Reference Units
Z_c	Consumers carbon	$\mathrm{mg}C\,\mathrm{m}^{-3}$
Z_n	Consumers nitrogen	$\mathrm{mmol}N\,\mathrm{m}^{-3}$
Z_p	Consumers phosphorus	$\mathrm{mmol}P\,\mathrm{m}^{-3}$
Φ_z	Total grazing of a consumer group	$\mathrm{mg}C\,\mathrm{m}^{-3}$
G_z	Total carbon (from prey) uptake rate	d^{-1}
$resp_z^{ss}$	Standing stock respiration rate	d^{-1}
$resp_z^{a}$	Activity respiration rate	d^{-1}
$resp_b$	Total consumer respiration rate	d^{-1}
exc_z	Specific excretion rate	d^{-1}
$mort_z$	Mortality rate	d^{-1}
Z_m^{POM}	Mortality products to POM (rate)	d^{-1}
Z_m^{DOM}	Mortality products to DOM (rate)	d^{-1}
Z_e^{POM}	Excreted products to labile DOM (rate)	d^{-1}
Z_e^{DOM}	Excreted products to semi-labile DOM (rate)	d^{-1}
ρ_n^z	Fraction of assimilated prey nitrogen	Dimensionless
ρ_p^z	Fraction of assimilated prey phosphorus	Dimensionless
G_n^{ass}	Assimilated flux of nitrogen intake	$\mathrm{mmol}N\,\mathrm{m}^{-3}\,\mathrm{d}^{-1}$
G_p^{ass}	Assimilated flux of phosphorus intake	$\mathrm{mmol}P\,\mathrm{m}^{-3}\,\mathrm{d}^{-1}$
G_n^{rec}	Recycled flux of nitrogen intake	$\mathrm{mmol}N\,\mathrm{m}^{-3}\,\mathrm{d}^{-1}$
G_p^{rec}	Recycled flux of phosphorus intake	$\mathrm{mmol}P\,\mathrm{m}^{-3}\,\mathrm{d}^{-1}$
G_s^z	Grazed silica fraction	$\mathrm{mmol}Si\,\mathrm{m}^{-3}\,\mathrm{d}^{-1}$
Ω_o	Oxygen limitation	Dimensionless
Ω_{nut}	Total nutrient limitation	Dimensionless
ϕ_n^z	Excreted inorganic nitrogen in the form of NH_4	$\mathrm{mmol}N\,\mathrm{m}^{-3}$
ϕ_p^z	Excreted inorganic phosphorus in the form of PO_4	$\mathrm{mmol}P\,\mathrm{m}^{-3}$

2.4 Decomposers module

2.4.1 Background review

Photosynthetically produced carbon can sink directly out of the euphotic zone under some conditions, but usually enters the marine food web in the surface waters in the form of DOM and POM through the activity of heterotrophs. Bacteria are primarily responsible for the processing of DOM in aquatic systems. The bacterial DOC utilization efficiency is an important factor determining the flow of carbon and energy through the microbial food web that leads to higher trophic levels. Heterotrophic bacteria are important to the maintenance of energy flow in aquatic systems in two main ways:

(1) Through assimilation of dissolved organic compounds. They may make them available to organisms higher up the food chain, although some energy is inevitably lost in going through the bacterial intermediary.

(2) Heterotrophic bacteria can mineralize organic compounds, thereby releasing inorganic substrates that can then be used by photoautotrophs. This mineralization is crucial to primary productivity, and thus to the maintenance of energy flow.

Dissolved organic matter utilization

Heterotrophic bacteria are major consumers and mineralizers of DOM in the ocean and the interaction between bacteria and DOM plays a key role in the aquatic carbon cycle. For that reason, all factors involved in the regulation of DOM production and consumption profoundly influence carbon fluxes. The availability of DOM to heterotrophic bacteria and its utilization depends on inorganic nutrient concentration in the water, and environmental factors like temperature [104]. The elemental balance of carbon and nitrogen restrains ammonium uptake vs. regeneration by heterotrophic bacteria. Unfortunately, predicting the role of bacteria in the ammonium cycle by *in situ* application of elemental balance models is prevented by the complex and unknown DOM composition in seawater. Likewise, studies of DOC cycling in aquatic ecosystems have focused primarily on the rates at which bacteria utilize DOC, with little emphasis on the identity of bacteria responsible for the uptake. So, this "microbial black box" approach [105] has dictated the use of a generic group of bacteria or decomposers in modelling efforts to assess their role.

In a more specific way, the C:N ratio of bacterial substrates like DOM is unknown, the same being true for growth efficiencies of bacteria that use them. Some studies have revealed that differences in DOC and DON cycling do occur and are greatest during phytoplankton blooms (e.g. [106]) because the dissolved material produced by algae during these events is mostly DOC with little or no nitrogen. The uptake of this DOC will result in a simultaneous uptake of inorganic nitrogen.

Research in the microbial food web processes [107] have revealed that 50% of organic matter generated by primary production is transferred to DOM and then utilized by heterotrophic bacteria. Bacteria are considered to be the main organisms using DOM as a substrate for growth [108, 109]. But the interaction between bacteria and DOM is far from being simple. In early models, heterotrophic bacteria were considered to be strict DOM consumers. However, recent studies [110] established that besides the rapid consume of labile DOM bacteria also produce refractory DOM resistant to decomposition. Earlier, McCarthy *et al.* [111] had already challenged the common paradigm that ocean reservoirs of dissolved material are predominantly derived from algal sources, by reporting that a substantial fraction of DON is of bacterial origin. They credit the intensive bacterial recycling of DOM coupled with similar dynamic bacterial removal by protozoan predation and viruses as the origin of this fraction of DON.

Semi-labile material is variously defined in different models, and thus the parameterization of its turnover vary. Some authors [112] assume that semi-labile material is only utilized after exhaustion of labile substrates, and with lower growth efficiency. In the other hand, others [72] define semi-labile material as molecules whose eventual assimilation by bacteria requires ectoenzyme hydrolysis to the labile pool. Many models therefore employ MMM kinetics to describe the turnover, which is usually passed to labile pools. However, estimates of kinetic parameters are rare.

Kinetics of DOM uptake

In 1942 Monod [113] showed that the relation between bacterial growth rate and subtract concentration could be expressed according to the empirical model know as the Michaelis-Menten-Monod equation:

$$\mu = V_{max} . \frac{S}{S + k_s} \tag{2.65}$$

in which S is the substrate concentration, V_{max} the maximal growth rate, and k_s the substrate concentration at which reaction velocity $=V_{max}/2$. This uptake kinetics was based on studies made where cultures were grown on simple monomers such as glucose. Some models have assumed this as the predominant form of substrate (e.g. [20]), but even when other forms of substrate were considered, the basic formulation has been retained.

The half-saturation constant, k_s, represents the substrate concentration at which growth is half the maximum. This parameter dictates at what level the substrate becomes limiting. At low food levels ($S << k_s$), the growth rate becomes directly proportional to the food supply:

$$\mu \cong \frac{V_{max}}{k_s} . S \tag{2.66}$$

In this case, the growth process becomes second-order.

The uptake of individual DOM components (carbon, nitrogen, phosphorus, etc.) can be modeled by standard MMM kinetics but, under certain circumstances, it may be adequate to describe the uptake as a first-order process, $uptake = \lambda.S$, where λ is a constant turnover rate and S the available substrate [114]. This simplification in the uptake parameterization has the advantage of making easier the incorporation of several components of DOM with different turnover rates. But this approach to substrate uptake, where the rate is constant and independent of the food supply only occurs at high food levels ($S >> k_s$). In this context the growth process becomes first-order:

$$\mu \cong V_{max} \tag{2.67}$$

This level is approximately 5 times the half-saturation constant [37]. Thus, the MMM kinetics adjusts the rate as a function of whether food is abundant or scarce.

Nevertheless, first-order reactions can be a valid approximation for modelling processes like the gross decomposition of sewage in oxygen balance models. However, when dealing with biological growth, the boundless nature of first-order growth begins to become inadequate. Hence the MMM formulation allows us to incorporate a limit to growth (food supply) into model kinetics. The introduction of such limits is characteristic of some eutrophication models and is reflective of the fact that unbridled growth is checked and moderated by finite resources in nature.

Nutrient uptake

Bacteria in water have the faculty to consume nutrients in both organic and inorganic form. Like producers, they can consume inorganic nitrogen and phosphorus directly from the water. But they can also extract the same nutrients from organic compounds, only in this case, nutrient uptake is directly linked with organic matter consumption. The MMM kinetics has been widely used in ecosystem models to describe the uptake of nutrients by different kind of organisms.

From the nutrient uptake MMM equation, two parameters are derived: V_{max} as the maximal rate of uptake, and k_s as the half-saturation constant. The affinity coefficient (k_s) is a measure of the nutrient affinity of a single uptake site, and V_{max} also known as the velocity coefficient, is a measure of the number of uptake sites per cell. Several authors have shown that k_s is independent on the nutrient status of the cell whereas V_{max}, increases with increasing nutrient limitation [115, 116]. Used as an index of a species potential competitive ability at low nutrient concentrations (usually in phytoplankton), k_s values vary considerably among different species with oceanic species having lower k_s values compared to neritic species [117]. Bacteria have a high affinity for dissolved nutrients (low relative k_s) because of their

small size but, as a consequence of the size, they are not able to take up nutrients as effectively at high nutrient concentrations (low relative V_{max}).

Like many other free-living organisms in the water column, bacteria float freely and are transported even by weak currents. This means that relative to the cell wall there is no current and these organisms must obtain substrate through diffusion. If the carriers involved in the binding and transport process of substrate into the cell have a constant frequency per unit surface area of cell membrane, the uptake is directly proportional to surface area.

Even without consensus on the existence of a theoretical basis (e.g., [118]), MMM formulation has been widely implemented in ecological models even though other hyperbolic functions can give a better fit to observed growth rates. Although useful to improve our understanding of microbial food webs, these Monod-type models prove difficult to use for detailed studies of bacterial DOM processing [119]. The motive underneath such difficulties is, according to Vallino *et al.* [120], because they do not account for the variable energy content and oxidation state of DOM.

To Baretta-Bekker *et al.* [29], the use of Michaelis-Menten nutrient kinetics in a previous model was a probable cause of discrepancies between observed and model-predicted concentrations of nitrogen and phosphorus. This hypothesis, based on a previous work [121], points out the fact that the MMM formulation does not allow intracellular nutrient storage or luxury uptake of nutrients.

In some models, bacterioplankton uptake of inorganic nutrients is not considered, and the carbon and nutrient uptake dynamics in phytoplankton groups are coupled. This approach implies fixed C:N:P ratios for the dissolved organic matter produced by the phytoplankton. As a consequence of these assumptions, bacterioplankton growth is always substrate-limited, depending on the excretion products of phytoplankton and if they contained sufficient organic nutrients to meet their nutrients requirements. Recent models, however, incorporate important mechanisms of the microbial food web (e.g. ERSEM model). Some of these mechanisms are the decoupling of carbon and nutrient dynamics in phytoplankton groups, allowing the excretion of nutrient-poor DOM (carbohydrates), and the uptake of inorganic nutrients by bacteria.

2.4.2 Basic module outline

The decomposers group addresses bacterial activity, specifically the consumption of DOM and inorganic nutrients by bacterioplankton. Although bacteria are modeled according to the standard organism concept, there are some significant differences in the modelling strategy (these differences will be highlighted in the description below). All organic matter components are subjected to bacterial activity but not all are considered as substrates that bacteria feed upon. Only labile dissolved organic matter can be consumed

by bacteria. All other substrates (semi-labile DOM and POM) are affected by bacterial activity (exoenzyme action) and changed, but are not incorporated in bacterial biomass. The conversion of POM and semi-labile DOM to DOM as a consequence of bacteria exoenzyme action is implicit in the model .

2.4.3 Carbon dynamics

Assimilation and respiration

The only source of carbon available for bacteria in the model is DOM carbon fraction (DOC). Carbon uptake follows a simple MMM kinetics but varies linearly with cell nutrient quota and with temperature. When the quota of one of the nutrients is near minimal, carbon uptake will become low, preventing the enhancement of nutrient limitation.

The realized uptake (ass_b) is determined as the minimum between the total amount of available substrate (S_c) and potential uptake $\left(ass_b^{pot}\right)$. The potential uptake is in turn dependent on temperature (Ω_T), nutrient quotas (Ω_{nut}), the maximum specific uptake rate at 10^oC (V_b^{max}), the DOM uptake half saturation constant $\left(k_b^{DOM}\right)$ and bacterial biomass (B_c) . The relation between these elements is expressed as:

$$ass_b^{pot} = \left[V_b^{max}.\left(\frac{[DOC]}{[DOC]+k_b^{DOM}}\right).\Omega_T.\Omega_{nut}\right].B_c \tag{2.68}$$

$$ass_b = \min\left(ass_b^{pot}, \frac{S_c}{\Delta t}\right) \tag{2.69}$$

The realized uptake is imposed as the minimum between the potential uptake and the available substrate to prevent the consumption of substrate once it drops below the amount calculated in the potential uptake. This mechanism prevents calculation errors, namely by substrate concentration becoming negative.

Temperature dependence (Ω_T) is calculated as in equation 2.17 or 2.18. The total amount of available substrate is the sum of all dissolved excreted and lysed products and the existing fraction of DOM.

While the rest or standing stock respiration is modeled in the same way as for consumers, the activity respiration is a fixed fraction of the uptake. Assimilation efficiency $\left(ass_b^{ef}\right)$, used to calculate total activity respiration, is not defined by a single rate as for consumers, but varies according to external oxygen concentration. If ambient oxygen concentration drops below a defined concentration (θ_b^o), assimilation efficiency will decrease.

Assuming that bacterial growth efficiency decreases under anoxic situations, this parameterization considers the differences in the energetics of metabolic reactions. Under low oxygen concentration, bacteria strive to

grow and usually only anaerobic bacteria thrive. Anaerobic bacteria are supposed to have a decreased efficiency because they need to respire more carbon in order to produce the same amount of energy.

The model does not take into account different types of bacteria but using different values for growth efficiency according to ambient oxygen concentration (θ_b^o) allows an implicit modelling of both anaerobic and aerobic bacteria.

$if\ \ [O_2] > \theta_b^o,$
$\quad then \quad ass_b^{ef} = ass_{norm}^{ef}$
$\quad else \quad ass_b^{ef} = ass_{low}^{ef}$

Bacterial respiration ($resp_b$) is then calculated as the sum of standing stock ($resp_b^{ss}$) and activity respiration ($resp_b^a$) according to:

$$resp_b^{ss} = \left(r_b^{10}.\Omega_T.B_c\right) \tag{2.70}$$

$$resp_b^a = \left[ass_b.\left(1 - ass_b^{ef}\right).(1 - \Omega_o)\right] \tag{2.71}$$

$$resp_b = resp_b^{ss} + resp_b^a \tag{2.72}$$

The limitation imposed by oxygen concentration (Ω_o) is calculated as in equation 2.56, where k_b^o is the oxygen half-saturation constant for bacteria.

Mortality

Bacterial mortality, a process where carbon and nutrients are lost to organic matter, differs from the standard organism concept because it has both density dependent and independent mortality factors. The density independent term is defined by a specific mortality rate $\left(m_b^{di}\right)$, while the density dependent varies according to bacterial biomass variations. This term is used as a simplistic approach to mortality by lysis caused by viral infection.

Because this is a density dependent process, a reference concentration value must be defined (v_b^m) and a specific density dependent mortality rate $\left(m_b^{dd}\right)$. The density dependent mortality depends on the actual bacterial concentration; it will increase or decrease whether bacterial concentration increases or decreases. The mortality caused by lysis is:

$$m_b^{lys} = m_b^{dd}.\frac{B_c}{v_b^m} \tag{2.73}$$

To account also for the specific density independent mortality rate, total mortality is assumed as the sum of the two mortality factors:

$$m_b = m_b^{di} + m_b^{lys} \tag{2.74}$$

Mortality products are partly dissolved and partly particulate, but the fraction diverted to each group is not defined as a constant (like in producers). Instead it varies around a defined value defined for POM fraction

$\left(q_b^{ref}\right)$, depending on the magnitude of the mortality caused by lysis. As mortality caused by lysis increases, the fraction diverted to POM decreases. This assumption is based on the fact that the result from cell lyses is mostly DOM.

The dynamic POM fraction $\left(q_b^{POM}\right)$ is calculated by:

$$q_b^{POM} = \min\left[\left(1 - \frac{m_b^{lys}}{m_b}\right), q_b^{ref}\right] \tag{2.75}$$

The resulting fraction for each organic matter pool is calculated according to:

$$\begin{aligned} B_m^{POM} &= mort_b.q_b^{POM} \\ B_m^{DOM} &= mort_b.\left(1 - q_b^{POM}\right) \end{aligned} \tag{2.76}$$

The carbon fraction of the resulting products from mortality will be further divided in the labile and the semi-labile pool. The division for each pool is controlled by the semi-labile dissolved organic carbon fraction parameter $\left(q_b^{DOM}\right)$. The division of DOM is then calculated:

$$\text{DOM pools} = \left[\begin{array}{ll} B_m^{DOMsl} = B_m^{DOM}.q_b^{DOMsl} & \text{semi-labile fraction} \\ B_m^{DOMl} = B_m^{DOM}.\left(1 - q_b^{DOMsl}\right) & \text{labile fraction} \end{array}\right] \tag{2.77}$$

2.4.4 Nutrient dynamics

The bacterial quota of a nutrient increases due to uptake and decrease due to excretion. Because only carbon content takes part is respiration process, the nutrient to carbon ratio will increase as a result of this process. As stated before, it is assumed that bacterial nutrient sources can be both organic and inorganic and so nutrient uptake follows two distinctive dynamics. Nutrients acquired from DOM follows the dynamic of DOC fixation while the uptake of inorganic nutrients depends on bacterial N:C and P:C ratios.

Assimilation and uptake

When bacteria consume DOM, the uptake of nitrogen and phosphorus $\left(\upsilon_j^{DOM}\right)$ will depend on their actual carbon to nutrient ratios. This means that the uptake of nutrients in the organic form is always a function of the consumed amount of dissolved organic carbon and on its quality (N:C and N:P ratios):

$$\upsilon_j^{DOM} = ass_b.\chi_j^s \quad , \; j = n, p \tag{2.78}$$

But the consumption of DOM is limited by bacterial nutrient quotas so that it starts to decrease as the nutrient to carbon ratios gets closer to

minimum values. The limitation to DOC consumption imposed by current bacterial N:C and P:C ratios (Ω_{nut}) is similar to the limitation by nutrients in producers (see equation 2.16) but instead of the Redfield ratio a minimum value $\left(\chi_j^{min},\ j=n,p\right)$ is used here.

The uptake of inorganic nutrients is calculated as a function of actual nutrient:carbon ratios and maximum and minimum ratios $\left(\chi_j^{min}$ and $\chi_j^{max},\ j=n,p\right)$ assumed for bacteria, which means that it is nutrient limited. In the inorganic nutrient uptake, when the quota is near minimal, uptake is high, and as the quota approaches a maximum, uptake ceases. The limitation for each nutrient is determined as:

$$\Omega_j = \max\left(\frac{\left(\chi_j^{max}-\chi_j\right)}{\left(\chi_j^{max}-\chi_j^{min}\right)},0\right) \quad \text{with} \quad j=n,p \tag{2.79}$$

Besides these limitations, the uptake also takes into account the external nutrient concentration of the nutrient and an affinity for the nutrient source $\left(k_b^{n1},\ k_b^{n2},\ k_b^{p}\right)$. For nitrogen, assuming no preference of one source, the uptake is then:

$$\upsilon_b^{n1} = k_b^{n1}.\Omega_n.\left[NO_3\right].B_c \quad \text{for nitrate} \tag{2.80}$$

$$\upsilon_b^{n2} = k_b^{n2}.\Omega_n.\left[NH_4\right].B_c \quad \text{for ammonium} \tag{2.81}$$

For the phosphorus inorganic source, the uptake is:

$$\upsilon_b^{p} = k_b^{p}.\Omega_n.\left[PO_4\right].B_c \tag{2.82}$$

Nutrient recycling

It is not assumed that decomposers recycle nutrients in the same way as consumers. Bacterial mineralization only takes place if nutrient ratios go above a specified maximum, in a process similar to the one described for both producers and consumers (eq. 2.39). Here the excreted amount is defined by ϕ_n^b for excess nitrogen and ϕ_p^b for phosphorus. This assumption in the parameterization reflects the current opinion that the role of bacteria in aquatic systems is more of sequestering rather than recycling nutrients [18].

2.4.5 Bacterial mediated organic matter hydrolysis

Bacteria affect the transformation of some components of organic matter without necessarily incorporating carbon or nutrients in the process. This happens through the action of exoenzymes released by bacteria to the substrate. The result is that a fraction of POM and DOMsl are converted into

Table 2.8: Parameters used in the decomposers module.

Symbol	Parameter	Reference Units
χ_n^{max}	Maximum N:C ratio	$\mathrm{mmol}N\,(\,\mathrm{mg}C)^{-1}$
χ_n^{min}	Minimum N:C ratio	$\mathrm{mmol}N\,(\,\mathrm{mg}C)^{-1}$
χ_p^{max}	Maximum P:C ratio	$\mathrm{mmol}P\,(\,\mathrm{mg}C)^{-1}$
χ_p^{min}	Minimum P:C ratio	$\mathrm{mmol}P\,(\,\mathrm{mg}C)^{-1}$
r_b^{10}	Rest respiration @ ref temperature	d^{-1}
V_b^{max}	Maximum specific uptake @ ref temperature	d^{-1}
k_b^{DOM}	Half saturation constant for DOM uptake	$(\,\mathrm{mg}C)^{-1}\ \mathrm{m}^{-3}$
ass_{norm}^{ef}	Assimilation efficiency	Dimensionless
ass_{low}^{ef}	Assimilation efficiency @ low oxygen	Dimensionless
Q_{10}	Q_{10} value	Dimensionless
q_b^{ref}	Fraction of mortality products to POM	Dimensionless
q_b^{DOMsl}	Fraction of DOM to semi-labile pool	Dimensionless
m_b^{dd}	Density-dependent mortality rate	d^{-1}
m_b^{di}	Density-independent mortality rate	d^{-1}
v_b^m	Mortality density dependent concentration	$\mathrm{mg}C\,\mathrm{m}^{-3}$
k_b^o	Oxygen half saturation constant	$\mathrm{mmol}O_2\,\mathrm{m}^{-3}$
θ_b^o	Oxygen concentration below which $ass = ass_{low}^{ef}$	$\mathrm{mmol}O_2\,\mathrm{m}^{-3}$
k_b^{n1}	Affinity for NO_3 (uptake rate)	$(\,\mathrm{mg}C)^{-1}\ \mathrm{m}^{-3}\,\mathrm{d}^{-1}$
k_b^{n2}	Affinity for NH_4 (uptake rate)	$(\,\mathrm{mg}C)^{-1}\ \mathrm{m}^{-3}\,\mathrm{d}^{-1}$
k_b^p	Affinity for PO_4 (uptake rate)	$(\,\mathrm{mg}C)^{-1}\ \mathrm{m}^{-3}\,\mathrm{d}^{-1}$
V_{hyd}^{POM}	Maximum rate for POM hydrolysis	d^{-1}
V_{hyd}^{DOMsl}	Maximum rate for DOMsl hydrolysis	d^{-1}
k_{hyd}^{POM}	POM hydrolysis half saturation constant	$\mathrm{mg}C\,\mathrm{m}^{-3}$
k_{hyd}^{DOMsl}	DOMsl hydrolysis half saturation constant	$\mathrm{mg}C\,\mathrm{m}^{-3}$

DOM. This is a fundamental step in order to make these substrates available to bacteria. Even though the process of hydrolysis is slow, by adding this process to the model, part of the organic matter that would be lost as particles or refractory can enter the system again.

The parameterization used to the bacteria mediated hydrolysis of POM and DOMsl is the same, a MMM kinetics limited by temperature (because it is an enzymatic process) and by bacteria concentration. All components, carbon and nutrients, are affected by this transformation. The only parameters varying between the equations are the maximum rate $\left(V_{hyd}^{POM},\ V_{hyd}^{DOMsl}\right)$ at which the reaction takes place and the semi-saturation constants $\left(k_{hyd}^{POM},\ k_{hyd}^{DOMsl}\right)$. This process is then calculated for carbon as follows:

$$\eta_c^i = V_{hyd}^i \left(\frac{i}{i + k_{hyd}^i}\right).\Omega_T.B_c \quad \text{with} \quad i = POM,\ DOMsl \tag{2.83}$$

and for nitrogen and phosphorus as:

$$\eta_j^i = \eta_c^i.\chi_j^i \quad \text{with} \quad i = POM_j,\ DOMsl_j \ \ ;\ \ j = n, p \tag{2.84}$$

2.4.6 Mass balance equations

The mass balance equations for the decomposer compartment are expressed by:

$$\frac{\partial B_c}{\partial t} = ass_b - resp_b - (m_b.B_c) - G_{B_c}^{z_c} \tag{2.85}$$

$$\frac{\partial B_n}{\partial t} = \upsilon_n^{DOM} + \upsilon_b^{n1} + \upsilon_b^{n2} - (m_b.B_n) - \phi_n^b - G_{B_n}^{z_c} \tag{2.86}$$

$$\frac{\partial B_p}{\partial t} = \upsilon_p^{DOM} + \upsilon_b^{p} - (m_b.B_p) - \phi_p^b - G_{B_p}^{z_c} \tag{2.87}$$

2.5 Biochemistry module

2.5.1 Background review

DOM modelling strategies

Because the bulk of DOM is still largely not characterized and its cycling is poorly understood from a mechanistic perspective [122], the effort to reduce the complexity of DOM biogeochemistry to representative and quantifiable structures in models is far from being an easy task. A diversity of approaches and model structures have been used over the last years, even with the limitation imposed by the uncertainty about concentrations and many

Table 2.9: Definition of variables used in the decomposers module.

Symbol	Variables	Reference Units
B_c	Decomposers carbon	$\mathrm{mg}C\,\mathrm{m}^{-3}$
B_n	Decomposers nitrogen	$\mathrm{mmol}N\,\mathrm{m}^{-3}$
B_p	Decomposers phosphorus	$\mathrm{mmol}P\,\mathrm{m}^{-3}$
ass_b^{pot}	Potential DOC uptake rate	$\mathrm{mg}C\,\mathrm{m}^{-3}\,\mathrm{d}^{-1}$
ass_b	Realized DOC uptake	$\mathrm{mg}C\,\mathrm{m}^{-3}\,\mathrm{d}^{-1}$
$resp_b^{ss}$	Standing stock respiration	$\mathrm{mg}C\,\mathrm{m}^{-3}\,\mathrm{d}^{-1}$
$resp_b^{a}$	Activity respiration	$\mathrm{mg}C\,\mathrm{m}^{-3}\,\mathrm{d}^{-1}$
$resp_b$	Total bacterial respiration	$\mathrm{mg}C\,\mathrm{m}^{-3}\,\mathrm{d}^{-1}$
m_b^{lys}	Mortality rate caused by lysis	d^{-1}
m_b	Mortality rate	d^{-1}
q_b^{POM}	POM fraction from mortality products	Dimensionless
B_m^{POM}	Mortality products to POM	$\mathrm{mg}C\,\mathrm{m}^{-3}\,\mathrm{d}^{-1}$
B_m^{DOM}	Mortality products to DOM[2]	$\mathrm{mg}C\,\mathrm{m}^{-3}\,\mathrm{d}^{-1}$
B_m^{DOMsl}	Mortality products to labile DOM	$\mathrm{mg}C\,\mathrm{m}^{-3}\,\mathrm{d}^{-1}$
B_m^{DOMl}	Mortality products to semi-labile DOM	$\mathrm{mg}C\,\mathrm{m}^{-3}\,\mathrm{d}^{-1}$
υ_n^{DOM}	Realized DON uptake	$\mathrm{mmol}N\,\mathrm{m}^{-3}\,\mathrm{d}^{-1}$
υ_p^{DOM}	Realized DOP uptake	$\mathrm{mmol}P\,\mathrm{m}^{-3}\,\mathrm{d}^{-1}$
Ω_o	Oxygen limitation	Dimensionless
Ω_p	Nitrogen limitation	Dimensionless
Ω_n	Phosphorus limitation	Dimensionless
Ω_{nut}	Total nutrient limitation	Dimensionless
υ_b^{n1}	NO_3 uptake	$\mathrm{mmol}N\,\mathrm{m}^{-3}\,\mathrm{d}^{-1}$
υ_b^{n1}	NH_4 uptake	$\mathrm{mmol}N\,\mathrm{m}^{-3}\,\mathrm{d}^{-1}$
υ_b^{p}	PO_4 uptake	$\mathrm{mmol}P\,\mathrm{m}^{-3}\,\mathrm{d}^{-1}$
ϕ_n^b	Excreted NH_4	$\mathrm{mmol}N\,\mathrm{m}^{-3}$
ϕ_p^b	Excreted PO_4	$\mathrm{mmol}P\,\mathrm{m}^{-3}$
η_c^{POM}	Bacteria mediated POM hydrolysis	$\mathrm{mg}C\,\mathrm{m}^{-3}\,\mathrm{d}^{-1}$
η_c^{DOMsl}	Bacteria mediated DOMsl hydrolysis	$\mathrm{mg}C\,\mathrm{m}^{-3}\,\mathrm{d}^{-1}$

key processes related with DOM production and consumption. Despite its heterogeneous nature and the inherent difficulty in characterizing different DOM compartments, models have categorized DOM in distinct classes in order to distinguish materials with high turn over ratios from those that accumulate and can potentially be exported.

For Kirchman *et al.* [114] models need to consider at least three DOC pools because of their different roles in biogeochemical processes: (1) a labile pool with turnover times of days or less, (2) a refractory pool with extremely long turnover times, and (3) a "semi-refractory" pool that varies on a seasonal time scale. Labile material is consumed rapidly (hours to days), semi-labile material degrades on seasonal time scales, and refractory material degrades very slowly and can even be biologically inert. Many ecological models consider both labile and semi-labile DOM without assuming this distinction as an analogy to monomers and polymers (e.g. [123, 124]).

Sometimes DOM is divided according to the molecular weight, more precisely in polymeric and monomeric pools. According to Chróst [125], enzymatic hydrolysis is required so that high molecular weight organic matter provides simple monomers that can be taken up by bacteria. The 'HSB' model [126] used this principle by including two polymeric pools, with fast and slow rates of hydrolysis by bacterial ectoenzymes, which are converted to a common monomeric pool that is consumed rapidly by bacteria. In this case, when C:N ratio of monomeric substrates is poorly balanced, bacteria take up ammonium and compete with phytoplankton for their nitrogen requirements. Other authors (e.g. [114]) also proposed that considering two distinct size fractions for DOM is a necessary condition to biogeochemical models. This approach, however, has some problems because the correlation between molecular weight and lability is weak in natural DOM. High molecular weight material can be highly bioreactive, while the bulk of oceanic DOM comprises small molecules that cycle slowly or are relatively unavailable to microorganisms [127, 104, 128].

The distinction between different kinds of DOM is important in most biogeochemical models because it can be used to estimate the *in situ* consumption of organic material and the export or sinking of the same. So, while local heterotrophic bacteria can consume the labile pool and part of the semi-labile DOM, because of its unavailability, refractory DOM can be useful to determine the production fraction that either sinks or is exported.

Another problem raised in the process of DOM modelling is the distinction between DON and DOC. Both are linked in the ocean and even if nitrogen-free DOC can exist, all organic compounds contain carbon and so if there is DON, DOC must also exist. In order to overcome the difficulties raised by assuming variable DOC/DON in models, two different approaches can be used:

(1) Include DOC without associated DON. This approach can be useful to simulate DOC accumulation and turnover. Because it neglects

the role of DON in nutrient recycling, this approach does not permit nitrogen to enter slow-turnover DON pools, and may result in overestimation of remineralization rates. A DOC-limited bacterial growth is assumed, and nitrogen requirements are taken from the inorganic pool (nutrients).

(2) DOC and DON can be included as separate state variables allowing dynamic C:N ratios. Models fitting in this category (e.g., [129, 72]) can perform a detailed examination of the roles of DOM in nutrient cycling as well as accumulation and export of DOC and DON. One problem related with this kind of models is the complexity in the C and N interaction parameterization.

Silica related processes

The cycle of silica in the water column essentially amounts to the production of opaline silica by utilization of dissolved silicon in some phytoplankton groups, and its dissolution following the death of organisms. So, the major cycle of silicon involves only inorganic forms. The importance of the silica cycle in aquatic systems lies in the fact that the growth of some plankton groups like diatoms tends to be silicon limited. Diatoms are the most abundant phytoplankton group making the silica biogeochemical cycle an important factor in the control of marine productivity. Because diatom productivity is frequently limited by the availability of dissolved silicon, this group is usually the dominant phytoplankton group in locations where dissolved silicon is abundant. Without Si limitation, diatoms can out-grow other phytoplankton groups because they assimilate nutrients faster than other pelagic phytoplankton groups. In silica bearing organisms the Redfield ratio is C_{105}:Si_{40}:N_{15}:P_1.

A great amount of all the silicon in the ocean is relatively inert because it is in the form of a constituent of mineral silicates. The dominant dissolved species of silicon at the usual pH and ionic strength of seawater is the silicic acid (H_4SiO_4) and most of the dissolved silicon is supplied by the dissolution of biogenic silica produced by phytoplankton (diatoms and silico-flagellates) and protozoa (radiolaria). The dissolution of biogenic silica ($BSiO_2$) is described by:

$$BSiO_2 + 2H_2O \longrightarrow H_4SiO_4 \tag{2.88}$$

The most significant mechanism involved in dissolved silicon removal from the water is the formation of siliceous hard parts by living organisms. Diatom productivity is also largely responsible for downward fluxes of biogenic silica. Silicon is removed from the surface layers of the ocean by the deposition of organic material derived from primary production. As a consequence, the biogenic silica constitutes a great percentage of the sediment composition.

Both biogenic and abiogenic silica precipitation produces an amorphous solid, called opaline silica, or opal. Due to its slow dissolution, silicon keeps

sinking and is regenerated at much greater depths than are nitrogen and phosphorus. For that reason the dissolved silicon concentration tends to be higher in regions where wind-driven upwelling occurs because nutrient-rich deep water is transported to the upper layers of the water column. When compared to other nutrients, this poorer recycling efficiency causes a greater degree of vertical and horizontal gradients.

Nitrification

One of the things that make the nitrification process so important in the study of water quality is that it causes oxygen depletion. Oxygen consumed in nitrification is about 30% of the oxygen consumed in oxidation of pure organic matter [37]. The way of modelling the nitrification process and its impact in oxygen concentrations has evolved. Because of its shortcomings, early attempts to model the impact of nitrification by way of using nitrogenous biochemical oxygen demand (NBOD) have been abandoned. This approach considered the total amount of oxidizable nitrogen as the sum of organic and ammonium nitrogen. This quantity is called total Kjeldahl nitrogen (TKN) and can be determined by analytical measurements. The search for a more efficient way to achieve it has led to the development of a more mechanistic approach that attempts to model organic nitrogen, ammonium, and nitrate explicitly.

2.5.2 Basic module outline

The biochemistry module abridges reactions and processes that are independent of any biological activity in the model (chemistry), but also processes that are influenced to some extent by organisms (biology). A short description of the organic matter dynamics and compartments is also addressed. Many processes and variables presented here have already been defined elsewhere in the description of the model above, and so repetitions are minimized. For a clear understanding of the innumerous sources and sinks in the mass balance equations presented, a look at tables 2.3, 2.6 and 2.8 may be helpful.

2.5.3 Organic matter

Organic matter is divided in two groups, particulate and dissolved, each one of them with a carbon, nitrogen and phosphorus fraction. This two detrital pools abridge the broad categories of non-sinking OM (which largely represents DOM and also colloidal small non-sinking POM), and of sinking POM. Both forms of organic matter, dissolved and particulate, are products of excretion/lysis and mortality of organisms. The dissolved fraction is divided in two subgroups, labile (DOMl) and semi-labile (DOMsl). It is assumed that labile DOM has a very short turnover time, becoming fully

Table 2.10: Parameters used in the biochemistry module.

Symbol	Parameter	Refrence Units
k_{nit}	First-order nitrification inhibition coefficient	$\mathrm{l\,mg^{-1}}$
I_{nit}^{ref}	Light intensity threshold for nitrification	$\mathrm{W\,m^{-2}}$
ν_{nl}	Nitrification rate	$\mathrm{d^{-1}}$
γ_s	Biogenic silica dissolution rate	$\mathrm{d^{-1}}$
$\delta_{o:c}$	Carbon-to-oxygen conversion parameter	$\mathrm{mg}O_2\,(\,\mathrm{mg}C)^{-1}$
$\delta_{o:n}$	Nitrogen-to-oxygen conversion parameter	$\mathrm{mg}O_2\,(\,\mathrm{mg}N)^{-1}$

available as substrate for bacteria within a short time after being produced. Nonetheless, it still can accumulate over time under favorable conditions. All organic matter components are parameterized by several state variables, one for each element. Taking labile dissolved organic matter as an example, we have DOCl, DONl and DOCl.

Particulate organic matter, commonly referred as detritus, is assumed to be the particle part of excretion products, leftovers from sloppy feeding and a fraction of the remains of dead organisms. This organic matter component, defined by three state variables, has a variable C:N:P ratio and is available for the degradation by the action of bacterial enzymes. The use of POM by bacterioplankton is defined in two steps: first POM is converted to DOM by enzymatic action and only them can it be consumed (see extended rationale on the Decomposer module section). Finally, a state variable is also used to address biogenic silica.

2.5.4 Nitrogen

Besides all the nitrogen dynamics induced by biological mediated processes, the model also considers the nitrification process. Assuming first-order kinetics, the nitrification process can be written as a series of first-order reactions. However, the two-step process of conversion of ammonium in nitrate is parameterized as having one step only. The two steps of the nitrification process are not actually represented here because nitrite is not defined as a state variable in the model. So, the rate used to define nitrification must take this assumption into account. The actual process of conversion of DON to ammonium is parameterized in detail in the decomposers module.

Some models (e.g. [32]) impose nitrification to occur only at low light levels (radiation $< 4.0\,\mathrm{W\,m^{-2}}$ averaged over the mixed layer) corresponding to winter conditions at high latitudes. Here a reference light intensity $\left(I_{nit}^{ref}\right)$ can be defined, acting as a threshold above which the nitrification process stops. Nitrification (ν_{am}) is then defined by:

$$\text{if } \; I_0 \leq I_{nit}^{ref} \quad \text{then} \quad \nu_{am} = \nu_{nl}.f_{nit}^{o}.\,[NH_4] \tag{2.89}$$

with ν_{nl} as the nitrification rate.

The use of an explicit simulation of the nitrification process can be realistic when compared to other modelling methods lacking this process. But it has some deficiencies nevertheless. The simple use of a rate to account for the nitrification does not consider the importance of limiting cofactors. And this is especially important for oxygen concentration in water, because the nitrification process depends on its availability. One way to minimize this shortcoming involves the inhibition of the reaction due to depressing oxygen levels. To achieve this, a limiting factor (f^o_{nit}) is multiplied by the rate:

$$f^o_{nit} = 1 - e^{-k_{nit}O} \tag{2.90}$$

where O is the oxygen concentration and k_{nit} the first-order nitrification inhibition coefficient. This factor is close to 1 for dissolved oxygen concentrations greater than 3 mgL-1. At lower levels the factor approaches a linear relationship. Thus as oxygen approaches zero, nitrification shuts down and eventually will be completely inhibited at zero oxygen concentration. With the adopted methodology, nitrification inhibition is then a function of both light intensity and dissolved oxygen.

2.5.5 Silica

Besides the silica quota in each silica-dependent producer compartment, there are two pools of silica in the model: dissolved silica $[DSi]$ and biogenic silica $[BioSi]$. Dissolved silica is frequently referred as silicate acid and so both terms are used here. Biogenic silica or silicate results from the production of fecal pellet (G^z_s) from all organism feeding upon silica-dependent producers. Unlike other nutrients, silica is not assimilated by grazers and so the fraction of silica in the ingested amount is excreted directly to the detritus silica pool in water in the form of silicate. Another source of silicate in water results from the death of silica-dependent producers.

The other pool, with dissolved silica, is consumed by phytoplankton and is produced as a result of biogenic silica dissolution in water. This process is modeled as:

$$\eta_s = \gamma_s . [BioSi] \tag{2.91}$$

with γ_s as the biogenic silica dissolution rate.

2.5.6 Oxygen

Biological activity accounts for both oxygen consumption and production. While consumers and decomposers groups only consume oxygen from the surrounding water, producers also have the ability to produce oxygen through photosynthesis. The photosynthetic reaction (eq. 2.8) is characterized by the consumption of carbon dioxide, nutrients and water to produce organic

Table 2.11: Variables used in the biochemistry module.

Symbol	Variables	Units
ν_{am}	Nitrification	$\mathrm{mmol}N\,\mathrm{m}^{-3}\,\mathrm{d}^{-1}$
f^{o}_{nit}	Oxygen limiting factor for nitrification	Dimensionless
η_s	Biogenic silica dissolution	$\mathrm{mg}C\,\mathrm{m}^{-3}\,\mathrm{d}^{-1}$

tissue and water. During this process the organism produces energy and releases oxygen. According to the photosynthesis simplified equation, for every mole of reduced carbon, a mole of oxygen is produced. The inverse occurs in the respiration process.

In order to calculate the amount of oxygen released or consumed from respiration or production rates, a carbon-to-oxygen conversion parameter is needed. A nitrogen-to-oxygen conversion ratio is also used to account for the oxygen deficit caused by the nitrification process. Both parameters are unit specific so they must be changed according to the unit system defined by the input values.

In the general equation for dissolved oxygen balance (eq. 2.107) a carbon-to-oxygen ratio ($\delta_{o:c}$) is multiplied to account for the unit difference. Also a nitrate-to-oxygen ratio ($\delta_{o:n}$) is multiplied by the nitrification rate to account for the deficit caused by nitrification.

When default units are used, both ratios ($\delta_{o:c}$) must be multiplied by 10^{-3} to account for the unit difference in the volume (because oxygen is quantified in l^{-1} while carbon and nitrogen are in m^{-3}). The nitrogen-to-oxygen then becomes $0.0588\ \mathrm{mg}O_2\ \mathrm{l}^{-1}\ \left(\mathrm{mmol}N\,\mathrm{m}^{-3}\right)^{-1}$.

2.5.7 Mass balance equations

Carbon

$$\frac{\partial DOC_l}{\partial t} = \left[\left(P_c^{DOM} + P_m^{DOM}\right).\varphi_P^l\right].P_c + \left(Z_c^{DOM} + Z_m^{DOM}\right).Z_c + B_c^{DOM}.B_c - ass_b + \eta_c^{DOMsl} + \eta_c^{POM} \quad (2.92)$$

$$\frac{\partial DOC_{sl}}{\partial t} = \left[\left(P_c^{DOM} + P_m^{DOM}\right).\varphi_P^{sl}\right].P_c + B_c^{DOMsl}.B_c - \eta_c^{DOMsl} \quad (2.93)$$

$$\frac{\partial POC}{\partial t} = \left(P_c^{POM} + P_m^{POM}\right).P_c + \left(Z_c^{POM} + Z_m^{POM}\right).Z_c + B_m^{POM}.B_c - \eta_c^{POM} \quad (2.94)$$

$$\frac{\partial CO_2}{\partial t} = (res - ass).P_c + resp_z.Z_c + resp_b \quad (2.95)$$

Nitrogen

$$\frac{\partial DON_l}{\partial t} = \left(P_m^{DOM}.\varphi_P^l\right).P_n + \left(Z_e^{DOM} + Z_m^{DOM}\right).Z_n + B_m^{DOM}.B_n - \upsilon_n^{DOM} + \eta_n^{DOMsl} + \eta_n^{POM} \quad (2.96)$$

$$\frac{\partial DON_{sl}}{\partial t} = \left(P_m^{DOM}.\varphi_P^{sl}\right).P_n - \eta_n^{DOMsl} \quad (2.97)$$

$$\frac{\partial PON}{\partial t} = P_m^{POM}.P_n + \left(Z_e^{POM} + Z_m^{POM}\right).Z_n + B_m^{POM}.B_n - \eta_n^{POM} \quad (2.98)$$

$$\frac{\partial NO_3}{\partial t} = -\upsilon_{n1}^{phy} - \upsilon_{n1}^{bac} + \nu_{am} \quad (2.99)$$

$$\frac{\partial NH_4}{\partial t} = \phi_n^{phy} - \upsilon_{n2}^{phy} + \varphi_n + G_n^{rec} - \upsilon_{n2}^{bac} + \phi_n^{bac} - \nu_{am} \quad (2.100)$$

Phosphorus

$$\frac{\partial DOP_l}{\partial t} = \left(P_m^{DOM}.\varphi_P^l\right).P_p + \left(Z_e^{DOM} + Z_m^{DOM}\right).Z_p + B_m^{DOM}.B_p - \upsilon_p^{DOM} + \eta_p^{DOMsl} + \eta_p^{POM} \quad (2.101)$$

$$\frac{\partial DOP_{sl}}{\partial t} = \left(P_m^{DOM}.\varphi_P^{sl}\right).P_p - \eta_p^{DOMsl} \quad (2.102)$$

$$\frac{\partial POP}{\partial t} = P_m^{POM}.P_p + \left(Z_e^{POM} + Z_m^{POM}\right).Z_p + B_m^{POM}.B_p - \eta_p^{POM} \quad (2.103)$$

$$\frac{\partial PO_4}{\partial t} = \phi_p^{phy} - \upsilon_p^{phy} + \varphi_p + G_p^{rec} - \upsilon_p^{bac} + \phi_p^{bac} \quad (2.104)$$

Silica

$$\frac{\partial DSi}{\partial t} = \eta_s - \upsilon_s^{phy} \quad (2.105)$$

$$\frac{\partial BioSi}{\partial t} = G_s^z + mort.P_s - \eta_s \quad (2.106)$$

Oxygen

$$\frac{\partial O_2}{\partial t} = \delta_{o:c}.\left[\sum_{i=1}^{n}\left(ass^n - res^n\right).P_c^n - \sum_{i=1}^{n} res_z^n.Z_c^n - resp_b\right] - \delta_{o:n}.\nu_{am} \quad (2.107)$$

Chapter 3

Assessing model performance

3.1 Introduction

Before any implementation to real scenarios, the model must be subjected to a number of tests to ensure that it is mathematically correct, and to check if it is able to describe the processes for which it was conceived. Some of these tests are: (a) simple long time runs to assess model stability over time and its capacity to converge to a repeating cycle; (b) mass balance checks over the whole period of simulation; (c) to ensure that the model operates under a wide range of conditions, testing its robustness with different initial conditions, forcing conditions and loading scenarios. In the present chapter, some of these considerations are addressed and some common techniques are used to test the model. It starts by analyzing model functions response to different sets of variables and parameters, discussing the results, followed by a test of model stability with a long time run. Then, the sensitivity to parameters and initial conditions is checked. In the process, model performance is checked against its own development guidelines, to see if it is able to address all the proposed processes, even if only from a theoretical point of view.

3.2 Function plots

Assuming one process p which can be a function of several parameters, forcing functions or other processes, $p = f(c, T, Q)$, the best way to visualize the dependence of this particular process solution on a set of parameters or over a range of a particular parameter values is by developing a plot of p versus c, T or Q. Prior to any assessment of model performance, these plots give an insight into the functional responses to different parameter sets of conditions. Despite its static nature, this analysis helps to understand the model outcome in dynamic simulations. For simplicity, plot results are divided by modules even though some processes are similar for more than

one module (e.g., temperature limitation).

3.2.1 Producers

The model has two distinct ways of calculating the temperature dependence of growth and of other physiological functions (equations 2.17 and 2.18). They have been implemented given the wide acceptance both have in literature. The difference between the two methods is portrayed in figure 3.1 (where "method 1" and "method 2" reflect equations 2.17 and 2.18, respectively). The methods have different performances, with method 1 having higher values, i.e., imposing a lower dependence from temperature. None of the methods assumes an optimum temperature for growth, hence result values increase with increasing temperature in both methods. At 30 °C, the defined reference temperature, both methods achieve no limitation ($\Omega_T = 1$). While having a 2 fold difference in results at 0 °C, estimations converge as the temperature increases. The choice of the temperature dependence method thus, greatly affect model results. As a general rule, however, as temperature increases, so will the rates of each temperature-dependent processes.

Nutrient limitation is a function of internal nutrient quotas (figure 3.1). As such, when nut:C ratios are near the minimum defined value $\left(\chi_j^{min}\right)$, limitation is more severe and total limitation ($\Omega_j = 0,\ j = n, p$) occurs when $\chi_j = \chi_j^{min}$. The Redfield ratio is the threshold for nutrient limitation, and so $\chi_j \geqslant \chi_j^R$ means no limitation to growth from nutrients ($\Omega_j = 1$). Even though there is no nutrient limitation when quotas go above the Redfield ratio $\left(\chi_j^R\right)$, a maximum ratio has to be defined. This higher ratio allows nutrient storage, sometimes referred as luxury uptake. Whenever ratios go above the maximum ratio, excretion will occur and the excess nutrient is released in a mineral form (ammonium or phosphate). Note that the normalized N:C ratio is used instead of real ratio values (x axis, fig.3.1). In this scale we have in the lower extreme the value 0 with the meaning that the actual quota equal the lower nut:carbon value defined, while on the other extreme we have 1 which means that the actual ratio is at its maximum value. This approach was chosen to facilitate the perception of full quota percentage.

Unlike nitrogen and phosphorus limitation, silica limitation in silica-dependent organisms is not a function of internal quotas but rather of the ambient silicate concentrations because there is no mechanism for luxury uptake of silicate. Being governed by MMM kinetics, silica limitation (figure 3.2A, considering $k_s = 0.3$ mmol$Si\,\mathrm{m}^{-3}$) doesn't vary linearly with dissolved silicon abundance in water. As silicon concentration drops below 2 mmol$Si\,\mathrm{m}^{-3}$ limitation values decrease dramatically, which means that the producer growth becomes silica limited. Above this concentration, limitation values tends to 1 implying that no limitation is imposed by silica

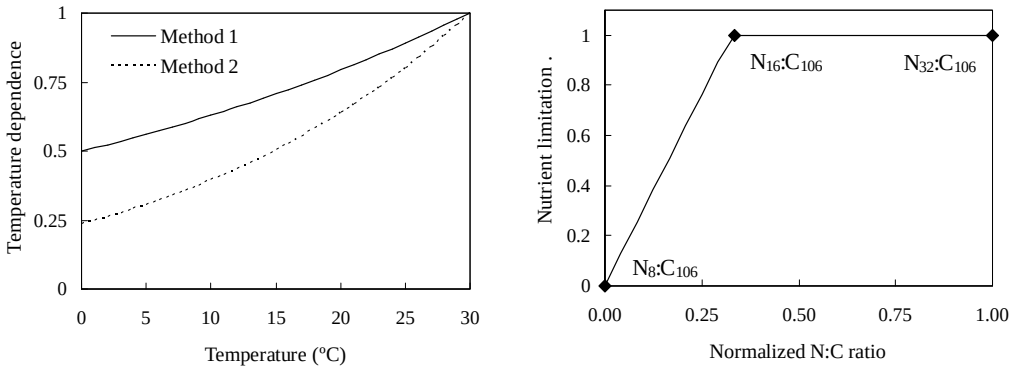

Figure 3.1: Temperature and nutrient limitation response. "Method 1" and "Method 2" addresses different ways by which the model quantifies temperature limitation (see text for details). Ratios in nutrient limitation refers to the predefined range of values: half the Redfield ratio, Redfield ratio, and twice the Redfield ratio. For simplicity only N:C ratio is presented.

shortage.

Silica quotas, however, affects the silica flux in the producer. The flux can be positive, meaning silica uptake whenever conditions are met for it to occur $\left(ass^{net} > 0\right)$, or negative, meaning silica excess release when $\chi_s > \chi_s^R$. Given silica dynamics parameterization (eq. 2.40), its quotas only affects silica excretion, silica uptake being only a function of net assimilation $\left(ass^{net}\right)$. The dynamics of silica flux, illustrated in figure 3.2B (with $ass^{net} = 1.5$, $r^s = 1$), is a function of Si:C (χ_s). The dotted line shows the Redfield ratio for silica, while the dashed line sets the boundary between silica uptake and excretion. As can be seen, while $\chi_s < \chi_s^R$ there is no excess silica release and so silica flux is positive and constant. From the point where $\chi_s > \chi_s^R$, as silica quota increases the amount of excreted silica excess $\left(\chi_s^R - \chi_s\right)$ will also increase, and the net flux will decrease, despite ass^{net} may stay constant. Finally, there will be a specific quota value (around 0.075, for the values combination presented here) where flux is 0 (uptake = excretion), and above which excretion will be higher than uptake and the resulting silica flux will be negative. This happens when, among other factor, external silica is not limiting growth.

The influence of different parameter values on the photosynthesis rate (eq. 2.20) is presented in figure 3.3. A detailed analysis of this parameterization can be found in the Geider *et al.* papers [64, 65, 41], and so only a brief analysis is presented here. Assuming all other parameters constant, photosynthesis rate $\left(P_c^{phot}\right)$ increases linearly with the increase of temperature dependence (Ω_T), as shown in figure 3.3A. This reflects the influence of Ω_T in photosynthesis maximum rate calculation, $P_c^{max} = r^{ass}.\Omega_T$. When

there is no limitation from temperature ($\Omega_T = 1$), P_c^{phot} will be regulated by other processes and parameters like light availability (I_o), Chl$a$:C ratio (χ_{chl}) and the chlorophyll light absorption coefficient $\left(\alpha^{chl}\right)$. It is also possible for temperature to increase the maximum photosynthetic rate (r^{ass}) when $\Omega_T > 1$ using the Q_{10} approach. Conditions for the results presented in figure 3.3A are $r^{ass} = 2.5$, $\alpha^{chl} = 3.0025$, $I_o = 200$, and $\chi_{chl} = 0.01$. Unless stated otherwise, the same values were used for plot B and C.

The direct influence of χ_{chl} and I_o on photosynthesis can be seen in figure 3.3, plots B and C. By assuming that photosynthesis rate is proportional to chlorophyll amount in the cell, expressed by χ_{chl}, the model estimates a faster increase in photosynthesis rate as chlorophyll quotas becomes higher (plot B). This simulates a simple functional response determined by the higher amount of photosynthetically active pigments. When the Chl$a$:C ratios are low (Chl$a$:C=0.005), higher radiation levels (above 600 $\mathrm{W\,m^{-2}}$ in this particular case) are necessary to achieve the maximum photosynthesis rate (P_c^{max}). Conversely, this rate is achieved at lower radiation levels (around 100 $\mathrm{W\,m^{-2}}$) when chlorophyll quota is high (Chl$a$:C=0.02). Eventually, photosynthesis rate will stabilize, constrained by its parameterization, even if radiation continues to increase, leading to $P_c^{phot} = P_c^{max}$. The same principle is illustrated in plot C, but this time with P_c^{phot} plotted against χ_{chl}. It is possible to conclude that when light radiation is sufficiently high P_c^{phot} tends to P_c^{max}, even at low χ_{chl}. Another relevant aspect is that the model photosynthesis parametrization is more sensitive to χ_{chl} at low radiation regimes. Photoacclimation imposes a down regulation of pigment content under high irradiance regimes, but also implicitly allows phytoplankton to maximize growth under unfavorable conditions like low irradiance. Based on observations for minimal Chl$a$ turnover in phytoplankton reported by several authors, Geider *et al.*[41] assumed the rate of Chl$a$ degradation to be proportional to the Chl$a$ concentration. However, in the present study this rate is assumed to be zero, an assumption based on previous works from these authors [65].

Photosynthesis is determined by Chl$a$ cell concentration, given that it is the Chl$a$ molecule which is responsible for the conversion of radiant energy into chemical energy (usually stored in the form of simple sugars). For this reason, photosynthesis is closely coupled to Chl$a$:C ratios and therefore dependent on the Chl$a$ synthesis. Chl$a$ production (P_{ac}, eq. 2.43) is mediated by a regulation term (ρ_{chl}, eq. 2.42) which is controlled by the light intensity (I_o), the photosynthesis rate $\left(P_c^{phot}\right)$, and Chl$a$:C ratio ($\chi_{chl:c}$). The Chl$a$ regulation dependency on irradiation is shown in figure 3.4A (with $P_c^{phot} = 2.5$, $\chi_{chl:c} = 0.02$, $\chi_{chl:n}^{max} = 3$, $\alpha^{chl} = 3.0025$), where it is clear it decreases strongly with increasing light intensity. The same happens in relation with the increase of $\chi_{chl:c}$, as portrayed in figure 3.4C. This adaptational mechanism of Chl$a$ synthesis regulation allows Chl$a$ production as

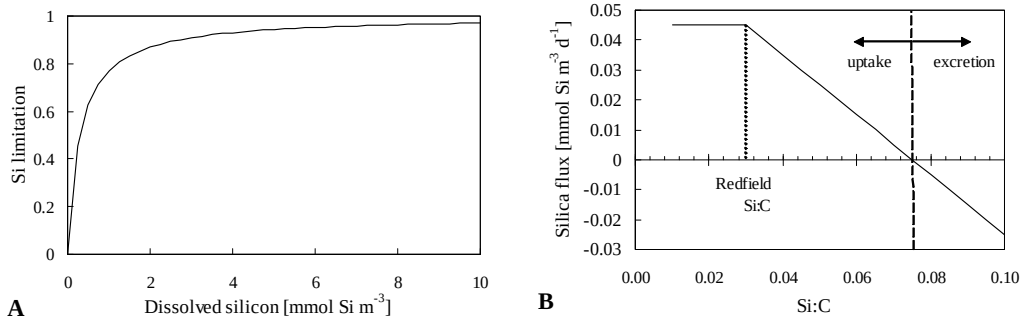

Figure 3.2: Silica dynamics in producers: (A) Silica limitation in producers as a function of dissolved silicon ambient concentration, and (B) silica flux dependence on silica quotas.

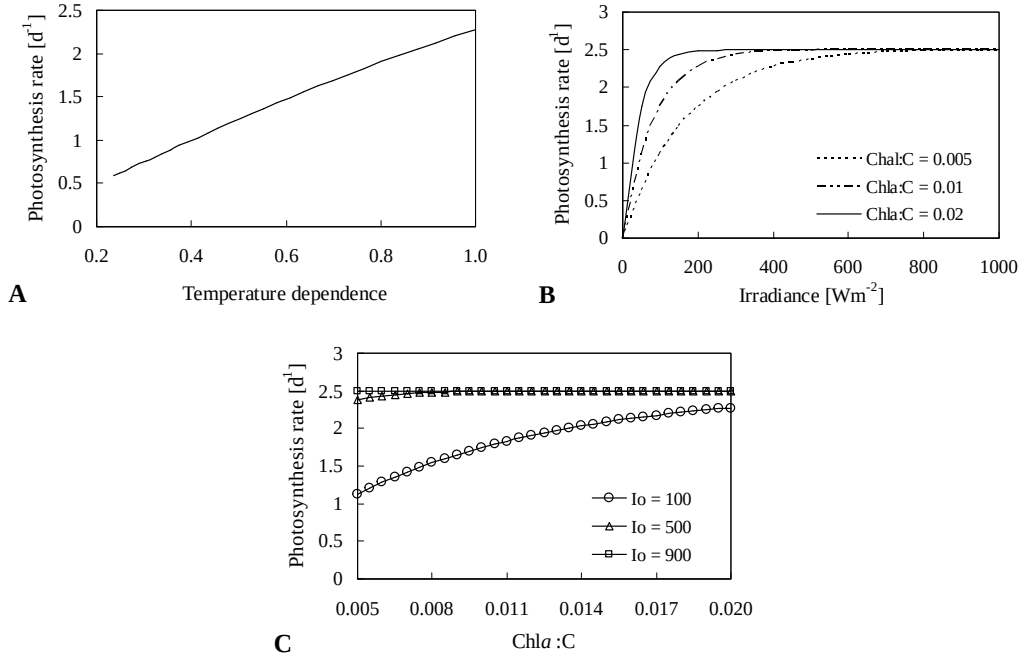

Figure 3.3: Plots of photosynthesis rate values as a function of different ranges of (A) temperature dependence (B) irradiance, and (C) Chl*a*:C.

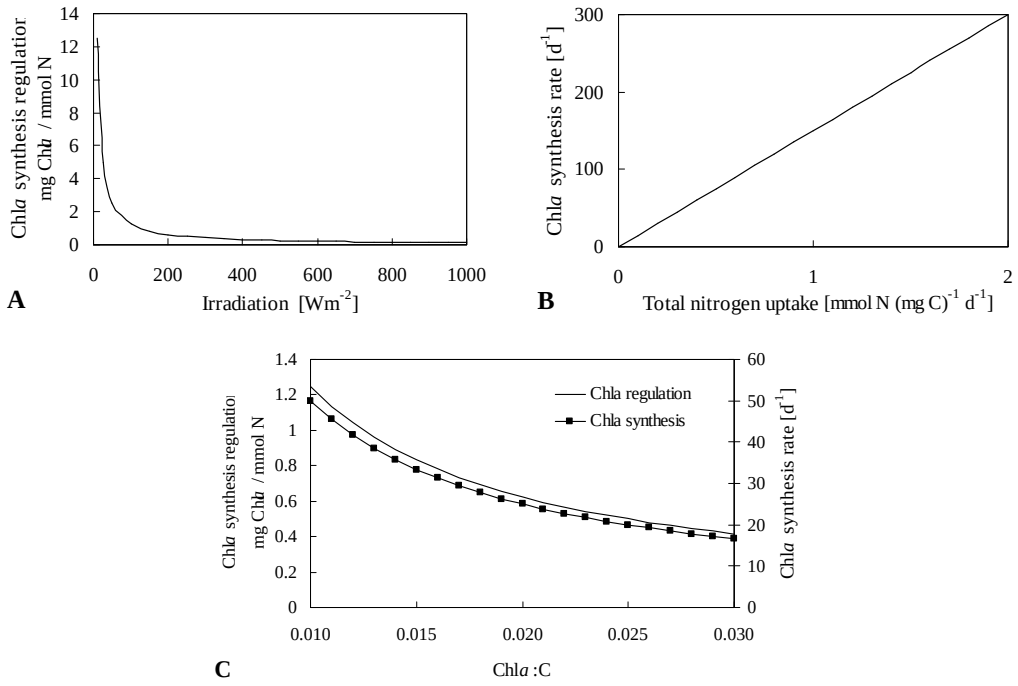

Figure 3.4: Variation of factors influencing Chlorophyll *a* production dynamics: (A) Chl*a* synthesis regulation as a function of light intensity; (B) Chl*a* synthesis rate dependence on total nitrogen uptake; and (C) Chl*a* regulation and synthesis for a range of Chl*a*:C ratios.

C fixation occurs through photosynthesis, but slows Chl*a* synthesis as $\chi_{chl:c}$ increases, acting as a control on $\chi_{chl:c}$ variation. Another aspects of this mechanism is the inverse response to light availability, which leads to higher Chl*a* production (imposed by higher values of ρ_{chl}) to compensate for lower light levels. Because at high light intensity levels, less Chl*a* is needed to convert the same amount of energy, the regulation term becomes low and as a response Chl*a* production is reduced. Another factor controlling Chl*a* synthesis is the nitrogen uptake, as presented in figure 3.4B (with $\chi_{chl:c} = 0.02$, $\alpha^{chl} = 3.0025$). As mentioned before, this simulates the need for this element in the production of proteins in the light harvesting complexes in the Chl*a* molecule. Finally, figure 3.4C (for $up_n = 0.5$, $\rho_{chl} = 1$ in the calculation of the Chl*a* synthesis rate) relates both terms of Chl*a* dynamics with $\chi_{chl:c}$. Unlike models with a static Chl*a*:C ratio (usually with no parameterization for Chl*a*), this approach to Chl*a* cell variable content enables the model to respond to different biotic and abiotic conditions, rendering the model more versatile and generic.

Several processes depend on the photosynthesis rate, one of them being the exudation rate of carbon (eq. 2.21). However, this particular process

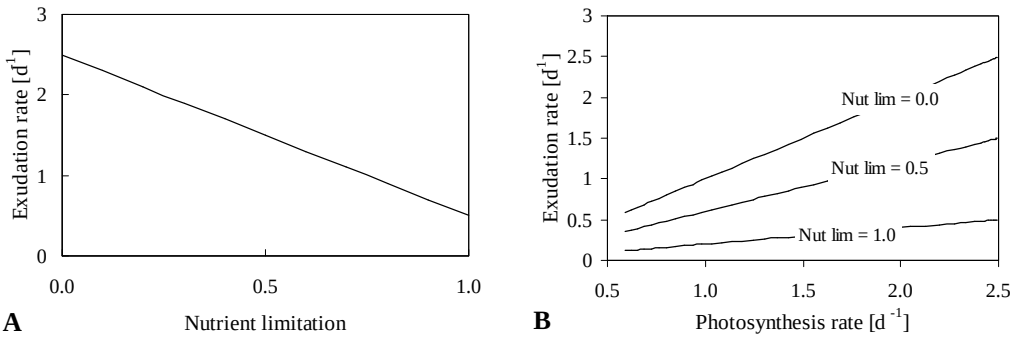

Figure 3.5: Exudation rate of carbon as a function of nutrient limitation (A), and its dependence on photosynthesis rate and nutrient limitation (B).

is also controlled by the nutrient status of the cells. The relation between theses processes is presented in figure 3.5 (with $\phi^{ex} = 0.2$). It is possible to verify that as stress induced by nutrient shortage increases, the exudation rate of C also increases. Contrary to this, lower stress of higher nutrient quotas means less C excreted because it is used to build biomass (illustrated in fig.3.5A, where $P_c^{phot} = 2.5$). In figure 3.5B it is possible to see the relation between exudation rate, photosynthesis rate and nutrient limitation. The increase of photosynthesis rate is reflected in the increase of exudation rate because a fixed fraction (ϕ^{ex}) of assimilated carbon is diverted to exudation products. But since this process is influenced by nutrient limitation, the state of nutrient quotas will also mediate C exudation. So, this amount becomes inversely proportional to the nutrient quotas; the lower the nutrient quotas, the higher the exudation of C.

As nutrients become non-limiting ($\Omega_{nut} = 1$) , exudation becomes $P_c^{phot}.\phi^{ex}$, so the fraction of exuded C is always a function of P_c^{phot} and its magnitude defined by the exudation rate (ϕ^{ex}). In the opposite scenario ($\Omega_{nut} = 0$) we will have $exu = P_c^{phot}$, meaning that all carbon fixated by photosynthesis is exuded. This regulatory mechanism prevents the enhancement of nutrient limitation by avoiding any more carbon fixation that might lead to lower nutrient:C ratios.

Subtracting the exuded fraction of C from the photosynthetically fixated (assimilated) fraction we have the fixed C $\left(ass^{inc}\right.$, see equations 2.22 and 2.23$\left.\right)$. Ultimately, the balance between this flux of carbon and respiration will define the net primary production $\left(ass^{net}\right)$. The respiration rate (eq. 2.24) comprises two terms, basal respiration as a function of temperature and activity respiration as a function of assimilated carbon, and their relation is portrayed in figure 3.6A (with $r^{bas} = 0.15$, $q^{res} = 0.1$). In the basal respiration component, as temperature rises, basal respiration will become higher expressing high metabolic rates induced by temperature. When $\Omega_T = 1$

the basal respiration will have the same value as the parameter expressing the basal respiration rate $\left(r^{bas}\right)$. When using the Q_{10} method for temperature limitation estimates this term of the respiration equation may become higher than r^{bas} (if $\Omega_T > 1$). Activity respiration will increase with the increase of ass^{inc}, reduced by q^{res} that reflects the fraction of assimilated C that is respired. The overall result, illustrated in figure 3.6A, is an increase in the respiration rate imposed by an increase in both temperature and C assimilation.

Producers natural mortality (eq. 2.25), or non-grazing related mortality, is only a function of a fixed minimum lysis rate $\left(r^{lys}\right)$ and nutrient cell quotas. As such, the realized lysis rate (lys) only varies in response to nutrient limitation variation; nutrient shortage contributes to higher mortality rates. Figure 3.6B shows how the minimum lysis rate and the nutrient limitation influence the mortality rate. In extreme cases, with acute nutrient limitation ($\Omega_{nut} = 0$) there will be a tenfold increase in r^{lys} expressing high mortality induced by cell lysis resulting from nutrient deficiency. When nutrient quotas are full ($\Omega_{nut} = 1$) the lysis rate will reach its minimum value, closer to r^{lys}.

The organic matter pools where the mortality products are routed also depends on cell nutrient quotas. Part of the products, controlled by q^{POM} (eq. 2.26), goes to the POM pool, while the rest is diverted to DOM. A fraction of intercellular nutrients are used to build biomass, but having the ability for luxury uptake, the excess or stored nutrients are kept in the cytoplasm. Hence, the closer the actual nutrient ratio will be to the maximum quota (normalized Nut:C closer to 1), the lower will be q^{POM} which means that a greater fraction of mortality products will be routed to the DOM pool (illustrated in fig. 3.6C). This way stored products inside the cell will be converted to DON and DOP. At around the Redfield ratio (pointed out in the graphic) the fraction for each organic matter compartment will be equal.

As with other physiological responses governed by nutrient limitation, sinking rate (σ_p, eq. 2.29) is also determined by nutrient content status. Increased nutrient stress (low Nut:C ratios) will cause the producer to sink faster, as can be seen in figure fig. 3.6D (with $\sigma_P^{str} = 5$, $\sigma_P^m = 0$). The nutrient stress threshold $\left(\Omega_{nut}^{sed}\right)$ sets the value below which sinking will start to occur. The higher this value, the sooner the organisms will start to sink when the Nut:C starts to drop (fig. 3.6D). So whenever $\Omega_{nut}^{sed} > \Omega_{nut}$, the organisms will start to sink, the speed also being determined by the reference sedimentation rate (σ_P^m) and the nutrient stress sedimentation rate $\left(\sigma_P^{str}\right)$. In cases where $\Omega_{nut} \geqslant \Omega_{nut}^{sed}$, the sinking speed will assume the fixed value of the fixed reference sedimentation rate $(\sigma_p = \sigma_P^m)$.

Nutrient uptake dynamics is regulated by external availability and internal cell quotas. Since external nutrient concentration control on uptake is defined as a linear relation, it will not be addressed here. But unlike this

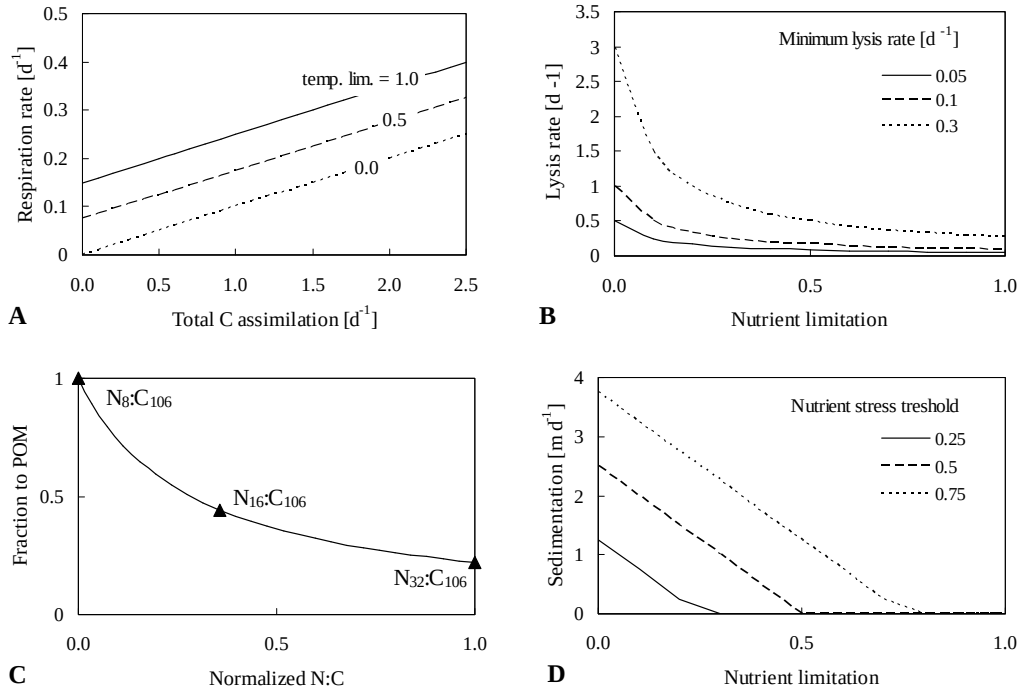

Figure 3.6: Assorted functional response plots for producers: (A) respiration rate as a function of temperature limitation and C assimilation; (B) lysis (mortality) rate as a function of nutrient limitation and for different values of minimum lysis rate; (C) fraction of POM as a function of nutrient cell quota; and (C) sinking speed as a function of nutrient limitation and for different nutrient stress threshold values.

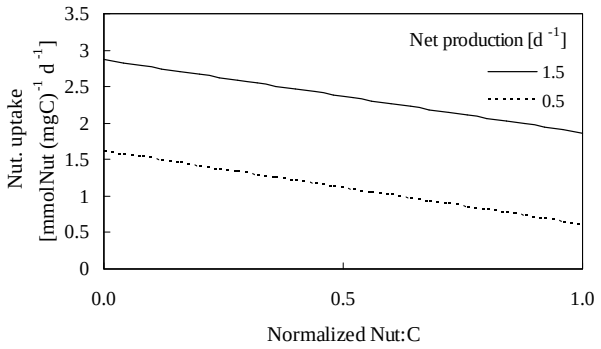

Figure 3.7: Nutrient cell quota and net production influence on nutrient uptake flux.

control, the constraints on nutrient uptake imposed by cell quotas (eq. 2.31) is rather complex, depending on photosynthesis net production $\left(ass^{net}\right)$ and on nutrient internal status $\left(\chi_j\right)$. The nutrient uptake process accounts for the amount of nutrients needed for growth, the nutrient equivalent for the amount of C fixed, and a quantity for storage. This last quantity of nutrient depends on the actual nutrient quota. Figure 3.7 (with $P_c = 50$, $Q_{max} = 1$, and χ_j^{max} twice the Redfield ratio) illustrates the influence of both net production and nutrient quotas on N uptake flux. Higher N uptake fluxes are observed when net production is higher, a response from the growth term of the nutrient uptake equation. This is a compensating mechanism to maintain nut:C ratios at its maximum.

The storage term, however, will tend to zero at nutrient quotas near the defined maximum, as is visible in figure 3.7 where nutrient uptake decreases as the normalized nut:C increases. This happens because as internal nutrient quotas are being filled, lesser amounts of nutrients are needed for storage. So, when $\chi_j = \chi_j^{max}$, the quota is full and storage stops, the uptake being $ass^{net}.\chi_j^{max}$ only used for growth. If $ass^{net} = 0$, when a balance is reached between incorporated and respired carbon, nutrient uptake is defined by storage needs, unless $\chi_j = \chi_j^{max}$, when all nutrient uptake ceases. Eventually nutrient uptake flux may become negative $\left(\text{e.g., } ass^{net} < 0 \text{ when } resp > ass^{inc}\right)$, implying a loss of nutrient from the cell. To avoid computation problems, this negative flux is not accounted for in the code, and instead a nutrient excretion process is used to release excess nutrient $\left(\text{if } \chi_j > \chi_j^{max}\right)$.

3.2.2 Consumers

Unlike producers and decomposers that have the ability to sequester nutrients in mineral or inorganic forms from the surrounding water, consumers

have to ingest them in organic forms. Only this way they acquire nutrients to build biomass and for proper cell function. But consumers are similar to decomposers in that both depend on organic matter as a C source, whereas producers depend on carbon dioxide. Through grazing, consumers ingest living organic matter, thus depending on this substrate for both nutrients and carbon. The model defines grazing according to MMM dynamics, and in this sense the grazing rate (eq. 2.50) is a function of prey availability (Φ_z), half-saturation concentration (k_z) and maximum specific uptake rate (V_z^{max}). Because it is a process controlled by a physiological response, it is also dependent on water temperature. Assuming no temperature limitation ($\Omega_T = 1$), and a fixed half-saturation constant ($k_z = 80$), the grazing rate increases with increasing abundance of prey, as it is depicted in figure 3.8A. In the same figure it is also possible to notice the effects of V_z^{max} on the grazing rate. As prey concentration increases, $\Phi_z / (\Phi_z + k_z)$ tends to one, and the grazing rate tends to stabilize at $G_z \cong V_z^{max}$.

The initial slope of the response curve is controlled by k_z, and so, independently of V_z^{max} the sharper increase in grazing rate is observed when $\Phi_z < k_z$. The influence of k_z on grazing rate at different values of V_z^{max} is presented in figure 3.8B (for $\Omega_T = 1$ and $\Phi_z = 80$). Higher k_z values means lower grazing rates inasmuch this parameters defines the inverse of the affinity to the substrate; low k_z reflects high affinity to the food source. At an hypothetical absolute affinity for a food source, $k_z = 0$, G_z would be defined as $V_z^{max}.\Omega_T$, meaning that consume would occur at the maximum rate with temperature controlling the magnitude of the rate. However, this kind of uptake dynamics is more likely to be found in bacteria and not in zooplankton.

Respiration and excretion (equations 2.53 and 2.54, respectively), are linked in consumers parameterization because they are controlled by the same set of variables and parameters, namely the uptake rate or grazing (G_z), the assimilation efficiency $\left(ass_z^{eff}\right)$, and the excreted fraction of non-assimilated carbon uptake (ϕ_z^{na}). Given that the last two parameters are static (i.e., they are defined by the user and do not change during the simulation), grazing becomes the major variable controlling respiration and excretion. Together with grazing, temperature limitation also controls respiration which is divided in two components: activity respiration ($resp_z^a$) dependent on grazing, and basal respiration ($resp_z^{ss}$) dependent on temperature. From this, it is possible to conclude that the contribution of $resp_z^{ss}$ to the total respiration rate varies according to the external temperature. In the example shown in figure 3.9A (with $G_z = 2$, $\phi_z^{na} = 0.5$, and $ass_z^{eff} = 0.5$) it is possible to see such influence for different values of the reference rest respiration at 10 °C $\left(r_z^{10}\right)$; the higher r_z^{10} is, the higher the respiration rate will be. At low temperatures $resp_z^{ss}$ contribution is reduced, while at $\Omega_T = 1$ it achieves it maximum, $resp_z^{ss} = r_z^{10}$ (not clear in the plot A because it

depicts total respiration rate and not $resp_z^{ss}$ alone).

The dynamics of the activity respiration term in the respiration rate equation is more complex, despite the linear dependence on every parameter. The lower ass_z^{eff} and ϕ_z^{na} are, the higher the activity respiration will be, contrary to the contribution of grazing to respiration, as represented in figure 3.9B (for $r_z^{10} = 0.02$, $\Omega_T = 1$, $\phi_z^{na} = 0.5$, and $ass_z^{eff} = 0.5$). Considering an hypothetical scenario of total assimilation of grazed carbon $\left(ass_z^{eff} = 1\right)$ or of total excretion of the non-assimilated fraction of carbon ($\phi_z^{na} = 1$), one would have no activity respiration ($resp_z^a = 0$). So, respiration would only be a function of temperature, $resp_z = resp_z^{ss}$. The parameter ϕ_z^{na} is the controlling (partitioning) factor of the destiny of non-assimilated carbon; $\phi_z^{na} = 0.5$ implies the same amount of diverted to respiration and excretion, $\phi_z^{na} > 0.5$ means more carbon excreted than respired activity respiration, $exc_z > resp_z^a$, and $\phi_z^{na} < 0.5$ the opposite scenario.

Together with grazing, mortality represents the last loss term of carbon in consumers. A particular consumer group can predate on other groups and on themselves, the parameterization used to address this process being the same as for grazing on producers and decomposers. In this process, the loss of carbon and nutrients is dependent on the grazing pressure by predators. Non-grazing mortality ($mort_z$), on the other hand, is defined by the characteristics of each group (namely by the oxygen-dependent, m_z^o, and temperature-independent, m_z^{ti}, mortality rates), the only external factor influencing it being the oxygen limitation (Ω_o). According to the mortality parameterization (eq. 2.55), the dissolved oxygen concentration on water determines the overall mortality rate as shown in figure 3.10A ($m_z^{ti} = 0.05$), where the mortality rate is calculated for different combinations of Ω_o and m_z^o. High values of Ω_o reflect more oxygen on water and, as a consequence, a lower mortality rate. Whenever dissolved oxygen is enough not to impose any limitation ($\Omega_o = 1$), there is no mortality induced by low oxygen stress, and mortality equals the temperature-independent mortality rate, $mort_z = m_z^{ti}$. The dependence on dissolved oxygen concentration is parameterized in a MMM fashion (eq. 2.56), controlled only by an half-saturation value for oxygen (k_z^o). In figure 3.10B the oxygen limitation factor dependence on dissolved oxygen concentration is illustrated at different values of k_z^o.

The nutrient dynamics in consumers are of particular relevance given their crucial role in the mineralization of organic matter in aquatic systems. As stated before, the model assumes that nutrient fixation by consumers is a function of their own Nut:C actual quotas $\left(\chi_j\right)$ and their range of minimum and maximum allowed quotas $\left(\chi_j^{min} \text{ and } \chi_j^{max}\right)$. And its the relation between these variables and parameters (equations 2.60 and 2.61) that defines the flux of assimilated and recycled fraction, as illustrated in figure 3.11. When consumers are severely limited by nutrients (χ_j approaching χ_j^{min}), the proportion of assimilated nutrients will reach its maximum, whereas,

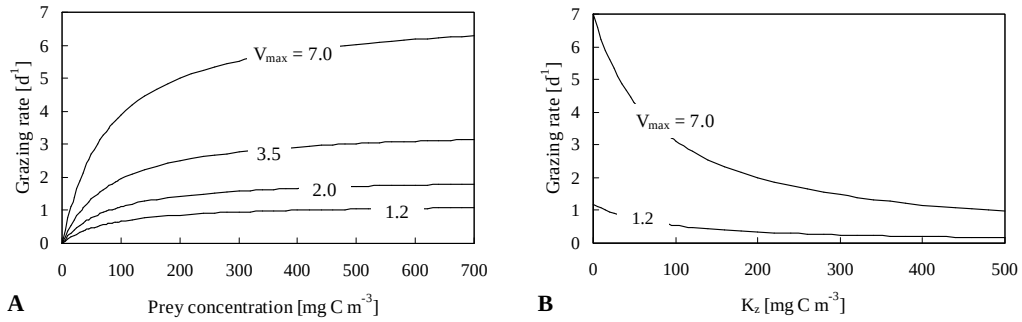

Figure 3.8: Consumer's grazing dynamics. Influence on grazing rate of: prey concentration and maximum specific uptake rate (A), and half-saturation concentration (B).

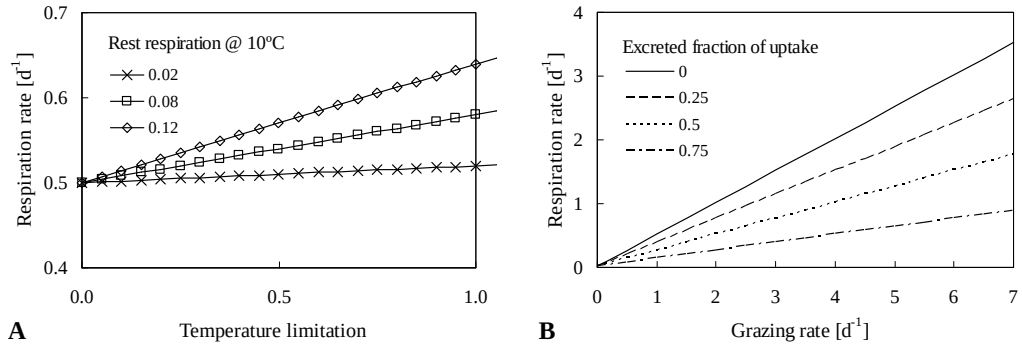

Figure 3.9: Respiration rate as a function of several parameter conditions in consumers: (A) respiration rate vs. temperature limitation plot for different rest respiration rate values; (B) respiration rate vs. grazing rate plot considering several values of excreted fraction of uptake.

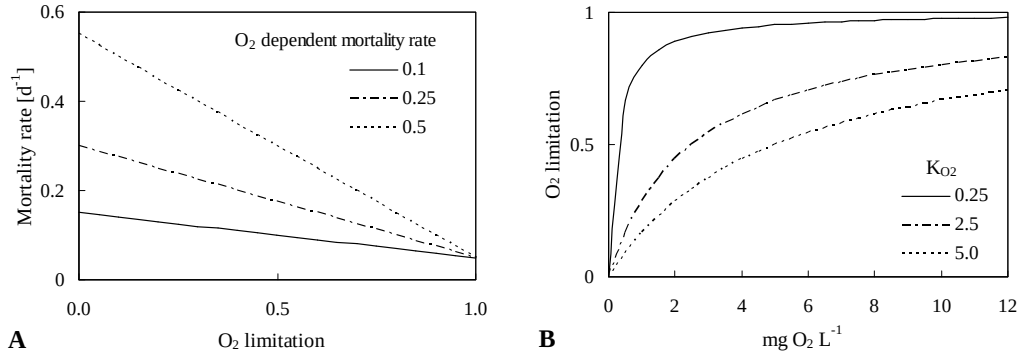

Figure 3.10: Mortality dynamics in consumers: (A) mortality rate as a function of oxygen limitation at different values of oxygen-dependent mortality rate, and (B) oxygen limitation factor at different half-saturation values.

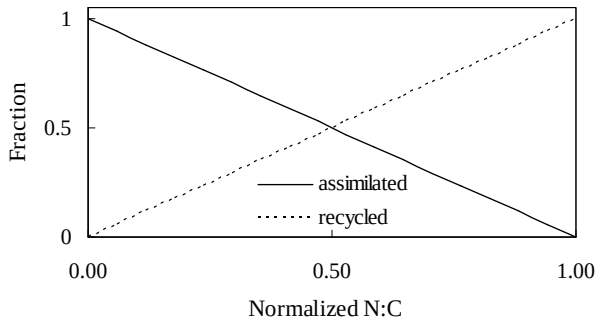

Figure 3.11: Fraction of assimilated and recycled nutrient from total grazed nutrient content.

when χ_j approaches χ_j^{max}, nutrients are no longer limiting and assimilation tends to zero while the recycled fraction will reach its maximum. Eventually, at nut:C ratios below χ_j^{min} all nutrients are assimilated, while at ratios above χ_j^{max} all nutrients are recycled or mineralized. So, whenever $\chi_j > \chi_j^{max}$, nutrient sequestering stop and all nutrients consumed by grazing are diverted to the recycled pool, being excreted in their inorganic forms. As nutrients become limiting for predators, the actual scheme implies that the rate of recycling decreases. Under these conditions, the organisms sequester the nutrient in order to restore the quotas. The opposite happens when nutrients are in excess and nutrients are diverted or recycled to the inorganic nutrient pools.

Zooplankton has been reported to have a rather rigid elemental stoichiometry [130], thereby justifying the assumption of consumer homeostasis common in many models. Using the model capability to define minimum and maximum nutrient quotas it is possible to implicitly impose this homeostasis by decreasing the range of variation in consumers stoichiometry. However, this capability renders the model more versatile, especially in the microbial loop related processes like mineralization. This parameterization of nutrient mineralization by consumers differs somehow from the one proposed by Baretta-Bekker *et al.* [28] in ERSEM because it allows recycling even when nutrient quotas are below the maximum. The simple excess release of a nutrient when quota rises above the maximum presented in other models implies a longer sequester period and those groups feeding on organisms with similar nutrient quotas will have a lesser contribute to the mineralization process. This approach is based on the stoichiometric axiom that as a nutrient element becomes limiting its excretion by the consumer tends to zero, in which case assimilated material would be exclusively used for new biomass [131].

3.2.3 Decomposers

Decomposer dynamics follows in many aspects some of the processes already described for producers and consumer. For that reason they will not be presented again. However, decomposers have one distinct process that is not shared with any other group, namely the mortality dependency on population density (equations 2.74 and 2.73). This parameterization of decomposer mortality was adopted because of the mounting evidence linking bacterioplankton mortality in natural systems with their abundance. In this context, bacterial infection by virus has been hypothesized as a natural control mechanisms. In the model, besides the density-independent mortality rate $\left(m_b^{di}\right)$, total mortality (m_b) is also determined by a term accounting for lysis $\left(m_b^{lys}\right)$. This in turn is defined by a constant density-dependent mortality rate $\left(m_b^{dd}\right)$, a reference bacteria density (v_b^m), and varies according to the actual decomposers concentration at any given time (B_c). Because it is assumed in the model that lysis increases linearly with the increase of population biomass, decomposers mortality also increases linearly as a consequence. This dependence of both rates on bacterial biomass is depicted in figure 3.12A ($m_b^{di} = 0.05$ and $v_b^m = 50$). Because here m_b^{di} is assumed to be relatively low, total mortality rate is slightly higher than lysis rate. It is possible to notice that when $B_c = v_b^m$, $m_b^{lys} = m_b^{dd}$, so at any double of B_c, lysis rate will also double.

The lysis rate also affects the final products of mortality through the ratio m_b^{lys}/m_b, as defined in equation 2.75. An increase in the lysis rate, reflecting an increase in decomposers concentration, leads to a decrease in the fraction diverted to POM $\left(q^{POM}\right)$. In figure 3.12B ($q^{ref} = 0.4$), the dashed vertical line is set where lysis rate is high enough to affect (decrease) the fraction of mortality products that goes to POM (when $lysis/mortality = 0.6$). The threshold is set by $1 - \frac{m_b^{lys}}{m_b} = q^{ref}$, so whenever $\frac{m_b^{lys}}{m_b} > 1 - q^{ref}$, the POM fraction decreases. below this threshold, the fraction that goes to POM assumes the value of the reference fraction $\left(q^{POM} = q^{ref}\right)$, while above, as lysis rate increases, more products are released to the DOM pool, as observed in natural bacterial populations under viral attacks.

Nutrient dynamics in decomposers are very similar to nutrient dynamics in producers, the only major difference being the acquisition method, given that decomposers can complement nutrient uptake by consuming them from DOM, unlike producers in the model. Models that do not assume uptake of inorganic nutrients by bacteria are always dependent on the nutrient contents of DOM (excreted by phytoplankton and/or produced by several processes) to meet their nutrient requirements.

Nutrient limitation in decomposers (equation 2.79) reflects their own internal nutrient quotas as shown in figure 3.13. So, at low nut:C, nutrient limitation values are high, leading to higher nutrient uptake of inorganic nu-

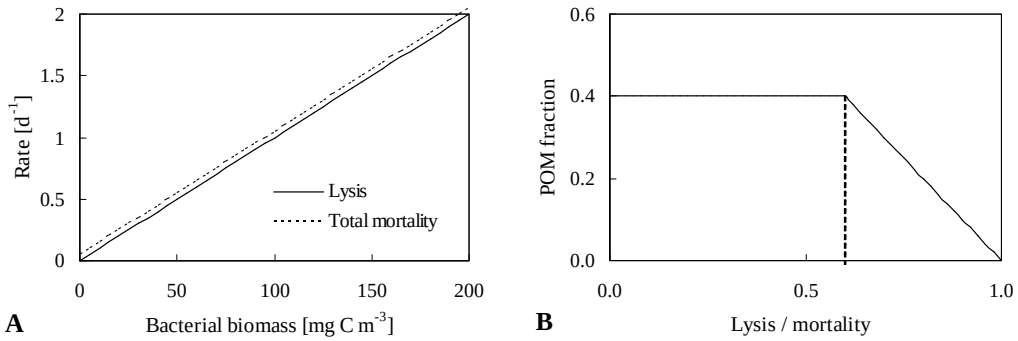

Figure 3.12: Decomposers mortality dynamics: (A) lysis and total mortality related with decomposers biomass, and (B) POM fraction as a function of lysis/mortality ratio.

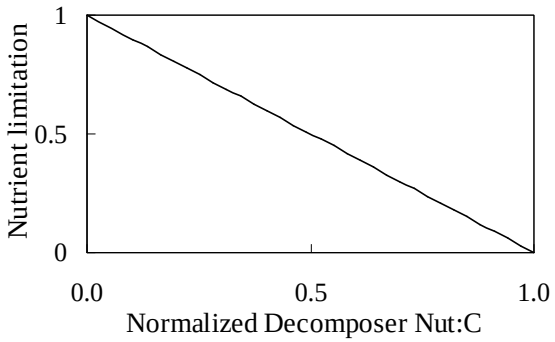

Figure 3.13: Normalized decomposers nut:C ratio influence on the nutrient limitation factor.

trients to compensate nutrient deficits. If $\chi_j \geqslant \chi_j^{max}$ (full nutrient quotas), then $\Omega_{nut} = 0$, imposing maximum limitation to uptake and as a consequence no uptake will occur. In this particular case there is an excess of nutrients and decomposers are carbon limited.

3.3 Long time run

3.3.1 Basic settings

In the basic setup of the model, primary producers are divided in four functional groups or size classes reflecting the same scheme presented in the ERSEM model: diatoms (20-200 μm), autotrophic flagellates (2-20 μm), picoalgae (0.2-2 μm), and mixotrophic flagellates (20-200 μm). Each group is defined by at least four state-variables: carbon, nitrogen, phosphorus and silica (only in diatoms). The consumer module includes microzooplank-

ton, heterotrophic flagellates and mesozooplankton. Here, unlike in ERSEM model, all consumer groups have the same parameterization being their different biology defined by their parameter values and prey preference. All other state-variables like decomposer components, organic matter groups and their components, and several nutrients are the same as presented in the previous chapters.

The initial conditions for some properties in the model are presented in table 3.1. For simplicity and to avoid redundancy, some values were left out. All producers initial N:C and P:C ratios follow the Redfield ratio (C_{106}:N_{16}:P_1). So, for a carbon content (P_c) of $1.0\,\mathrm{mg}C\,\mathrm{m}^{-3}$, the nitrogen ($P_n$) and phosphorus ($P_p$) content is $\sim 0.01257\,\mathrm{mmol}N\,\mathrm{m}^{-3}$ and $\sim 0.000786\,\mathrm{mmol}N\,\mathrm{m}^{-3}$, respectively. The same ratios are defined for the initial N and P components of consumers, labile DOM and POM. For diatoms, the Si:C content was also defined according to the Redfield ratio C_{106}:Si_{14}[132] and so P^1_{si} is $0.01\,\mathrm{mmol}Si\,\mathrm{m}^{-3}$. In all producers, chlorophyll content is initialized as 0.01 $\mathrm{mg}Chla\,\mathrm{m}^{-3}$, reflecting a C:Chl$a$ of about ˜ 100. Finally, bacteria nutrient content was set according to the C_{76}:N_{18}:P_1 ratio [38].

Parameter values used in this simulation for each module (producers, consumers, decomposers and biochemistry) are presented in tables 3.1 to 3.5. Parameters were chosen within typical ranges of oceanic systems, in an attempt to be as realistic as possible. So, most of these values are the same of ERSEM reference runs [28, 29] because they were derived from experiments using nutrient enrichment in mesocosms or estimated from analyzing data sets from the North Sea. Whenever this is not the case, the origin of the values is mentioned. All other values are educated guesses based on several previous simulations (results not shown). Unless otherwise stated, all parameters and initial values used in any further simulations are the same presented in tables 3.1 to 3.5.

3.3.2 Trophic relations

As a consequence of the generic group approach of *mohid.Life.1.0* code arrangement in respect to producers and consumers modules (without a rigid pre-defined trophic chain), any trophic relation (predator-prey interaction) can be defined. In this sense, any consumer can potentially feed upon any other consumer, producer or decomposer (plus on itself). This is also true for any producer group provided that the mixotrophic behaviour option is activated. Again, the trophic structure and prey availability (table 3.6) is adapted from ERSEM reference runs [28, 29].

The availability of each prey is not always assumed as total (where $\beta^{predator}_{prey} = 1$, reflecting 100% availability) because each functional group (whether it addresses a producer, consumer or decomposer) comprises a range of prey dimensions and not all can be consumed by the predators.

Table 3.1: Initial values used in the reference run. Note that not all state-variables are mentioned here (see text for details).

Symbol	**State-variables**	**Value**
producers		
P_c^1	Diatoms	1.0
P_c^2	Autotrophic flagellates	1.0
P_c^3	Picoalgae	1.0
P_c^4	Mixotrophic flagellates	1.0
consumers		
Z_c^1	Microzooplankton	0.5
Z_c^2	Heterotrophic flagellates	0.5
Z_c^3	Mesozooplankton	0.5
decomposers		
B_c^1	Heterotrophic bacteria carbon	1.0
B_n^1	Heterotrophic bacteria nitrogen	0.0198
B_p^1	Heterotrophic bacteria phosphorus	0.0011
organic matter		
POC	Particulate organic carbon	1.0
$DOCl$	Labile DOC	1.0
$DOCsl$	Semi-labile DOC	0.0
others		
$BioSi$	Biogenic silica	0.0
NO_3	Nitrate	10.0
NH_4	Ammonium	4.0
PO_4	Phosphate	1.0
Si	Silicate acid	6.0
O_2	Oxygen	8.0

Table 3.2: List of parameter values used as reference for producer groups. Four values correspond to the four functional groups in the following order: diatoms, autotrophic flagellates, picoalgae and mixotrophic flagellates. Two values are for diatoms and all others. Only one value is provided if the value is the same for all functional groups. All values are from Baretta-Bekker [28], except [a] from Brzezinski [132], [b] from Geider *et al.* [41] and [c] from Moore *et al.* [32].

Symbol	Parameter	Value
χ_n^R	Redfield N:C ratio	0.011261
χ_n^{min}	Minimum N:C ratio	$0.5 \times \chi_n^R$
χ_n^{max}	Maximum N:C ratio	$2 \times \chi_n^R$
χ_p^R	Redfield P:C ratio	0.000786
χ_p^{min}	Minimum P:C ratio	$0.5 \times \chi_p^R$
χ_p^{max}	Maximum P:C ratio	$2 \times \chi_p^R$
χ_s^R	Standard Si:C ratio	0.01^a
α^{chl}	Chl$a$ – specific initial slope of the photosynthesis-light curve	3.0025^b
$\chi_{chl:n}^{max}$	Maximum Chl:N ratio	3.0^c
Q_{10}	Q_{10} value	2.0
r^{ass}	Maximum assimilation rate	$2.5; 2.7; 3.0; 1.5$
ϕ^{ex}	Exudation under nutrient stress	$0.05; 0.2; 0.2; 0.05$
r^{bas}	Basal respiration rate	$0.15; 0.1$
q^{res}	Respired fraction of production	$0.1; 0.25$
r^{lys}	Minimum lysis rate	0.05
sed_P^{str}	Nutrient stress sedimentation rate	$5.0; 0; 0; 5.0$
sed_P^m	Minimum sedimentation rate	0
Ω_{nut}^{sed}	Nutrient stress threshold	$0.70; 0.75$
Q_{max}	Maximum rate of storage filling	1
k^{n1}	Affinity for NO_3 (uptake rate)	$0.0025; 0.0025; 0.0; 0.0025$
k^{n2}	Affinity for NH_4 (uptake rate)	0.0025
k^p	Affinity for PO_4 (uptake rate)	0.0025
r^s	Release rate of excess silicate	1
k_s	Silicate uptake Michaelis constant	0.3
φ_P^{sl}	DOM fraction diverted to semi-labile pool	0.1

Table 3.3: List of parameter values used as reference for consumer groups. Three values correspond to the three functional groups in the following order: microzooplankton, heterotrophic flagellates and omnivorous zooplankton. Only one value is provided if the value is the same for all functional groups. Values in parenthesis refer to the grazing behavior by mixotrophic flagellates. All values are from Baretta-Bekker *et al.* [29].

Symbol	**Parameter**	**Value**
χ_n^{max}	Maximum N:C ratio	0.0167
χ_n^{min}	Minimum N:C ratio	0.015
χ_p^{max}	Maximum P:C ratio	0.00185
χ_p^{min}	Minimum P:C ratio	0.0017
r_z^{10}	Rest respiration @ 10^oC	0.02
ass_z^{ef}	Assimilation efficiency	$0.5; 0.25; 0.5; (0.4)$
ϕ_z^{na}	Excreted fraction of uptake	0.5
Q_{10}	Q_{10} value	2.0
q_z^{POM}	Fraction of excretion to POM	0.5
m_z^o	Oxygen-dependent mortality rate	0.25
m_z^{ti}	Temperature-independent mortality rate	0.05
k_z^o	Oxygen half saturation constant	0.25
V_z^{max}	Maximum specific uptake @ 10^oC	$1.2; 7; 7; (3.5)$
k_z	Half saturation value for uptake	$80; 300; 40; (300)$

Table 3.4: List of parameter values used as reference for decomposers. All values are from Baretta-Bekker *et al.* [28] except when marked with *; [a] taken from Cochrane *et al.* [25].

Symbol	Parameter	
χ_n^{max}	Maximum N:C ratio	0.019720*
χ_n^{min}	Minimum N:C ratio	0.016652*
χ_p^{max}	Maximum P:C ratio	0.0016652*
χ_p^{min}	Minimum P:C ratio	0.0010955*
r_b^{10}	Rest respiration @ 10^oC	0.01
V_b^{max}	Maximum specific uptake @ 10^oC	$5*$
k_b^{DOM}	Half saturation constant for DOM uptake	10.6^a
ass_{norm}^{ef}	Assimilation efficiency	0.5
ass_{low}^{ef}	Assimilation efficiency @ low oxygen	0.2
Q_{10}	Q_{10} value	2.95
q_b^{ref}	Fraction of mortality products to POM	0.4
q_b^{DOMsl}	Fraction of DOM to semi-labile pool	0.2*
m_b^{dd}	Density-dependent mortality rate	0.5
m_b^{di}	Density-independent mortality rate	0.05
v_b^m	Mortality density dependent reference concentration	100*
k_b^o	Oxygen half saturation constant	0.01
θ_b^o	Oxygen concentration below which $ass = ass_{low}^{ef}$	1.6
k_b^{n1}	Affinity for NO_3 (uptake rate)	0.025*
k_b^{n2}	Affinity for NH_4 (uptake rate)	0.025*
k_b^p	Affinity for PO_4 (uptake rate)	0.025*
V_{hyd}^{POM}	Maximum rate for POM hydrolysis	1*
V_{hyd}^{DOMsl}	Maximum rate for DOMsl hydrolysis	1*
k_{hyd}^{POM}	POM hydrolysis half saturation constant	32**
k_{hyd}^{DOMsl}	DOMsl hydrolysis half saturation constant	200*

Table 3.5: List of parameter values used as reference for the biochemistry module. Reference key: [a] Chapra[37]; [b] Moore *et al.* [32]; [c] Baretta-Bekker *et al.* [133].

Symbol	Parameter		Units
k_{nit}	First-order nitrification inhibition coefficient	0.6^a	$\mathrm{l\,mg^{-1}}$
I_{nit}^{ref}	Light intensity threshold for nitrification	4^b	$\mathrm{W\,m^{-2}}$
ν_{nl}	Nitrification rate	0.04^b	$\mathrm{d^{-1}}$
γ_s	Biogenic silica dissolution rate	0.02^c	$\mathrm{d^{-1}}$
$\delta_{o:c}$	Carbon-to-oxygen conversion parameter	2.664	$\mathrm{mg}O_2\,(\,\mathrm{mg}C)^{-1}$
$\delta_{o:n}$	Nitrogen-to-oxygen conversion parameter	0.0588^a	$\mathrm{mg}O_2\,\mathrm{l}^{-1}\left(\,\mathrm{mmol}N\,\mathrm{m}^{-3}\right)^{-1}$

As an example, one can look at the predation of microzooplankton on diatoms. The low availability of diatoms to microzooplankton $\left(\beta_{P1}^{Z1} = 0.1\right)$ is explained on the similarities in size, because both functional groups range between $20\,\mu$m and $200\,\mu$m. From a theoretical point of view, a percentage of microzooplankton can be smaller then some diatoms and so they cannot ingest them.

3.3.3 Simulation

The model was run over a period of 5 years with a 3600 seconds time step. Physical processes affecting the properties over time (advection, sinking, etc.) were left out. In this simplified 0D scheme without any physical transport processes, the sources and sinks terms of each property are a function of chemical and biological processes occurring inside the water quality model alone. This approach enables a detailed study of model performance independently from any transport scheme. In all the theoretical application described from now on, the study "site" represents a "virtual mesocosm". It consists of a 10 meter deep tank with a simple square geometry and with only one layer.

3.3.4 Model Forcing

Monthly mean values of surface water temperature used to force the model are from a station located off Lisbon (latitude 38^o49'N and longitude 09^o05'W). In this first model implementation, where a detailed spatial discretization on the temperature is not needed, only one value per month is used as a rough characterization of the characteristic temperature throughout the year (Fig. 3.14a). There is in fact a wide variation within each month, but for the aim of this application it is not relevant. The solar radiation at surface used to force the model was obtained from a simple function inside *MOHID* that calculates the radiation for any chosed latitude and longitude. This function uses random numbers in some calculus (e.g. cloud cover) and so it does not repeat the same pattern each time the model is run. However, this is only relevant in comparing runs with different sets of parameter values, like in sensitivity analysis. In these simulations, 38^o49'N latitude and 09^o05'W were defined as the reference coordinates for the surface radiation model. As can be seen in figure 3.14 (b and c) the surface radiation model can reproduce with a satisfactory degree of accuracy both the diel (light cycle in a day) and seasonal variation (intensity and light period). In multi year runs the same set of data is repeated.

Table 3.6: Trophic relations definition: values represent availability of prey to predator and no value is provided if predator-prey relationship doesn't exists.

Predator	Micro-zooplankton	Heterotrophic flagellates	Meso-zooplankton	Mixotrophic flagellates
Prey				
Diatoms	0.5	–	0.2	–
Autotrophic flagellates	0.2	0.2	0.3	–
Picoalgae	–	1	–	1
Mixotrophic flagellates	1	–	–	0.5
Microzooplankton	0.2	–	0.2	–
Heterotrophic flagellates	0.6	0.2	0.2	–
Mesozooplankton	–	–	0.2	–
Bacteria	0.1	1	–	0.1

3.3.5 Results

Looking at the producer biomass results for the simulation period (figure 3.15) it is possible to see the existence of an adjustment period, characterized by "chaotic" oscillations in properties concentrations over time. These fluctuations reflect the model response to the initial conditions and show its capacity to converge to an dynamic steady state. In this particular case, the equilibrium or steady solution is achieved after just one year of simulation, a pattern also observed in all other properties. However, the equilibrium is not a repeated cycle. Some minor variations can be seen from year to year, as in the gradual decreasing concentration of mixotrophic flagellates in the last three years (fig. 3.15b). The high-frequency oscillations observed in producer results are explained on the basis of the diel light fluctuations that cause minor variation in producers biomass, together with grazing pressure. The effect of this pressure is more pronounce during night when producer growth rates are lower.

This minor annual change is not in itself an example of inter-annual variation. This kind of variation is not expected in a schematic application like the one implemented here, only because the external forcing conditions are repeated every year and there is no addition of nutrients over the simulation period. Nevertheless, the results clearly show annual or seasonal variation with higher concentrations during spring and summer months. This variations occurs mostly as a response to the seasonal cycle of radiation and water temperature in the forcing conditions (figure 3.14). This physical control on biological parameters has a cascade effect because organisms themselves have the ability to influence external nutrient concentration, which in turn affects other organisms. Hence, seasonal variation results from feedback mechanisms both from physical and biological/chemical processes. Overall, the model has produced apparently reasonable predictions for producer dynamics in the water column.

The undulatory pattern of producers evolution in time is also shaped by the combination of top-down and bottom-up control mechanisms. Even with seasonal fluctuations, most explicitly in ammonium and nitrate (figure 3.16), the relatively stable nutrient availability over the spring-autumn period implies that a bigger control can be ascribed to processes other than nutrient limitation (bottom-up). Together with water temperature and radiation levels, results combine the contribution from biological and chemical processes like uptake, competition, mineralization, nitrification, etc. But the greatest control pressure is apparently made by grazers (top-down).

Apart from the forcing mechanisms, no other physical processes affect the evolution of properties over time. In natural systems, late summer/early autumn blooms are induced by the increase in mixing in the water column bringing nutrient rich waters to the surface layer where nutrients have been depleted during summer [101]. This physical control is absent here, given

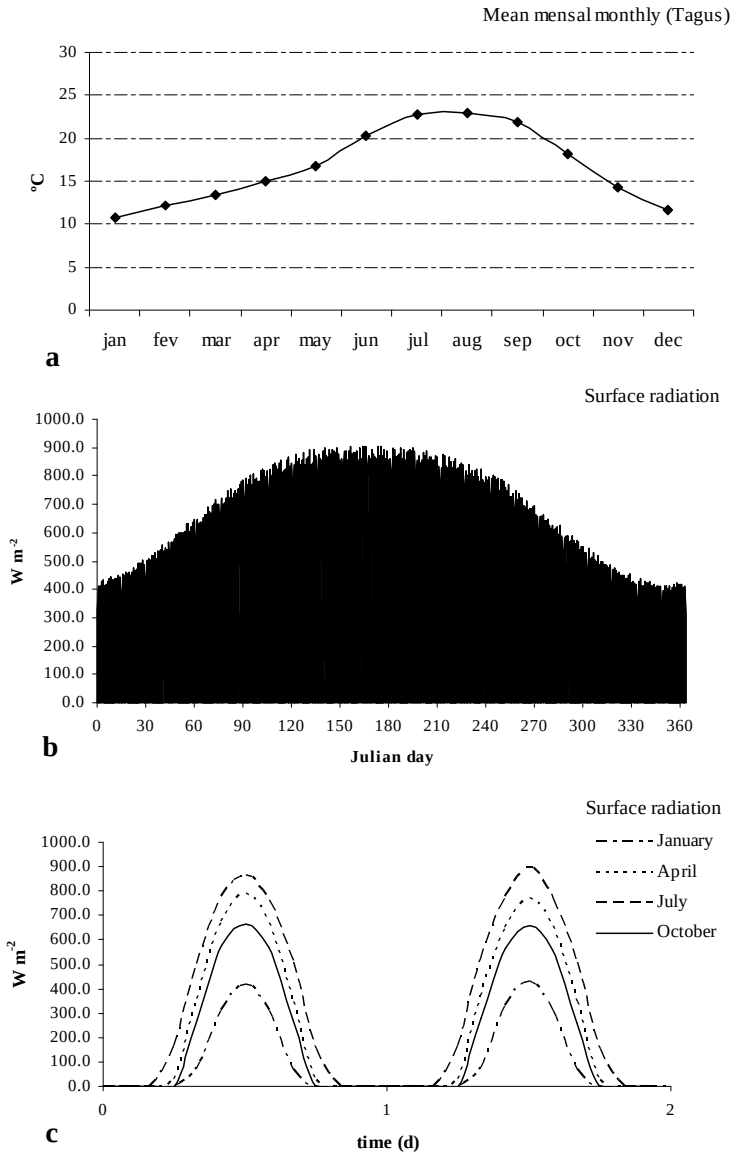

Figure 3.14: Environmental parameters used to force the model: (a) Monthly mean surface water temperature from a station located at Tagus estuary (latitude 38°49N and longitude 09°05W). (b) Surface radiation calculated inside MOHID for the same coordinates of the station where the temperature was measured. (c) A period of two days at the beginning of different months where the variation in the length of the light period and light intensity is portrayed.

the geometry and circulation constraints imposed in the simulation. Sometimes, however, model results can mimic this pattern if nutrient recycling during summer achieves enough impact to boost continuous blooms throughout summer while radiation levels are high enough to maintain significant growth rates. In the present application, this process can explain the higher concentration observed from spring to mid autumn (figure 3.15c). The model shows algal succession, frequent in natural systems (figure 3.15b). This succession is determined by different grazing pressure, growth rates, nutrient dependency, among other factors.

The temporal evolution of producers populations and of decomposers has in turn an effect on consumers populations. Looking at figure 3.17 one can see that the overall pattern is similar to the pattern observed in producers. Because a consumer group feeds upon several prey groups (producer and bacteria), the population variations tends to follows the trend of producers as a whole, with the expected time lag. Comparing producers and consumers results is possible to notice that total consumers biomass (figure 3.17c) is generally slightly higher than producer total biomass (figure 3.15c) While producers reach a maximum between 40 and 45 $\mathrm{mg}C\,\mathrm{m}^{-3}$, consumers go over 50 $\mathrm{mg}C\,\mathrm{m}^{-3}$. Following the producers and decomposers seasonal patterns, consumer maximum values are also reached in spring as a consequence of the food supply.

Besides the contribution of producers to consumers biomass, there is also the decomposer's contribution because they are also a food source. Decomposers time series (figure 3.18) shows that bacterial biomass throughout the year can be twice as high as consumers biomass, with peaks above 100 $\mathrm{mg}C\,\mathrm{m}^{-3}$. These results imply that much of consumers biomass is supported by bacterial production. In the trophic structure defined for this simulation (table 3.6) both picoalgae and bacteria are fully available prey to heterotrophic flagellates $\left(\beta_{P3}^{Z^2} = \beta_{B}^{Z^2} = 1\right)$. Given the high biomass values of decomposers and picoalgae, the contribution of these two groups sustains in part the consumers biomass. The importance of the grazing on decomposers is paramount to nutrient recycling. Consumers recycle nutrients by respiring C and excreting the associated nutrients. Since decomposers have higher N:C and P:C ratios than producers and consumers, a diet where they are abundant will lead to a greater amount of inorganic nutrients excreted by consumers.

Despite the different peaks in producers occurring at different times, it is still possible to notice a succession pattern characterized by an initial autotrophic dominance phase with increasing phytoplankton production, followed by a heterotrophic phase with decline in primary production and increased bacterial and consumers biomass. This is a realistic pattern that has been observed and modeled in enclosure experiments [134], as well as in natural systems.

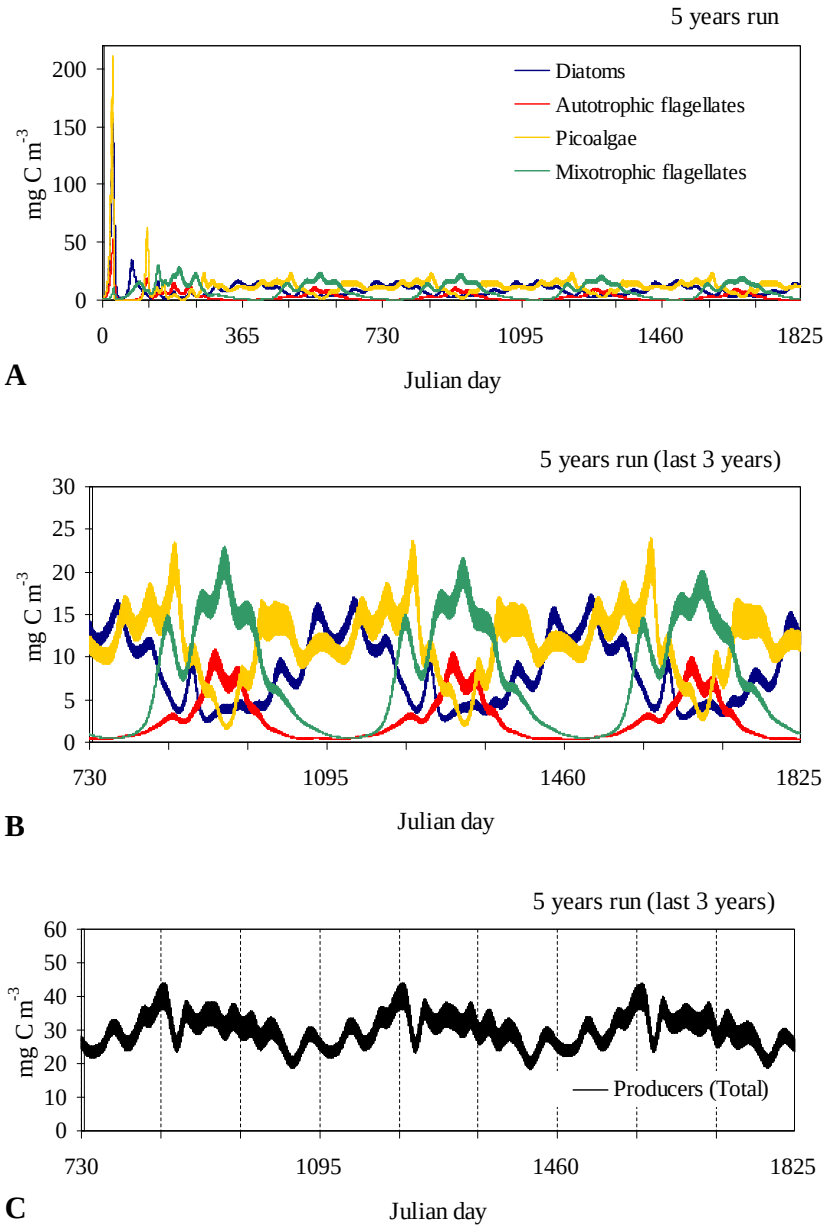

Figure 3.15: Simulation results for producers: (a) variation over the five years run; (b) variation over the last three years; (c) total producers biomass over the last three years.

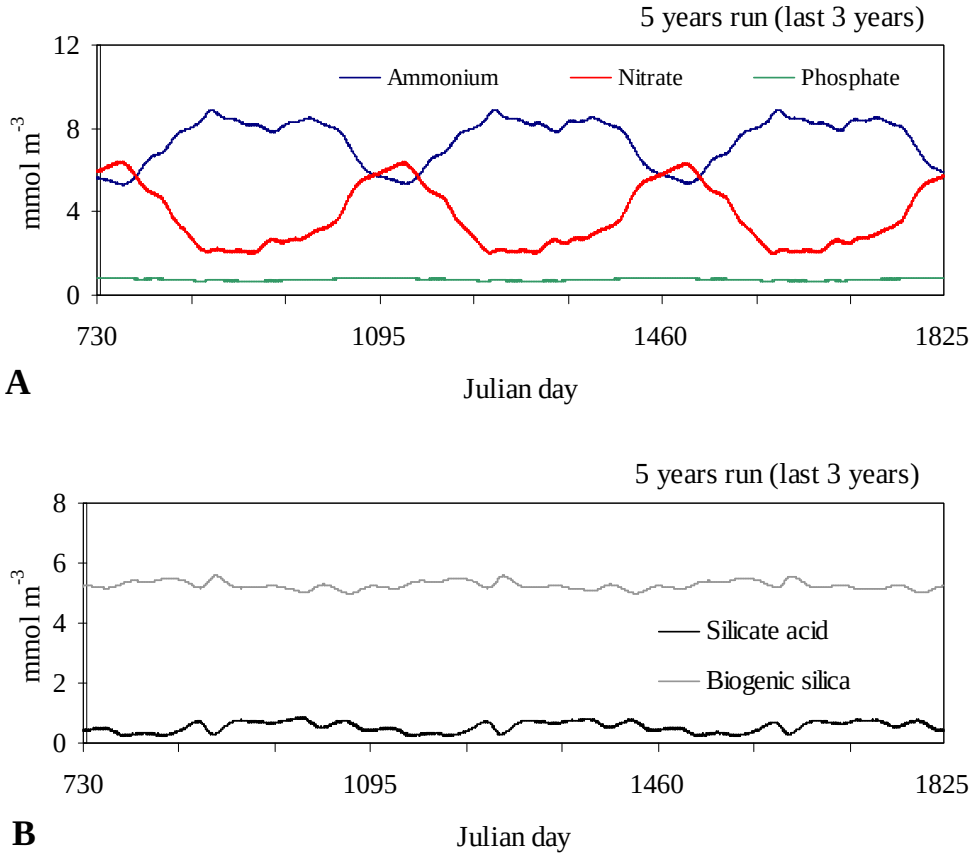

Figure 3.16: Nutrients time-series for the last three years of the five years simulation: (a) ammonium, nitrate, and phosphate ; (b) silicate acid. Biogenic silica is also shown.

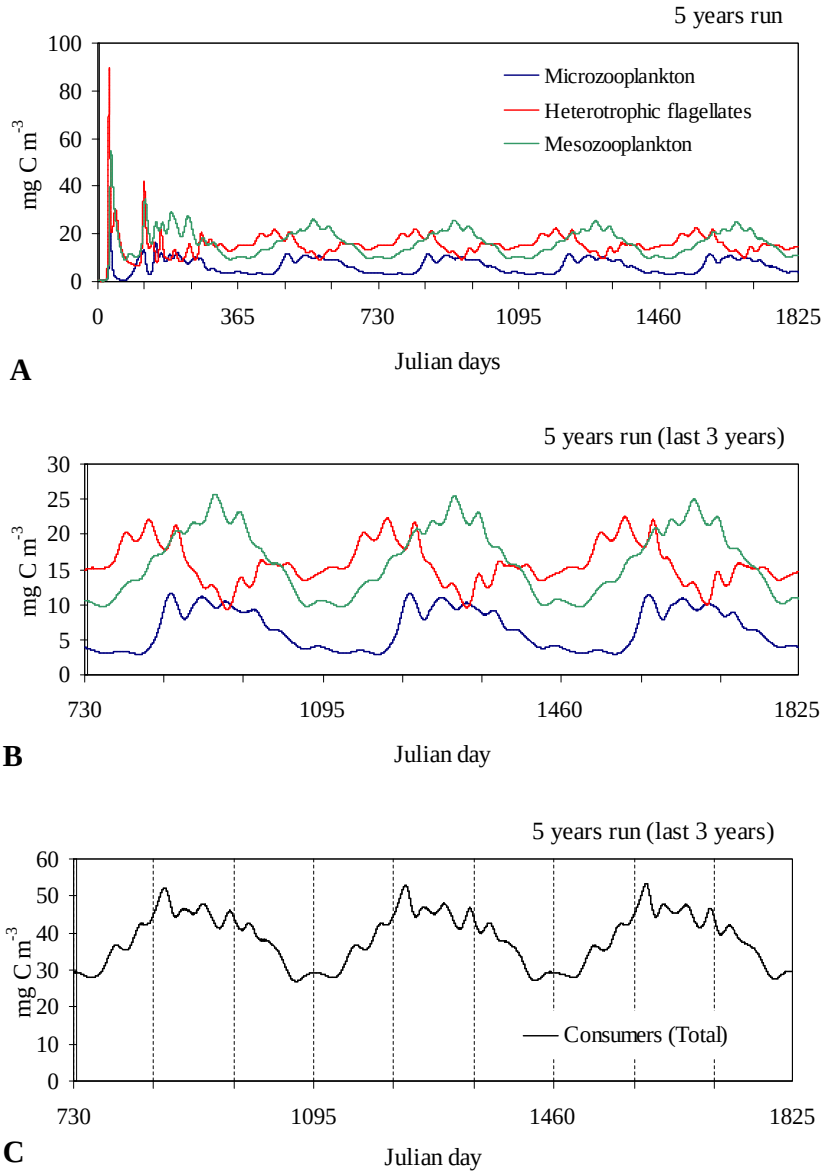

Figure 3.17: Simulation results for consumers: (a) variation over the five years run; (b) variation over the last three years; (c) total consumers biomass over the last three years.

As expected, there is a strong correlation between bacterial abundance and chlorophyll concentration. Since there is no allochtonous DOM, bacterioplankton C dependency relies on DOM produced in the system with primary producers as the main source. The abundance relation between producers, decomposers, and consumers is shown in figure 3.19. As it can be seen, the P:C ratio (producers:consumers) is always higher than the $P : D$ ratio (producers:decomposers), which implies that producer and consumers bulk quantity tend to be closer than producers and decomposer. At least during winter, P:C ratio goes above 1 reflecting a dominance of producers biomass over consumers biomass. Looking at figure 3.18b it is possible to see that decomposers abundance is lower in winter reducing the growth of consumers predating on bacteria, and this occurrence might explain the lower P:C in this season. The values of $P : D$ ratio around 0.5 implies that decomposer biomass is usually twice as high as producers biomass. Situations have been reported where bacteria dominates the microbial biomass of the system, consuming a significant amount of fixed C (DOC), probably mostly released directly by phytoplankton or via herbivores [135]. This is typical for oligotrophic conditions where nutrient availability is mainly determined by heterotrophic mineralization of organic matter via decomposers and consumers. In this particular simulation setting, without allochtonous nutrient sources (by physical processes or imposed as a boundary condition), the model is able to simulate an oligotrophic mesocosm, where all production as to be supported by autochthonous nutrient sources resulting from biochemical processes.

Decomposers evolution in time reflects the availability of organic matter. Organic matter components variation in time is portrayed in figure 3.20. Labile DOM concentrations remain relatively low because they are readily consumed by bacteria as a carbon source. In figure 3.20 we notice an accumulation of DOCl in the first year, with concentration above 200 $\mathrm{mg}C\,\mathrm{m}^{-3}$ as a result of the excretion by producers and by consumers to a lesser extent. When nutrient concentration drops to low values, as observed during the first year (figure 3.16a), bacteria are nutrient limited and not able to use the DOCl substrate as a carbon source, resulting in its accumulation. After the first year of spring, the system settles into a repeating cycle and nutrient availability increases and decomposers growth becomes C limited instead. In this situation, DOCl is consumed as it is being produced, and no accumulation is observed. However, it is possible to notice smooth DOCl peaks resulting from producers blooms in spring. DOMsl concentrations are relatively high and follow the decomposers abundance because bacteria mediate its hydrolysis to DOMl. Nevertheless the process is slow and so DOMsl concentration remain high, unlike POM with a higher rate of hydrolysis.

The model assumes competition for inorganic nutrients between producers and decomposers. Part of the observed concentrations for these groups are shaped by this interaction. Given the explicit parameterization of N, P

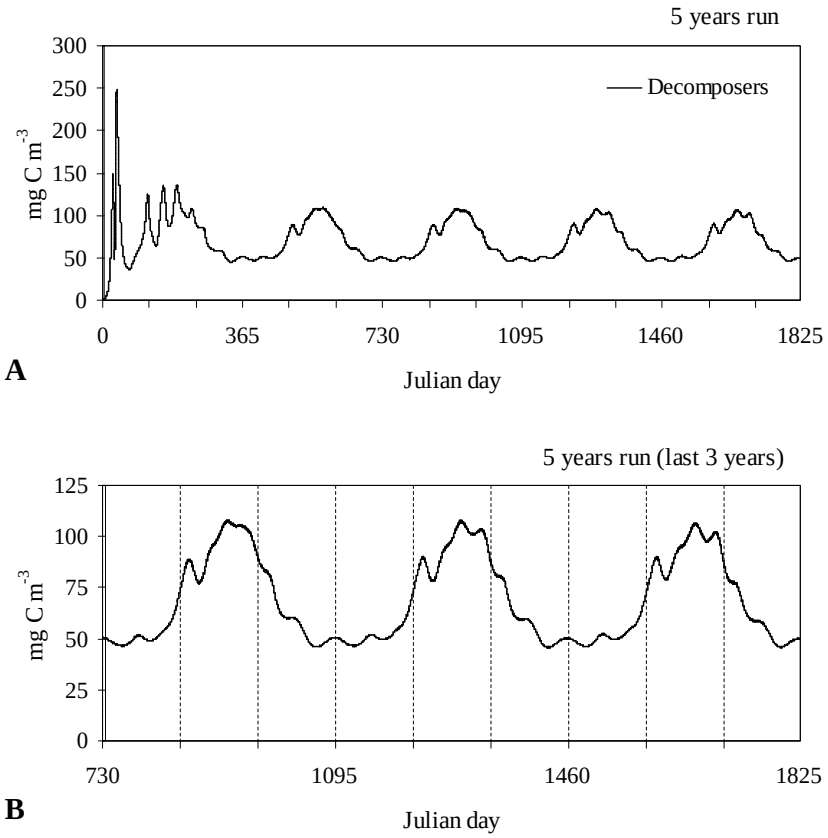

Figure 3.18: Simulation results for decomposers: (a) results of the five years run; (b) total decomposers biomass over the last three years.

and C cycles and dependency of growth on them, it is possible to have a situation with producers growth limited by N or P and decomposers by C.

This schematic application of the model is sufficient to demonstrate the functionality and complexity of the microbial loop, with regeneration of nutrient from organic matter within the system performed by decomposers and consumers. It also captures the dynamics of the competition for inorganic nutrients by decomposer and producers.

Mass balance

When using a "control volume" methodology in the development of any model it is necessary to check whether the model conserves mass. By performing a simple test, taking into account the balance between sources and sinks of each nutrient (currency), it is possible to determine the correctness of the model. The test is particular useful because it enables the debug-

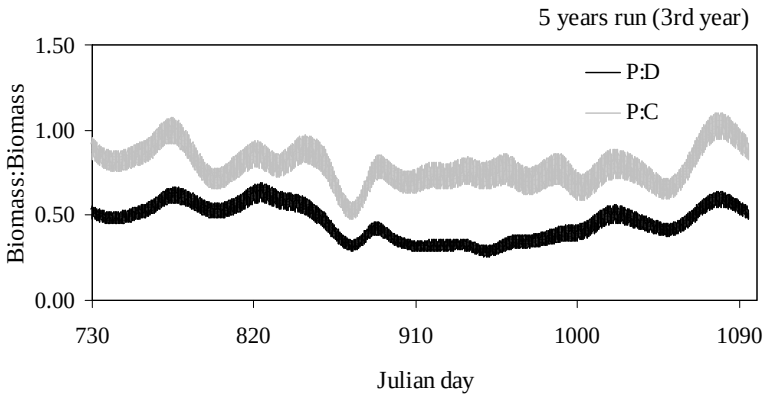

Figure 3.19: Producers:decomposers (P:D) and producers:consumers (P:C) ratios. Results for the third year of simulation only.

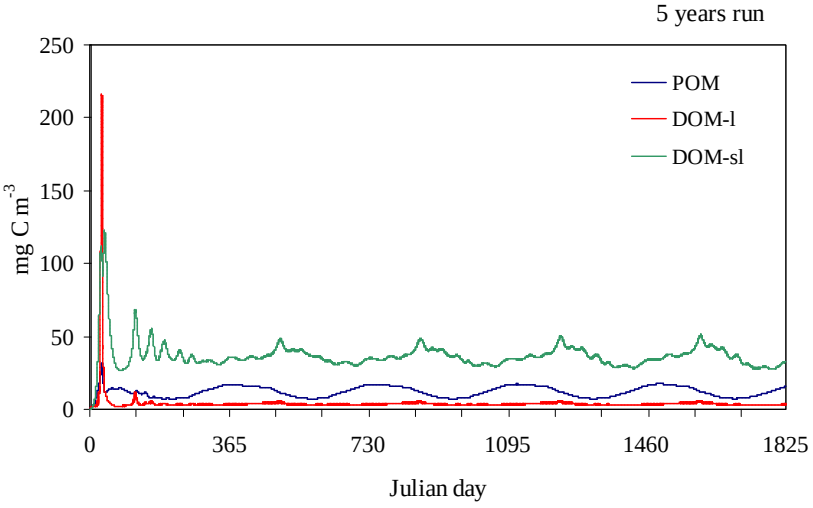

Figure 3.20: Simulation results for organic matter components over the five years run.

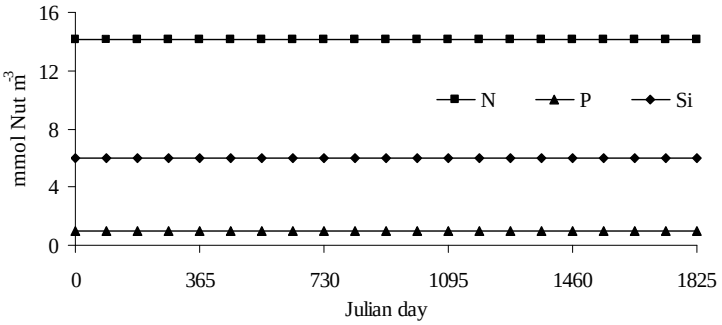

Figure 3.21: Mass Balance check for all nitrogen (N), phosphorus (P) and silica (Si) compartments during the simulated period.

ging of the algorithms of the water quality model of any errors causing mass conservation violation (before source and sink terms from transport are considered).

The mass balance test considers each nutrient compartment in the model, weather it is the organism cell quota, the organic matter nutrient quota or in the inorganic form. A simple algorithm was added to the code to sum all compartments for each nutrient at each time step. Taking nitrogen as an example, this calculation is then:

$$Total\ N = \sum_{i=1}^{j} P_n^j + \sum_{i=1}^{j} Z_n^j + B_n + DOMsl_n + DOMl_n + POM_n + NH_4 + NO_3 \tag{3.1}$$

With this check it is possible to control the mass conservation or variation in time, being the simplest way by just plotting the result of each sum at any given moment, as in figure 3.21. In the present case, it can be seen that the model conserves mass, which shows that there is a consistency in the code regarding the source and sink terms and also in the mass balance equations. Based on this, the contribution of processes other than the ones inside the water quality module can be correctly assessed and studied in 1D, 2D or 3D applications.

Only N, P and Si are mentioned because C and Chl*a* are not parameterized to conserve mass. The model assumes a system saturated with carbon (DIC in the form of CO_2) and so sources and sinks do not have to be balanced. As for chlorophyll, because it is only produced and degraded inside phytoplankton cells, there is no point in speaking of mass conservation.

3.3.6 Dynamic elemental composition

Being one of the major guidelines for the *mohid.Life.1.0* development, the capacity to have a variable stoichiometry or elemental composition must

also be addressed in the assessment of model performance. To achieve this purpose, some results are shown to illustrate the model capacity to calculate the internal organism nutrient quotas as a function of other internal and external parameters and processes. The same is done for organic matter components, given that its elemental composition also varies in time according to the "quality" of residues resulting from all the biological processes addressed by the model. Unless otherwise stated, all the results presented are from the third year of the simulated period.

Starting with producers, as stated before their evolution in time is shaped by interactions like competition and predation, response to external nutrient concentrations and light availability. Some of these factors have an effect on the internal element composition of producers (chlorophyll and silica concentration and nutrient quotas). This influence is not the same for all the elements. While nutrient quotas and silica concentration tend to be more dependent on nutrient availability, chlorophyll will depend more on available light.

The model is able to simulate a physiological response by producers to seasonal changes, and this behaviour is particularly evident in Chl*a*:C ratios (bold line in figure 3.22). In contrast to Chl*a*:C static ratios, a dynamic approach allows Chl*a* internal concentration to fluctuate in response to light availability and nitrogen availability. So, Chl*a*:C values are not necessarily related with Chl*a* concentration values, and it is possible to have low Chl*a* concentration and still to maintain a high Chl*a*:C ratio (e.g., last trimester in figure 3.22 B). There is a clear seasonal pattern in Chl*a*:C ratios, consisting of higher values in autumn and winter (low radiation) and lower values during spring and summer (high radiation). This is a clear response to light availability; as light availability decreases, producers compensate by synthesizing more Chl*a*. This adjustment mechanism provides an adaptation to environmental conditions which can be seen on a seasonal scale, but also on a diurnal scale. This daily variation is represented in Figure 3.23 only for two producers groups because they represent the higher and lower range of values of Chl*a*:C ratios. Notice that higher values occur at night (around 6 a.m.) and, consequently, lower values during day time (around 4 p.m.). Again, this is a response to light availability. The adaptation mechanism is sensitive enough to adapt to diel cycles, yet without allowing Chl*a* concentration to increase too fast. In addition, the C assimilation in the light and C respiration in the dark also contributes to this pattern. Therefore, the model is able to impose an adaptation period before production increases when sporadic periods of light availability are higher but still enabling a response to conditions in order to show a seasonal trend.

Silica quota also varies in diatoms (figure 3.24), with the variation closely related with carbon dynamics. Silica differs from N and P dynamics because there is only one reference value for the Si:C ratio and not a range defined by a maximum and minimum quota. As such, variation around the defined Si:C

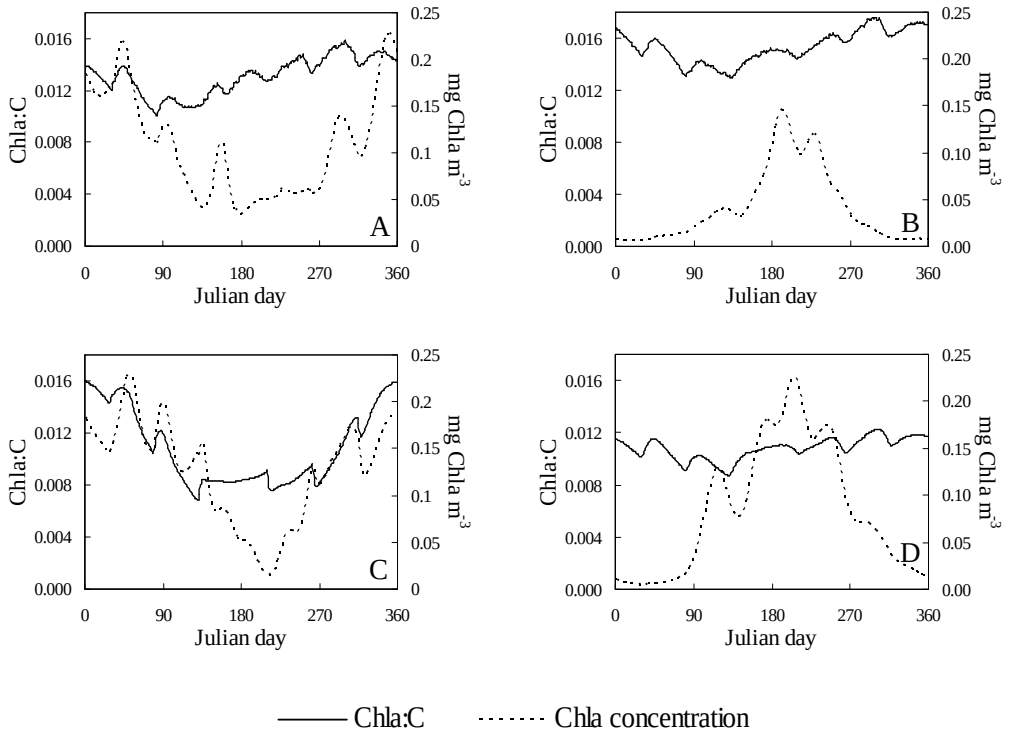

Figure 3.22: Chl$a$ concentration (dashed line) and Chl$a$:C (bold line) dynamics. Key to producer groups: (A) diatoms; (B) autotrophic flagellates; (C) picoalgae; (D) mixotrophic flagellates.

ratio are minor. Nevertheless, if DOC is excreted the ratio will eventually increase and the model compensates that by excreting the excess silica to maintain the ratio around the predefine value (χ_s^R in equation 2.40).

Looking at figure 3.25 it is possible to evaluate the nutrient cell content (quota) of each producers group during the simulated period. The percentage of full nutrient reserves were chosen in the graphics instead of actual ratios (mmolNut/ mg$C$) because it facilitates the interpretation of nutrient quota status. Diatoms and autotrophic flagellates have a similar pattern of nutrient quotas, with reserves values always above 87% of full. The lowest values of both nutrient quotas are observed during the third trimester reflecting in part the low levels of nitrate and the slight depression in ammonium after the late spring peak (figure 3.16A).

Picoalgae show a clear limitation by nitrogen, a pattern that can be explained on the nitrogen availability for this particular group. Unlike other producer groups, picoalgae do not have the cellular machinery to reduce nitrate, relying only in ammonium as the only source of N. So, the availability of this nutrient to picoalgae is always reduced when compared to other

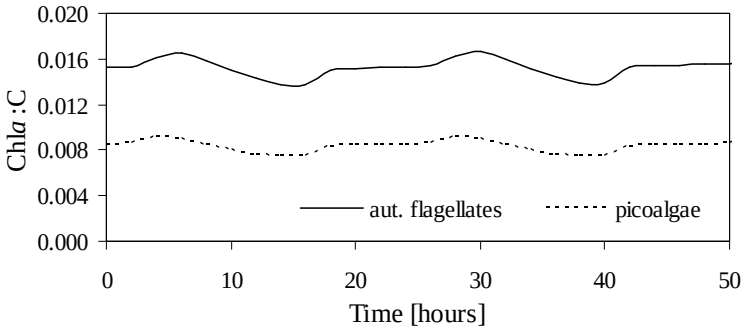

Figure 3.23: Dynamics of Chl*a*:C ratio over a period of approximately two days. Only autotrophic flagellates and picoalgae variation is shown.

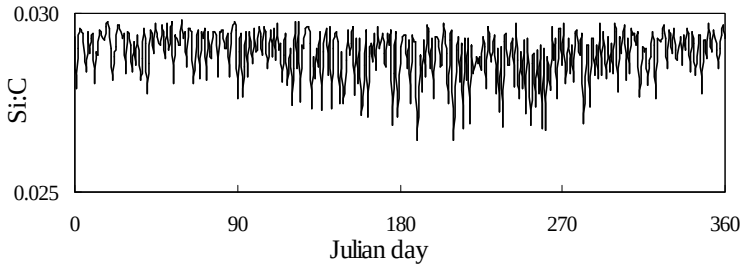

Figure 3.24: Dynamics of Si:C ratio in diatoms.

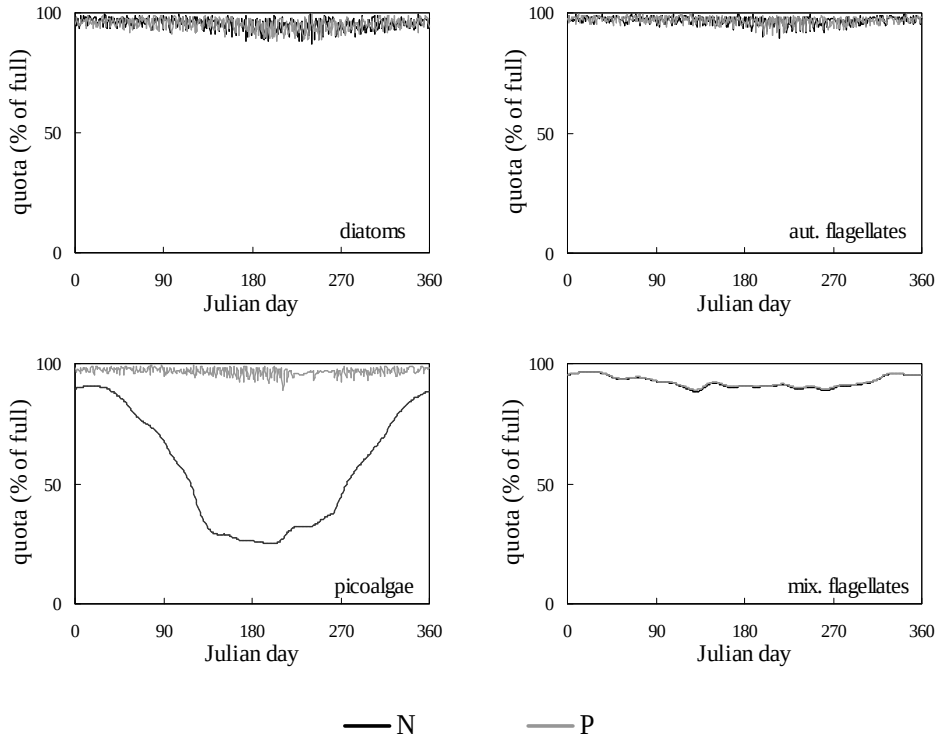

Figure 3.25: Dynamics of the physiological state of producer groups, graphing internal nitrogen (dark line) and phosphorus (grey line) quota (percentage of maximum quota).

groups.

High nutrient quota values denotes a limitation by factors other than nutrient availability, usually by light. So, the growth of producers groups in this condition is not nutrient dependent. In picoalgae, where only P:C quota show this behaviour, N is limiting production. Nutrient quota pattern in diatoms and autotrophic flagellates and P quota in picoalgae are a result of the underlying biological response to the daily light cycle (assimilation, respiration, exudation, etc.) and the daily fluctuation in nutrient availability (as a result of biological activity). However, this pattern is not observed in mixotrophic flagellates despite their sharing the same processes (quota variation is represented by a smooth line). The difference is explained by their hybrid parameterization combining both producers and consumers processes. Hence, they are not as dependent on external nutrient concentrations as other producers because they have an extra nutrient source in their heterotrophic feeding behaviour. Their nutrient quota mechanisms are also different from other producers because they possess the typical nutrient assimilation/recycling parameterization of consumers.

Consumer nutrient quotas are significantly lower than producers quotas, as it can be seen in figure 3.26 showing all heterotroph (mixotrophs excluded) quotas. For simplicity, here also is shown the nutrient quota status rather than the actual nutrient:carbon ratio. Unlike producers and decomposers that excrete nutrient excess directly, consumers release (mineralize) nutrients in a constant flux imposed by their parameterization of assimilated and recycled fraction of grazing products (see equations 2.60 and 2.61). This explains the fact why nutrient quota values are so low when compared with producers. In addition, consumers parametrization philosophy does not consider nutrient storage in the same way as producers. As a consequence, the "quality" of a nutrient source for consumers (prey nutrient content) can change the consumer nutrient quota slightly. The feeding dynamic (preys, feeding rates, etc.) impact on the nutrient quotas of each consumer is illustrated in figure 3.26. Another way where the "food quality" is evident is in P quotas that are systematically lower than N quotas. Taking into consideration prey maximal P:C ratios (producers and decomposers in table 3.7), it becomes clear that consumers have higher P:C ratios than its prey and so they will always have a P deficit. But prey nutrient content is more significant to the amount of nutrient that is recycled, i.e., the higher the nutrient prey content, the higher the recycled flux will become.

Decomposers are the only group of organisms where both quotas are kept full throughout all the simulation period, independently of seasonal cycles or predation pressure (figure 3.26). Explaining this occurrence is the fact that besides sequestering nutrients taken from DOMl, they are also able to uptake nutrients in their inorganic form. Eventually their nutrient:carbon ratios go above the defined maximum and mineralization takes place. In the process, DOM nutrient:carbon ratio plays a decisive role influencing the mineralization. Because all organisms require carbon, nitrogen and phosphorus in a certain proportion to growth, when nutrient quotas are full they become carbon limited, as happens with decomposers in this particular situation. Though C:N and C:P ratios are higher in decomposers substrate (DOMl in figure 3.27; values in table 3.7), implying more carbon in proportion, C is in shortage to decomposers given their extra nutrient uptake from mineral forms.

Each organic matter compartment has its own nutrient:carbon dynamics. Because there are no additions to the system (i.e. allochtonous element source), all organic matter components are produced and used within the system. For this reason all nut:C ratios tend to be constant, depending exclusively on biological activity.

The relation between all organism groups and OM components regarding the maximum values of nut:C ratios is presented in table 3.7. Of all functional groups, producers have the highest nut:C ratios because they are allowed to store as much as twice the Redfield ratio. This characteristic, however, is user-defined and so lower values can be established according

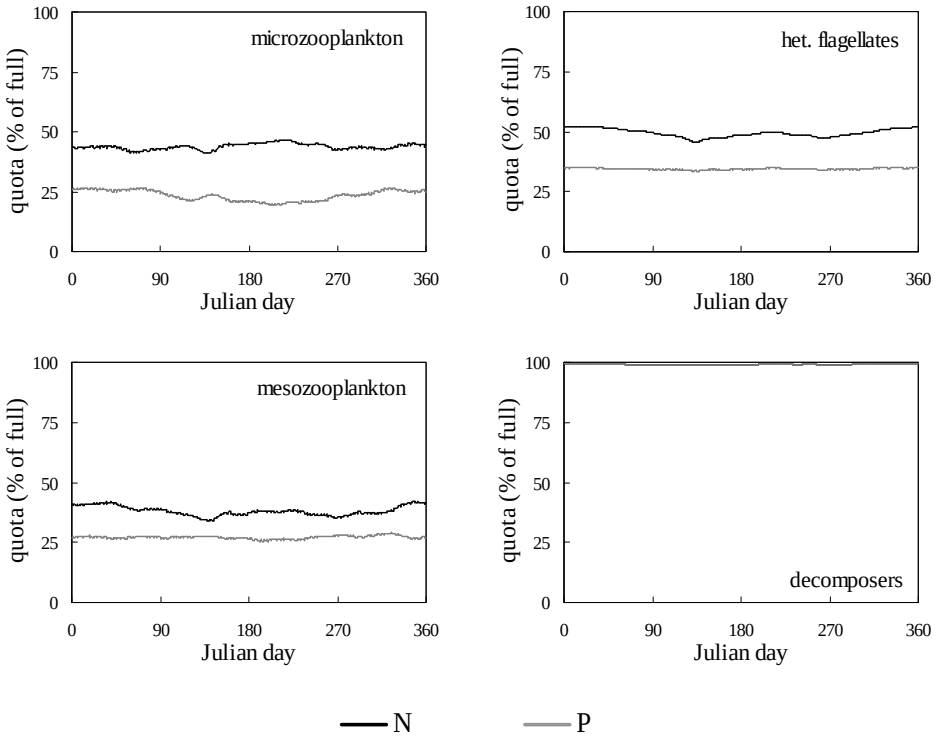

Figure 3.26: Dynamics of the physiological state of consumers groups and decomposers: internal nitrogen (dark line) and phosphorus (grey line) quota (percentage of maximum quota).

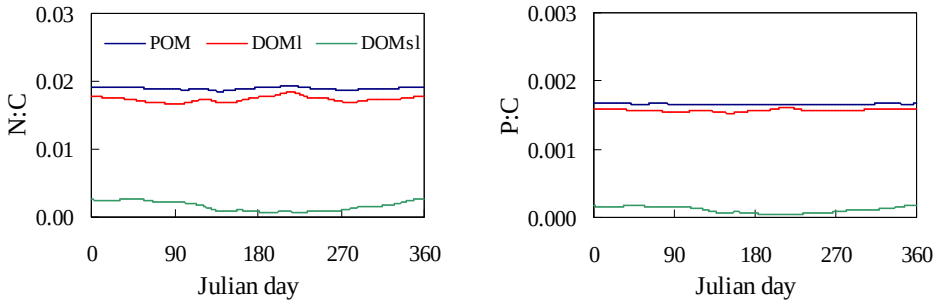

Figure 3.27: Dynamics of nutrient ratios in all organic matter components: particulated (POM), dissolved labile (DOMl) and semi-labile (DOMsl).

Table 3.7: Maximum values (approximated) of N:C and P:C observed in the results for each model compartment.

	maximum (mmol/ mg)	
	N:C	**P:C**
Producers	0.024	0.0015
Consumers	0.016	0.0017
Decomposers	0.019	0.0016
POM	0.019	0.0017
DOMl	0.016	0.0015
DOMsl	0.0023	0.00015

to the systems and the producer groups addressed. In this particular case, producers have higher ratios than bacteria, which is not usual in natural systems. In OM groups, semi-labile DOM (DOMsl) has the lowest nutrient content. This occurrence is determined by the sources for DOMsl components. DOMsl carbon has an additional source from phytoplankton exudation that is not present in nitrogen and phosphorus dynamics. This additional source of carbon for DOMsl is responsible for keeping nut:C ratios low.

3.4 Testing temporal resolution

The rate of change (or flux) of a given property C in a particular time step, Δt, is proportional to the product $\Delta C \Delta t$. From this it is possible to conclude that the rate of change in the property is proportional to the slope of the line denoting concentration variation between two successive time intervals, and this line also indicates the errors associated with the choice of t. As a rule of thumb, the smaller the time step, the smaller the introduced error will be, because numerical dispersion is, among other factors, a function of time. But on the other hand, a small time step means that the total running period will be divided in smaller temporal segments, and consequently more calculations will have to be made, increasing the total computation time.

As the spatial resolution is increased (i.e. the separation between grid points is reduced) the time step must be decreased to maintain computational stability, at least for the explicit techniques that are generally used. But the desire to increase the resolution of a model may be constrained by the speed and storage capacity of the computer. Assuming that the model will be implemented in 2D/3D scenarios, the additional requirements in computational cost of the water quality time step must be considered, despite the fact that a control volume approach is implemented.

The physical characteristics of the modeled systems usually dictate the necessary resolution, both spatial and temporal. As a consequence of the control volume approach around which the model was developed, in this

particular study the assessment of the time step influence on the solution is only restricted to water quality processes, not having to deal with spatial derivatives. The water quality model is independent of any transportation scheme, so it has its own time step defined solely on the basis of the biological/chemical processes considered in the model. The process scales covered by the model range from a few hours in some processes rates mediated by decomposers up to the scale of months in some cases of organic matter degradation. To assure stability and accuracy, the typical reaction time scales must be longer than the constant model time step, and the choice for an acceptable time step must take this into account. Given the nature of most modeled processes, a relatively fine temporal scale is required. Usually, for models of this nature a time step of 3600 seconds is considered acceptable.

To test the model robustness or sensitivity to the time step, some simulations were made running the same set of conditions (the same as for the standard long time run) with different time steps. To cover different magnitudes, tested time steps were 90, 900 and 3600 seconds. As it can be seen in figure 3.28 where the temporal evolution of several properties is portrayed for the different time steps, the solution remains stable irrespective of the time step used. However, some expected fluctuation can be seen in some properties evolution in time, specially in flagellates, microzooplankton and decomposers. Comparing all time steps, the higher time step (3600 s.) shows the biggest differences (figure 3.29). A systematic difference between 3600 and 90 seconds can be noticed and its magnitude varies in time, but never higher than 20%. For a forty-fold increase in the time step, a 20% variation does not seem relevant.

The other tested time steps show a striking convergence in results which implies that below 900 seconds there is no significant change in results induced by the time step. This does not mean, however, that a time step of 3600 seconds must be avoided. By pondering the computation time cost and the model performance in such a scenario, a time step of one hour is fairly acceptable. To support this claim, a look at figure 3.28 shows that the overall results of the simulation are not changed by any of the tested time steps.

Stability connotes with errors that are not amplified as the computation progresses, i.e., are not amplified by the solution scheme. An instable solution is one where errors can corrupt the true solution. Implicit integration methods have better stability properties than explicit methods [136], but at least for growth equations, an explicit scheme is better for the stability of the model. Nevertheless, explicit schemes are known to be conservative, but for sufficiently large time steps they may compute negative values for non-negative state-variables. A small time stepping may avoid this outcome but with a potential high cost, namely an enormous increase of the computational effort. As a result, these schemes may lose their practical relevance

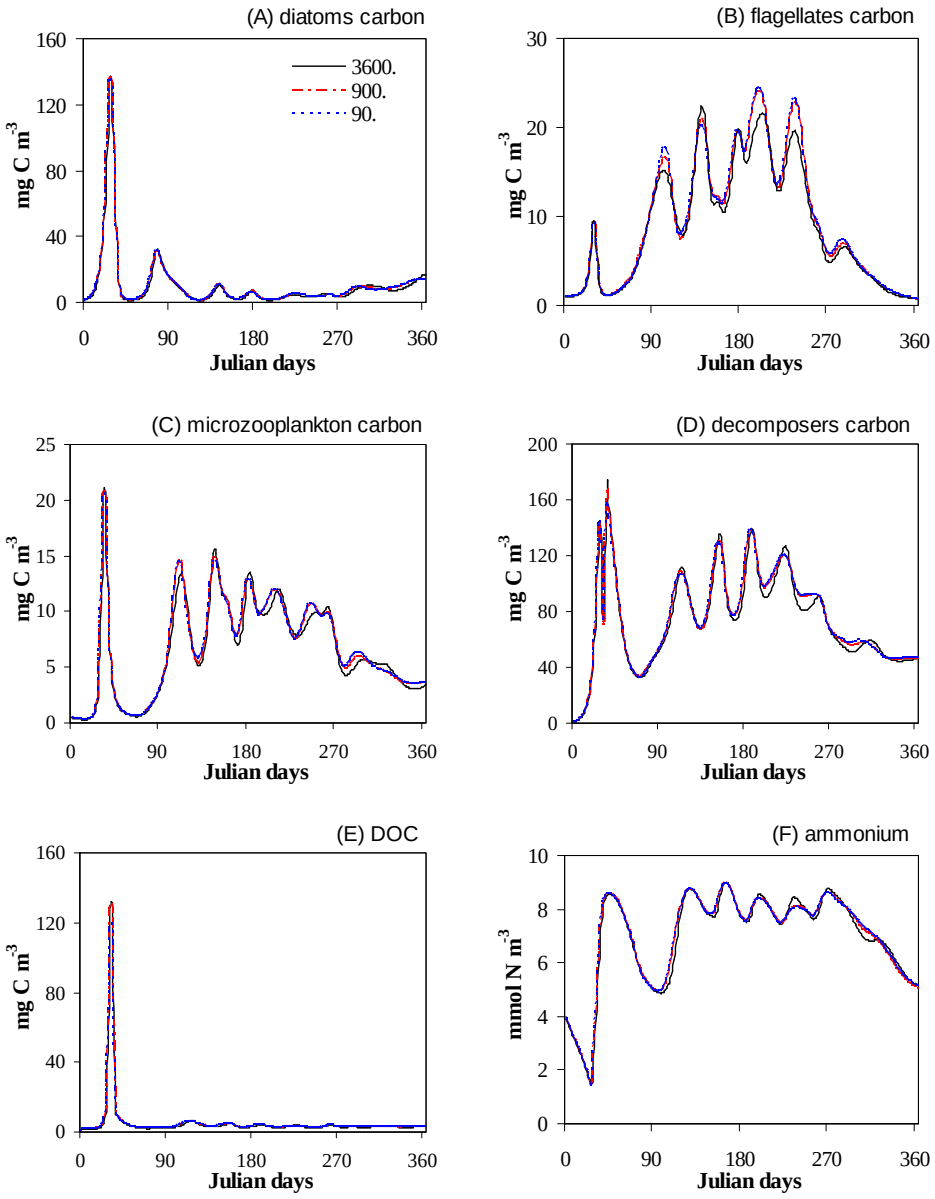

Figure 3.28: Comparison between runs with the same basic setup but with different time steps (3600, 900, and 90 seconds): (A) diatoms carbon, (B) flagellates carbon, (C) microzooplankton carbon, (D) decomposers carbon, (E) DOC, and (F) ammonium. Properties were chosen to have at least one representative of each group, namely, producers, consumers, decomposers, organic matter, and nutrients. None of the remaining properties show any relevant difference between time steps.

in some contexts.

Overall, the results show that for the wide range of time steps evaluated, the solution never become unstable for any time step. Even an increase in the reference time step (to 5400 seconds) didn't result in any undershoots, but instead the model converged to the same solution (figure 3.30). Ultimately, this result is true for the 0D case where there are no spatial gradients. So, this conclusion must be carefully extrapolated to other scenarios such as 3D settings where steep vertical gradients can occur. Because the specific influence of a given time step to the overall outcome of the model is a difficult task given the complexity of relations in the model and of little profit in the present context, it will be not attempted here. Ultimately, comparing model outcome with different time steps only makes sense strictly in the actual set of conditions. Hence, using the same model with different values in some rates will result in a different response to the time step.

3.5 Sensitivity analysis

Sensitivity analysis can be broadly described as a process by which the contribution of input parameters to uncertainties in the model outcome is evaluated. Several parameters in ecosystem models represent specific process coefficients that are only measured with difficulty (if possible at all). As a consequence, there are uncertainties related with the parameterization and the nonlinearity of interactions within the model. This raises two basic questions: (a) how sensitive is the model to changes in individual parameter values, and (b) which parameters or associated processes have most influence on specific output variables? The answer to the first question may reveal which parameter values might need further attention and where possible modifications should focus to achieve robustness is model results. The answer to the second question will help to understand the simulated system. One way to try to answer these questions and assess model performance can simply be addressed via a systematic sensitivity analysis (SA) by which variations of single parameters effect on specific output variables are studied.

Sometimes the large number of input values in the habitual "one at a time" SA perturbation method requires excessive computation times. In addition, it is aggravated by serious difficulties in visualizing the results in a comprehensive manner. This is usually the case of complex ecosystem models, nesting physical and biological parameterization. To avoid a sensitivity matrix with numerous columns or rows, some proposed methodologies analyze not single parameters but rather clusters of related parameters in group-collecting sensitivity analysis, reducing the total amount of required variations by at least a factor 1/9 [137]. In those cases, however, not just the parameters of ecological models are analyzed, but also from the transport, and all external inputs. Despite all the advantages of such SA tests,

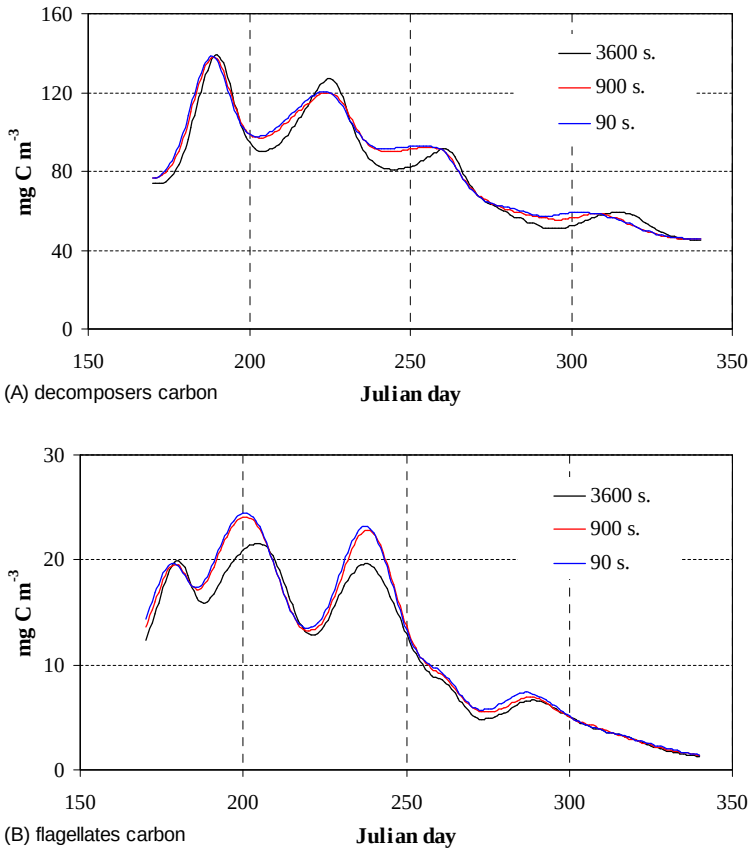

Figure 3.29: Evolution of two properties in response to different time steps: (A) decomposers, and (B) flagellates carbon. Results were choose for a specific temporal window for a better illustration of the changes induced by the time step.

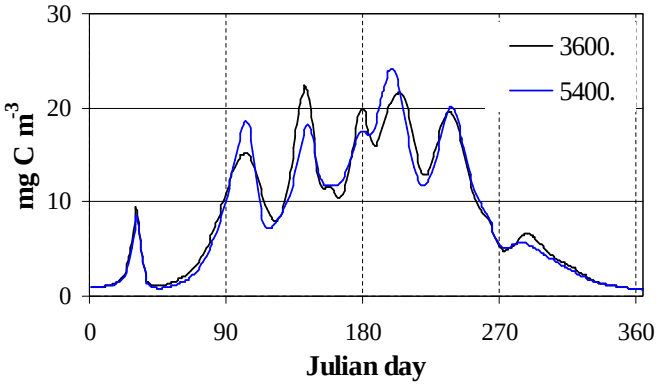

Figure 3.30: Flagellates carbon response to a time step of 3600 and 5400 seconds. Despite the obvious differences in the temporal evolution, the model is still able to stick to the same pattern and arrive at the same final solution. This means that a time step of 5400 seconds would still be feasible under certain conditions.

one of its drawbacks is that it can mask the importance of some individual parameters in model performance.

3.5.1 Methodology

Given that *mohid.Life.1.0* is independent of any transport scheme, only the parameters exclusive to this model are analyzed. To reduce the amount of information and aiming for simplicity in the analysis, the reference simulation for this study is simplified by considering only one producer and one consumer. All other state-variables remain the same. This can be done because the code is the same for all producers (except for silica dependence and mixotrophic behaviour) and for consumers. A full sensitivity analysis would require not just the study of individual effects of each parameter, on their own and in combination with other parameters, but also the changes in sensitivity of variables over time. For the purpose of this study, the sensitivity analysis aims at gaining some additional insight into the processes driving the model and so a simple analysis was undertaken.

The modeled mean state is defined as the "standard" run, which provides a base for a series of parameter sensitivity analysis. The results of the sensitivity analysis are classified by distinguishing model parameters with a qualitatively different effect on model results. With this set of simplified conditions, a single parameters effect analysis on model performance was used. The impact of initial properties values on the overall result of the simulation are also analyzed. This was achieved by singly and sequentially altering the standard parameterization with up- and down-variation of each

parameter, by 10% up and down in a series of separate runs, while holding all other terms constant. A raised and lowered 10% of parameter perturbation is frequently adopted ([25, 23]), hence its use in the present study. The initial value of variables was also disturbed to study the model sensitivity to initial conditions.

Sensitivity index

The definition of a sensitive index is not universal. Among the several indexes used to quantify parameter sensitivity, it was chose for this study one quantifying normalized sensitivity but with the ability to reveal up and down variation. Normalized sensitivity, $S_{(p)}$, is defined as the relative change in model output divided by the relative change in the parameter value. It is calculated as:

$$S_{(p)} = \frac{\left(V_{(p)} - V_s\right)/V_s}{\left(p - p_s\right)/p_s} \tag{3.2}$$

where all variables with an S in the lower index represent standard case values (V_s the value of a given variable for the standard case with parameter p_s), and $V_{(p)}$ is the value for the case when the parameter is given the value p. This method was proposed by Fasham *et al.* [40] and adopted in other studies (e.g. [23]). According to this sensitivity index, a negative parameter perturbation (10% below in this case) with a negative index result means a positive perturbation in the end result (meaning a higher end value compared with the reference run value) of a given property, whereas a positive index result means a negative perturbation in the result (a lower end value compared with the reference run value). Conversely, a positive parameter perturbation (10% above) will give a negative index result if a negative end result is achieved, and a positive index result with a positive end result. The degree of model sensitivity towards a given parameters can be defined as sensitive (S>0.1, meaning a change of more than 1% in the result when compared with the reference value), highly sensitive (S>1, meaning a change of more than 10%), and extremely sensitive (S>1, meaning a change of more than 100%). Whenever S<0.1, it can be said that the model is not sensitive to that parameter. However, it must be kept in mind that the bias achieved by omitting some variations is a frequent or potential error that might occur in a systematic SA. In addition, it is difficult to choose the magnitude of parameter perturbation in a way which avoids non-realistic values but at the same time covers the interesting span [137].

Variables of interest

Given the high number of state variables within the model, the choice of result variables to monitor the sensitivity of parameters must be case-specific. Considering too many variables in this study might prove to be ineffective

by reducing the comprehensibility of the analysis. Hence, only some meaningful variables were chosen and others were combined in integral measures (table 3.8) to compare the values after perturbation with the unperturbed value.

The choice of sensitivity indicators was based on the major lines of development behind the present model (e.g. multi-nutrient cycles, bacteria-phytoplankton interactions, variable Chl*a* quotas, etc.). So, the biomass of functional groups and the concentration of nutrients and labile-DOC in water are of interest in this study, as it is the chlorophyll content. The $P_c : B_c$ was chose to evaluate the varying microbial community composition in response to different parameters values. Finally, and to complement the study, another variable is added in the form of an index to quantify the system behaviour over the whole range of different trophic levels, from substrate (organic matter) to top predators. It is the Shannon-Wiener Index (SWi_c) of diversity, applied to all carbon reservoirs (i.e. carbon biomass in organisms and organic matter) in the model. It is defined as:

$$SWi_c = -\sum_{i=1}^{X_c} \frac{C_i}{T_c} \ln\left(\frac{C_i}{T_c}\right) \tag{3.3}$$

in which X_i is the number of carbon fluxes, C_i the carbon content of the ith reservoir, and T_c the sum of all carbon reservoirs. This particular use of the Shannon-Wiener Index follows part of the methodology proposed by Köhler and Wirtz [137].

Simulation runs

All simulations were forced with the same environmental data presented in figure 3.14, and run over two years. In order to save on computing time and to avoid the "chaotic" oscillations characteristic from the first year run, the test runs started with the variable concentrations obtained after an initial running period of a year and four months with the standard parameterization (tables 3.1 to 3.5). The analyzed values were taken by the end of July in the second year and compared with values from the reference run observed at the same temporal moment. The running time window for the sensitivity analysis comprised a period of 90 days during the second year, starting on the 1st of May and ending on the 1st of August. All result variables show seasonal behaviour. Hence, this particular time window was chosen to include the formation and destruction of a spring bloom, avoiding a period of model stasis. Results of the reference run are illustrated in figure 3.31. Despite almost all variables show seasonal behaviour, parameters impact on this variability is only mention if found relevant. Almost all variables addressed in this analysis correspond to state variables defined in the model (except $P_c : B_c$ and SWi_c). As such, the term "variable" will be loosely used throughout the sensitivity analysis discussion.

Table 3.8: List of selected result variables to assess model sensitivity.

Symbol	Description
P_c	Biomass of producers
Z_c	Biomass of consumers
B_c	Biomass of decomposers
NH_4	Concentration of ammonium
NO_3	Concentration of nitrate
PO_4	Concentration of phosphate
Si	Concentration of silicate
$Chla$	Chlorophyll concentration of producers
$Doml$	Concentration of labile DOM
$P_c : B_c$	Producers ratio to decomposers
SWi_c	Shannon-Wiener diversity index of total carbon

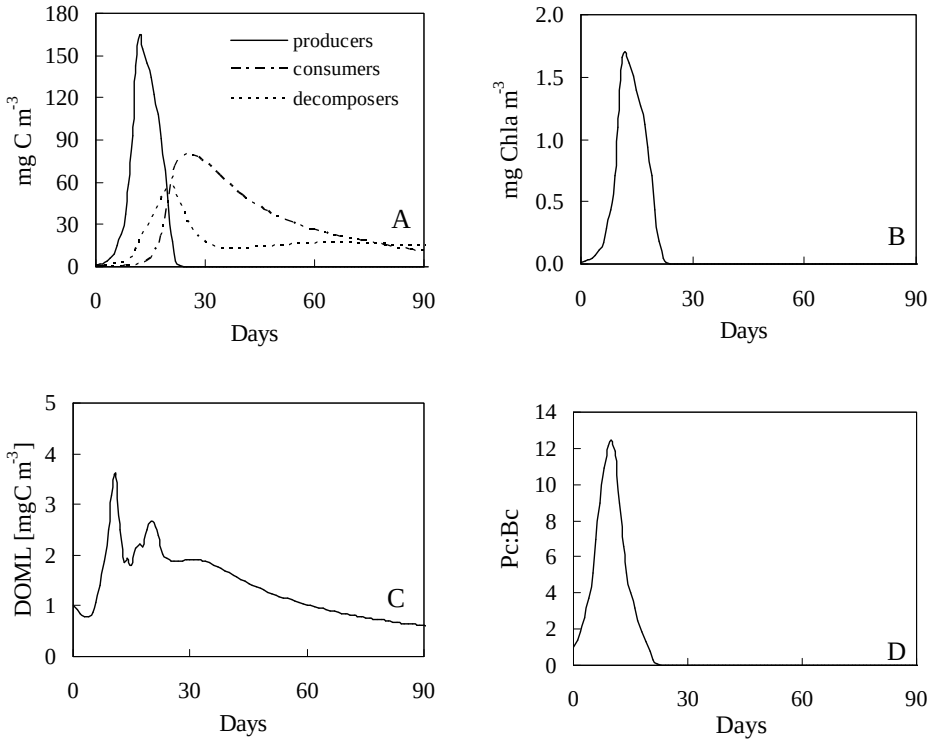

Figure 3.31: Results used as reference in the sensitivity analysis: (A) producers, consumers, and decomposers carbon biomass, (B) Chl$a$, (C) DOMl, and (D) $P_c : B_c$.

3.5.2 Result matrix and discussion

Given the high number of parameters used by the model, the result matrix of the SA is extremely extensive. To minimize superfluous information, only the most relevant parameter influence on model results, i.e. denoting moderate or high model sensitivity toward that parameter, are more thoroughly discussed. In addition, results are shown and discussed on a qualitative basis (interval of values) and only occasionally on a quantitative basis (the specific result value). Only general patterns are addressed in this analysis, and only a few striking relationships between individual result variables and a variety of parameters are highlighted.

Except for the maximum rate for DOM hydrolysis (V_{hyd}^{DOMsl}), DOMsl hydrolysis half saturation constant (k_{hyd}^{DOMsl}), producer affinity to phosphorus (k^p), decomposers assimilation efficiency at low oxygen concentrations (ass_{low}^{ef}) and oxygen half-saturation constant (k_b^o), the model is moderately sensitive to most parameters. The lack of model response to the last two mentioned parameters is due to permanent high oxygen concentrations in the entire running period. The observed sensitivity, however, is not noted in all model compartments, implying that a single parameter may have the capacity to have an impact on one or a group of state variables, but not on the overall result of the model. Under the present set of chosen parameter and variable values, only one parameter, namely the reference temperature in decomposers, shows the potential to influence model results as a whole (expressed in the Shannon-Wiener Index). Even so, the model sensitivity to it is rather low (<0.2 in both upper and lower parameter value disruption, meaning an overall change below 2%). From this observation, it can be said that though some parameters may lead to pronounced changes in some variables, the Shannon-Wiener Index was mostly insensitive to them.

Of all variables studied in this SA, nutrients were the least affected in terms of number of parameters to which they are sensitive. Model nutrients components sensitivity to parameters perturbation never exceeded 10% upper or lower variation in the final result. From this, it is possible to conclude that nutrient variables are the most robust. Silica is the variable affected by the lower number of different parameters, probably because of its dependence of producers dynamics only. Remarkably, none of producer parameter disruption cause any significant change in the final outcome of silica. Biogenic silica dissolution rate upper and lower perturbation, produced a minor impact (<10%) on silica which implies that although controlling the transition between two forms of silica, the model is not very sensible to it. Besides this, the other parameters to which the model silica compartment is sensitive are related to consumers grazing activity, namely the reference temperature, assimilation efficiency and the maximum specific uptake at a reference temperature. Based on these results, it can be stated that it is the grazing pressure that has a higher control on the silica abundance, probably

because it diverges silica that has been incorporated by producers to biogenic silica and/or it controls producer abundance modifying silica consumption.

Phosphate only reflects the variation of two parameters: the positive perturbation of maximum and the negative perturbation of the minimum P:C consumers ratio. By defining the ratio range of consumers, both parameters affect directly the immobilization and mineralization of phosphorus. Hence, their perturbation has a direct impact on phosphate, even though not a significant impact (also below 10%). Since nitrate is not a product of mineralization, it is not affected by any consumers or decomposer parameters. In this case, nitrate is only affected by the nitrification rate change (both positive and negative) and by the maximum N:C producer ratio. Again, the perturbation is less than 10%. Because it mediates the transformation of nitrogen forms, nitrification rate also affect ammonium results. The only producers parameters able to change ammonium model outcome are the maximum and minimum N:C ratio, the positive perturbation of the affinity for nitrate $\left(k^{n1}\right)$, and the reference temperature. The same is observed for decomposers N:C maximum and minimum ratios. Of all groups, consumers have more parameters affecting ammonium dynamics probably because of its important role in nutrient mineralization through grazing and subsequent nutrient recycling. Almost all grazing activity parameters have a minor effect on ammonium ($Temp_{ref}$, ass_z^{ef}, V_z^{max}, k_z, and $\beta_p^{Z^i}$). Curiously, many results lie within the expectations given their influence on some variables, while others revealed unexpected insensitivities or extremely sensitive responses.

Because a detailed analysis of the results would pose some difficulties of interpretation in terms of the model response and lead to conclusions of doubtful accuracy, the remaining results are presented in tables, a table per functional group, where the impact of each parameter is mentioned in a qualitative way. The tables provide a condensed view of the complexity of the interrelations between parameters and variables within the model. These tables can be used as look-up tables to identify sensitive responses in real cases applications. Some specific results need to be addressed more carefully given their relevance in changing some variables outcome and the particular model sensitivity towards them.

General parameters

In table 3.9 it is possible to see the model sensitivity towards some parameters that are not necessarily related with any functional group. The list is reduced to only three parameters because all others do not cause any significant impact (above 1%) on variable results. Biogenic silica dissolution rate (ν_{nl}) perturbation induces a moderate change in results, especially in producers (also reflected in chlorophyll) and consequently on the producers:decomposers ratio. This impact is probably due to producers limitation

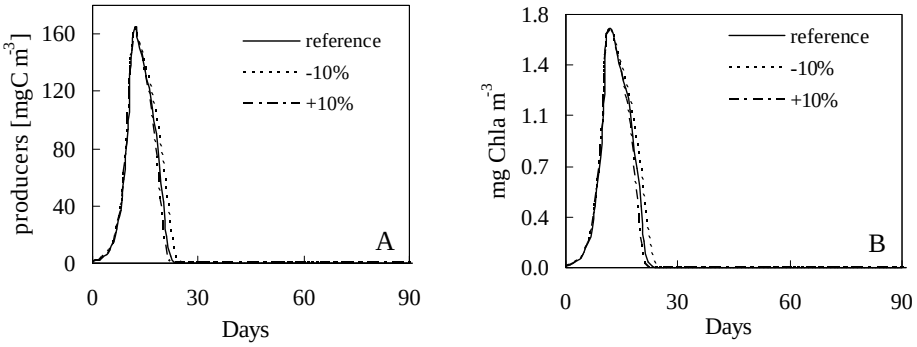

Figure 3.32: Time evolution of two variables considered in the sensitivity analysis: (A) producers carbon and (B) producers Chl*a*. Despite being extremely sensitive to POM hydrolysis maximum rate, the model evolution in time is not affected by the disturbance of this parameter. Parameter perturbation result lines coincide with the reference result in both cases.

by silica in this particular run. It can be hypothesized that model sensitivity to nutrient dynamics related parameters will increase with increased nutrient limitation. As already mentioned above, V_{hyd}^{POM} and k_{hyd}^{POM} are able to induce small changes in nutrient variables. Despite the small influence on nutrients, both parameters have a high impact on producers, specially V_{hyd}^{POM}, able to induce a change in some variable results one order in magnitude. This value alone can wrongly lead one to assume a drastic change in model dynamics induced by this parameter alone. However, by plotting the results together (figure 3.32, reference and both upper and lower parameter perturbation) it is possible to notice that the model behaviour is not affected at all. Hence, the extreme sensitive to this parameters is only achieved at extremely low variable values (it must be consider that most values are compared to the 16th decimal house). Nevertheless, this change might induce different scenarios if conditions are met for the variable values increase again in time.

By controlling the rate at which DOM originated in POM hydrolysis becomes available substrate to decomposers, these parameters influence bacterial production. This, in turn is reflected on producers dynamics through nutrients competition. Curiously, the impact on decomposers is rather small. Nevertheless, the influence is obvious; a negative perturbation of V_{hyd}^{POM} increases producers total biomass and a positive perturbation decreases it. This means that higher V_{hyd}^{POM} values means higher availability of DOM and better conditions for decomposer to grow. The outcome is a decrease in producers biomass.

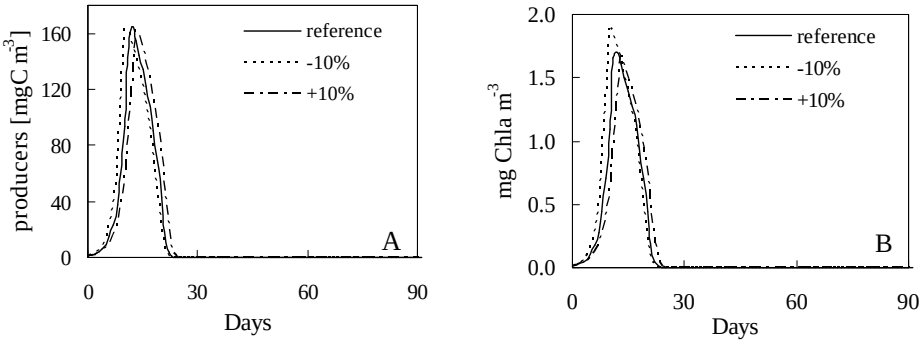

Figure 3.33: Time evolution of the response of two variables to $temp^{ref}$ perturbations in the sensitivity analysis : (A) producers carbon and (B) producers Chla. As it can be noticed, there is a slight change in producers response, denoting the model sensitivity.

Producers parameters

The sensitivity analysis of producers parameters, shown in table 3.10, revealed a relatively low or insignificant impact of their perturbation in the result of consumers and decomposers, the exception being for r^{ass} and $Temp_{ref}$ with a sensitivity of S<0.1 in consumers. Overall, the nutrient affinity to both forms of nitrogen were the parameters with less effect on variables. The model is extremely sensitive (S>10) only to three producers parameters, namely, exudation under nutrient stress (ϕ^{ex}), maximum assimilation rate (r^{ass}), and the reference temperature ($Temp_{ref}$). Their effect is particularly relevant in producer related variables like producers carbon and Chl*a*. The effect can be explained based on the conditions of the run. After the bloom, the values continuously decrease throughout the run, reflecting a lack of response by producers biomass conditioned by nutrients availability. So, by the time the run ends, the nutrient stress is high and parameters governing growth and response to nutrient stress have a more dramatic effect when compared to others. This is observed in the decrease of ϕ^{ex}, meaning lesser exudation under nutrient stress, which results in a positive perturbation on producers carbon. The higher sensitivity index value observed is for the $Temp_{ref}$ upper perturbation in Chl*a*. Overall, $Temp_{ref}$ is the parameter to which producers are more sensitive, an expected occurrence given the control of temperature on several physiological processes. Figure 3.33 illustrates the magnitude of change in producers carbon induced by the perturbation of this parameter. While being able to increase or decrease the peak of producers carbon in the bloom, the parameter perturbation didn't cause any change in the pattern or magnitude in the model response, in this variable or any other.

Consumers parameters

Generally speaking, consumer parameters prove to be the set of parameters to which the model is more sensitive. Looking at table 3.11 it possible to notice that only one parameter (minimum N_:C ratio, χ_n^{min}) did not cause any change in results. All other parameters cause a shift in the results to a greater or lesser extent. The model shows relatively low sensitivity to all parameters related with consumer ratios. The remaining parameters are highly or extremely sensitive to producers carbon and chlorophyll, consumers, and $P_c : B_c$. Parameter sensitivity to decomposers and $DOMl$ proves to be low (S<1). From this, it is possible to observe that consumers parameterization is important to the control of both producers and consumers groups, and not so relevant for the decomposers and organic matter dynamics.

Other relevant aspects of the sensitivity analysis of consumers parameters can be summarized as follows:

- Except for the nutrient:carbon ratios, only m_z^o, q_z^{POM}, k_z^o, and $\beta_b^{Z^i}$ were sensitive to variables (always S<1).
- None of the parameters is extremely sensitive to consumers (S<10 for all parameters).
- Only the variables P_c and Chl$a$, and as a consequence $P_c : B_c$, are extremely sensitive to some consumer parameters.
- The highest sensitivity values observed were (in decreasing order): ass_z^{ef} and $\beta_p^{Z^i}$, both for Chl$a$ and P_c. The sensitive index observed in ass_z^{ef} for Chl$a$ is the highest sensitive index registered in the sensitivity analysis.

Given the extremely high sensitivity of some model variables to ass_z^{ef}, an illustration of its effects on the same variables is useful to understand the change in model dynamics induced by a parameter perturbation. In figure 3.34 it is possible to see how ass_z^{ef} perturbation shifts the variable values from the reference value throughout the simulation period. Despite not being so sensitive to Z_c and B_c, this parameter shows a greater influence on their dynamic during the run than on P_c and Chl$a$.

Based on the results of consumers parameters, and comparing them with other parameters, it is possible to conclude that this group has the strongest effect on model behaviour. According to the results, it is possible to infer that this is achieved through grazing control on producers. In a sense it can be said that at least in this particular set of conditions, the system is top-down controlled.

Decomposers parameters

Of all biological groups, decomposers have the lower number of parameters for which variables are extremely sensitive. In the list of decomposers parameter sensitivity presented in table 3.12 it is possible to notice that variables are only extremely sensitive (S>10) towards $temp^{ref}$ perturbation

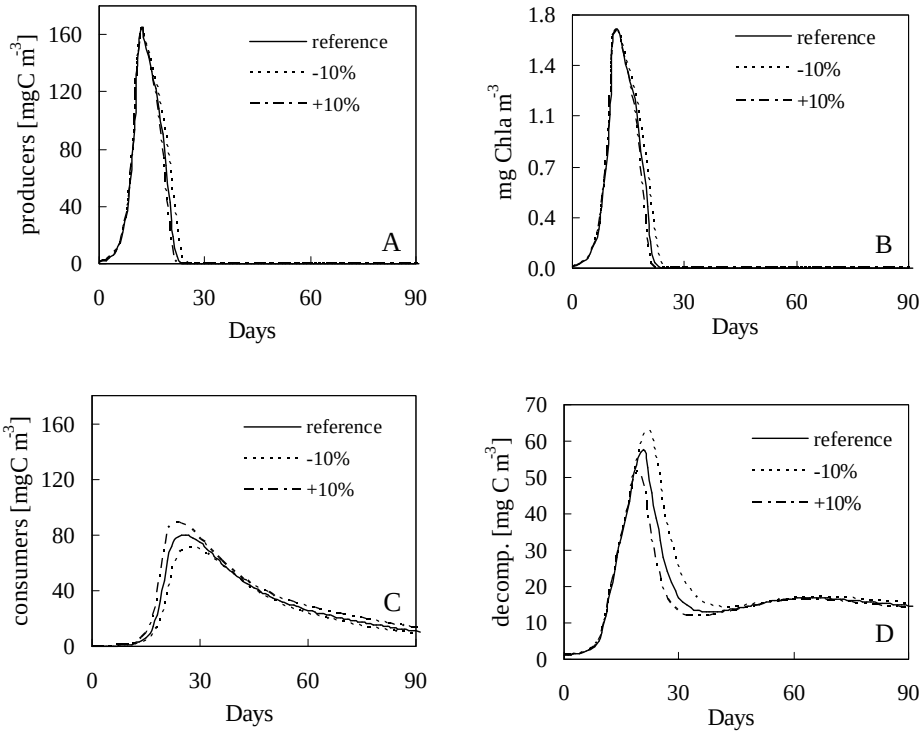

Figure 3.34: Time evolution of the response of four variables to perturbations of ass_z^{ef} in the sensitivity analysis : (A) producers carbon, (B) Chl$a$, (C) consumers, and (D) decomposers.

(particularly P_c, Chl$a$ and $P_c : B_c$). It is also possible to see in table 3.12 that this parameter is the only one for which all variables are sensitive to a greater or lesser degree (without considering nutrient variables as discussed above). By looking at figure 3.35 it is possible to notice that despite being extremely sensitive to some variables, the change in the behaviour of the variables is almost unnoticed. Again, and as in consumers, this is due to the response function to environmental conditions expressed in the control of temperature in various physiological processes. Producers related variables are the most sensitive to decomposers parameter perturbation. Considering all the processes addressed by the model (the microbial loop), any change in the processes controlled or influenced by decomposers will produce an effect on producers given their trophic relation of competition for nutrients or commensalism.

Without taking nutrients into account in the present discussion, Z_c and B_c where more robust variables to decomposers parameters perturbations, with all sensitivity indexes <1, i.e., without showing to be high sensitive to any parameter. Even so, they only reveal any sensitivity (S>0.1) to two parameters: $Temp_{ref}$ and r_b^{10} for Z_c, and $Temp_{ref}$ and m_b^{di} for B_c. DOMl, on the other hand, shows to be the least robust variable to consumers parameters when compared with the sensitivity to other biological groups parameters. Only among decomposers parameter set is possible to find some parameters to which DOMl shows high sensitivity, namely the parameters that directly affect the processes of DOMl uptake dynamic: $Temp_{ref}$ (it is possible to see the influence induced by this parameter perturbation in figure 3.35), V_b^{max}, and k_b^{DOM}. Intuitively it is possible to explain this occurrence on the basis of the DOMl sinks and sources parameterization. While there are many sources to the DOMl pool, there is only one sink, the bacterial consumption. Hence, any degree of variation on this flux is supposed to cause a more relevant effect on the entire DOMl dynamic (see fig. 3.35E).

Generally, all mortality related parameters show a high sensitive to some variables, denoting an important control on the model. As in consumers sensitivity indexes, nut:C ratios also show a lesser influence on the model performance. But unlike consumers, assimilation efficiency in decomposers (ass_{norm}^{ef}) prove to have an insignificant impact. This observation an be explained solely on the different parameterization of consumption in both groups and substrate type organisms in consumers and organic matter in decomposers). The affinity for nutrient does not show any relevant disturbance on model response, in a similar way as observed for producers.

Initial conditions

The perturbation of variables initial values impact on model performance in such controlled and theoretical conditions helps to assess how important slight variations can be to the model outcome. Contrary to parameters that

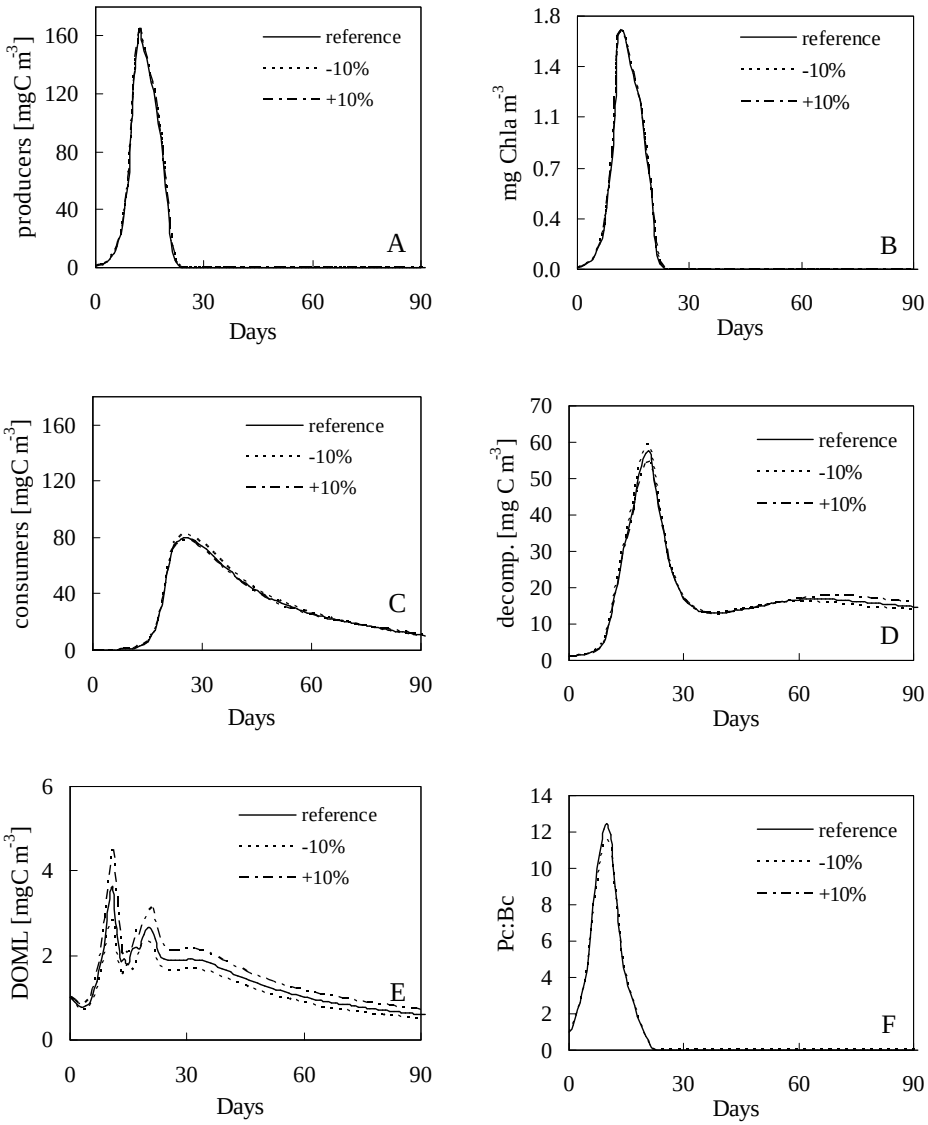

Figure 3.35: Time evolution of the response of six variables to perturbations of decomposers $Temp^{ref}$ in the sensitivity analysis : (A) producers carbon, (B) Chl$a$, (C) consumers, (D) decomposers, (E) DOMl, and (F) $P_c : B_c$.

condition model evolution in time because they are used throughout all the running period, initial values only set an initial conditions from which the model departs. Its impact is not made in successive incremental contributions but rather in one contribution whose effect may be influential by amplification or become minimal by fading during the simulation. Depending on model sensitivity to some variables, the magnitude of the impact will vary. Considering this punctual perturbation on the model (the starting point), it is expected that the model solution will not diverge on such minor perturbation. Looking at the impact of value perturbation on nutrients (table 3.13) it is possible to see that only the initial value of some state-variables induces relevant change in their own outcome. Most of these responses denotes a relatively low sensitivity (S<1), and only PO_4 and Si perturbation reveals high sensitive to theses variables. At least for PO_4, the perturbation is only noticed in its own result.

The remaining result sensitivity matrix of variables initial values is presented in table 3.14. A general analysis of the results shows that the model is moderately sensitive to a few variables (namely Z_c and Si), but overall it proves to be insensitive to initial conditions perturbations, with some variables without any impact on the model at all (e.g., $DOMsl$ and $BioSi$). As mentioned above for some Z_c related parameters, here too producers initial values prove to be sensitive to model behaviour trough their impact on consumers. The results show that the direction of perturbation results in the same direction of change in the final results of producers, and consequently on Chl$a$ and $P_c : B_c$. Finally, the impact of silicate acid initial value must be highlighted because its shows the higher sensitive values in the this particular analysis. As already mentioned, the extremely sensitivity notice around silicate acid (in this case the availability) is exaggerated inasmuch that only one producer (silica-dependent) is considered. So, a possible silica controlled production will have a high control on producers evolution and throughout the food web (noticed in high sensitivity of Z_c to silica initial values).

A closer look at the impact of silica initial values on model performance reveals that the influence of initial conditions is propagated during the simulation period, as seen in some variables illustrated in figure 3.36. But despite some fluctuations around the reference values obtained with the initial value, the pattern is not affect and model eventually converges to the same solution. Here too the model outcome shows high resilience to the proposed amount of parameters and initial values perturbation. Only silica initial value perturbation is illustrated because it achieved the highest values in the sensitivity analysis of all initial conditions. The variables whose evolution is portrayed in figure 3.36 were chosen because they are the most sensitive to silica initial conditions.

SA results synthesis

Nutrient variables are the least affected in terms of number of parameters to which they are sensitive, with sensitivity to parameters perturbation never exceeding 10% variation. So, it is possible to conclude that nutrient variables are the most robust.

There are only three producers' parameters for which the model is extremely sensitive: exudation under nutrient stress, maximum assimilation rate, and reference temperature. Overall, reference temperature ($Temp_{ref}$) is the parameter to which producers are more sensitive, an expected occurrence given the control of temperature on several physiological processes.

Results show that consumers parameterization is particularly relevant to the control of producers and consumers groups, and not so important for decomposers and organic matter dynamics. In addition, consumers' parameters have the strongest effect on the behavior of the model, probably through grazing control on producers.

Decomposers have the lower number of parameters for which variables are extremely sensitive, namely one parameter, $Temp_{ref}$.

In conclusion it can be said that this study shows that the proposed degree of variation in the initial conditions (and also in the standard parameterization) does not yield a much different scenario or lead to any significant change in the model performance.

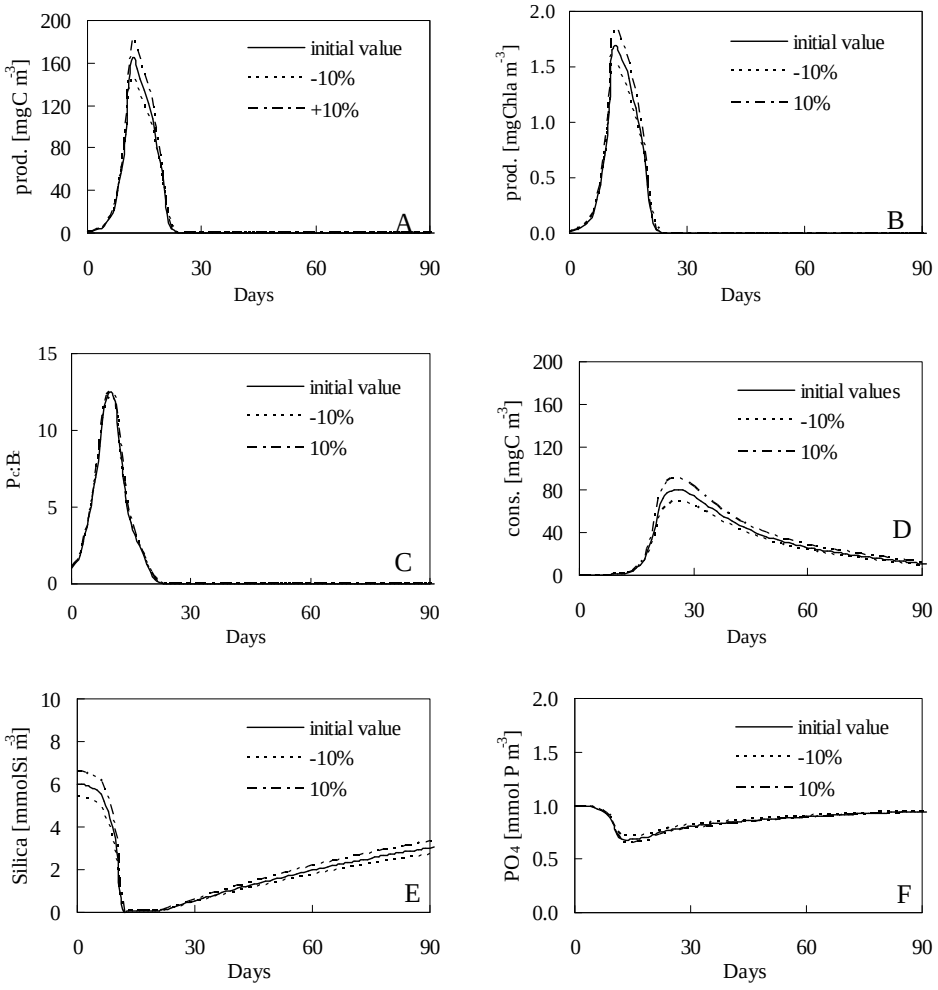

Figure 3.36: Time evolution of the response of six variables to perturbations of silica initial value in the sensitivity analysis : (A) P_c, (B) P_{Chla}, (C) $P_c : B_c$, (D) Z_c, (E) Si, and (F) PO_4.

Table 3.9: Analysis of normalized sensitivity of chosen results variables. Parameters varied ±10%. Signs (+ and -) indicate the direction of change, i.e., a (+) sign on a lower parameter perturbation denotes a negative impact expressed in a lower final value, whereas the same sign (+) on a upper perturbation means that the final result was greater than the reference value (for details see text). The magnitude of change in final results is expressed by: + or - for sensitive (S>0.1), ++ or - - for highly sensitive (S>1), and +++ or - - - for extremely sensitive (S>10). Values below 0.1 are left blank.

	P_c		Z_c		B_c		$Chl\,a$		$DOMl$		$P_c : B_c$	
Symbol	-10%	+10%	-10%	+10%	-10%	+10%	-10%	+10%	-10%	+10%	-10%	+10%
ν_{nl}	++	++					++	++	+		++	++
k_{hyd}^{POM}	++	++			-	-	++	++	-		++	++
V_{hyd}^{POM}	- - -	- -	-	-	-	-	- - -	- -	-	-	- - -	- -

Table 3.10: Analysis of normalized sensitivity of chosen results variables in response to producers parameter perturbation. Parameters varied ±10%. Signs (+ and -) indicate the direction of change, i.e., a (+) sign on a lower parameter perturbation denotes a negative impact expressed in a lower final value, whereas the same sign (+) on a upper perturbation means that the final result was greater than the reference value (for details see text). The magnitude of change in final results is expressed by: + or - for sensitive (S>0.1), ++ or - - for highly sensitive (S>1), and +++ or - - - for extremely sensitive (S>10). Values below 0.1 were left blank.

	P_c		Z_c		B_c		$Chla$		$DOMl$		$P_c : B_c$	
Symbol	-10%	+10%	-10%	+10%	-10%	+10%	-10%	+10%	-10%	+10%	-10%	+10%
χ_n^{min}	-						-			-	-	
χ_n^{max}	++	++					++	++	+	-	++	++
χ_p^{min}	-						-				-	
χ_p^{max}		-						+	+			+
$\chi_{chl:n}^{max}$	++	++					++	++		-	++	++
α^{chl}	++	++					++	++		-	++	++
k^{n2}							-		+			
k^{n1}	-						-				-	
ϕ^{ex}	- - -	- -					- - -	- -	+		- - -	- -
φ_P^{sl}	-	-					-	-			-	-
r^{ass}	++	+++	-	-			++	+++		-	++	+++
Q_{max}									-			
r^{lys}	- -	- -					- -	- -	+		- -	- -
$mort_P^{sl}$	-	-					-	-			-	-
$Temp_{ref}$	- - -	- -	-	-			- - -	- -	+		- - -	- -
r^s	- -	- -					- -				- -	
r^{bas}	- -	- -					- -		+		- -	- -
q^{res}							- -	- -	+		- -	- -
k_s	- -	- -					- -	- -	+		- -	- -
Ω_{nut}^{sed}												

Table 3.11: Analysis of normalized sensitivity of chosen results variables in response to consumers parameter perturbation. Parameters varied ± 10%. Signs (+ and -) indicate the direction of change, i.e., a (+) sign on a lower parameter perturbation denotes a negative impact expressed in a lower final value, whereas the same sign (+) on a upper perturbation means that the final result was greater than the reference value (for details see text). The magnitude of change in final results is expressed by: + or - for sensitive (S>0.1), ++ or - - for highly sensitive (S>1), and +++ or - - - for extremely sensitive (S>10). Values below 0.1 were left blank.

	P_c		Z_c		B_c		$Chla$		$DOMl$		$P_c : B_c$	
Symbol	-10%	+10%	-10%	+10%	-10%	+10%	-10%	+10%	-10%	+10%	-10%	+10%
χ_n^{max}									+			
χ_p^{max}	-						-		-		-	
χ_n^{min}												
χ_p^{min}		+						+		+		+
ϕ_z^{na}	- - -	- -	+	++	+	+	- - -	- -	+	+	- - -	- -
m_z^o	++	++			+		++	++			++	++
q_z^{POM}	++	++	+	+	+	+	++	++	+		++	++
m_z^{ti}	++	+++	-	-	+	+	++	+++	-	-	++	+++
k_z^o	++	++			+		++	++		-	++	++
$Temp_{ref}$	++	+++	++	++	+	+	++	+++	+	+	++	+++
r_z^{10}	++	+++	- -	- -	+		++	+++	-	-	++	+++
ass_z^{ef}	- - -	- -	++	++	+	+	- - -	- -	+	+	- - -	- -
V_z^{max}	- - -	- -		-	-	-	- - -	- -			- - -	- -
k_z	++	+++	-	-	+	+	++	+++	-	-	++	+++
$\beta_p^{Z^i}$	- - -	- -	-	-			- - -	- -		-	- - -	- -
$\beta_b^{Z^i}$	- -	- -	+	+	-	-	- -	- -	+	+	- -	-

Table 3.12: Analysis of normalized sensitivity of chosen results variables in response to decomposers parameter perturbation. Parameters varied ± 10%. Signs (+ and -) indicate the direction of change, i.e., a (+) sign on a lower parameter perturbation denotes a negative impact expressed in a lower final value, whereas the same sign (+) on a upper perturbation means that the final result was greater than the reference value (for details see text). The magnitude of change in final results is expressed by: + or - for sensitive (S>0.1), ++ or - - for highly sensitive (S>1), and +++ or - - - for extremely sensitive (S>10). Values below 0.1 were left blank.

	P_c		Z_c		B_c		$Chla$		$DOMl$		$P_c : B_c$	
Symbol	-10%	+10%	-10%	+10%	-10%	+10%	-10%	+10%	-10%	+10%	-10%	+10%
χ_n^{min}		-						-		-		-
χ_n^{max}	+						+				+	
χ_p^{min}									+			
χ_p^{max}										-		
ass_{norm}^{ef}									+			
ass_{low}^{ef}												
m_b^{dd}	++	++					++	++	+	+	++	++
v_b^m	- -	- -					- -	- -	-	-	- -	- -
V_b^{max}	-	-					-	-	- -	- -	-	-
k_b^{DOM}	+	+					+	+	++	+	+	+
q_b^{DOMsl}	++	++					++	++			++	- -
q_b^{ref}	++	+					++	+			++	+
m_b^{di}	++	++			+	+	++	++	+	+	++	++
k_b^o	+	+					+	+	+	-	+	+
θ_b^o												
r_b^{10}	++	++		-			++	++		-		
$Temp_{ref}$	++	+++	+	+	+	+	++	+++	++	++	++	+++
k_b^{n1}												
k_b^{n2}									+			
k_b^p												

Table 3.13: Analysis of normalized sensitivity of chosen results variables in response to perturbation of variables initial values. Values varied ± 10%. Signs (+ and -) indicate the direction of change, i.e., a (+) sign on a lower parameter perturbation denotes a negative impact expressed in a lower final value, whereas the same sign (+) on a upper perturbation means that the final result was greater than the reference value (for details see text). The magnitude of change in final results is expressed by: + or - for sensitive (S>0.1), ++ or - - for highly sensitive (S>1), and +++ or - - - for extremely sensitive (S>10). Values below 0.1 were left blank.

	NH_4		NO_3		PO_4		Si	
Variable	-10%	+10%	-10%	+10%	-10%	+10%	-10%	+10%
NH_4	+	+	+	+				
NO_3	+	+	+	+				
PO_4					++	++		
Si	+	+	+	+		++	++	++

Table 3.14: Analysis of normalized sensitivity of chosen results variables in response to perturbation of variables initial values. Values varied ± 10%. Parameters varied ± 10%. Signs (+ and -) indicate the direction of change, i.e., a (+) sign on a lower parameter perturbation denotes a negative impact expressed in a lower final value, whereas the same sign (+) on a upper perturbation means that the final result was greater than the reference value (for details see text). The magnitude of change in final results is expressed by: + or - for sensitive (S>0.1), ++ or - - for highly sensitive (S>1), and +++ or - - - for extremely sensitive (S>10). Values bellow 0.1 were left blank.

	P_c		Z_c		B_c		$Chla$		$DOMl$		$P_c : B_c$	
Variable	-10%	+10%	-10%	+10%	-10%	+10%	-10%	+10%	-10%	+10%	-10%	+10%
P_c	+	+					+	+			+	+
Z_c	++	++					++	++		-	++	++
B_c		-					+	-				-
$DOMl$		-						-				-
$DOMsl$												
POM		-						-				-
NH_4								-				
NO_3	-							-			-	
PO_4												
Si	- - -	- -	++	++			- - -	- -	+	+	- - -	- -
$BioSi$												
O_2	-	-					-	-			-	-

Chapter 4

Real case application: the Tagus estuary

4.1 Introduction

In conformity with the aim of the present work, this chapter addresses the application of *mohid.Life.1.0* to a real system. Even though the model was developed for a pelagic system, the Tagus estuary was selected as the study site for this application given the previous accumulated experience gained studying the trophic state of this system with *MOHID* and the knowledge gained from it[1]. Besides, the choice of Tagus estuary could also benefit from the available data sets gathered in monitoring studies. The main goal of this chapter is to assess the performance of the model in complex scenarios and to evaluate its ability to reproduce observed biological patterns when forced by several known variables like atmospheric parameters, river discharges and tide. As such, an in-depth study on the dynamics of the estuary, either from a hydrodynamic or ecologic perspective, falls outside the scope of this application. Nonetheless, the following aspects will be addressed even if only subjected to a superficial analysis:

- To identify the critical processes controlling carbon and nutrients dynamics in the system
- To examine the potential role of physical forcing and the behaviour of the biological variables included in the model.
- To provide a formal, quantitative and dynamic framework for the synthesis of the results of the various components inside the estuary.
- To compare the model results with previous modelling efforts made to study this estuary with a simpler water quality model available in the *MOHID* modelling system.

[1] Detailed information on this study can be found at http://www.maretec.mohid.com/TroficLevel/

4.1.1 Basic concepts in estuarine ecology

Being a transitional zone from two distinct aquatic systems, fresh water and salt water, estuaries have their own set of conditions that shape their ecological structure. Usually, estuaries have more similarities with the marine than with the freshwater environment. In marine and estuarine systems the fundamental principles of the throphodynamic structure and functions are very similar, with the exception of gelatinous plankton, which does not occur in freshwater. Nevertheless, it is clear that physical, chemical and biological factors, with different strength in oceanic and estuarine environments, shapes the biological patterns from nekton to microbial communities. The abundance of microorganisms is a major characteristic of estuarine systems, an evidence of the importance of microbial processes in these ecosystems.

The typical features of oceanic pelagic systems encompass autochthonous organic material and oligotrophic conditions with characteristic small cell size phytoplankton. A rather different scenario is found in estuarine ecosystems, where a high content of allochtonous material is observed, as well as high concentration of nutrients (comprising mesotrophic and eutrophic conditions), larger cells like diatoms, and high bacterial diversity. In addition, and imposing a major control on system behaviour, oceanic systems have a relatively seasonally-stable regime while estuaries have a strong-seasonal regime. Also, steep physical, chemical and biological gradients are an important aspect of estuaries.

Estuaries are usually divided in two classes defined by their vertical density profile. When the currents of riverine fresh water inflow and tide are similar, turbulence is the major mixing agent. This process is induced by the periodicity of tidal action. In this case the vertical salinity profile is less variable because most of the energy dissipates in the vertical mixture, originating a rather complex set of layers and water masses. Under these conditions, estuaries are considered partially mixed or moderately stratified. In completely mixed and vertically homogeneous estuaries, however, the tidal action is strongly dominant and the water column is well mixed from surface all the way down to the bottom. Major salinity and temperature changes are more frequently observed horizontally rather than vertically and this spatial heterogeneity is thought to affect nearly every aspect of population dynamics, species interactions, and community structure.

The water circulation inside an estuary is capable of changing the conditions of the ecosystem over a much smaller temporal scale, when compared with neritic or oceanic areas. The hydrodynamic inside an estuary are driven by a complex interplay of mechanisms, all with a strong influence on biological processes. The water circulation is conditioned by tidal currents, river discharges, wind and local topography. The resulting circulation patterns may have a large effect on the abundance and production of the microbial community by controlling the supply of allochtonous organic matter, con-

centrating and retaining locally produced organic matter inside the system. They also produce conditions for long-term coupling of bacterial production and autochthons sources of organic matter. Because an estuary is not a closed system, tidal currents act as an oscillating conveyor belt with the coastal zone, moving plankton, organic and inorganic materials, and sediments back and forth, creating complex distribution patterns.

The estuarine environment is often reported as extremely productive, with high rates of primary production and bacterial production, and supporting dense planktonic communities. The major transformation processes of organic and inorganic nutrient pools that reach the main body of the estuary are related to biological processes associated with bacterioplankton [138].

4.1.2 Tagus estuary characterization

The Tagus Estuary (38 °44′N, 9 °08′W), the largest estuarine system on the Portuguese coast (Figure 4.1), is a relatively shallow estuary with an open boundary to the Atlantic. It is a mesotidal system (mean tidal range of 2.2m) with semi-diurnal tides and tidal amplitudes ranging from 1 to 4 meters. It has a surface area of about 320 km^2 and a mean volume of 1900×10^6 m^3. The intertidal areas are composed mainly by mudflats with a total area ranging from 20 to 40% of the total estuarine area.

The hydrographic conditions of the estuary are mainly determined by the inflow of the saline water from the Atlantic and a considerable riverine input of freshwater with a clear seasonal pattern. The estuary receives a modal freshwater inflow of 400 $\mathrm{m}^3\,\mathrm{s}^{-1}$. From March to December the Tagus River has a rather constant monthly average flow of around 330 $\mathrm{m}^3\,\mathrm{s}^{-1}$. Higher values are recorded from January to March. The Tagus river is the major contributor of fresh water to the estuary, but two other smaller rivers have fresh water inputs to the system, namely the rivers Sorraia and Trancão. The estuary receives also effluent discharges, mainly from urban (with over 10 WWTP's discharge points inside the estuary), industrial, and agricultural sources.

The wind regime over the estuary area is characterized by predominant winds from south and southwest during winter, rotating progressively to winds from northwest and north during spring, and maintaining these directions throughout the summer months. Given the seasonal variability of meteorological conditions and river discharges, the estuary is characterized by a strong seasonal variability of both hydrodynamic and biogeochemical conditions. Besides this seasonal pattern, inside the estuary there is also a strong horizontal pattern as a result of the hydrodynamic conditions controlled mostly by the tidal regime. Middle estuarine areas (and upper areas to a lesser extent) have more stable and homogenous conditions, with a high residence time, while lower estuarine areas are characterized by a high

variability influenced by the tidal regime.

The relatively high flow associated with the shallow depth prevents the formation of a late-spring thermocline, characteristic of temperate waters. Hence, there is no thermal stratification inside the estuary during spring and summer months. The system is vertically well-mixed all year around, and has a mean tidal prism of 600×10^6 m^3, about a third of the mean volume.

High winter concentrations of inorganic nitrogen and phosphorus are prerequisites for a strong development of the phytoplankton in spring, the beginning of which is triggered by the increase in radiation levels. Several factors control the blooms (zooplankton grazing, residence time, etc.), given that frequently limiting nutrients (nitrogen and silica) are never depleted inside the estuary. Also, the turbulent mixing in early autumn that usually triggers the autumn bloom does not occur inside Tagus estuary. Here too, the lack of a marked seasonal regime is a consequence of the transport regimes that prevent the formation of a thermocline. Several groups of primary producers can be found inside the estuary and also in the surrounding coastal waters. Despite the different composition in phytoplankton communities inside the estuary (specially Bacillariophyceae, Chlorophyceae, and Dinophyceae), diatoms dominate the phytoplankton in the entire estuary [139].

4.2 Methods

4.2.1 Model implementation

Hydrodynamic model setup

A coherent interpretation of any ecosystem must rely on a study analysis with an integral approach. As such, the interplay between physical, chemical and biological processes, as well as the interaction of the different compartments of the system must be considered. It is also essential for the study to include the different factors that may control the fluxes of energy and matter inside the system.

For a better description of the hydrodynamic control on the biogeochemical processes inside the estuary, the model domain was extended to encompass the adjacent coastal area outside the estuary, as well as a section of the upstream area of Tagus river just before its widening into the estuary. The *MOHID* hydrodynamic model was used to achieve an accurate characterization of the flow regime for the whole study area. Its governing hydrodynamic equations have been described elsewhere [51, 52, 53], so only a brief overview of the model is presented here. The main forcing mechanisms for the circulation considered in the model are the tides, the wind regime and the river outflow into the estuary.

The model uses a full 3-D hydrodynamic formulation with hydrostatic

Figure 4.1: Enhanced satellite image of the Tagus estuary. Green dots indicate the monitoring sites. Model stations (MS) where time series were taken to assess model performance were set to coincide with the data collection points. The location of the meteorological monitoring station is marked in blue. River discharge points are marked by yellow dots: Tagus river on the top right corner, Sorraia and Trancão rivers on the left and right margin of the estuary, respectively. Red dots mark the location of WWTP's discharging to the estuary.

and Boussinesq approximations [49], and the general ocean turbulence model GOTM for the turbulent closure [140]. However, in the present application the model is set as a 2D depth-integrated model. It was assumed that the study area has an intense vertical mixing, implying a homogeneous water column. Based on this assumption, a single water layer was defined for the entire study area with variable depth defined by the bottom topography of the modelled area.

The model domain is characterized by a variable square grid with 73x94 computation points (figure 4.2), with higher resolution inside the estuary where each cell covers an approximated area of 3.72 $\mathrm{k\,m^2}$. The geographic location of the domain is defined by the following coordinates: $38\,^{\circ}30\,'$-$39\,^{\circ}N$ and $8\,^{\circ}51\,'$-$9\,^{\circ}51\,'W$. Meteorological forcing, boundary conditions and river discharges are explicitly imposed, all with temporal variability. For the tide solution, the hydrodynamic model was forced with tide gauge elevations at the open boundary.

An Eulerian formulation for the transport model is adopted, coupled to the hydrodynamic module. Interactions between atmosphere and water column occurring at the surface (e.g., heat fluxes, wind stress, solar radiation) are handled by the surface module and the interaction between the bottom and the water column (e.g., cohesive sediments resuspension and deposition) by the bottom module.

The model runs with a time step of 60 seconds for a period of 20 months, starting in April 2003 and ending in January 2005. Given the control of suspended sediment concentration on the ambient light, special attention was paid to achieve an accurate description of cohesive sediments, both in the water column and on the bottom of the estuary. The methodology adopted for modelling sediment dynamics consisted in starting the simulations with a layer of 10 $\mathrm{kg/\,m^2}$ of bottom sediments in the entire domain and a constant concentration of 100 $\mathrm{mg\ l^{-1}}$ in Tagus river discharges. Then the model runs for 2 months with cohesive sediments, POM (C, N and P), and biogenic silica as the only properties considered in the simulation. This period was assumed as a reasonable time to achieve a proper bottom sediment pattern inside the estuary with deposition and erosion areas already defined. All other properties were only simulated after this initial period. A simple sediment model was included to account for POM and biogenic silica diagenesis. A fixed mineralization rate of $0.1\mathrm{d}^{-1}$ was defined for all these properties. PON and POP are converted to ammonium and phosphate, respectively, and biogenic silica to reactive silicate.

Ecological model setup

Mohid.Life.1.0 model was coupled to the transport model as a zero dimensional water-quality/ecological model. Unlike the schematic applications presented earlier, in this application only two producers are considered, one

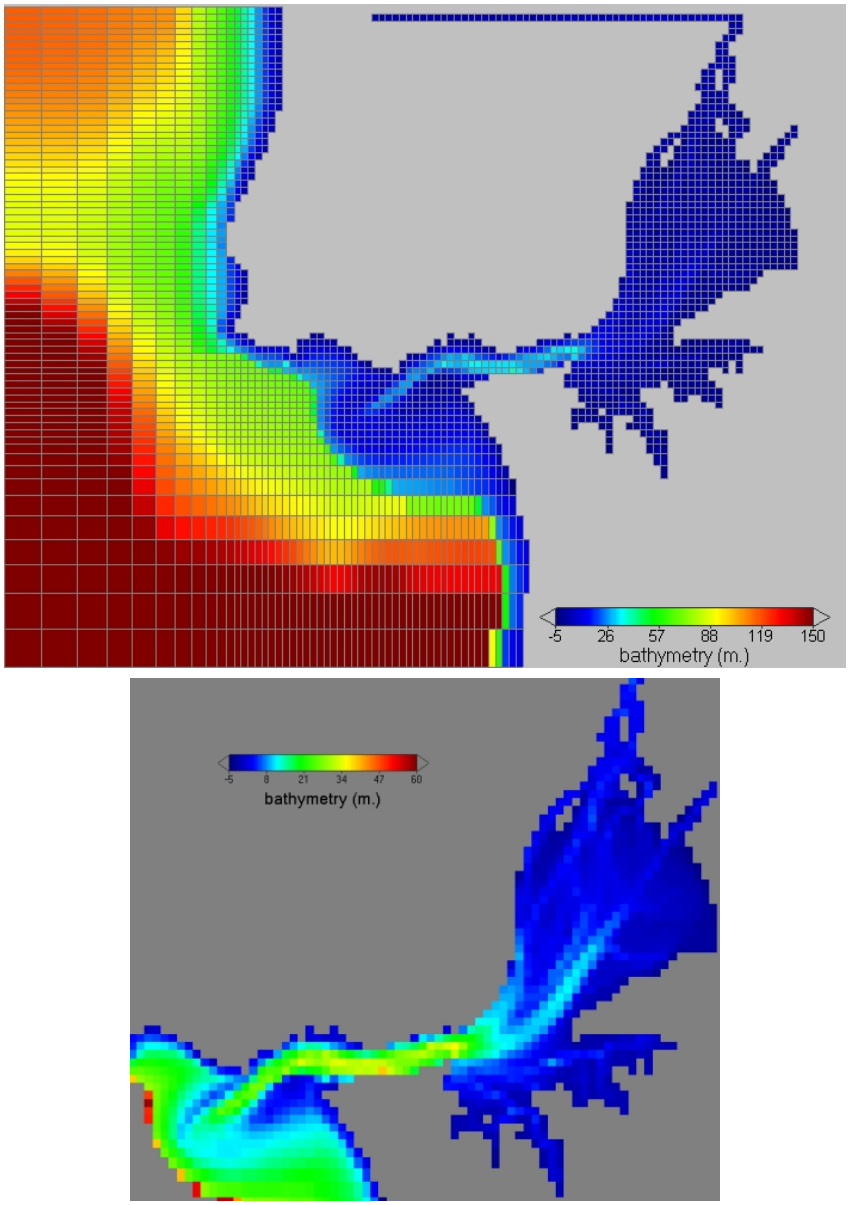

Figure 4.2: Computational grid with variable spatial resolution used in the model domain (top) and a close-up at the estuary area to show the bathymetry (down). A smaller cell size is defined inside the estuary given the higher spatial variation and velocities of the hydrodynamic regime.

silica-dependent and the other silica-independent. This simplified approach was devised to consider the two main phytoplankton groups: diatoms and flagellates. The parameter values correspond to diatoms and autotrophic flagellates values taken from the same sources presented before. Only one group of consumers was added to the simulation, acting as the closure of the food web. The microzooplankton parameter values were chosen to parameterize the consumer. However, to compensate for the lack of top predators feeding on this group, a quadratic density dependent term (such that grazing rates decline at low prey biomass) was adopted as an alternative method to establish a mortality criteria for consumers. Evidences for such a threshold effect on grazing have been reported in essays with natural microzooplankton assemblages in the Sargasso sea [141].

Finally, bacterioplankton were also included in the model setup, given their important role in estuarine ecology. The trophic structure was defined on the simple basis of a predatory action of the consumer group on both producers, on bacteria, and on itself. The prey availability was set to 0.5 for diatoms and autotrophic flagellates, 0.8 for bacteria, and 0.2 for microzooplankton.

Taking advantage of the model generic unit system, all element concentrations are expressed in $\mathrm{mg\,l^{-1}}$, except for the chlorophyll cell content in producers that were kept at $\mathrm{mg\,m^{-3}}$. The penetration of light through the water column is dependent on phytoplankton chlorophyll and cohesive sediment concentration in the water column and is computed within the model system.

Unlike the hydrodynamic model with small time-step requirements (60 seconds in this application), the ecological model iterates every 3600 seconds, the regular time-step already tested in the previous applications. The ecological model runs for 18 months, starting after a two months run of the hydrodynamic module to setup the sediment pattern on the bottom of the modelled domain.

When possible, the values of parameters used in the model have been selected from relevant studies or to lie within the range of values used in similar models. Some model parameters, generally those for which precise estimates were unavailable like grazing rates and prey availability, were set by calibration of the model output against observed values of some state variables.

External conditions

External conditions included forcing functions (for example irradiance, temperature), inputs (nutrient discharges, etc.), and boundary conditions (concentrations of each state variable in the adjacent Atlantic boundaries).

The data used in the model for climatological forcing, boundary and initial conditions were obtained, where possible, from measurements made

in the last years. The lack of comprehensive data sets makes it difficult to have a detailed description of some properties. So, it is impossible to achieve a high frequency in forcing in most situations. To fill in the gaps in the scarce data sets, estimated guesses had to be made based on available information and some hypothesis had to be formulated. Not all forcing functions, boundary conditions, and river loads data used in the simulation were compilations from the same year. The lack of detailed available information conditioned the use of data for the same year. To build a complete data set for some properties with seasonal variation, values from different years had to be included.

Atmospheric forcing

Photosynthesis was driven by light using observed values measured at a meteorological station near Tagus estuary mouth, located at 9^o26'48"O and 38^o41'48"N (figure 4.3). Besides radiation levels, there were also values of wind (direction and intensity), air temperature, atmospheric relative humidity and precipitation. All these properties were used as a high frequency atmospheric forcing, giving the detailed data set available with an hourly resolution between measurements for a full year. The measurements used were made during 2004.

River and WWTP's discharges (inputs)

Three distinct points of river discharge are defined inside the estuary. The most relevant is without doubt the Tagus river discharge (figure 4.3). Tagus river flow data were obtained from Instituto Nacional da Água (http://www.inag.pt). The other two rivers, Trancão and Sorraia, despite the much lower flow regime, have an important nutrient and organic matter contribution to the system, a fact that justifies their inclusion. River discharges are defined by the flow, temperature, salinity, concentrations of cohesive sediments, nutrients, organic matter components, and biological constituents. Because there is a marked seasonal pattern in the flow and properties concentrations, a monthly value was used whenever available or estimated when not.

Nutrient loading (calculated from publicly accessible data of the National Water Institute, INAG, Portugal) derived mainly from fixed stations monitoring measurements. Carbon and phosphorus fractions of both dissolved (labile and semi-labile) and particulate organic matter was inferred from the nitrogen fraction, assuming a Redfield ratio composition, typical of fresh organic matter. The same principle was used to determine the nutrient and carbon content of primary producers. The fragmented data available for each discharge makes it necessary to build the data set used to define the discharge from a compilation of several disperse measurements and estimations. Most of the data came from the Portuguese Water Insti-

tute (INAG) historical data set compiled for the study area and available online (incomplete monthly values sets ranging from 1989-1993), as well as from field measurements.

Because Tagus River represents by far the major contribution to the estuary, only its hydrological regime is addressed here. The characteristics of the Tagus river inputs are represented in figure 4.3. The annual river flow depends partly on rainfall, with years of very high flow interlaced with periods of drought. Rainfall and water retention by dams contributes to the already sharp seasonal and interannual differences in freshwater inputs. Throughout the year, the mean daily freshwater flow varies abruptly between seasons, with peak winter flows ranging from 400 to 920 $m^3 s^{-1}$ and a minimum of about 100 to 250 $m^3 s^{-1}$ in summer. The temperature time series show a clear seasonal pattern with low temperatures in winter ($\tilde{}12\,^{\circ}C$), gradually increasing throughout the year, and reaching their highest values in summer months ($>20\,^{\circ}C$). Nutrients show different pattern; nitrate concentrations are higher during spring months and decrease in mid-summer, while phosphate concentrations are lower in spring and higher in winter months. Ammonium has a distinct pattern with a constant concentration the entire year only interrupted by a peak in June with an almost tenfold increase in concentration. The remaining properties, silicate acid, oxygen, organic matter components, don't show any seasonal pattern. Biogenic silica discharge was defined as constant value of 1 $mg Si\ l^{-1}$.

The discharges of WWTP's inside the system were also considered in this study. The values used for the flow, nutrient and organic matter loads were taken from previous impact assessment studies made in the Tags estuary using *MOHID* (for details see [142]).

Boundary conditions

When it comes to boundary conditions, the *MOHID* system parameterization enables simulations ranging from estuaries to large scale current systems like ocean basins. Its code flexibility allows the *MOHID* hydrodynamic model to simulate the interface zone of estuary system and coastal systems where processes characteristic of each overlap.

Boundary conditions imposed on the open oceanic boundaries were taken from values compiled by NODC for the area off Lisbon[2]. To correctly achieve seasonal variation, a mean value should be used for each month whenever possible. In this particular case, the conditions are quite stable throughout the year, given the oligotrophic conditions of such areas. Nevertheless, given the lack of data and the small contribution of these oceanic areas to estuarine dynamics, the focus of the application, such detailed characterization of conditions was not adopted. Instead, a constant value for each property was assumed as sufficient to properly define the boundary conditions.

[2] available at http://www.nodc.noaa.gov/

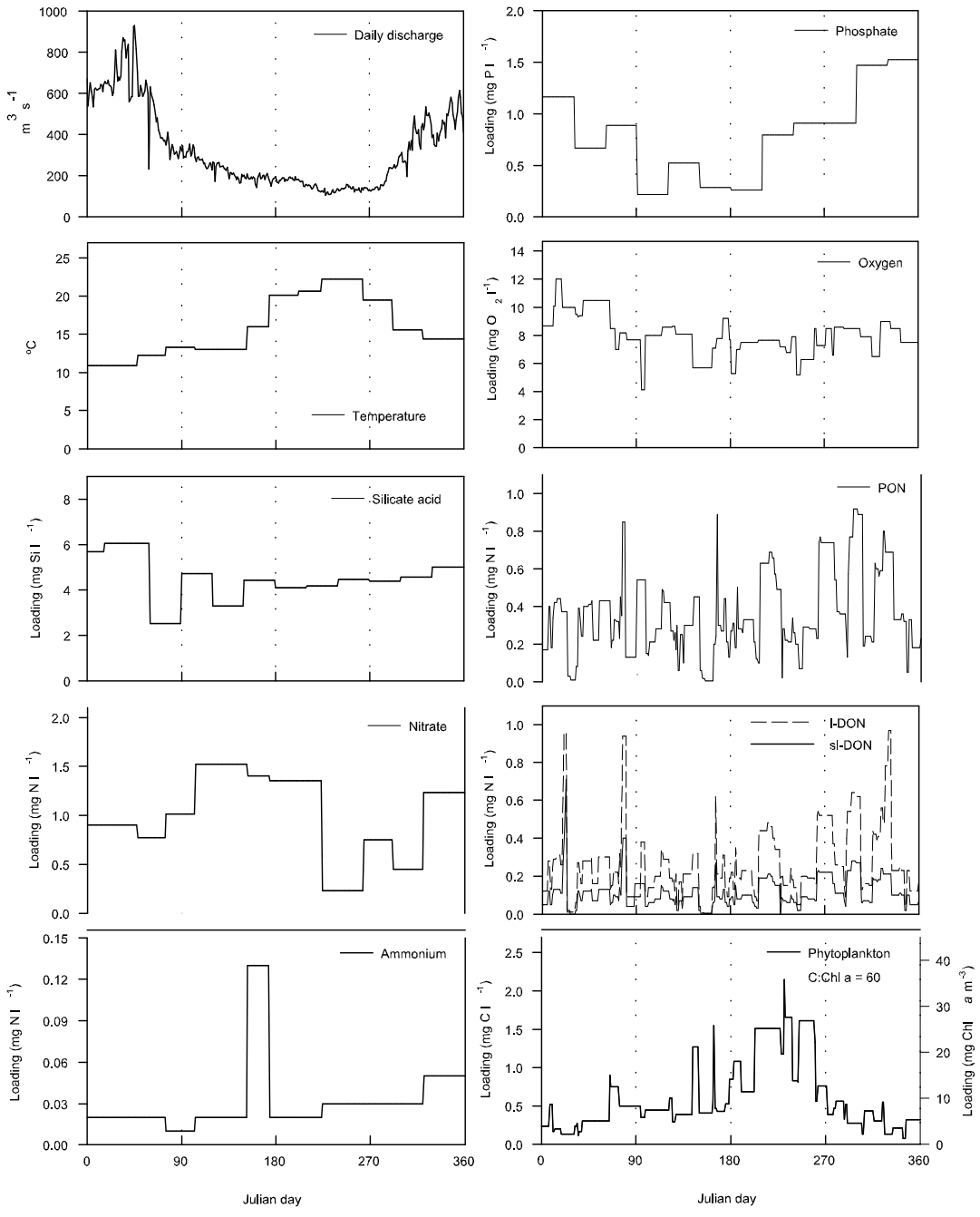

Figure 4.3: Data from the Tagus river discharges used to force the simulation as the main freshwater input into the Tagus estuary. Flow, temperature, chlorophyll, and nutrient data comes from station measurements (located upstream in river Tagus). Phytoplankton biomass was determined from a fixed C:Chl*a* ratio of 60. Organic matter loads correspond to estimates made from nitrogen inputs data. All missing carbon and nutrient composition (for phytoplankton and organic matter) were calculated based on Redfield ratios.

The Dirichlet boundary condition is the most commonly used type of boundary condition in water-quality modelling [37]. As such, it was adopted in this simulation by simply specifying the concentrations at the boundary.

4.2.2 Monitored sites and model calibration

Four virtual sampling sites (figure 4.1) were established along a NE-SW transect to monitor model properties evolution in time, starting in the mid-estuary area and extending all the way down to the coastal estuarine zone at the river mouth (referred herein as MS1, MS2, MS3, MS4). Model stations are numbered from the mid-estuary areas to the river mouth. The virtual stations distribution tries to cover major areas of the estuary that may be controlled by different parameters and/or processes. The purpose of this regionalization is to provide more accurate interpretation of model estimates inside the estuary and to help identify possible controlling mechanisms. The choice of the sites to check model performance was also made based on the location of some sampling sites monitored in the estuary during 2004. These sites where data has been collected are referred as site 1 to site 4, following the same numbering scheme as adopted for the model stations.

The calibration was made in a step-by-step approach in a series of successive model runs, starting with a standard set of parameter values and sequentially changing some of them after checking the results at the end of each new run. Parameter values were constrained within limits that were considered to be biologically realistic. Considering the enormous range of different values that could lead to a reasonable fit between model results and *in situ* measurements, the "optimal" solution can be found when a satisfactory fit is achieved by changing the minimum set of parameters.

The model calibration was made mainly by comparing model results for MS1 with field data from *in situ* measurements for the year of 2004 at site 1. To achieve a realistic comparison between model results and field data, the location of the virtual stations was set to coincide with the location of the sampling stations also shown in figure 4.1 (green dots). Although the data set comprises several sampling stations scattered inside the estuary, only values for site 1 were used in the calibration effort. Whenever multiple measurements were available for the same time instance at the same site (sampling at different depths in the water column), the average from all the samples was used to compare with model results. Monitored data comprise ammonium, nitrate, chlorophyll, and oxygen concentration values for each station. The temporal resolution of the data can be considered satisfactory; despite only one monthly value is available for each property and the limited data for winter months, there is enough resolution to portray the seasonal patterns of the system.

For simplicity, and also because data temporal resolution constraints, results are analyzed on a seasonal scale and not a diurnal or tidal time scale

(on the order of hours). Only the results of the last year of the simulation (2004) are presented and discussed. To avoid an excessive information, only the major features are highlighted in the results. A more detailed result analysis is also restricted to the properties whose values are available from *in situ* observations. But in accordance with the aim of the application, other results will be analyzed and discussed whenever found relevant to understand the model dynamics and/or explain some characteristics of the system.

4.3 Results

4.3.1 Model calibration

As a preliminary step to the model calibration, ranges where checked for each of the major model parameters whenever available. For the reference situation, the adopted parameters values were the same used in the previous chapter for diatoms (used to characterize the silica-dependent group) and flagellates (used to characterize the non silica-dependent group).

A better fit for chlorophyll concentration was achieved by adjusting the Chl*a*-specific initial slope of the photosynthesis light curve $\left(\alpha^{Chl}\right)$ to a smaller value (see equation 2.42). The adopted value of 1.7 $\mathrm{mg}C\,\mathrm{m}^2(\,\mathrm{mg}Chl\,\mathrm{W\,d})^{-1}$ is a standard value found within the ranges mentioned by Geider *et al.* [41] for some phytoplankton groups. Another parameter governing phytoplankton growth (silica-dependent producers) that was changed by model calibration was the silicate uptake Michaelis constant (k_s). The adopted value was 0.08 $\mathrm{mg}Si\ \mathrm{l}^{-1}$. Half-saturation constant concentrations values for silicate reported in the literature range between 0.000843 to 0.094663 $\mathrm{mg}Si\ \mathrm{l}^{-1}$ [143] for marine and coastal diatoms.

The defined value for biogenic silica proved to be too low to account for a recycling of silica in the system. So, to avoid unrealistic shortage of silicate, the silicate dissolution rate was doubled. For the dynamics of semi-labile and POM hydrolysis mediated by bacteria, some empirical values were chosen ($V_{hyd}^{POM} = 0.5\,\mathrm{d}^{-1}$ and $V_{hyd}^{DOMsl} = 1.5\,\mathrm{d}^{-1}$; see table 2.8 for details). Finally, to adjust model results to the observed concentration of ammonium and nitrate in the system, the nitrification light limitation was removed and the nitrification rate slightly increased to 0.1 d^{-1}.

4.3.2 Data from sampling sites

In situ data show a seasonal trend in ammonium concentration, with lower values observed during summer months in all monitored sites, as portrayed in figure 4.4 where discrete values are plotted. Site 1 shows consistently the highest measured values, reaching $0.25\,\mathrm{mg}N\ \mathrm{l}^{-1}$ in late October. The same seasonal trend can be observed for nitrate concentrations, but its only

evident in data from sites 2, 3 and 4, where a marked decrease is evident in summer. Nitrate concentrations reveals a clear longitudinal distribution pattern with decreasing concentrations from upper areas of the estuary (station 1) to the river mouth (station 4). Like ammonium, higher values ($>0.8\,\mathrm{mg}N\ \mathrm{l}^{-1}$) are found in site 1, only in winter. Table 4.1 summarizes the mean values for each monitored variable at each site. The results clearly show that values are systematically higher at site 1 and decrease towards site 4.

Of all measured parameters, chlorophyll a has the most striking seasonal pattern. Data shows the typical pattern of a spring/summer bloom after low concentrations in winter ($< 2\,\mathrm{mg}Chla\ \mathrm{m}^{-3}$). After winter period with low values, chlorophyll concentration starts to increase in mid-spring, reaching its highest values ($> 10\,\mathrm{mg}Chla\ \mathrm{m}^{-3}$) in summer. By the start of Autumn (measures made at September 22), chlorophyll concentration shows a clear decreasing trend. The most obvious spatial and temporal pattern appears to be the higher chlorophyll concentrations inside the estuary (sites 1 and 2).

Finally, the oxygen concentration is very spatially homogenous (see Table 4.1). Values range from 6 in winter to $10\,\mathrm{mg}O_2\ \mathrm{l}^{-1}$ in summer. Only a slight increase in concentrations can be noticed during summer, coinciding with the increase in chlorophyll concentrations. There is also a slight increase by the end of the year that falls outside the seasonal pattern observed during the entire year.

All monitored variables show a seasonal fluctuation but with different magnitudes, both spatially and in time. It is evident by looking at these results that there is a link between all parameters, easily explained by the chlorophyll values. As already mentioned, the increase in chlorophyll is in phase with the increase of dissolved oxygen in water, as a result of the increase in production and consequent oxygen production. The same is true for ammonium and nitrate, only here the increase in chlorophyll overlaps the decrease in these nutrients as a result of uptake. However, it must be stressed that the influence of river discharge cannot be ruled out of this explanation. By looking at figure 4.3 it is possible to infer the importance of the Tagus river on each property evolution in time and space (discussed below).

4.3.3 Temperature and salinity

Model results for temperature show the typical pattern of mid-latitude estuarine system, both spatially and seasonally. In figure 4.5 (for simplicity only results for MS1 and MS4 are shown) its possible to see that temperatures are higher during summer months, reaching 25 °C at MS1. In addition, the spatial differences are also easily noticed because lower temperatures (˜17 °C) are observed at MS4 in the same time period. Besides, the temperature range is much greater inside the estuary (12-24 °C at MS1 and

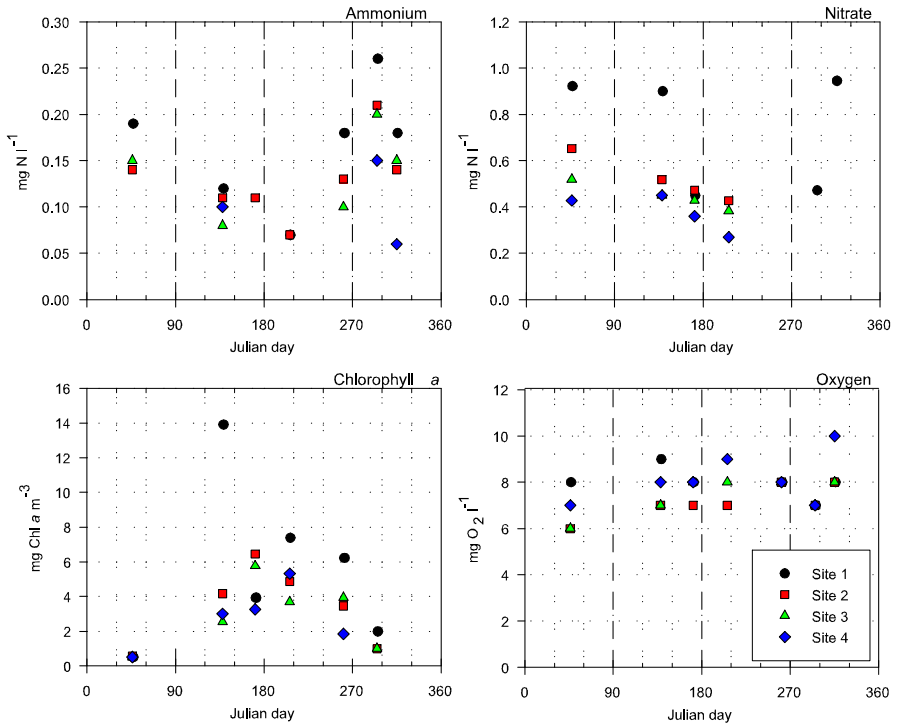

Figure 4.4: Comparison of measured parameters between all monitored sites.

Table 4.1: Anual average for measured parameters at each monitoring site in Tagus estuary during 2004.

Site	**Ammonium** mg$N$ l^{-1}	**Nitrate** mg$N$ l^{-1}	**Chlorophyll** mg$Chla$ m^{-3}	**Oxygen** mgO_2 l^{-1}
1	0.17	0.74	5.66	8
2	0.13	0.52	3.42	7.14
3	0.12	0.46	3.5	7.67
4	0.1	0.37	3.13	7.79

only 14-18 °C at MS4). Upper estuarine areas have both higher and lower temperature values, reaching both temperature extremes. The temperature fields at different times of the year, illustrated in figure 4.6, allow a detailed look at the temperature variation inside the studied system, especially the horizontal gradients.

Salinity follows the same general patterns of temperature (figure 4.5), with a wider range of values observed up inside the estuary (from less than 5 PSU up to a little over 25 PSU observed at MS1) and small variations at the estuary mouth (27-35 PSU at MS4). Also like temperature, salinity values reveal a strong seasonal fluctuation, specially in the inner areas of the estuary. But unlike temperature, higher values are observed at the river mouth and lower salinity concentrations in the upper areas. Salinity shows a stronger signal of tidal influence with marked fortnightly fluctuations caused by the spring/neap cycle. Salinity fields at different times of the year are represented in figure 4.7.

4.3.4 Cohesive sediments

The concentration of cohesive sediments in the water column also shows a great variation, both in time and in space. Taking MS1 as an example (figure 4.5), concentrations range from 42 to 111 mg l^{-1}. Higher values are observed during winter months, while late summer months register the lowest concentrations for the entire system. This observation becomes obvious when comparing cohesive sediments concentrations at different stations, with values consistently higher at MS1 when compared with MS4. Lower estuarine areas show a much narrower range of variation (43 to 45 mg l^{-1}). The spatial discrepancy in suspended sediment concentration is particularly evident in winter months (figure 4.8).

4.3.5 Nutrients

Model output and *in situ* data for ammonium are shown in figure 4.9, where model results and data are compared for all stations. A fairly reasonable agreement between observations and model results is attained for all stations, both in respect to the seasonal patterns and the concentrations magnitude. Nevertheless, the model reveals a sharper seasonality in ammonium concentrations, especially in upper stations. As mentioned earlier, *in situ* data shows that concentrations are very similar among stations, but with station 1 having the higher measured values (figure 4.4). Model results, however, show a clear decrease in ammonium concentrations from the upper estuary areas to coastal zone, notice in figure 4.9, possibly as a result of the river discharges in winter and of mineralization in summer. A major difference between model station results is that the marked seasonal pattern observed in MS1 tends to decrease in magnitude as we move towards MS4,

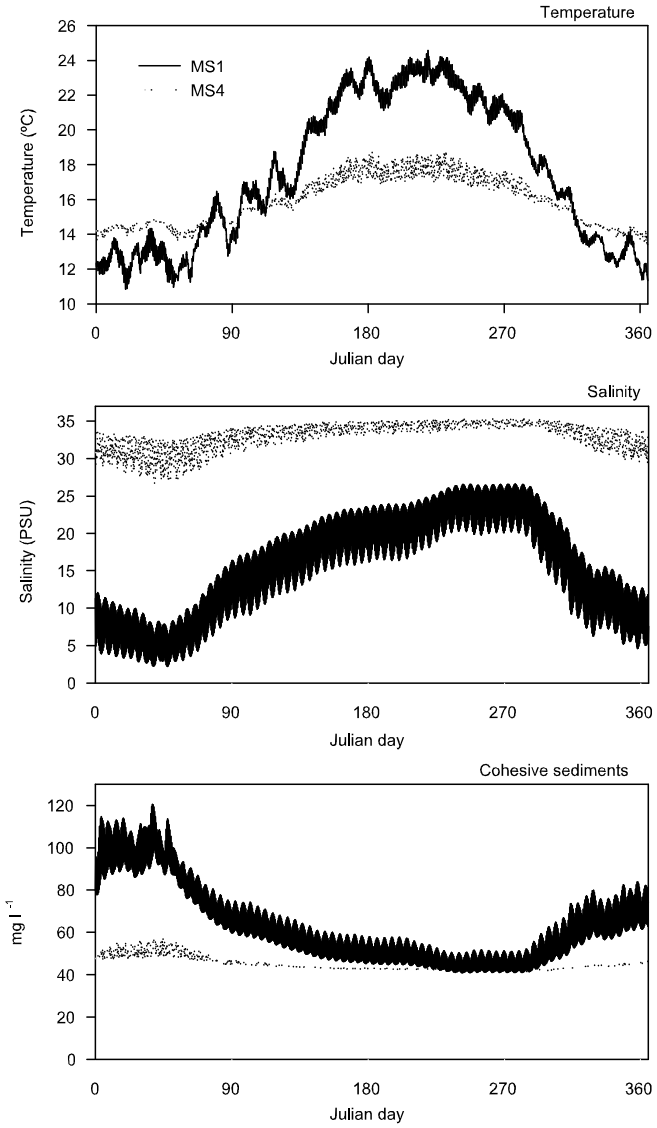

Figure 4.5: Temperature, salinity and cohesive sediments concentration evolution calculated by the model at MS1 and MS4.

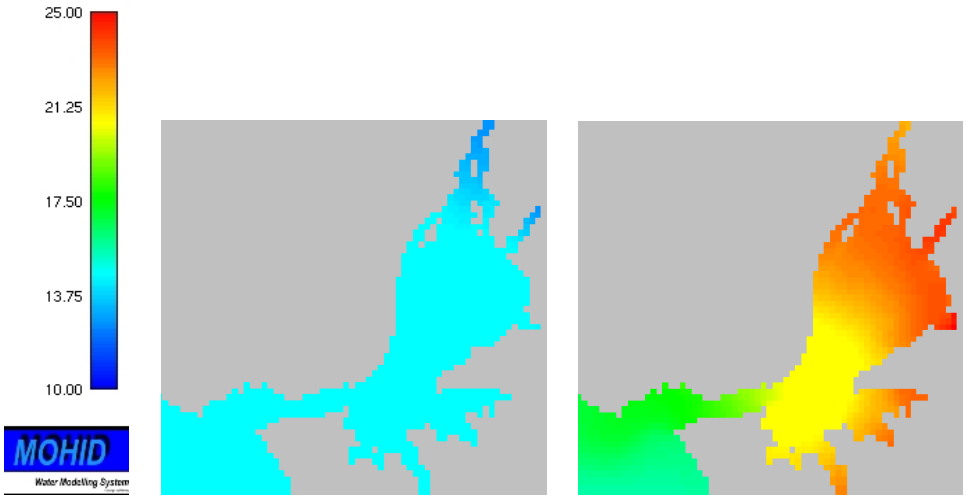

Figure 4.6: Model results for the temperature field ($^{\circ}C$) in Tagus estuary area in winter (left) and summer (right) conditions. Model predictions for Julian day 43 and 177 for winter and summer results, respectively.

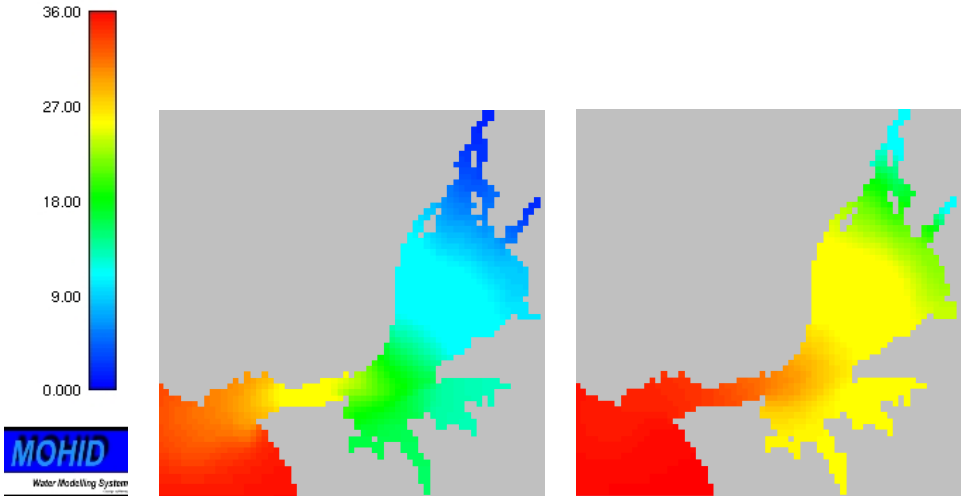

Figure 4.7: Model results for the salinity field (PSU) in Tagus estuary area in winter (left) and summer (right) conditions. Model predictions for Julian day 43 and 177 for winter and summer results, respectively.

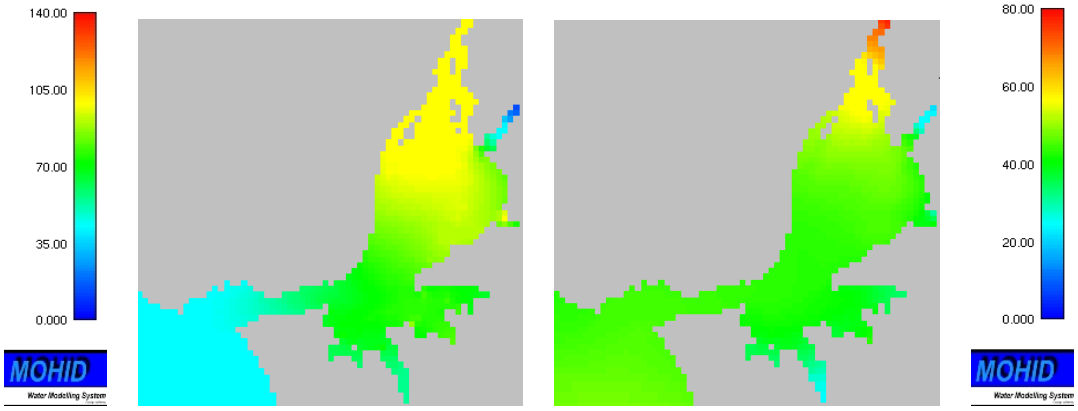

Figure 4.8: Model results for suspended cohesive sediment (mg l^{-1}) distribution in Tagus estuary area in winter and summer conditions (left and right, respectively). Different color scales are used to enhance the spatial pattern. Model predictions for Julian day 43 and 177 for winter and summer results, respectively.

denoting a decrease influence from river discharges.

The spring decrease in ammonium concentrations begins earlier in model results, but shows agreement with the observations. The lower summer values are produced correctly, but usually with slightly higher values in model results in sites 1-3 and lower in station 4 (with concentrations below 0.15 mg$N$ l^{-1}) when compared with sampled values. In MS1 it is possible to notice that the model shows the lowest values (0.1 mg$N$ l^{-1}) by the end of summer, a fact that clearly contradicts the observations. The sharp increase in Autumn's observations is not correctly reproduced by the model because it only returns to previous summer value range. Nevertheless, the model is able to match measured values. Model results for ammonium reaches highest concentration in winter ($>$ 0.6 mg$N$ l^{-1}), but the lack of measurements at this time of year prevents any validation.

Nitrate concentrations showed a similar marked seasonal pattern in all studied sites (figure 4.10), with higher values in winter and a sharp decrease in summer. By comparing model results with *in situ* data, it is possible to notice that the model captures the yearly fluctuation in nitrate values, but a correct match between model and observations is seldom achieved (e.g., MS1). As an example, the observed decrease in summer for nitrate values observed in all monitored sites (figure 4.10) are reproduced accurately by the model but not its absolute values. Therefore, the model reproduces the seasonal pattern observed in the monitored sites and gives a fairly approximation to the measured values. As with ammonium concentrations, nitrate seasonal pattern is not so evident in MS4, where concentrations tend to remain low the entire year (always below 0.5 mg$N$ l^{-1}). It must be highlighted

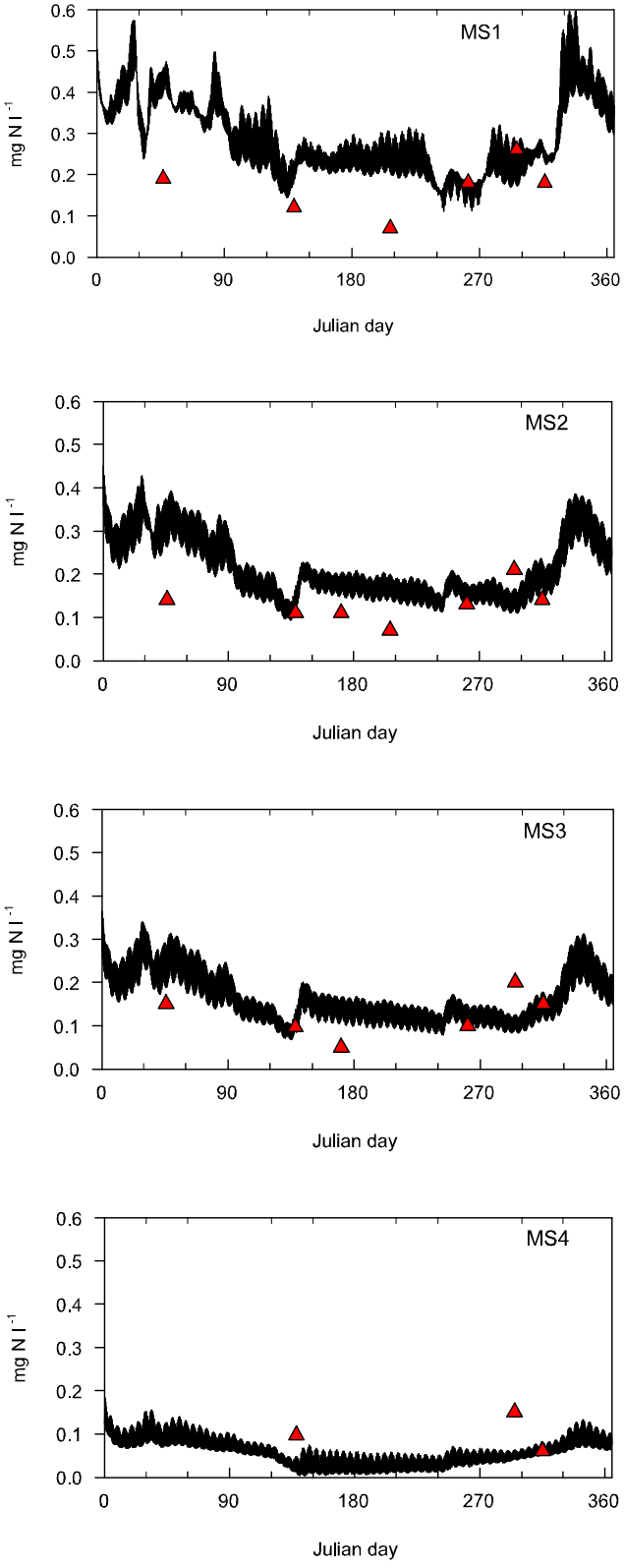

Figure 4.9: Ammonium values from sampling sites versus time series output from model stations.

that the model systematically overestimates ammonium in the system and at the same time it underestimates nitrate concentrations. Even so, results are still in the same order of magnitude of measured values.

Nitrate results also share with ammonium results the marked depression in concentrations at MS1 by the end of the summer. Unlike for ammonium, there are no sources of nitrate by mineralization and so its decrease is more pronounced, almost being depleted. It must be stressed that data is unavailable to allow any kind of validation of this result. Also in MS4 very low concentration values of nitrate are observed in the model, only in this case during the entire bloom period. The model clearly fails to converge to the observed values at this station.

There are no phosphate and silicate acid data available to compare with model results. As such, only model results are presented for each model station in figures 4.11 and 4.12. Both nutrients show a seasonal pattern with higher concentration in winter months, decreasing towards summer when the lower values are observed, and then increasing again as autumn advances. In addition, both nutrients show marked depression in concentrations during summer months, more pronounced in upper estuarine stations given the great difference between winter and summer concentration values (between 0.1 and 1.35 $\mathrm{mg}P\ \mathrm{l}^{-1}$ for phosphate, and 0 and above 6 $\mathrm{mg}Si\ \mathrm{l}^{-1}$ for silicate acid). The same spatial pattern is observed in phosphate and silicate acid, namely, a decrease in concentrations and seasonal values amplitude from MS1 to MS4.

In situ data resolution is detailed enough to suggest that there is a general spatial and temporal pattern of nutrient concentrations in the system, with higher values observed in autumn/winter months and in the upper estuarine areas, denoting a clear influence from the river Tagus discharge. Nutrient concentrations tend to be lower with increased distance from the upper estuary areas. So, the nutrient availability in the estuary is seasonally related to river flow. Nutrient concentrations decrease in summer is a result of a marked decrease in the discharges and of increased demand by producers.

The model is able to portray this temporal and spatial variation. The rate and timing of the marked decrease of nutrients in the water is generally correct, as is the subsequent increase in autumn. These patterns, however, are better observed with horizontal concentration field plots as shown in figure 4.13 for nitrate, inorganic phosphorus and silicate acid at different times of the year. Profiting from *MOHID* post-processing software tools these fields are easily constructed, allowing a better perception of model performance. All nutrients follow the same approximated pattern, changing only in the magnitude of the concentration values.

Of particular relevance in model results is the fact that, while experiencing variable periods of low concentrations, none of the nutrient is entirely depleted in the system during summer.

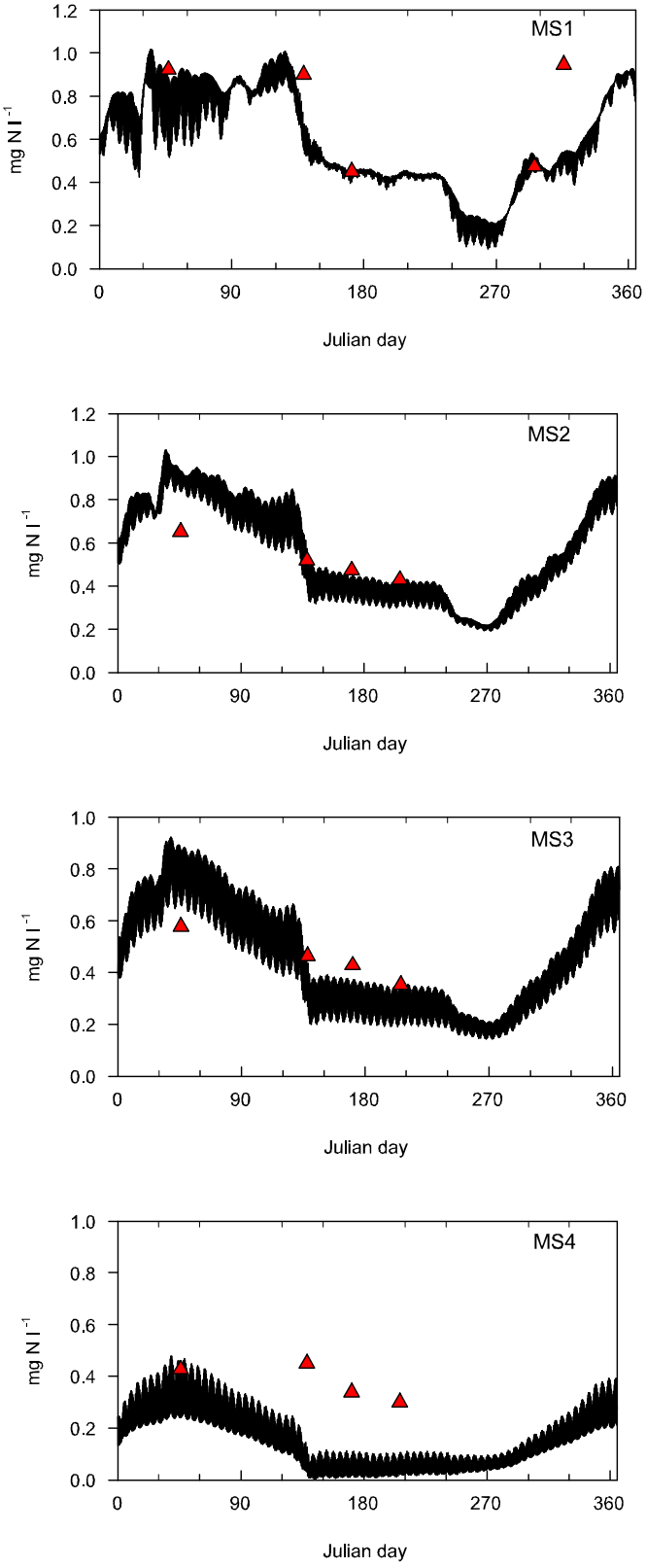

Figure 4.10: Nitrate values from sampling sites versus time series output from model stations.

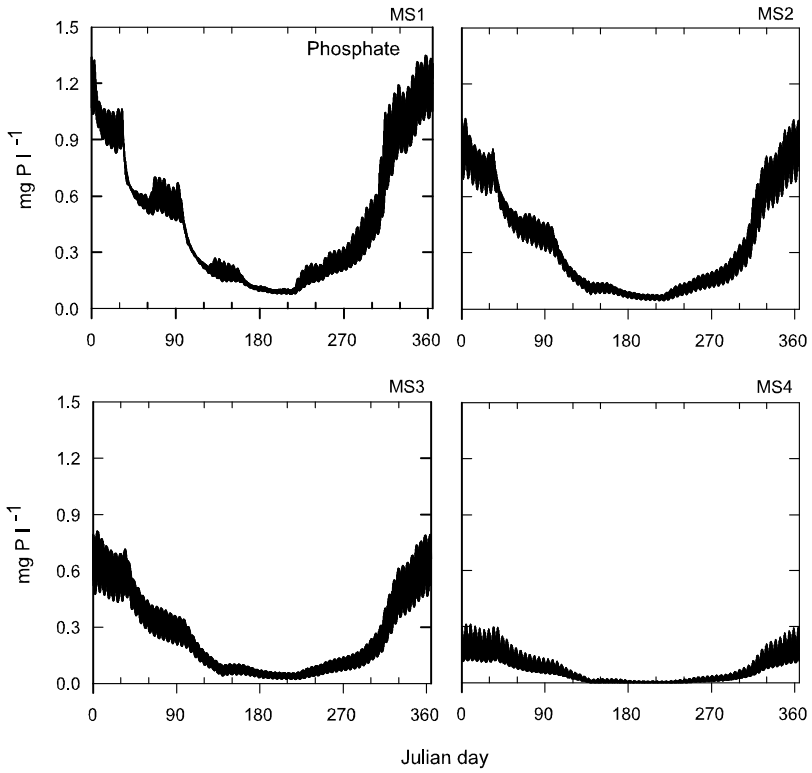

Figure 4.11: Model predictions for phosphate evolution in time at all model stations.

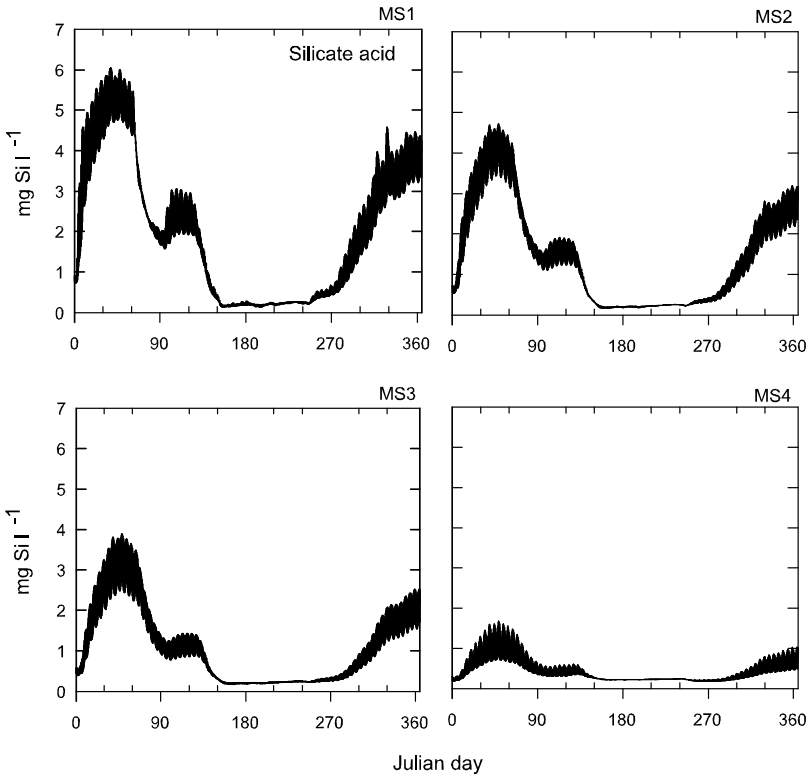

Figure 4.12: Model predictions for dissolved silica evolution in time at all model stations.

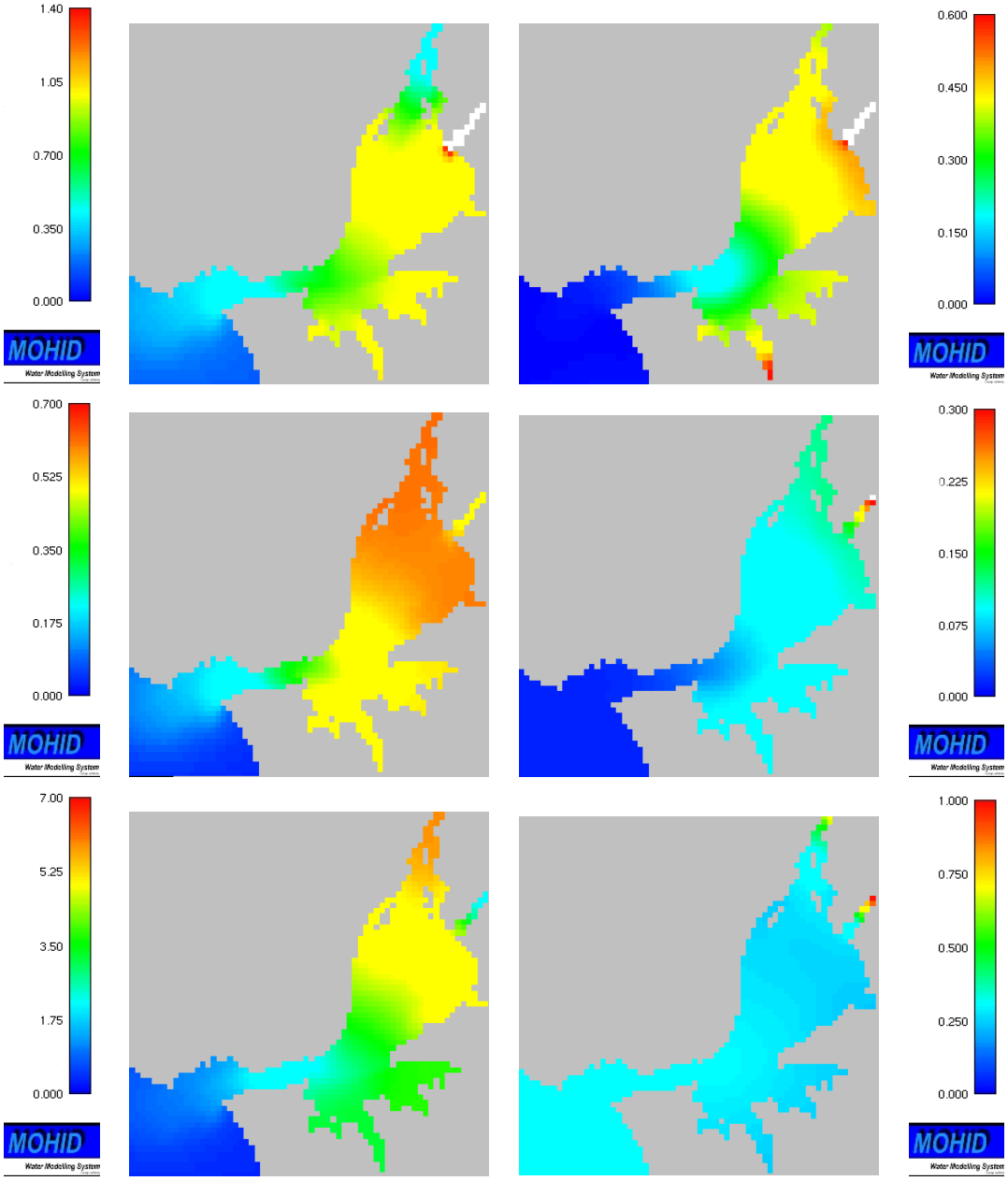

Figure 4.13: Model results for nitrate (top, $mgNl^{-1}$), inorganic phosphorus (middle, $mgNl^{-1}$) and silicate acid (bottom, $mgSil^{-1}$) horizontal distribution inside the estuary. Model predictions for Julian day 43 and 177 for winter (left column) and summer (right column) results, respectively. Different scales are used for winter and summer to enhance spatial pattern.

4.3.6 Dissolved oxygen concentrations

By comparing the oxygen concentrations of model results and measured data (figure 4.14) it is possible to acknowledge that the model is able to reproduce the general tendency of the evolution of this property. The different interval range of dissolved oxygen in data in the various check points is reproduced reasonably well for all sites. Nonetheless, the observed higher values in summer are not reproduced by the model for MS3 and MS4. Results denote that the oxygen balance in the system is satisfactorily achieved. However, some discrepancies are observed, mostly in sites 3 and 4 and also in MS1 and MS2 in February. The oxygen concentration value observed in November at site 4 (10 $\text{mg}O_2\ \text{l}^{-1}$) is probably an outlier and, therefore, must not be considered as representative.

4.3.7 Phytoplankton

The simulated phytoplankton chlorophyll distribution (figure 4.15) shows that the model reproduces the observed strong seasonal variation with a late spring/early summer peak in abundance, although with a lower magnitude in most cases. Measured values for the late-spring and summer months show consistently higher values for chlorophyll than those obtained from the model. Taking MS1 as an example, while *in situ* data reaches 15.5 $\text{mg}Chla\ \text{m}^{-3}$, model results only reach a total (sum of the chlorophyll of both groups) maximum of 13.3 $\text{mg}Chla\ \text{m}^{-3}$ at the bloom peak. But while missing the timing and magnitude of the bloom peak, the model shows a good fit for June and July at this site. The strong oscillation seen in the results, induced mainly by the diel light regime and the tide, can account for this fit The discrepancy between model predictions and data is more pronounced in MS2 and MS3 for the long term.

Observations indicate that despite being triggered at the same time, the timing of the maximum bloom peak is different among sites. Model results, on the other hand, show a slightly different scenario with the bloom peaking simultaneously in May at sites 2, 3 and 4, and some later at site 1. In addition, the decay of the simulated bloom is faster than the observed distribution suggests. After an initial bloom, total chlorophyll estimated by the model starts to decrease. Data reveal a decreasing tendency too, most clearly noticed at site 1 and 3. But while retaining this pattern, observed values and model results does not coincide as well everywhere. The model predicts smaller subsequent peaks in phytoplankton in late summer. However, observations to support the existence of this feature were insufficient or not available. The spatial distribution of chlorophyll in the estuary, portrayed in figure 4.16 for diatoms, reveals some curious patterns. In winter, higher concentrations of chlorophyll can be found in mid estuarine areas and in the south banks, while in summer there is a clear gradient from low con-

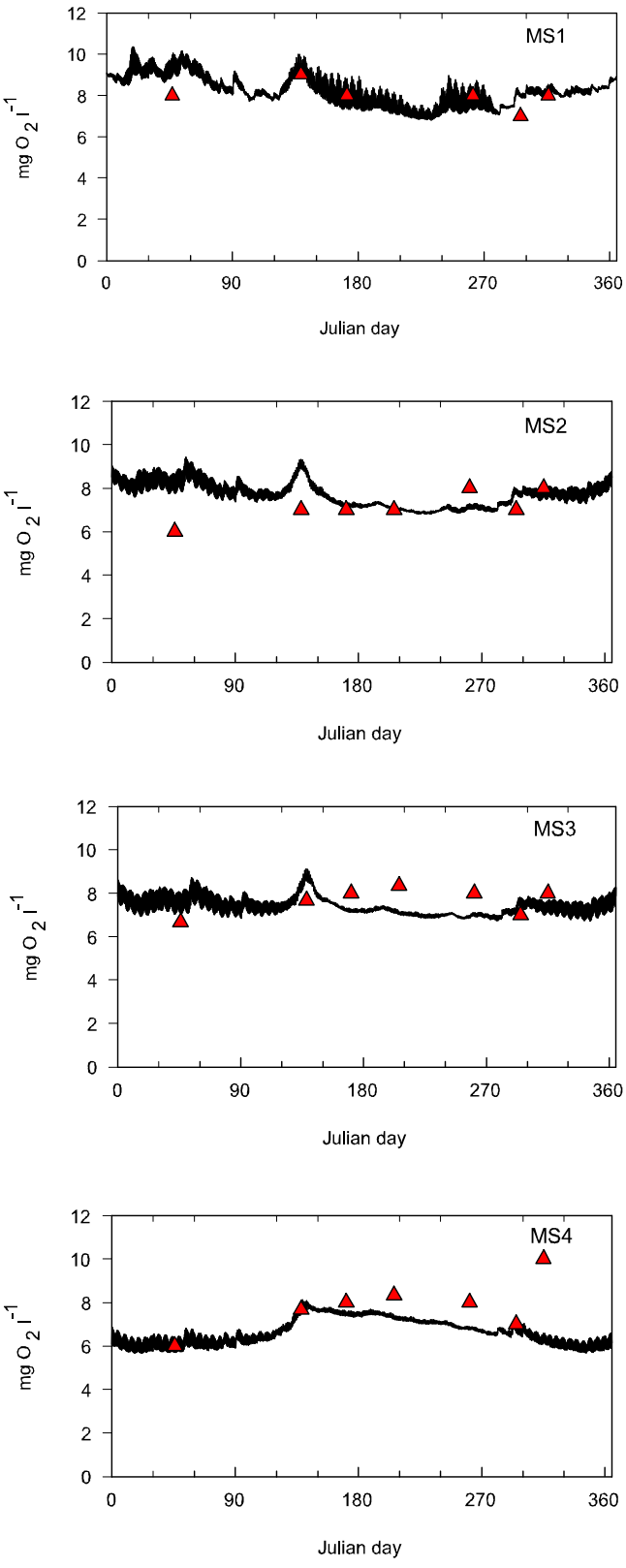

Figure 4.14: Dissolved oxygen values from sampling sites versus time series output from model stations.

centrations in the lower estuarine area to high concentrations in the upper areas.

Time series for chlorophyll distribution and C:Chl$a$ ratio evolution obtained by the model are represented in figures 4.17 and 4.18 for diatoms and non silica-dependent producers, respectively. Chlorophyll concentrations in diatoms tend to decrease along the transect, with higher values observed for MS1 and lower values at MS4. In all station, however, it is possible to identify the seasonal fluctuation. An inverse pattern is observed for non silica-dependent producers, that show higher values at MS4 and lower values at MS1. Hence, diatom dominance decreases and non silica-dependent producers dominance increases seaward.

A common feature to both producers groups in all model station is the seasonal fluctuation in C:Chl$a$ ratio (figures 4.17 and 4.18). There is a general pattern of lower values of C:Chl$a$ during Autumn/Winter months and higher values in Spring/Summer. The values for C:Chl$a$ vary around a minimum of 46 and 44, and a maximum of 114 and 102, in diatoms and non-silica dependent producers, respectively. Despite the constant fluctuation in the ratio, the increasing and decreasing tendency seen throughout the year shows a clear adaptation to the changing conditions of the system. Besides the clear temporal pattern in the C:Chl$a$ ratio, there is also a spatial pattern, though not so obvious. Even with a small difference in values between stations, they are systematically lower in upper areas when compared with the observed ratios at the river mouth. Taking diatoms as an example, the mean annual C:Chl$a$ ratio increases from 78 in MS1 to 88 in MS4, reflecting the better underwater light climate in the outer estuary.

4.3.8 Decomposers

Decomposers biomass distribution in time does not show any distinctive pattern. Bacterial biomass is relatively constant when analyzed at a smaller time scale (days), but it varies monthly and seasonally. Model results show that except for MS4, higher values are usually found during autumn and winter (figure 4.19). In addition, concentrations are more steady in this period of the year. MS4 has a reversed pattern with higher values observed during summer. However, when comparing values at the different stations, higher values are found up inside the estuary in late-summer, reaching 0.32 $\mathrm{mg}C\ \mathrm{l}^{-1}$ in MS1.

Because bacteria depend on organic C substrate for growth, but also of inorganic nutrients, its distribution patterns and abundance follow the abundance of DOM and nutrients inside the estuary. For that reason, decomposers biomass is usually higher in winter conditions and in upper estuary when the river flow is higher, discharging high loads of nutrients and OM in the system (middle row in figure 4.16).

The alternation in the allochtonous and autochthonous control is obvious

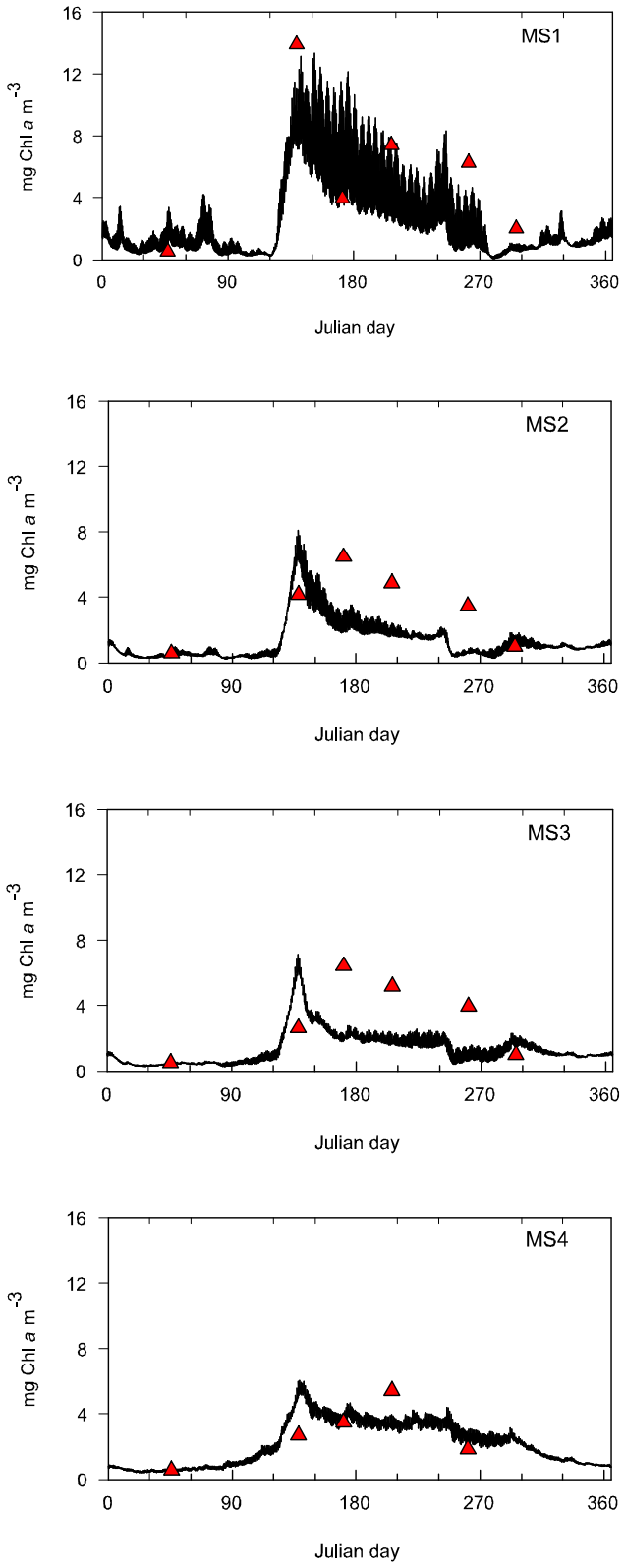

Figure 4.15: Chlorophyll values from sampling sites versus time series output from model stations. Model results are from total chlorophyll, i.e., the sum of the chlorophyll content from both producer groups.

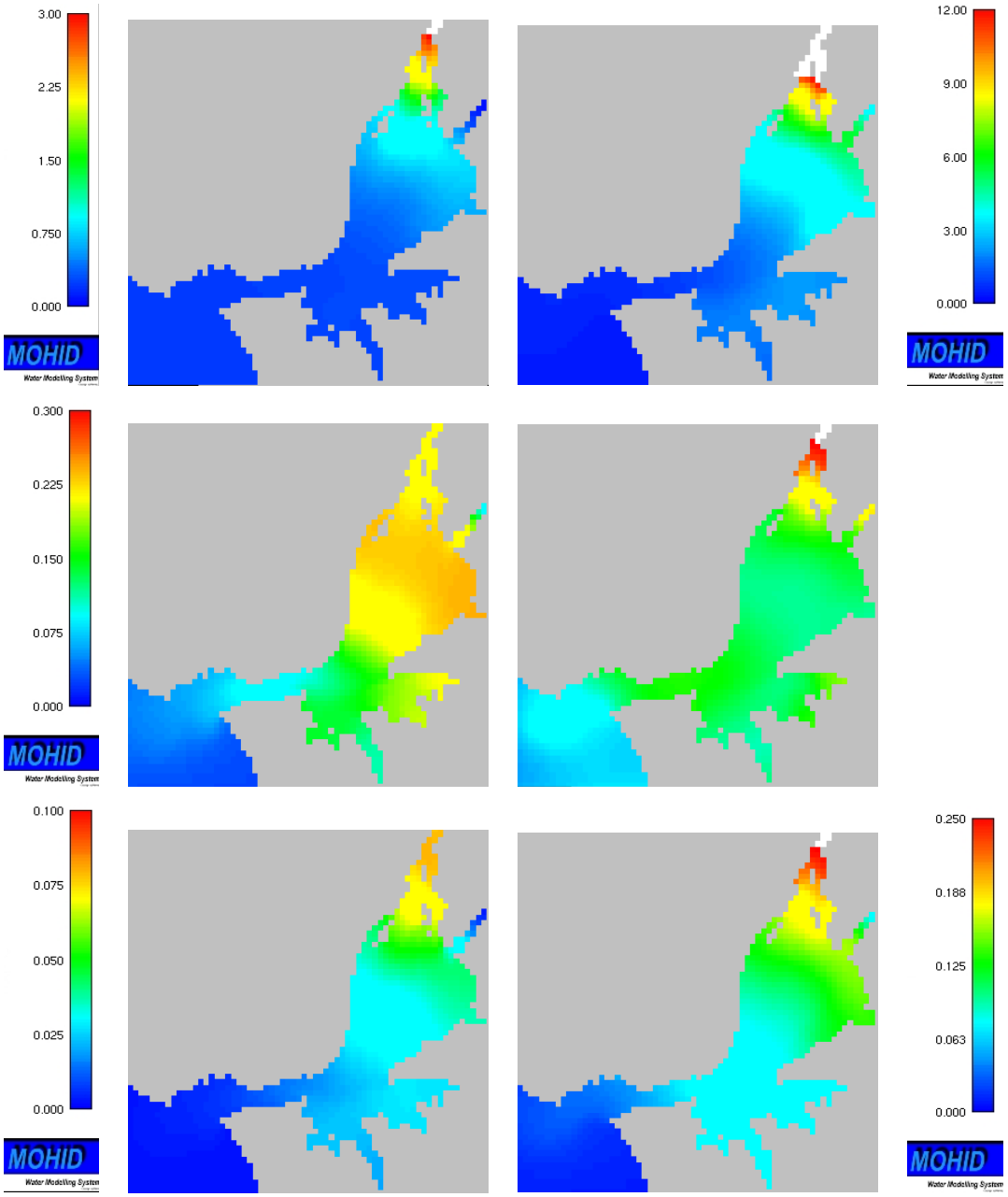

Figure 4.16: Model results for diatoms chlorophyll content (top, $mgChaam^{-3}$), decomposers biomass (middle, $mgCl^{-1}$), and consumers biomass (bottom, $mgCl^{-1}$) horizontal distribution inside the estuary. Model predictions for Julian day 43 and 177 for winter (left column) and summer (right column) results, respectively. Different scales are used for winter and summer to enhance spatial pattern.

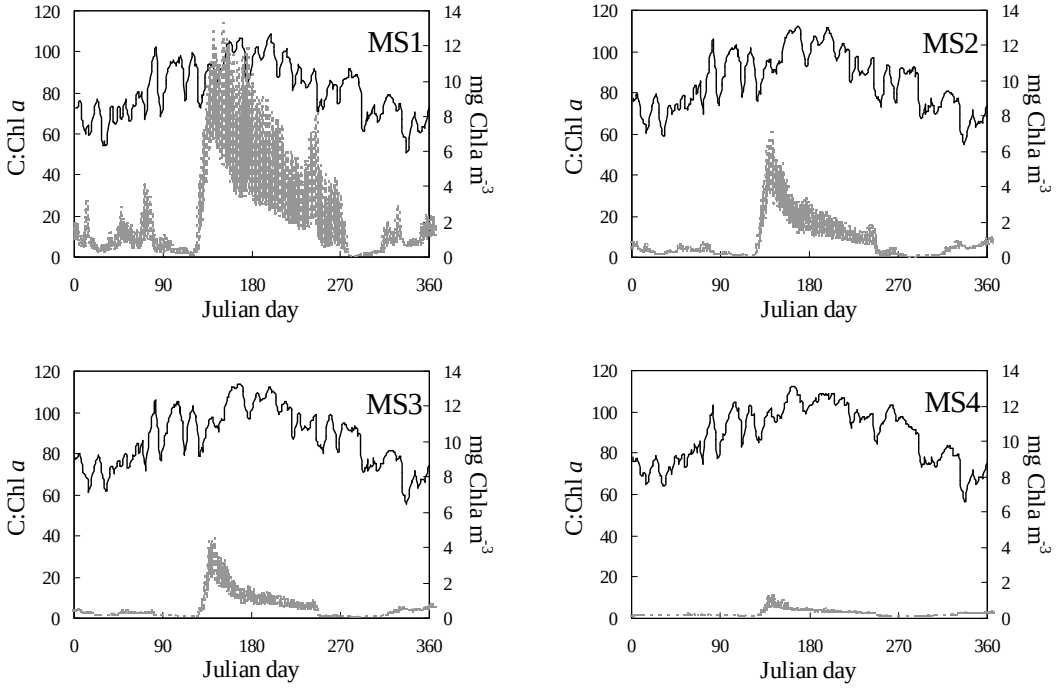

Figure 4.17: Model results for diatom Chla concentration (grey line) and C:Chl*a* ratio (bold line) dynamics.

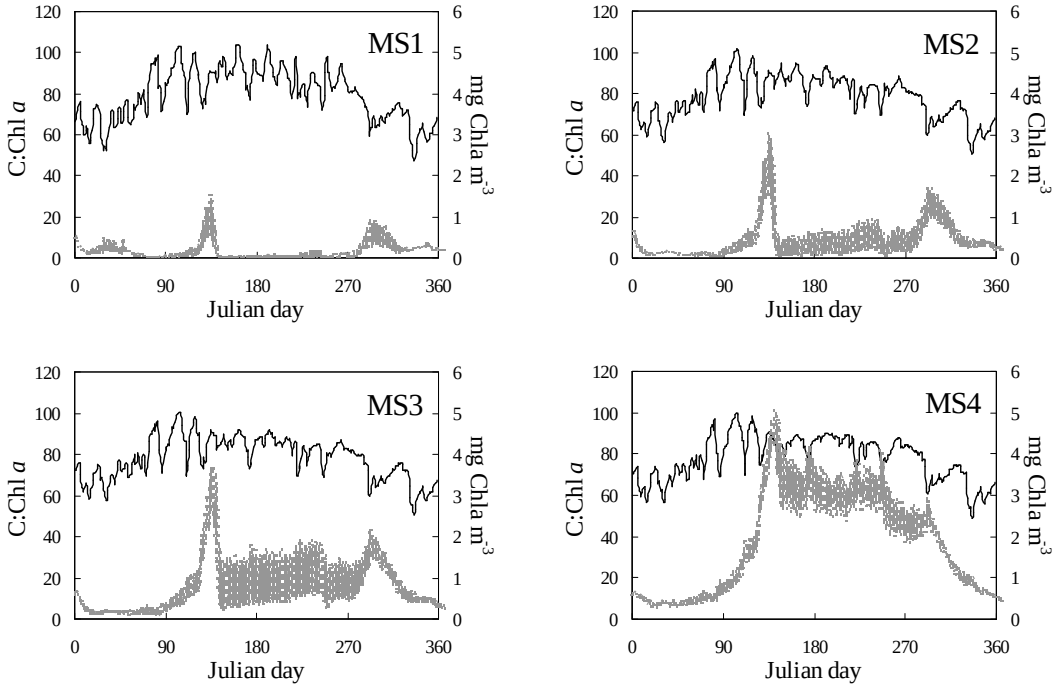

Figure 4.18: Model results for non silica-dependent producers Chla concentration (grey line) and C:C:Chl$a$ ratio (bold line) dynamics.

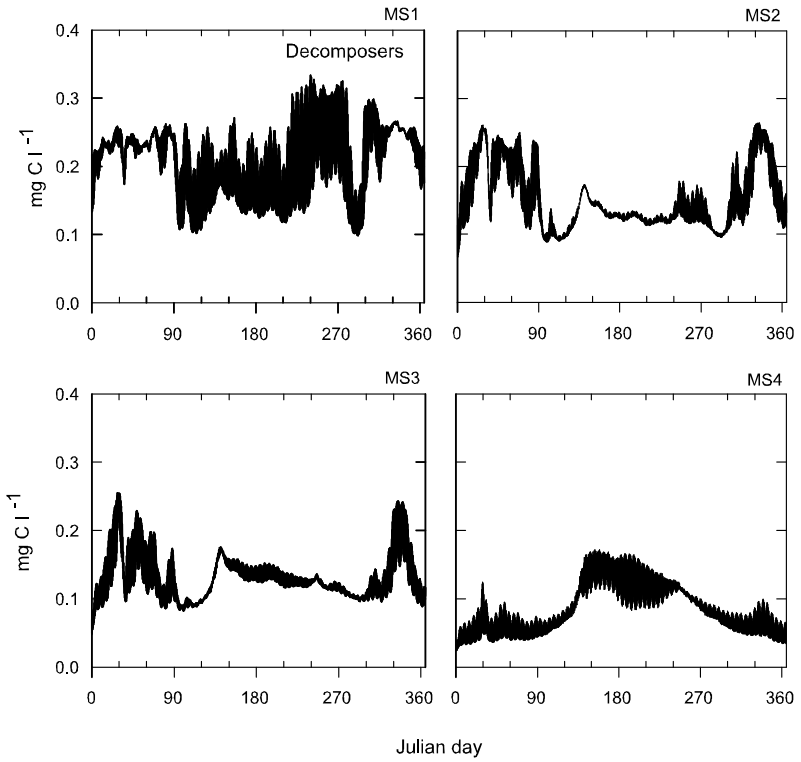

Figure 4.19: Bacterioplankton carbon biomass calculated by the model at the monitoring sites.

in the distribution of OM and nutrients. Both are usually depleted during summer when there is not sufficient inputs to ameliorate its shortage. During this time, the OM matter produced inside the system is the main source of C substrate.

4.3.9 Consumers

Given its dependence on living biomass as source of C and nutrients (either in the form of producers or decomposers), consumers biomass and distribution patterns are determined by the abundance of prey and temperature. As such, the abundance of consumers is a consequence of the availability of prey. Looking at figures 4.16 and 4.20, it is possible to see that the higher concentration in summer are a direct consequence of the abundance of producers and decomposers. As expected, consumers biomass reaches higher values in the upper estuary all year around as portrayed in figure 4.16 (bottom row).

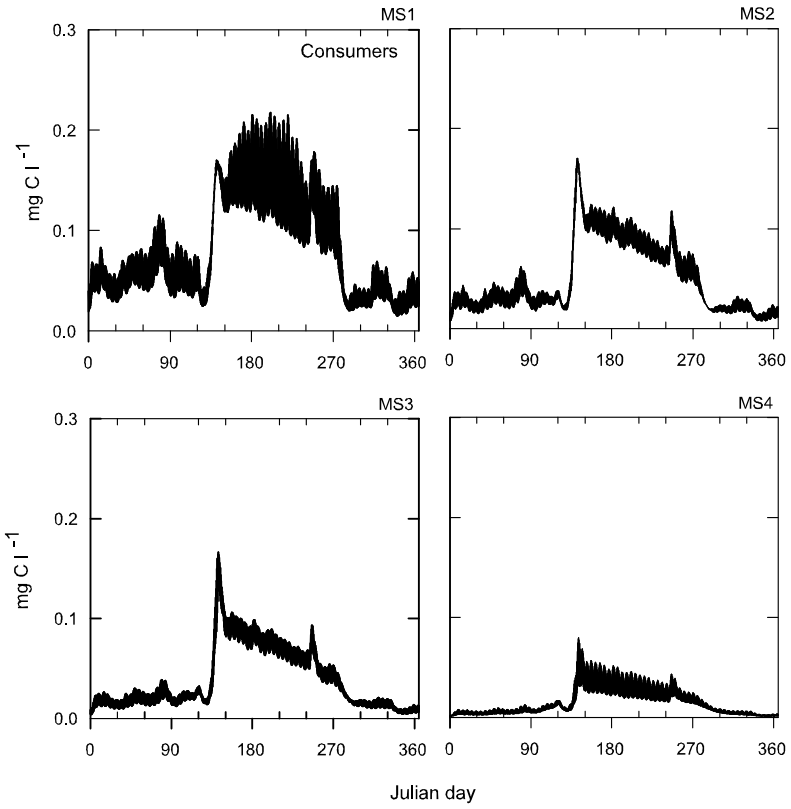

Figure 4.20: Consumers carbon biomass calculated by the model at the monitoring sites.

4.3.10 Organic matter and biogenic silica

The abundance of organic matter in the estuary is clearly linked to organisms activity and discharges to the system. The influence of the discharges is most clear in POM and labile DOM concentrations. As with inorganic nutrients, the Tagus river discharge contribution is more evident in the OM distribution patterns and concentrations in the system. Also because Tagus is the major source of OM to the system, its availability decreases with increasing distance from the river, as can be seen in figures 4.21 to 4.23. In the case of POM, river flow not only provides an input to the system, but it also contributes to the resuspension of deposited POM along with the all the processes conditioning the hydrodynamic regime like the tidal prism.

The contribution of biological activity to the OM balance is more obvious when looking at semi-labile DOM concentrations. While POM and DOM either sediment or are consumed by decomposers, the increased sinking rates and decomposers demand helps keeping concentrations low during summer months when the river discharge is low. Because DOMsl is not readily available for consumption by decomposers, it tends to accumulate in the system, as can be seen in figure 4.23. The spring/summer blooms explain the increase in DOMsl concentrations observed in this time of year.

Biogenic silica, much like OM, shows a clear relation with Tagus discharge, their concentrations being higher in months of high river flow (figure 4.24). There is a clear depression in the concentration around May, followed by a continuous increase during summer. The sudden change can be attributed to the loss of influence from the river and the increased influence of biological activity. High values of biogenic silica during summer, particularly at MS1, are a result of diatoms mortality, either natural or due to grazing.

All forms of OM and also biogenic silica have the same spatial distribution pattern inside the estuary, much like the pattern already observed for other properties. An example of this pattern can be seen in figure 4.25. At the same time instance, higher values are usually observed in the upper areas of the estuary where the river influence is greater.

4.4 Discussion

Considering that observational data sets always include components of variable or uncertain accuracy and gaps in temporal/spatial coverage, using such data sets to evaluate model performance and balancing their mutual deficiencies is a major challenge. Rigorous model evaluation requires broad compatibility between resolution and accuracy in models and observations - temporally, spatially (horizontal and vertical) and in parameter range [5]. Even with a low temporal resolution, especially during winter months, there is enough available data for a satisfactory characterization of seasonal pat-

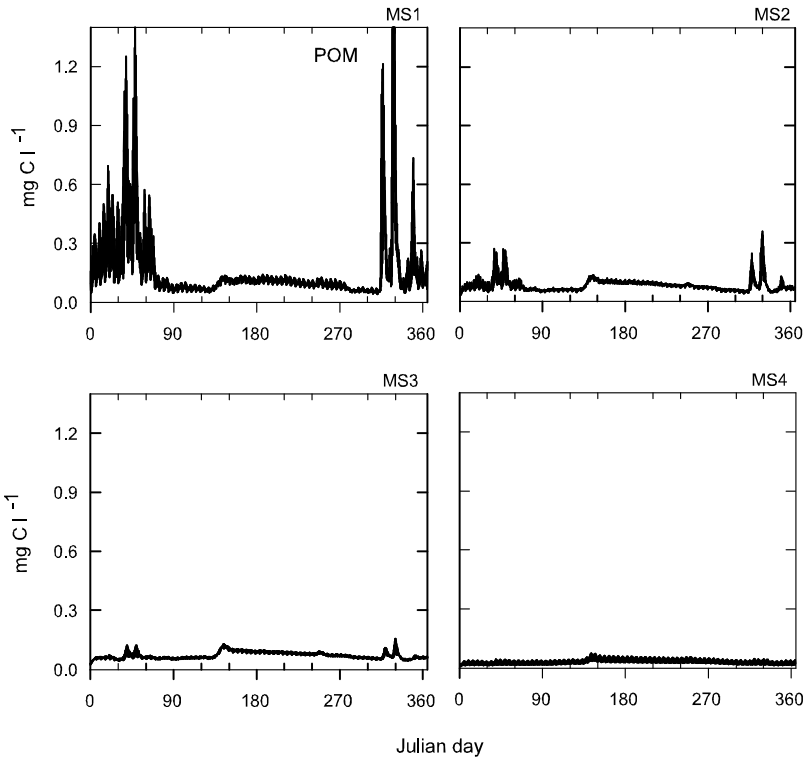

Figure 4.21: POM concentration calculated by the model at the monitoring sites.

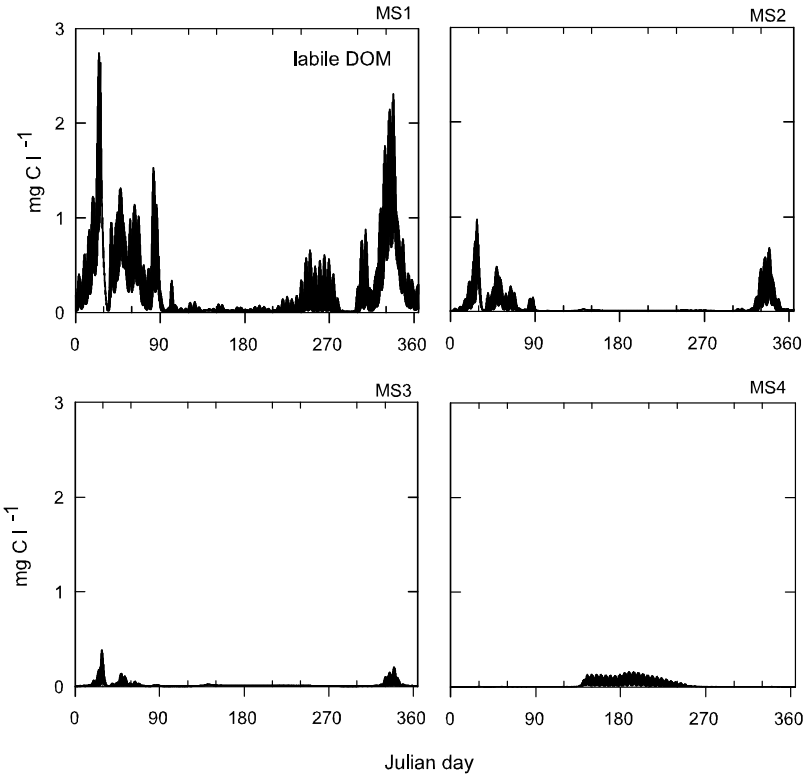

Figure 4.22: Labile DOM concentrations calculated by the model at the monitoring sites.

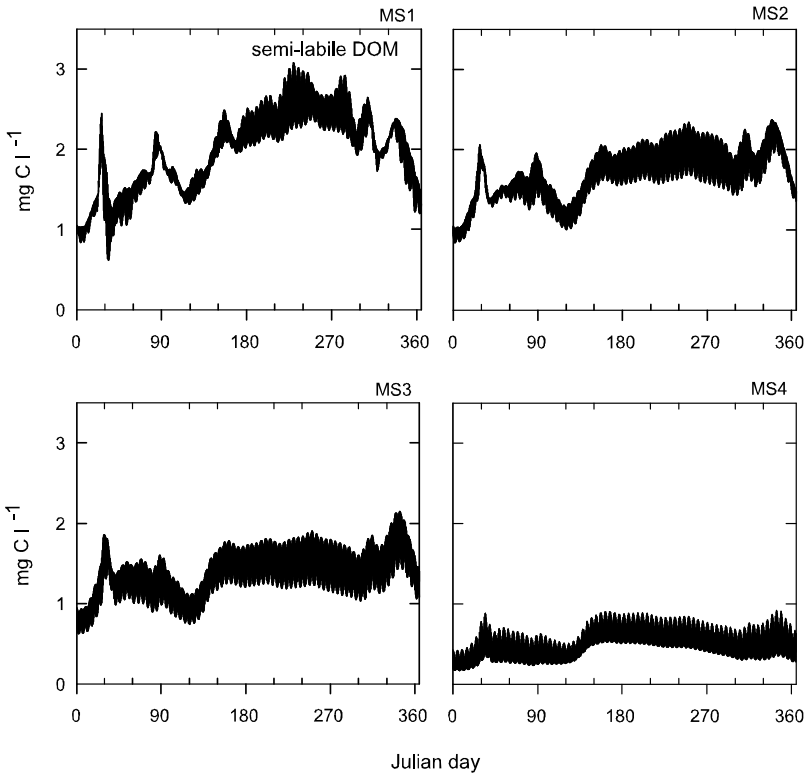

Figure 4.23: Semi-labile DOM concentrations calculated by the model at the monitoring sites.

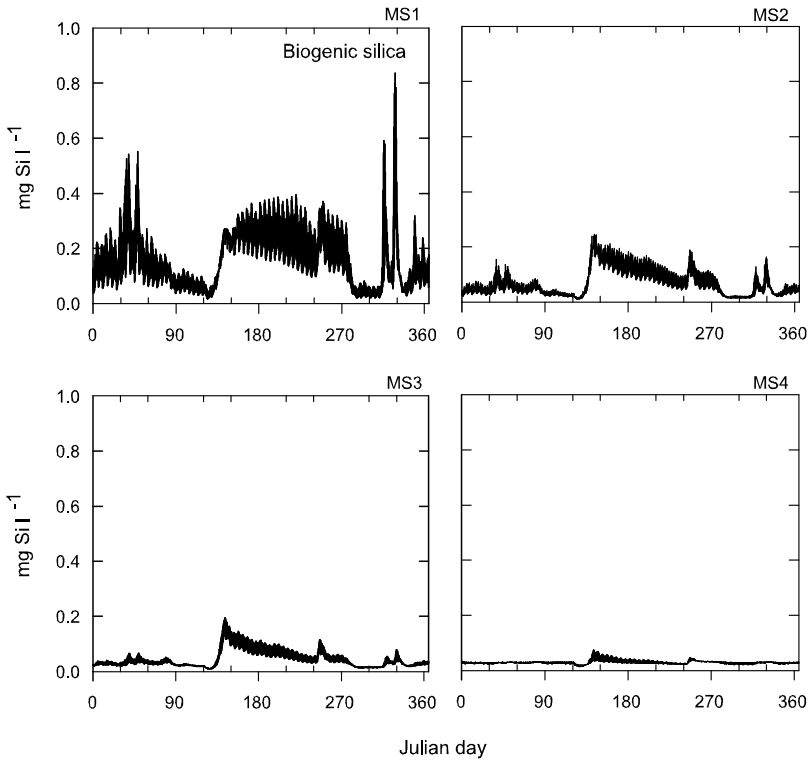

Figure 4.24: Biogenic silica concentrations calculated by the model at the monitoring sites.

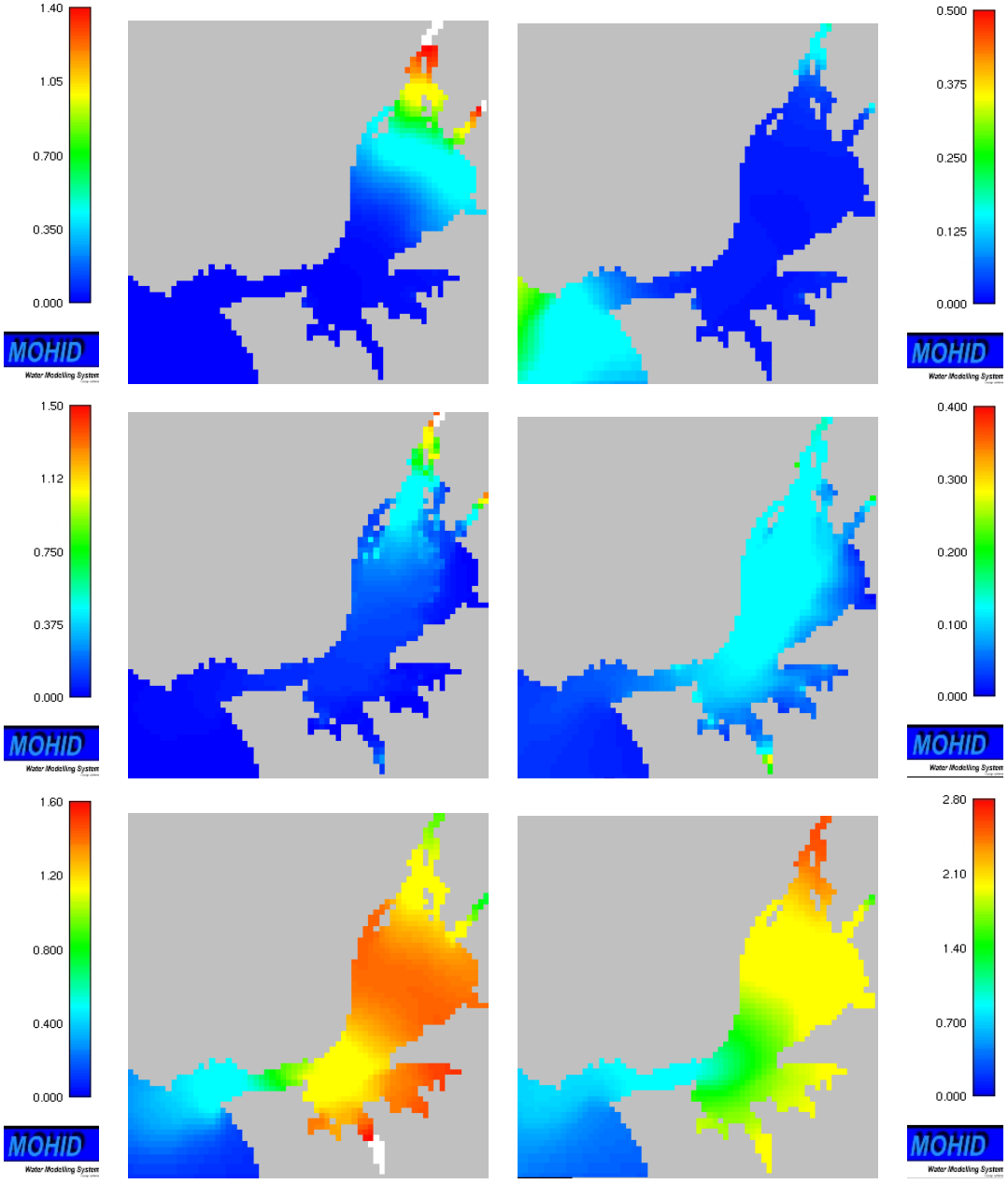

Figure 4.25: Model results for POC (top), DONl (middle), and DOCsl (bottom) horizontal distribution inside the estuary. All values im $mgCl^{-1}$. Model predictions for Julian day 43 and 177 for winter (left column) and summer (right column) results, respectively. Different scales are used for winter and summer to enhance spatial pattern.

terns. The same can be said about the spatial resolution because it enables the identification of spatial patterns inside the estuary.

Reproducing the timing and magnitude of events such as spring blooms, is usually a basic achievement expected from any pelagic ecological model. The discrepancy between model output and observations in some properties sometimes can indicate limitations in the model, inadequate or unrealistic parameterization, lack of detailed input values for river discharges and loads, absence of significant hydrodynamic processes, or even inappropriate initial conditions. As an example, the failure of the model to simulate the biomass peak may either have been the result of (1) low input values of phosphorus in the Tagus discharge, (2) flawed assumptions (e.g., extremely high grazing pressure), or (3) incorrect values for the production parameterization (chlorophyll synthesis, growth rates, etc.).

The model limitations are somehow clear, given the fact that being a model for the water column, it neglects the importance of benthic processes that play an important role in a shallow system such as Tagus estuary. As for the parameterization used in this model application, despite being based on published sets of values or derived from calibration, they still need further assessment and validation for each particular case. So, part of the error in the solution is undoubtedly related to the adopted parameterization. Finally, to avoid the additional uncertainties that might come from the inputs to the system, a detailed set of flow values and loads is required for all discharges.

Nevertheless, for the scenarios investigated here, the observation of biogeochemical parameters could be qualitatively reproduced and sometimes a satisfactory quantitative agreement was achieved. There are many reasons why a better quantitative agreement has not been attained. The most obvious have already been mentioned above, but the identification of other possible factors impairing model performance will still need a more detailed approach.

4.4.1 Hydrodynamic processes

The strong dependence of biogeochemical parameters on the applied turbulence closure scheme is obvious in this scenario. The transport scheme is important for food webs in marine systems since much of the observed structure in plankton populations results from the effects of the circulation patterns. And these patterns are particularly relevant in estuaries given their complex flow regimes. The choice to implement a 2D hydrodynamic model to the domain are clearly justified on the know characteristics of the estuary, namely its shallowness and hydrodynamic regime. Previous modelling experiences using *MOHID* hydrodynamic model [54, 144] have shown that 3D effects are only relevant close to the mouth and during high flow periods. As such, the limited area does not justify a full 3D application

because the benefits would not outweigh the cost of such a computationally demanding scenario. The Tagus estuary is a typical well mixed estuary where vertical stratification, whether induced by temperature, salinity, or both, is absent. Except for a few confined areas in the upper-estuary, where the hydrodynamic regime might be characterized by high residence times, stratification is unlikely to occur. Nevertheless, the model has the ability to address such complex physical-biological interactions usually observed in stratified systems if conditions so require.

Being outside the aim of the present study, no special attention was paid to the hydrodynamic regime along the coastal shelf outside the estuary. This area is characterized by upwelling events in late spring and summer [145], with nutrient enrichment of surface waters and an associated high productivity. By not taking this process into account, it is possible that the simulation may fail to correctly represent some parameters like chlorophyll and nutrient distribution in the estuary, because production and nutrients in the upwelling areas can be imported into the system, ultimately enriching the lower estuary during low river flow months.

4.4.2 Abiotic conditions

Temperature and salinity inside the estuary are both strongly controlled by river discharges and the tidal-induced circulation. The evolution in time (scale of weeks to months) of their spatial pattern is clearly linked to the fluctuations of the Tagus river flow. In the case of temperature, the seasonal variations in the light regime characterized by the increase of radiation reaching the surface and being absorbed by water molecules and suspended matter contributes to the temperature increase in summer. Seasonal variations also induce an increase in the atmospheric temperature, leading to heat transfer from the atmosphere to the water. Together, irradiance and atmospheric temperature, account for the increase of water temperature from late-spring months, all through summer, and only decreasing whit the start of autumn.

Salinity inside the estuary shows the extent of the influence of the River Tagus and of the saline intrusion controlled by the tidal oscillations. In winter months, with Tagus River flow reaching maximum values (~920 $m^3 s^{-1}$, figure 4.3), salinity distribution inside the estuary is characterized by lower values when compared with summer months. In summer, with river discharges reaching minimum values, the hydrodynamic regime controlled mainly by tidal cycles leads to a much more extensive saline intrusion to the estuary.

Given that the cohesive sediment concentrations in the water have two possible sources, river discharge and resuspension, its evolution in time has a clear seasonal signal induced by the variation in the Tagus river flow, another signal influenced by the fortnight cycles of neap/spring tides, and finally a semi-diurnal signal determined by the tidal cycle. Because cohesive

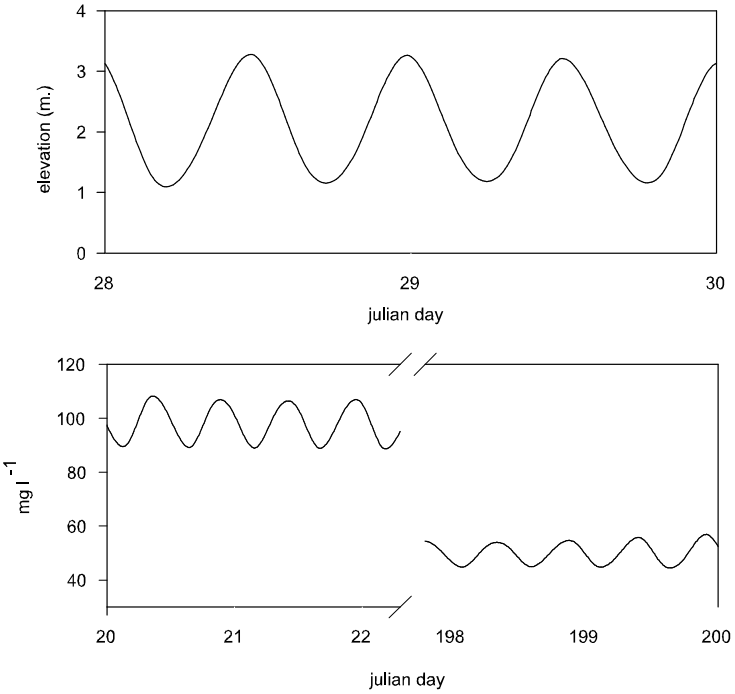

Figure 4.26: (a) Surface elevation for a period of two days, and (b) cohesive sediment concentration in winter and summer. Results from MOHID hydrodynamic model at MS1.

sediments decrease light penetration in the water column, they have a direct influence on phytoplankton production. Therefore, the daily, monthly and seasonal fluctuation in sediments eventually shape the production patterns inside the estuary. River discharge can be considered as the major input to the system during winter, while resuspension can be considered as the major source during summer when river discharge reaches the lowest values. In figure 4.26 it is possible to see the concentration of cohesive sediments in water at MS1 in winter and summer regime. The concentration of sediments in water varies among seasons, revealing the strong influence of Tagus discharge. Also in figure 4.26 it is possible to see the semi-diurnal tidal cycle (expressed in the surface elevation) that strongly controls the sediment deposition and resuspension dynamics inside the estuary.

No attempt was made to calibrate or validate model results for temperature, salinity and sediment dynamics. Given the long history of successful applications of the *MOHID* hydrodynamic model ([54, 142, 144, 146, 55]), with Tagus estuary among many others, these features have already exhaustively tested and the calibration and validation properly achieved. As such, this study relies on the assumption that the model correctly simulates these

properties in the system based on past successful applications.

4.4.3 Limitation to production

The controlling mechanisms on the production of estuarine and coastal systems are usually summarized in five major conditions: (1) nutrient availability, (2) temperature, (3) grazing, (4) ambient light, and (5) transport. The model application confirms to some extent that though the residence time may shape the chlorophyll patterns in the system, it does not act as a limiting factor, as has already been observed with a simpler ecological model application to this system [144].

Usually, the large signal from nutrient variability draws attention away from other relevant processes. However, both experimental [139, 147] and numerical studies [148, 144] have pointed out light as the major limiting factor both inside the estuary and in coastal areas influenced by the river plume with high concentrations of suspended matter [147]. The results obtained by the model corroborate this scenario. But while imposing a limit on the production inside the system, results imply that the light climate, together with the hydrodynamic processes that regulate nutrient availability and temperature, strongly shape the observed zonation.

The model application reveals a complex interplay of physical, chemical and biological factors shaping the biological patterns inside the estuary. A seasonal cycle is evident in the results, mostly governed by irradiance and the Tagus river discharges. Organic matter, phytoplankton and bacterioplankton biomass values found in this study are in the same range of values observed in other estuarine systems [149] with higher values in inner estuarine areas, with a limited circulation, and lower values in the main channels with high hydrodynamic regimes. This implies that despite differences between model results and data, the model can still capture the main features of such a system.

Production in estuaries is usually limited by nutrient availability, light, or both. The results suggest that each limitation process may play a role inside the Tagus estuary, and sometimes they may act together to maintain the producers biomass relatively low. Some contrary effects may also occur. In summer months, the decrease in the input of fresh water and lower nutrients is somehow compensated by the increase of water transparency. However, the Tagus hydrodynamic features imposes a relatively high sediment resuspending regime which helps to maintain high concentrations of sediments in the water column, therefore compromising the light penetration.

4.4.4 Residence time

The formation of blooms inside the estuary is controlled by local conditions and transport-related mechanisms that govern biomass distributions. Bio-

mass abundance at any particular place and time is a function of (a) spatial variability of population dynamics, and (2) spatially variable transport of water. As such, the analysis of the results must be made with these different controls in mind.

The first control can be defined by the local combinations of both biotic and abiotic parameters responsible for the balance between production and loss (turbidity, nutrients, grazing pressure, etc.). Therefore, local conditions control net population growth at a particular spatial location. The second major control - transport - determines biomass concentration and distribution, thus controlling if and where a bloom actually occurs (favorable conditions for patchiness vs. dispersion of mass through the domain, etc.). The transport inside the estuary determines the residence time of the water in different parts of the system, determining if phytoplankton stay the necessary time to generate a bloom, but also conditioning the exchanges between sediment and water column.

The relation between freshwater flow and accumulation of phytoplankton biomass in estuaries is complex. In some estuaries where the processes of material transport are mostly driven by tidal fluxes, the semi-diurnal variability will prevail over seasonal effects. In the Tagus estuary, considering the high flow from the Tagus river, transport is driven by both tidal fluxes and river discharge. River discharges are particularly relevant in winter months characterized by high flow values. While high freshwater inputs can stimulate primary production by importing nutrients into the system, the development of blooms is only possible when the net rate of biomass accumulation exceeds the losses (either by biotic or abiotic means). Therefore, low river inputs causing long water residence times allow the accumulation of phytoplankton and may act as the triggering factor of a bloom. The link between river discharges and the start of the spring bloom (both in model results and *in situ* data) clearly reveals the influence of the residence time controls mainly by the river discharges that are decreasing in this time of year.

Chlorophyll distribution inside the estuary shows a clear dependence on the hydrodynamic circulation. Optimal bloom conditions only occur in mid and upper estuarine areas, a fact that is explained by the high residence times in these regions. Previous studies of the residence time inside the estuary using the *MOHID* tools [144] have shown that in the middle areas of the estuary the residence time is around 25 days, whereas in the narrow areas near the river mouth the residence time is much shorter influenced by advection. The tidal flat areas located in the south and southeast margins of the estuary also have residence times lower than 10 days. In these areas, the renewal efficiency is regulated by the exchange of water with the central part of the estuary. Also, the water exchange between the riverine and coastal system allows a faster dilution of bloom in these areas while the more stagnant conditions in the upper estuary keeps the bloom together. Ulti-

mately, the hydrodynamics influence the chlorophyll patterns in the estuary, defining where blooms may occur. By comparing the Tagus flow and the timing of the bloom formation it is possible to notice that lower river inputs and long water residence times during summer enhance the accumulation of phytoplankton.

4.4.5 Underwater light climate control

Together with the shallowness of the estuary, the balance between freshwater and saline water controlled daily by the strong tidal currents and influenced seasonally by the river contributes to the absence of a vertical stratification. River inflow, reflecting climate variability, affect biomass through fluctuations in flushing, but also induces changes in the growth rates through fluctuations in total suspended solids. Despite there may be several regulatory mechanisms acting at the same time or with particular spatial/temporal relevance, the results indicate light availability as the major control inside the estuary. This is a common feature to other estuaries [138]. The resuspension of fine sediments induced by the strong tidal currents determines the underwater light climate. Tidally driven resuspension, and riverine source of sediments might be important mechanisms influencing suspended matter concentration, determining the photic depth in the water column. So, even when nutrient concentrations are relatively high, light availability will be the key limitation.

The high turbidity inside the estuary, typical of mesotidal estuaries along the European Atlantic seaboard, resulting from strong tidal currents and resuspension of fine particles, will limit phytoplankton growth. Hence, in this kind of systems, light is a key limiting factor for pelagic primary production [150]. Because the estuary is well mixed, phytoplankton populations have to adapt to continuously changing irradiance conditions ranging from complete darkness to saturating light. Under such conditions, a photo-adaptation mechanism like the production of chlorophyll in response to environment optical conditions is a better approximation to the estimation of chlorophyll than the use of fixed C:Chl$a$ ratios.

The results denote the higher control of light in Autumn/Winter as a consequence of: (1) higher river discharges and sediments and organic matter in the water column, and (2) the natural light regime characteristic of temperate zones. To compensate for lower light levels, the model increases the chlorophyll content of the cells, explaining the observed patterns (figures 4.17 and 4.18). Despite the correct characterization of the evolution of the C:Chl$a$ ratio, the values are relatively higher than would be expected. Because the chlorophyll synthesis also depends on the nitrogen uptake, the observed fluctuation in the C:Chl$a$ ratio in model results are explained by the variable uptake of this nutrient. A quick look at the variation of both ammonium and nitrate makes this point clear. Higher biomass values were

found in the upper estuary reflecting the higher availability of nitrogen, both recycled in the system and added via river discharge, but also because of the higher residence time in this area of the estuary. The lower values were observed near the main channel (MS2 and MS3) as a consequence of the higher hydrodynamic circulation imposed mostly by tidal regime and magnitude. Despite the wind-induced oceanic circulation in the outer estuarine zone, the conditions are still favorable to an accumulation, explaining the increase in chlorophyll concentration from MS2 to MS4.

There is a clear control by light inside the estuary as it can be seen by the result analysis. This control has already been revealed by a detailed modelling effort using the *MOHID* hydrodynamic model with a coupled NPZ water qualify model [56]. In a study to assess the effect of different nutrient loads to the Tagus system, a two-fold increase in the loads has proved to have minor effects on the total primary production inside the system. This previous application with the *MOHID* modelling system has reinforced the concept of light limitation already proposed by other experimental and numerical studies ([139, 147, 148]).

4.4.6 Temperature and predation

Water temperature has an impact on the dynamics of the system because it regulates all biological rates. Therefore, the clear seasonal fluctuations in producers, consumers and decomposers is influenced by temperature. Because temperature fluctuation over the year follows the radiation fluctuation closely, its influence on producers is difficult to be separated from light influence. Results suggest that both forcing functions influence producers.

In some systems, predation is considered as the major control on phytoplankton abundance. There are no data available for the Tagus estuary that allow an assessment of this control by consumers. The lack of data on the trophic structure in the estuary makes it impossible to determine the full magnitude of this control. Model results show that consumers abundance follows prey abundance closely, but a control on prey populations cannot be inferred from this observations alone. Consumers have a clear regulation by temperature, as can be seen in figure 4.20. Consumers concentration are relatively low during winter. Results reveal that during this period of the year, mainly decomposers support consumers standing stock. The marked increase in late-spring that extends throughout summer is a response to the producers concentration increase, but also an increase in the growth rate induced by higher water temperatures.

As far as any inference from model results may go, temperature and predation exert an ambient and top-down control, respectively. Such control, either from temperature or predation, can be considered as a shaping factor for producers standing stock temporal and spatial distribution, but not as a limiting factor inside the system.

4.4.7 Nutrient control

In this study, nutrients do not limit production in the system but appear to exert some control on the producers group dominance. This is particular relevant for silica, because there is a clear decrease in diatoms dominance from inner estuarine areas towards the estuary mouth. *In situ* data does not seem to agree with this limitation given that high values of silicate acid have been observed in the coastal areas outside the estuary in summer months [147]. As mentioned before, the discrepancy between model results and observations may be explained by the upwelling phenomena observed in summer months that enrich the surface layer with inorganic nutrients, silica included.

On some occasions, model results suggest a phosphorus limitation. But before any statement can be made about a possible nutrient limitation in summer, a detailed set of values for phosphorus input via river must be evaluated to determine any possible underestimation in the loads used in this study.

The constant values of ammonium observed in the measured data imply that a great part is produced inside the system, and that this production is particularly relevant during summer when the river discharges are lower. Horizontal nutrient gradients reflect the considerable loadings of nutrients (N, P and Si) discharged by the Tagus river. The clear zonation observed in model results reflects the impact of river discharges in autumn/winter on one hand, and of biological activity in spring/summer on the other. These contributions help to explain the consistent higher ammonium concentration in upper areas, where the discharge contribution is higher and also biological production and mineralisation. Despite the high demand for ammonium by producers to maintain the high biomass values found in this areas, mineralisation (by consumers and decomposers) balances the sinks, keeping ammonium concentration high in summer. The overestimation of ammonium and underestimation of nitrate concentrations in the estuary may indicate insufficient nitrification due to incorrect parameterization.

The model shows no signs of severe nutrient depletion in the summer, supporting the claim that the control of production in the system is not made by nutrients. The available data for ammonium and nitrate support this result. Limitation of phytoplankton growth by DIN has already been established in the upper areas of the estuary during summer [151]. Nonetheless, both model results and *in situ* observation tend to disagree with this. So, it can be hypothesized that such limitation is not a common occurrence in the estuary (since in situ data used in this study does not point that way) or that the model is failing to reproduce this limitation.

Given the model assumption of a variable nutrient quotas, it is possible to have an idea of the influence of nutrient deficiency that may determine production at any given time. Such nutrient influence can be seen in figures

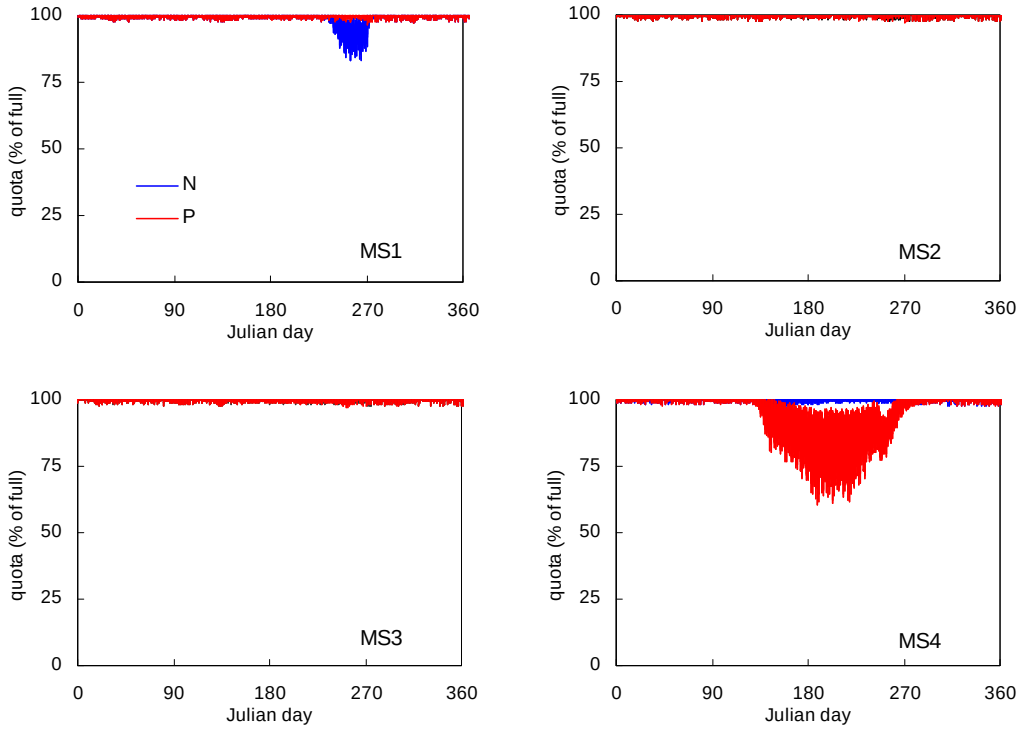

Figure 4.27: Nutrient (N and P) limitation in diatoms observed at model stations during the entire year. The limitation is expressed in state of nutrient reserves (quotas).

4.27 and 4.28, where the nutrient quotas variation in time is shown. In this case it is possible to notice some mild nutrient limitation during summer months, especially for phosphorus. For both producers, the limitation is consistently higher at the mouth of the estuary where the nutrient supply is limited. Most of the nutrients discharged by the river are consumed in the upper areas, with only a fraction of it, along with regenerated nutrients inside the estuary, reach the outer zone of the estuary. This is particularly relevant in summer months when the river flow is significantly reduced, decreasing the its importance in the estuary nutrient enrichment. During this period, nutrient recycling inside the system becomes more important, as well as the enrichment via coastal water entering the estuary.

The lack of *in situ* data for silica and phosphorus prevents any conclusion regarding its role in the control of production. The model clearly limits diatoms growth as a consequence of silicate acid shortage. Phosphorus limitation for phytoplankton growth has been observed in the Tagus coastal areas [147], a fact that highlights the relevance of explicitly modelling its cycle in this particular system. Model results suggest that there is no ap-

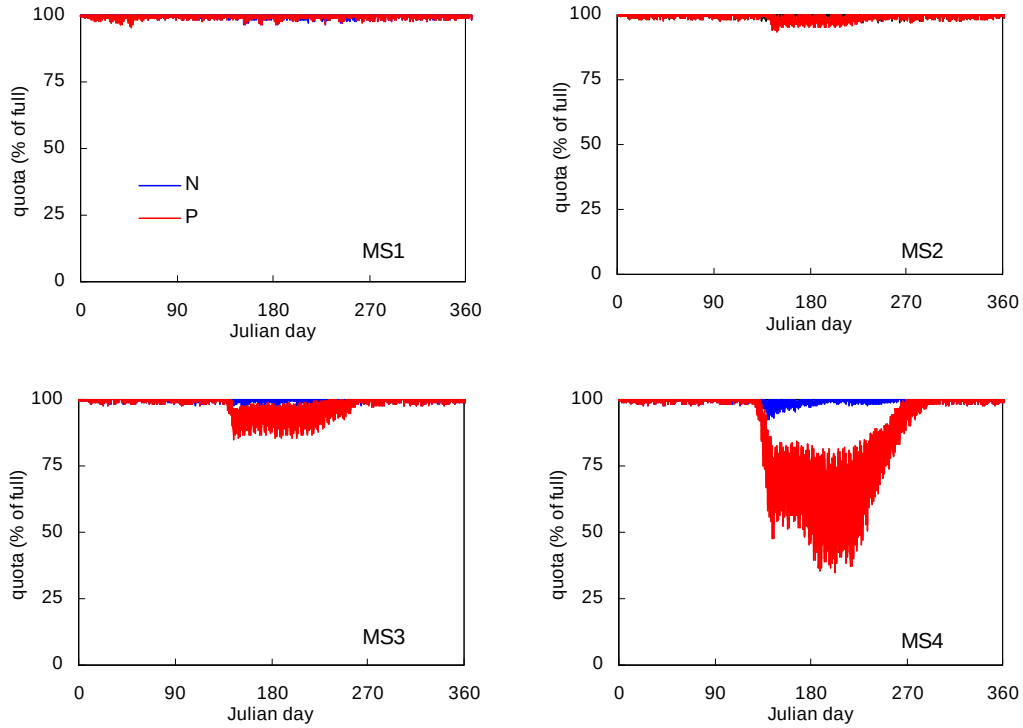

Figure 4.28: Nutrient (N and P) limitation in flagellates producers observed at model stations during the entire year. The limitation is expressed in state of nutrient reserves (quotas).

parent limitation by phosphorus (figures 4.27 and 4.28) except for flagellates in MS4, in agreement with observations.

Using the same hypothesis for silica can only be done with *in situ* data. Despite the clear relations between silica availability and diatoms concentrations denoting a strong control, the high concentration referred in the literature for the mouth of the river area [147] shows that there is a shortage of silica in the model, either as a results of low inputs to the system or excessive sink (lost as biogenic silica and mineralized outside the system).

The lack of a "typical" nutrient control scenario is of particular relevance in the Tagus estuary case. The estuary receives the discharges from more than 10 WWTP's, spread inside the estuary, acting as point sources of nutrient supply. The estuary receives a nutrient input corresponding to about 3×10^6 population equivalents (PEQ), resulting from domestic and industrial discharges [152]. Some more additional WWTP's are projected and, therefore, the nutrient load is expected to increase in the near future. Hypothetically, this increase in nutrients will not result in a net production increase up to problematic levels. Nonetheless, the input of anthropogenic nutrients (N & P) may induce a change of Si:N in the system, possible leading to conditions that allow flagellate dominance over diatoms.

Previous modelling approaches have pointed out the potential role of seaweeds in the control of the nitrogen balance in the system, by removing large amounts of this nutrient from the water [148]. *MOHID* comprises a macroalgae model already implemented to another Portuguese estuarine system [153]. This module, however, is not compatible with *mohid.Life.1.0* modelling philosophy (multi-nutrient). Hence it was not included in the present study.

4.4.8 Producers chlorophyll biomass

Assuming that the circulation inside the estuary is well simulated, the underestimation of producers chlorophyll content reflected in the chlorophyll concentrations can be caused by a number of factors. In their application of an improved ERSEM application to the global ocean, Vichi *et al.*[154] point out that some of the model biases in chlorophyll distributions in the results might be related to deficiencies in the simulation of physical processes or attributed to inadequate parameterization of important physiological mechanisms such as light acclimation. Other reasons could be found in what Holt *et al.*[155] mention as the major model limitations: errors in formulation; errors in parameterization; poor knowledge of the initial conditions; and poor knowledge of external environmental forcing. Based on results of their modeling study of eutrophication of the Southern North Sea, Allen *et al.*[156] found out that one key area where the model parameterization is weak is the attenuence of photosynthetically available radiation (PAR) in coastal waters. In the Tagus case, with suspended sediments controlling the

underwater light ambient (discussed above), the results can be conditioned by a similar limitation in the parameterization.

The reasons for the incorrect timing of bloom peak and summer abundance in the model are not entirely clear, but possibly the parameter value for the maximum rate of uptake is too high, leading to a net population growth when both radiance and water temperature increases in mid-late spring.

Chlorophyll values estimated by the model are in the usual average range for this type of system, 2.6 to 20 mg$Chla$ m^{-3} [157]. However, both *in situ* data and published data shows higher Chl$a$ concentrations in some bloom events in different parts of the estuary. In the coastal areas, intense phytoplankton blooms have been observed, with chlorophyll concentration ranging from 15-39 mg$Chla$ m^{-3} [147]. These observations also shows the importance of the mixing process between estuary and the coastal stratified waters that may explain the high Chl$a$ values observed in the Tagus coastal areas during summer months. The range of values for phytoplankton and bacteria biomass, and POC in model results are within the range of values observed for the same parameters in Ria de Aveiro [158], a smaller estuary located in the north of the Portuguese coast.

The initial C:Chl$a$ ratio, as well as the C:Chl$a$ assumed for all discharges, was defined assuming the canonical value of 60 [159]. To assess the influence of this assumption on the overall result of the model, a similar run was made assuming an initial ration of 100. Despite some minor changes in the C:Chl$a$ throughout the simulated period, this change does not produce any significant change in the outcome, as it can be notice in figure 4.29. During summer, when chlorophyll values are higher, the results converge to almost identical C:Chl$a$ ratios. Taking as an example the diatoms chlorophyll concentration shown in figure 4.29 (top), one can assume that the model is not highly sensitive to the initial C:Chl$a$ in this kind of scenarios.

The C:Chl$a$ spatial pattern reflects the simultaneous control on Chl$a$ synthesis of the light ambient in the water column and the uptake of nitrogen regulated by its availability. The shallow upper estuarine areas are more prone to sediment resuspension which affects the light penetration. As a consequence, higher chlorophyll synthesis production rates are expected. Nevertheless, because the model implementation is 2D, the available light used to force the model is depth-integrated in the water column. As such, deeper areas like the main channel where MS2 and MS3 are located have lower light levels, which induces the synthesis of Chl$a$, lowering the C:Chl$a$ ratio. The nutrient availability has a concurrent effect. Since ammonium and nitrate concentrations are systematically higher in the upper estuary, chlorophyll synthesis is expected to be higher. For this area of the estuary, the model result show no significant nutrient limitation.

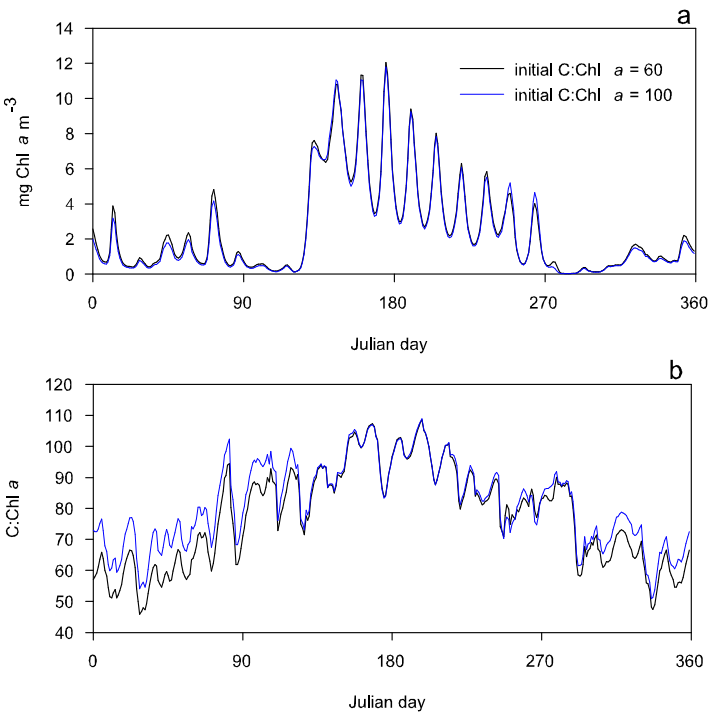

Figure 4.29: Model outcome for different initial and forcing C:Chl*a* ratio conditions: (a) diatoms chlorophyll concentration, and (b) C:Chl*a* evolution in time. Model predictions for MS1.

4.4.9 Producer groups

Field studies have shown important differences in species composition in the Tagus estuarine system [139, 151]. So far, these differences in phytoplankton composition have never been considered in any modelling study of the system. Therefore, this study can be considered as a first step of a numerical assessment of the role of two functional producer groups in the estuary.

Model results show that diatoms dominate the phytoplankton in the entire estuary during the entire simulation period. This pattern has been observed in field studies over a one and a half year period [147], implying that the model is able to correctly reproduce the dominance of these primary producers. The low levels observed for the non silica-dependent producers can also be validated by observation of quite low levels of dinoflagellates in the estuary, when compared with diatoms biomass [151]. Dinoflagellates are not representative for the general functional group of flagellates; nonetheless their abundance can reveal general patterns of non silica-dependent producer's concentration. When moving towards the estuary mouth, diatoms dominance tends to fade out and instead the non silica-dependent producers become dominant. This is a clear response to systematic shortage of dissolved silica observed in the low estuary area, specially in the summer months with little or none influence of flushing from the river.

At least one study [139] reports a growing contribution in the percentage of dinoflagellates in the total producers population in the estuary from mid estuary to lower estuary; at the estuary mouth values ranging from 5 to 16 % in total phytoplankton were estimated. Model results do not reproduce this contribution quantitatively, but nonetheless they capture the pattern of increasing non silica-dependent producers towards the estuary mouth.

4.4.10 Heterotrophic bacterial patterns

Many studies of aquatic systems have revealed that bacterioplankton abundance and production is positively correlated with phytoplankton biomass or production [18, 135, 122]. These observations have lead some researchers to suggest that the growth of bacterioplankton and phytoplankton is somehow coupled, with phytoplankton directly stimulating the growth of bacterioplankton [86]. The correlation is usually explained on the bacterioplankton dependence on DOM excreted by phytoplankton as a C-source.

The results show a clear dissociation between phytoplankton and bacterioplankton production, denoting an independence of DOM excreted from phytoplankton as the common C-source. Bacteria and producers distribution and abundance patterns are usually related in aquatic systems given the bacterioplankton dependence on DOM release by phytoplankton. Given the high loads of nutrients and organic matter in estuaries, bacteria are not dependent on producer by-products for their own survival. As such, the

strong relation between bacterial and primary production observed in the open ocean and in lakes is not usually found estuarine systems [160]. Other carbon sources (allochtonous inputs) may be equally available as substrate for bacteria. Allochtonous inputs will tend, in this case, to uncouple bacterial abundance and production from phytoplankton abundance and primary production patterns, affecting the natural pattern of both communities.

Some works show that in coastal surface waters, bacteria commonly make up 5 to 20% of the microbial biomass with phytoplankton usually making up most of the rest [161], although in summer when dissolved nutrients are sparse, bacterial biomass sometimes exceeds that of phytoplankton. In estuaries also this can be observed, even though the controlling mechanisms are not the same because there is usually a constant nutrient enrichment from rivers or land runoff alleviating nutrient depletion.

Estuarine waters are 1-3 orders of magnitude richer in bacterioplankton than the open ocean [162]. In shallow estuarine systems, bacterial abundance can be homogeneous down the water column or even higher near the bottom [163]. In plankton communities, an important indicator of ecological dynamics is the relative balance between the biomass of heterotrophic bacteria and autotrophic phytoplankton [164]. Generally, the ratio of bacterial biomass to phytoplankton biomass increases down a gradient of productivity, and equals or exceeds unity in waters of low chlorophyll concentration [135, 165, 166]. Comparison of bacterial production to primary production is a well-accepted indication of the trophic state of a system. Ecosystems where bacterial production is lower than primary production are dominated by allochtonous inputs of organic carbon and are by definition heterotrophic [167]. Contrarily, systems in which bacterial production is in deficit of net primary production are characterized as autotrophic [168]. The bacteria:phytoplankton biomass ratio, although less informative of the functional nature of communities than the ratio of productivity [164], is related to factors such as the turnover rate of phytoplankton, the presence of detritus supporting heterotrophs, and the export of autotrophs reducing support of heterotrophs [169].

A recent analysis of published literature indicates a bacteria:phytoplankton biomass ratio of 1.00 for the open ocean, and 0.62 for coastal waters [169]. By comparing producers and bacteria biomass results (not production rates) inside the estuary, it is possible to notice that the Tagus is dominated by allochtonous inputs that fuel heterotrophic organisms like bacteria. This explains the ratio between producers and decomposers biomass found in the results. The variation inside the estuary (both diurnal induced by tides and seasonal) generates a wide range variation of ratio values between different estuarine areas and throughout the year. Nevertheless, when mean annual values are calculated for each model station, it is possible to acknowledge that the ratios are on the same order of magnitude (2.8 for MS1 and MS2, 2.2 for MS3, and 0.7 for MS4). These results show a clear prevalence of bacterioplankton in the upper estuarine area where substrate concentrations are

higher, but also sediment concentrations that attenuate light in the water column limiting phytoplankton growth.

Some studies suggest that the variation in the rates of bacterial activity in eutrophic and mesotrophic ecosystems might primarily be regulated by temperature, with substrate supply playing a lesser role [170]. In oligotrophic systems the reverse situation occurs, with substrate supply being more important in the regulation of bacterial growth than temperature [171]. This pattern is found in the results to some extent since the substrate availability for decomposers decreases from upper-estuarine areas to coastal areas. As such, the control on bacterial production shifts from temperature in the inner estuary (since it is possible to assume that there is no nutrient limitation) to a probable C-source limitation outside the estuary.

An independence of phytoplankton from bacteria-mediated nutrient recycling is suggested by model results. In this application, like in any other open system (i.e., with open boundaries with the input of nutrients), the material cycle is open and so primary producers survive without the presence of decomposers or any other mineralizers. This happens because they are still supplied by the external input of nutrient into the system. But bacterioplankton growth appearing to be independent from phytoplankton production cannot be used to dismiss the explicit modelling of this group. The results suggest that thanks to the abundance of C-sources and associated nutrients to support bacterial growth, bacterioplankton play an important role in the remineralization of organic matter. This process enriches the inner-estuary areas, keeping a satisfactory supply of nutrients to support phytoplankton production.

Given their lower C:Nut ratios, bacteria have a higher demand for nutrients. This requirement can explain the marked phosphorous limitation observed at MS4 (figure 4.30). Since there is no evidence for nutrient limitation, and nutrient concentrations are relatively low (both organic and inorganic forms), model results for summer months observed at the other model stations suggest that the production and consumption of nutrients in the system may be at an equilibrium. As such, nutrients are possible consumed at the same time as they are being introduced in the system, either by resuspension (POM), mineralization, transport, or from any other source. The results for nutrient limitation for decomposers (figure 4.30) also shows that since there in no apparent nutrient limitation for bacterial growth, carbon has to be the limiting resource for growth.

The composition of microbial assemblages varies along physical and chemical gradients. In estuarine environments a high bacterial diversity is expected due to the mixing of seawater and freshwater and the transportation of particles from many sources, including salt marshes, mudflats, rivers and bottom sediments, all present in Tagus estuary. It has been shown that the bacterial composition of estuarine environments differs from oceanic waters [172]. The model does not account for those differences in composition.

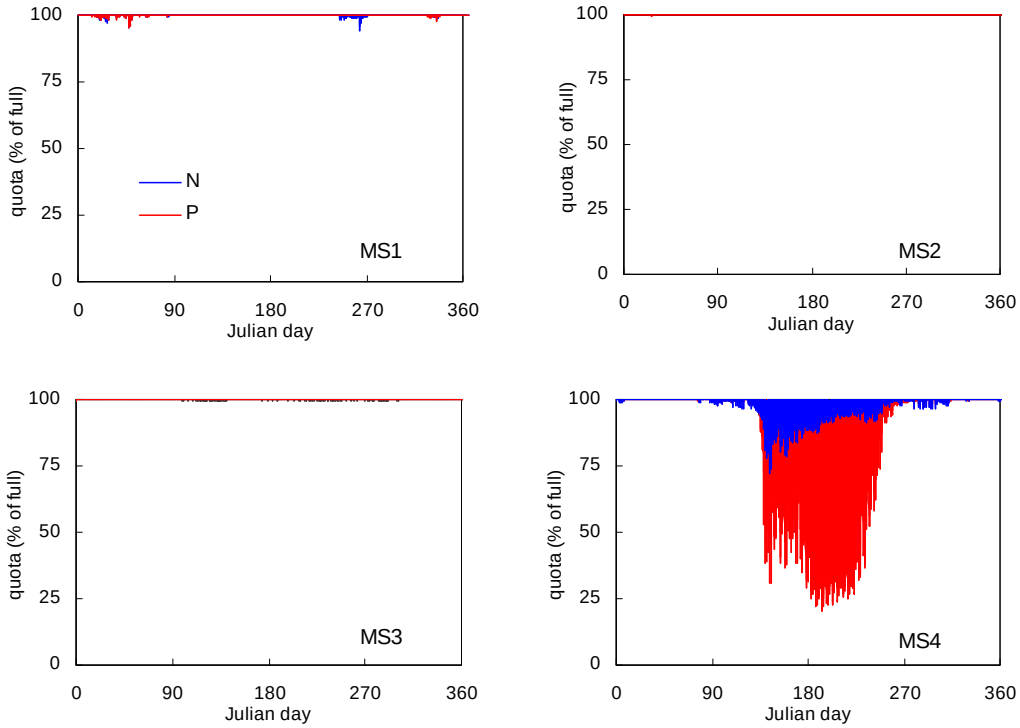

Figure 4.30: Nutrient (N and P) limitation in decomposers observed at model stations during the entire year. The limitation is expressed in state of nutrient reserves (quotas).

From an ecological perspective, capturing the function (mineralization of organic carbon and nutrients) of bacterioplankton in the system may well be enough for this type of model and its scope of applications.

Like for other groups, bacterial biomass data was not available to compare with model results. While bacterioplankton studies have been carried out in other Portuguese rivers and estuaries like the Ria de Aveiro ([158, 173]), the Tagus estuary has been scarcely studied. As such, data on the microbial community and relevance in this estuary is missing, making impossible any verification of model results. But the incorporation of a microbial loop into the model is still important. The same approach has been made by other authors (e.g. [25]). The absence of any studies regarding bacterial production in the water column inside the estuary prevents the verification of the model results. Despite this shortcoming, it is possible to conclude that the model can reproduce a correct pattern of bacterioplankton distribution based on the nutrient and organic matter discharges from the rivers, as well as from the internal dynamics of the system.

4.4.11 Nutrient cycles

The choice to explicitly address N, P and Si cycles may be questioned for the Tagus estuary because N is assumed to be the limiting nutrient. In some systems like the Oosterschelde estuary (Netherlands) silica is assumed to be the limiting nutrient and so, nitrogen and phosphorous modelling can be considered irrelevant [43]. So, the limiting nutrient depends on the specific characteristics of each estuarine system. Having a numerical tool that is able to account for all major nutrient cycles enables the use of the model to a wider set of scenarios.

Several studies based on observed data (experiments and *in situ* measurements) and modelling simulations have pointed out nitrogen as the limiting nutrient in the particular case of the Tagus estuary. But this condition might well change in the future as already observed in several coastal systems. If the nitrogen to phosphorus ratio of the inputs remains the same in future, or nitrogen inputs become relatively lower, there is no need to change this assumption. However, if phosphorus inputs start to show a relative decrease compared to nitrogen or silicon, P might become the limiting nutrient. Therefore, estimating the impact of an increase or decrease in nutrient loads may not be very relevant assuming only one nutrient as a possible limitation to growth. As an example, once nitrogen limitation is decreased (by increasing the inputs), phosphorus will then control production. The same is true for silica if both nitrogen and phosphorous loads are increased. In Tagus this scenario seems unlikely in the near future. Besides, previous studies using the *MOHID* system have revealed that an increase in the nitrogen load to the system will not result in a significant change in the overall production given the light limitation that is taken to be the major

control [142].

Cultural eutrophication reflects the enrichment of catchments areas like estuaries induced by human activities with nutrients like N and P, but not with silica. For some time now this unequal nutrient enrichment has been hypothesized as the cause of the shift from diatom dominance to non diatom dominance in the phytoplankton composition [174]. Eutrophication conditions, with an increase in nitrogen and phosphorus and not in silica, forces a change in N:Si and P:Si ratios that are favorable to flagellate blooms and unfavorable to diatoms.

The transition from diatom-based to non-diatom-based phytoplanktonic communities in aquatic systems has been associated with a degradation of the water quality [175]. Such occurrences have been observed in at least one estuary in the south of Portugal, Guadina estuary, where a change in Si:N and N:P ratios have induced a change in phytoplanktonic composition, favouring potentially noxious species [176]. For future studies these factors cannot be completely discarded considering that a total of sixteen WWTP's will be operational in the near future. In some systems, WWTP's discharges represent an addition of N and P (but not Si), enhancing silica-limitation. The natural characteristics of Tagus estuary, especially its size and hydrodynamic regime, makes negligible the impact of such discharges on the system as a whole.

For the time being, the WWTP's discharges appear to have little effect on the overall enrichment of the system. To assess the influence of WWTP's discharges in the system, a parallel run was made with the same simulation settings used in this study, only this time without considering any additional nutrient and organic matter sources besides the three rivers discharges. As it can be seen in figure 4.31, there are no significant differences between model predictions at MS1 for the two simulated scenarios. To assess possible local influences of the WWTP's discharges, some additional comparisons are made in figures 4.32 and 4.33, only now portraying the entire estuarine system.

Looking at the spatial distribution some slight differences can be seen. The contour plots show that WWTP's discharges do induce some minor changes in the system. Taking nitrate concentration as an example (figure 4.32), it is possible to see that there is a clear enrichment of the system more marked in summer when Tagus discharges reach minimum values. Nitrate concentration is also higher at the south margin in middle estuary and in all upper estuarine area. However, this enrichment does not induce any significant growth in phytoplankton (figure 4.33, top row), again highlighting the fact that production is the system is not limited by nitrogen. Another problem that can be aggravated is the oxygen consumption due to the OM matter loads introduced in the system, followed by bacterial reduction. But comparing the oxygen concentrations contour fields for the two scenarios (figure 4.33, bottom row) it is possible to acknowledge that OM degradation has a minor impact, only noticed in the upper estuary.

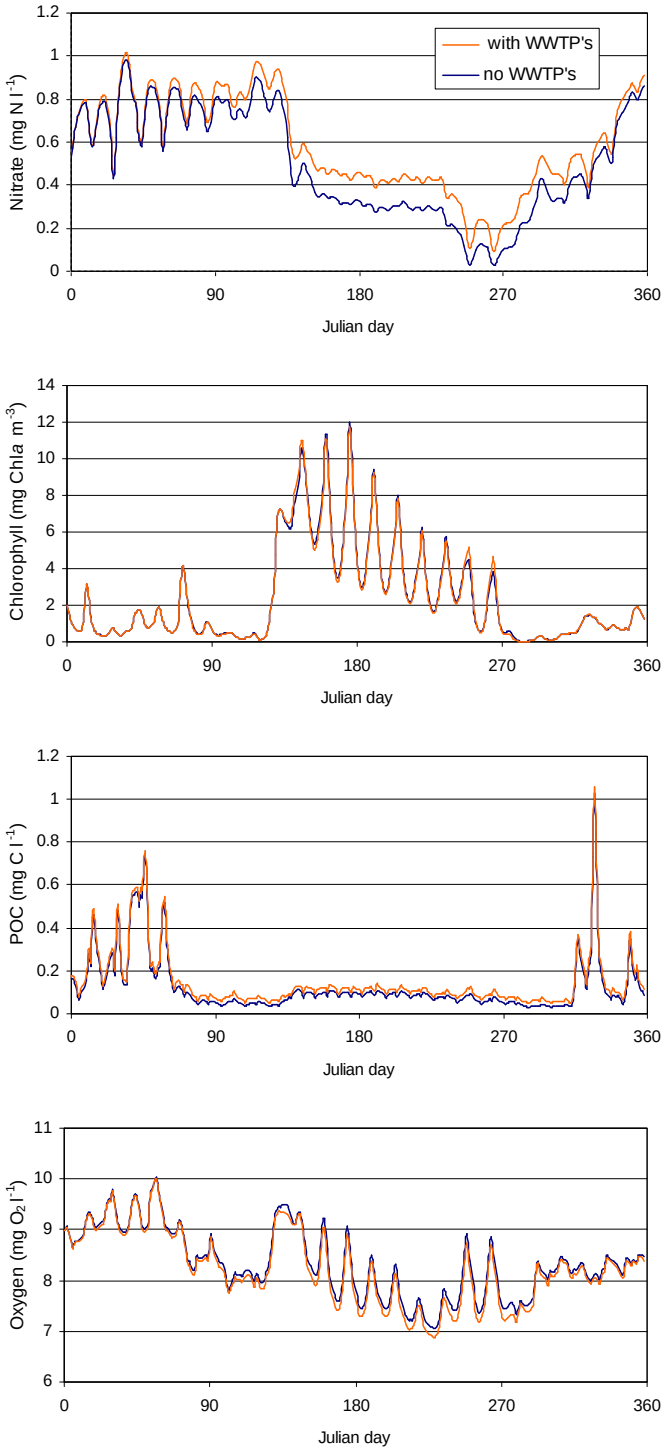

Figure 4.31: Model results for selected variables at MS1 for two different scenarios: reference situation (with WWTP's discharges) and another scenario without any discharge from the WWTP's inside the estuary.

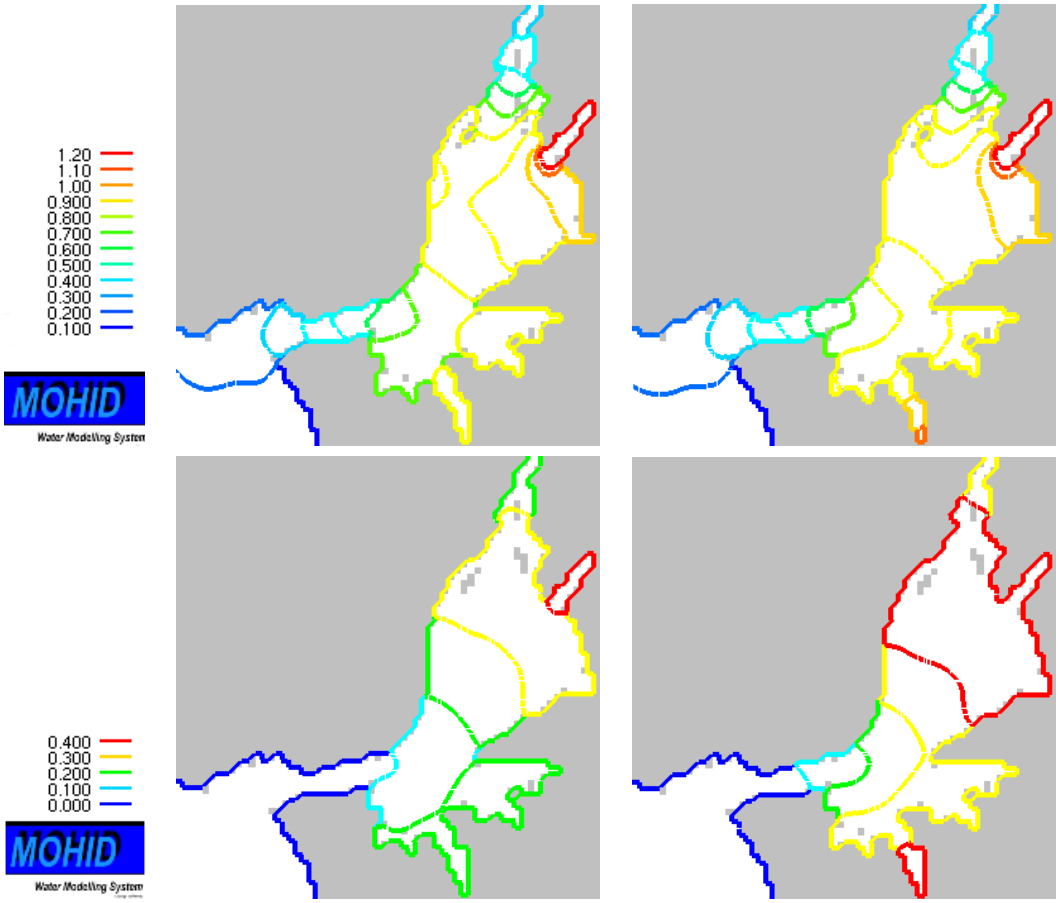

Figure 4.32: Contour plots for the nitrate concentration mgl^{-1} inside the estuary during winter (top) and summer (bottom) conditions. The first column corresponds to a scenario with no WWTP's discharging inside the system, while in the second column are the results for the reference scenario with WWTP's discharges. Model predictions for Julian day 43 and 177 for winter and summer results, respectively.

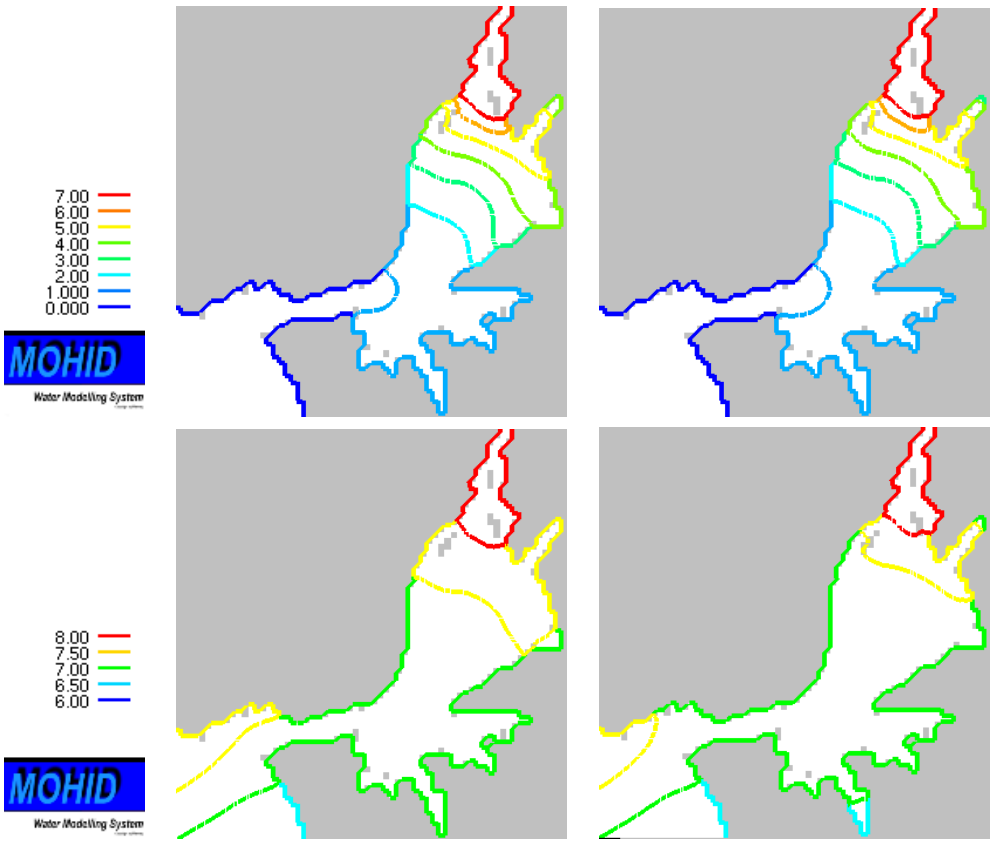

Figure 4.33: Contour plots for the diatoms chlorophyll concentration ($mgChlam^{-3}$, top row) and oxygen concentration (mgO_2l^{-1}, bottom row) inside the estuary during summer conditions (Julian day 177). The first column corresponds to a scenario with no WWTP's discharging inside the system, while in the second column are the results for the reference scenario with WWTP's discharges.

Based on the results of this test it is possible to hypothesize that given the hydrodynamic characteristics of the Tagus estuary, the actual situation does not enhance any eutrophication process in this system.

For now, the model may reveal certain trends for the Tagus estuary or even highlight hypothetical future problems related with nutrient enrichment. Nevertheless, direct or indirect inferences must depend on a comprehensive and reliable data set, especially for the nutrient loads discharged to the estuary. Above all, the dominance of non-silica dependence producers in same parts of the estuary or at some points in time observed in model results must be weighted against the limitations of the chosen scenario. As already mentioned, there is no nutrients enrichment of the coastal areas by oceanic circulation (e.g. upwelling). As a direct result, the lower estuarine areas are more prone to nutrient deficiency, specially from silica. This ultimately justifies the sharp shift in the silica-dependent to non silica-dependent ratio in producers observed. Aside from that, there no other indications of potential problems in Tagus that might be induced by nutrient limitation or excess.

The N:P ratio also plays a role because it can have an influence on interspecific competition, as a consequence of species-specific nutrient requirements, and because the production of toxins by certain toxic species increases under phosphorus deficiency conditions (as shown in [177]). If so, a model considering several phytoplankton groups as well as several nutrient cycles may help to identify potential conditions for HAB events. Sometimes large blooms of dinoflagellates occur in estuaries giving rise to the well known episodes of red tides. Among other things, the tides may lead to high fish mortality and can spread to coastal areas outside the estuary. Organic pollution and stable water conditions may trigger these episodes. Because HAB occurrences are frequent near shore, local nutrient inputs are usually thought to be a causative factor. The shift in nutrient ratios caused by anthropogenic factors is also discussed as a significant factor responsible for HAB formation and effects.

4.4.12 Relevance of sediment processes

In muddy cohesive sediments, such as those found in Tagus Estuary, there is considerable biotic activity. The result is a complex interaction of biological and physical processes that control much of the sediment dynamics. As a pelagic model, *mohid.Life.1.0* doesn't have any benthic state-variables or accounts for benthic mineralization, photosynthesis or any other processes such as oxygen consumption that takes place in the sediments. However, the modular arrangement of the *MOHID* system allows a simple parameterization of mineralization of any property in the sediments. Even with the lack of any reference rates for this particular system, the option to include this mineralization approach was taken considering the importance of sediment diagenesis in estuarine systems.

Despite their important role in the food web, bottom fauna has not been imposed as a forcing function. Likewise, benthic primary producers have been left out of the simulation. Even so, the inclusion of this biological component in the simulation of Tagus Estuary should be pondered given the extensive areas of tidal flats (up to 40% of the total estuary area). Special attention should be given to benthic diatoms because the role of their extracellular polymeric substances (EPS) influencing tidal flats sediment stability in Tagus Estuary has been found important [178].

4.4.13 Improving the operational tool

Human actions are resulting in large scale modification of the hydrologic, chemical and biological factors that regulate phytoplankton production within estuaries [138, 179]. These phenomena are particularly relevant in high-density urban areas typical in coastal zones and major estuarine zones. In the last decades, many estuaries have experienced massive human-induced modifications of external and internal organic matter supply and subsequent perturbations in the nutrient cycles. In this context, predicting food-web responses to future manipulations of organic matter supply, both planned and unplanned, is becoming an important assessment strategy.

So far, the impact studies made with *MOHID* for the Tagus estuary rules out the hypothesis of any change in the trophic status of the estuary under the present identified organic matter loads, even when doubling the actual loads. Yet, the continuous monitoring requirements to evaluate the evolution of the trophic state of the system under EU guidelines, demand an exhaustive modelling effort. Planning and decision-making can be improved by model forecasting of ecosystem state by means of an operational ecosystem model. For the time being, an operational version of *MOHID* with an NPZ model for the Tagus is already implemented[3] to evaluate the water quality of the system. But to reflect the state-of-the–art in operational modelling, the *MOHID* system will have to adopt complex ecological models somewhere in the future.

Recent trends in operational modelling show an increasing application of complex hydrodynamic modelling effort, but also the use of ERSEM-complexity type of ecological models [39], despite all the constraints usually associated with their complexity. However, the uncertainty related with parameter values and the difficulty to explain simulation results of models such as the one presented here can be smoothed by data assimilation. Assimilation refers to techniques used to integrate model and observed information in an optimal way, taking into account the uncertainties or errors in the model and the observations.

[3] Results can be seen online in real-time at http://www.mohid.com/tejo-op/

4.5 Preliminary conclusions

The model implementation here presented is the first attempt to incorporate all the major groups, from microbes to zooplankton, in a single numerical simulation scenario of the Tagus estuary. Overall, it provided a reasonable first estimate of the major trends in biomass of a highly dynamic and interactive community, where indirect effects had considerable influence on the abundance of the components. Since the main purpose of the model application to the Tagus was to test the model behaviour and not so much achieve a detailed description of the system dynamics, the analysis was based exclusively on standing stocks and abundances. Rates and fluxes would provide much more insight in the functioning of the system. So, the output of rates and fluxes is now being implemented in the model by adapting algorithms that are already available in MOHID.

Of even more interest are the model results that provide information about regional differences in the internal structure and functioning of the system and how these vary in time and space. Finally, the model provides a valuable tool for synthesizing and evaluating these interactions in a framework that can be replicated and rigorously tested. In addition, it can be further developed in parallel as new knowledge on the system becomes available. It also provides a tool for analysis and prediction of the system response to human manipulation.

Benthic-pelagic interactions and benthic dynamics in general had to be ignored in the absence of a benthic model. As such, the role of potential major influences on the ecological dynamics and water quality inside the estuary were impaired in the simulation, adding difficulties to the model calibration. However, the relevance of such processes must be carefully assessed (computational time requirements, complexity, etc.), prior to their full inclusion to achieve a more accurate representation of the system. To minimize this limitation, a benthic module already available in the *MOHID* system was adapted and used (even in an incipient form) in the simulation. Future work will encompass a development of a detailed benthic associated model. Only by doing so, a correct assessment of the contribution of mineralization inside the system can be accomplished.

The model generates far more results than we can ever hope to verify with *in situ* data, given the scarcity of relevant observational and experimental data on almost all aspects of the microbial food web. This shortcoming should not be considered as reason to avoid the use of such complex models, nonetheless. The authors of the ERSEM I model have reported the same limitation of data without discarding the development of complex ecological models [133]. Model results, even when not validated or evaluated against data, can still be useful to give relevant information on the processes they address, and eventually help to test hypotheses or even raise additional relevant questions. But, on the other hand, the choice to use models with

this degree of complexity and constraints must only be made if conditions so require.

The increased knowledge about the mechanisms controlling the functioning of aquatic systems and the experience gained in the last decades with ecological models have revealed that a proper modelling strategy to study estuarine system dynamics, whether to understand their basic ecological processes or to assess the implications of human-originated nutrient loads to the trophic status of the system, must be done not only with a multi-nutrient approach but also considering different producers groups. However, because much of the production controlling factors in the Tagus estuary have been studied and identified by means of simpler models (EPA nitrogen based model coupled with *MOHID* hydrodynamic model) validated by field observations, a complex model can prove to be redundant in some aspects like the estimation of the impact of increased nitrogen loads. But complex ecological models may be necessary to understand the role of each functional group in the system, as well as the interplay of multi-nutrient control on production. For a better understanding of the differences between the two ecological models available in the MOHID system, namely *mohid.Life.1.0* and *WaterQuality*, a brief comparison is provided in Appendix A.

A previous research effort must be done before the application of models with this degree of complexity, namely the implementation of enclosure experiments to estimate rates and fluxes, and to determine the proper trophic matrix. This is usually the standard methodology in recent model applications (e.g., [29, 180]). In such complex systems as estuaries and coastal areas, with a great amount of uncertain forcing values and some unknown parameters ranges, the calibration effort is always impaired. Under these circumstances, models are usually calibrated by changing the ecological model parameters, sometimes using unreal values. In this sense, enclosure and/or mesocosm experiments are the best way to calibrate the model prior to its application to such systems. Only with the proper calibration approach it is possible to make precise analysis of model results. Nevertheless, without a specific calibration experiment for a given system, the model application may provide a good basis to raise hypotheses and to infer possible explanations.

Chapter 5

General discussion

5.1 Bulk quantity models vs. structured based models

Most pelagic ecological models treat phytoplankton and zooplankton as bulk quantities, meaning that no distinction made between species, groups or sizes. With this approach, the rates included in the model represent population or community averages. The outcome is that such models integrate large ranges of possible values and can only provide an average distribution, which may or may not be consistent with the available data for calibration and verification [36]. Since a full description of the biology of every species is not feasible, all ecological models must assume some kind of simplification to deal with different organisms. The usual procedure consists of the aggregation of these biological components into functional groups representing the main functional roles of production, consumption, and decomposition [39]. With this approach, individual organisms within a functional group are assumed to be identical.

This modeling approach has been implemented in the MOHID systems as its first ecological model for the water column. While it may be adequate to study some ecological aspects of ecosystem dynamics, ranging from seasonal patterns to excessive nutrient impacts, it can be reductive in others. So, the adoption of a structured based modeling philosophy is justified on the need of broadening the scope of applications and detail in the ecological dynamic of the modeled systems. As an example, the advantage of having a structure-based model is found in modelling the ecological dynamics in stratified coastal areas, with the typical phytoplankton succession scenario [181].

Based on the results presented above (both in the schematic setting and in the Tagus application), it is possible to conclude that more information can be drawn from an application based on this principle. The exercise in the schematic case portrays a theoretical study of the controlling factors for

each group temporal evolution. In that sense, it helps to shed some light in the producers and consumers behavior in general, but also in the behavior of each particular group. The relevance of this feature is clearly seen in the Tagus case, where the dominance of producers has a spatial variation.

The addition of a structure based on size or distinct features of a population (e.g. silica dependence or mixotrophy) adds realism to the models. At the same time it allows the explicit inclusion of important phenomena dismissed in bulk models, especially the control of abiotic conditions (nutrients, light, etc.) on different populations. Also, the biotic control expressed mostly on nonlinear interactions is only possible in models that include multiple types of predators and prey.

Predicting plankton community structure and changes in that same structure is an important aspect of forecasting the effects of natural, and especially man-induced ecosystem changes. This is particularly relevant when it comes to evaluate the development of optimal conditions for HABs events. But such model a prediction, even if in an incipient phase, requires models that include a realistic representation of the physical environment as well as realistic ecosystem structures. These are just some of the reasons behind the need to equip the MOHID system with a structure based ecological model.

Eventually, both modeling principles, bulk quantity and structural based, will achieve the same general results (as reported by the example in Appendix A). However, the philosophy here developed enables to take the knowledge on the system much further, and adds versatility to the model.

5.2 Photoadaptation and dynamic C:Chl*a* ratios

Photoadaptation, involving the adjustment of pigment synthesis to irradiance levels, temperature and nutrient availability, is a universal feature of algal physiology. Photoadaptation responses have been observed in several aquatic systems, expressed mainly in the adaptation of pigment content in natural phytoplankton assemblages. Despite common, this process has been observed to differ among groups of producers [65]. Its effect on the rate of primary production in natural systems, however, has been difficult to evaluate in face of the irradiance fluctuation over a wide range of time scales and difficult to mimic in controlled environments. Nevertheless, this experimental limitation does not imply that such process cannot be addressed in primary production models. The great importance of this regulatory mechanism and its response to environmental light conditions point to its relevance and inclusion in models.

Many models have focused on photosynthetic responses that occur on short time scales of minutes to hours (see [10]). The Geider *et al.* model [41] was chosen as the methodology to assess photoadaptation given its ability to estimate photoadaptation of pigment content on longer times scales of our

to days. The ERSEMII scheme [182] was also a possible choice. However, ERSEMII scheme for the chlorophyll assessment uses a diagnostic method and does not account for explicit chlorophyll production. For that reason, the more recent version of ERSEM has adopted also the Geider *et al.* model (Job Baretta, *personal communication*). This implies that such mechanism is in fact relevant, but also that the Geider *et al.* model is a reliable choice.

Since chlorophyll *a* is the most widespread index of phytoplankton abundance in water [183], its explicit inclusion in production models has become an important aspect of model development. The down-regulation of pigment synthesis at high irradiance has been well documented in both prokaryotic and eucaryotic phytoplankton [184, 185, 186], along with its reflex on C:Chl*a* ratios. Hence, rather than simply defining primary production based on carbon or nitrogen and then extrapolate to chlorophyll *a* concentrations based on fixed C:Chl*a* or N:Chl*a* ratios, this approach render more realism to the model. According to Chapra [37], the opposing effect of nutrients and light on the C:Chl*a* ratio seems to sharpen up growth events, allowing models to better simulate both temporal and spatial gradients of carbon and chlorophyll in natural systems (e.g., spring blooms and deep chlorophyll layers). Typically, it is assumed that acclimation serves to increase growth rates under suboptimal ambient conditions over the value that would be achieved if cellular chemical composition were static. Its importance to phytoplankton population in diverse aquatic systems is indicated by variations in of C:Chl*a* observed in vertical profiles, as well as along horizontal transects.

The variation of the C:Chl*a* is also particularly relevant during the spring bloom because changes in the light and nutrient environment can be dramatic. In addition, there may be the highly variable mixing depth throughout the diel cycle [187], causing the intermittent exposure of phytoplankton to limiting and saturating irradiances during the bloom event. Under such conditions it is expected a physiological adjustment of C:Chl*a* ratios, with consequent effects on phytoplankton growth.

The gradual accumulation of data on the temporal and spatial distributions of Chl*a* in coastal and neritic provinces of the ocean is a direct result of the increased use of direct measurements, using optical instruments like remote sensing of Chl*a* concentration from satellites and aircraft, and by continuous measurement using *in vivo* fluorescence in ship-based or moored instruments. However, this situation leads sometimes to a well documented spatial and temporal distribution of phytoplankton biomass in a given system that does not directly benefit the use of models unable to account for Chl*a* dynamics. Oceanographers and modelers often relate Chl*a* concentrations to primary producers biomass by means of empirical factors. But because it varies, chlorophyll is a deceptive measure of true biomass, and so this procedure has been recognized to be doubtful given the lack of precision of these factors. Using Chl*a* spatial maps to determine biomass can be misleading, especially if fixed C:Chl*a* ratio models are used, or any other

models that do not even account for chlorophyll. In phytoplankton cultures C:Chl*a* ratio varies from <10 to >100 [188], a range that is also expected to occur in natural systems. For this reason, chlorophyll is a poor measure of phytoplankton biomass [183]. Consequently, addressing C:Chl*a* ratio conditional factors and mechanisms is essential in improving model estimations and usefulness.

Based on the model application to the Tagus estuary presented in the previous chapter, the adaptation mechanism to different light climates on the system is well portrayed in C:Chl*a* evolution time series (see figure 4.17). Fixed C:Chl*a* used in conversion to estimate chlorophyll concentrations may produce good results under some circumstances, but will eventually fail to correctly depict the evolution of a system with a strong seasonal and spatial heterogeneity. Using model results for MS1 in the Tagus case as a reference, figure 5.1 illustrates the difference in chlorophyll concentrations calculated by the model (with variable C:Chl*a* ratios) and by calculating chlorophyll from carbon or nutrient biomass using fixed ratios. In this case, the estimates were made from diatom carbon biomass. It is possible to notice that there is a difference between winter and summer; higher C:Chl*a* is better suited to estimate chlorophyll content in summer conditions (expressed in a better adjustment between C:Chl*a* ratio of 100 line with the variable C:Chl*a* line), while a lower ratio (C:Chl$a$ = 60) is a better choice for winter conditions. Curiously, besides the seasonal difference, there are also a spatial differences (shown in Tagus results). This is another reason why a fixed ratio is unfit, given that distinct areas in the same system can have different C:Chl*a* ratios at the same temporal instant.

These observations may lead to conclude that when conditions are more stable, whether from nutrient availability or light climate (like in MS4 where the river discharge is not so strong, as well as it seasonal signal), a fixed rate might be a reasonable choice. However, when conditions have strong changes of nutrient availability and light conditions, a photoacclimation mechanism becomes an essential requirement for reliable chlorophyll biomass estimates.

A final argument on the importance of having a chlorophyll synthesis adapted to the availability of light and nutrients can be found in studies where different fixed ratios have been used to determine the fluxes of produced material. In one study, Jassby *et al.* [157] demonstrates that a change from a C:Chl*a* ratio of 50 to 35 resulted in a decrease of 17 tons y^{-1} and a net transport loss increase of 2 tons y^{-1}.

5.3 Production control

Since a large fraction of carbon in aquatic systems is now thought to flow through bacteria, the knowledge of factors controlling bacterioplankton production is relevant to the understanding of biogeochemical cycles function-

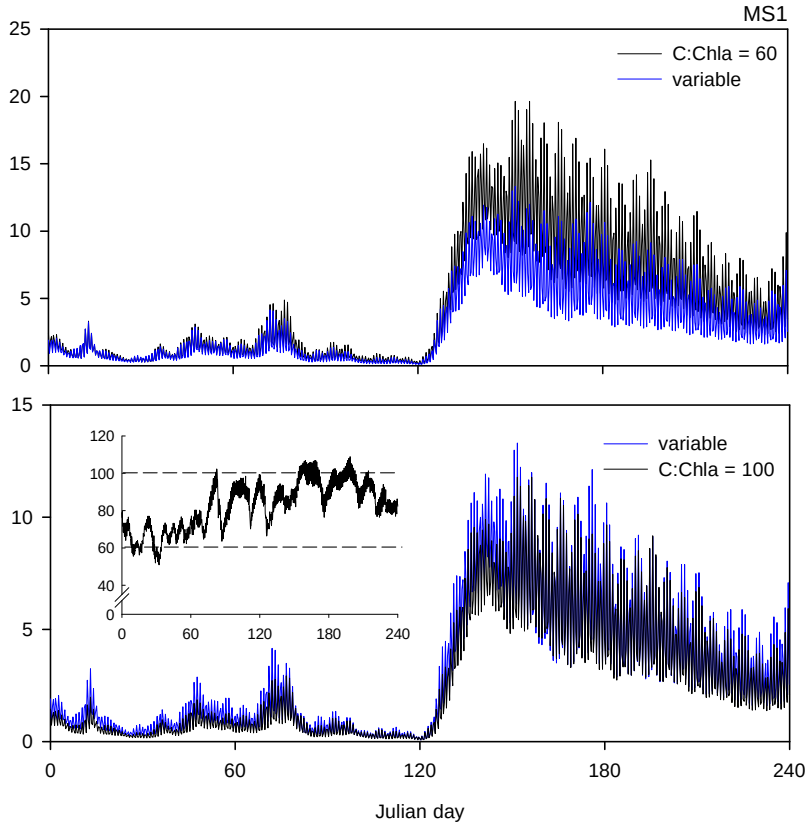

Figure 5.1: Chlorophyll concentrations (mg Chl$a$ m^{-3}) obtained by the model (variable C:Chl$a$) and calculated from diatoms carbon biomass using fixed C:Chl$a$ ratios. C:Chla ratios of 60 (top) and 100 (bottom) were used as reference values. Inset plot shows the actual C:Chl$a$ at each time instant calculated by the model based on diatoms C and Chl$a$ content.

ing and, particularly, to the prediction of their evolution after perturbation. The main factors regulating bacterial growth (availability of organic and inorganic substrates, temperature, predation, viral lysis, etc.) have been considered in the model development and reasonably modelled. However, such an attempt is a first step in including these processes given that qualitative and quantitative relationships among these factors are still poorly understood.

Several potentially important processes are excluded from the model given their complexity in parameterization or incipient knowledge about their real impact. The model does not account for producers viral infection, an important process influencing some algal blooms ([189, 190, 191]) as it can be noticed by the fact that during a bloom period of phytoplankton, free viruses in the water varied by a factor of >30 [192]. The sharp reduction of phytoplankton biomass sporadically observed by remote sensing in some estuaries suggests that this process may control the end of blooms to some extent.

Phytoplankton absorb incident light as a function of wavelength, pigment concentration, cell geometry and the presence of other attenuating components in the water column. Also, the spectrum of absorption coefficients for the pigment assemblage is characteristic for each phytoplankton species. While some models take most of these characteristics into account (e.g. [11]), only a few are considered in the model here presented.

5.4 The microbial loop and organic matter components

Several factors highlight the importance of incorporating bacterioplankton in model components. As already mentioned, their role as decomposers is fundamental in estuarine systems. But they are also relevant in open ocean systems, as mentioned by Kirchman *et al.* [106] based on observations of rapid DOC turnover by bacterioplankton during the spring bloom in the North Atlantic Ocean. Considering the general scope of potential applications of *mohid.Life.1.0* to both eutrophic and oligotrophic systems, the role of bacterioplankton must be addressed explicitly. The trophic gradient change from eutrophic to oligotrophic, influenced basically by the bacterioplankton to phytoplankton ratio, is now beyond dispute [193]. In this context, the particular role of bacterioplankton has been pointed out as having paramount importance [194], a fact that justifies by itself the incorporation of a detailed microbial loop dynamics in aquatic ecological models.

In ERSEM model a short turnover time is assumed for labile DOM, meaning that this fraction of organic matter does not accumulate over time into considerable concentrations, and is instead consumed by bacteria as it is produced. These assumptions are at the base of a model simplification

by not representing labile DOM as a state variable. In the model presented here, however, labile DOM is defined as an explicit state variable. The reason for this assumption lies on the fact that under certain circumstances, labile DOM can accumulate in the water column and reach considerable concentrations. Because all DOM compartments have a variable C:N:P, one can define an hypothetical situation where labile DOM has a low nutrient to carbon ratio and there is no inorganic nutrients in the water. With these constraints, bacteria will be unable to consume DOM at the risk of aggravating the need for nitrogen and phosphorus.

Integrating the microbial food web is essential to understand the dynamics of ecosystem behaviour and any consequences of perturbations in the forcing of such complex systems. But as the application to the Tagus estuary reveals, the scarce or absent data on bacterioplankton and DOM quantity and quality (composition), prevents any validation effort. In such cases, even if only a qualitative validation can be attained, some conclusions on the microbial dynamics can still be inferred from the results.

5.5 Sensitivity analysis

Two potential problems must be faced when developing ecosystem models: first, complex models may not behave as the sum of their components parts, and the second is that some aspects of a model which may be unimportant in one particular situation may become significant under different conditions. Some of these problems highlight the importance of carrying out a sensitivity analysis to determine which parameters the model is most sensitive to, and how large an error may be introduced by poorly constrained parameter values. However, such analysis does not tell us why a particular parameter is important. Even so, this exercise helps in the identification of parameters which may have a greater impact on the model outcome.

The sensitivity analysis performed in this study has pointed out such parameters, and in that sense proved to be an essential step in the evaluation of the model output. The sensitivity analysis indicates that the function controlling predation kinetics are very important in determining model performance. The same result is mentioned by Davidson [17] after reviewing several ecological models with a microbial food web. This author also implies that the lack of rigor applied to the choice of the ingestion function may result in serious shortcomings in the final model. Overall, the model showed little sensitivity to most parameters and, in this sense, the complex ecosystem model can be considered robust. Further conclusion could be drawn by a more detailed analysis but in the present context they fall outside the scope of this work.

Chapter 6

Concluding remarks

The present work consisted mainly of the development of a generic model for the dynamics of marine plankton communities and subsequent testing. The construction of the model, the sensitivity analysis undertaken, the application to a real system and the attempts to calibrate it have all revealed a number of uncertainties in existing knowledge regarding the rates of various processes, as well as on the processes themselves (DOM degradation kinetics, etc.). In terms of the objectives listed in the introduction, the modelling exercise was largely successful, i.e., the development of a process-oriented biogeochemical model for pelagic systems reflecting the state of the art inside the MOHID modeling platform, and its subsequent testing. But the model is by no way in a final form inasmuch it has been conceived to be easily changed to fit to specific needs. This means that there is still work in progress and as such it will be subject to changes in time. The scope of changes will range from code re-arrangement to facilitate the manipulation of the large amount of input information, minor changes in some in the parameterization of processes and above all, the inclusion of new processes of state-variables or exclusion of some already existent as knowledge on their particular relevance advances.

Two additional steps will assist further in the development of the model. These are: (1) a comprehensive sensitivity analysis, and (2) attempts to validate the model by applying it to the existing, applicable data sets or to a new data set collected for this purpose. Both tasks have been undertaken to a certain extent. But a detailed study of a particular system with the model can be improved by performing these tests with the object of study in mind. Insights gained from the above, in conjunction with those obtained from this initial exercise, could lead to improvements in the model, in the form of structural or parameter changes. Once confidence has been gained in an improved model, it should be possible to delineate experimental programs. These can go from assisting in the design of plankton sampling and monitoring exercises, to the preliminary testing of related hypothesis, prior

to the validation in the field or laboratory.

The structure of the model makes it straightforward to add other components or to adapt some of the already existent (having in mind an adaptation to benthic processes). Moreover, taking advantage of the *MOHID* system characteristics, the model can be applied to other environments by changing parameter values, its trophic structure, and the input biomass spectrum. The model was designed as simple as possible to allow a thorough model analysis, but sufficiently detailed for an appropriate description of relevant ecological processes (with both biotic and abiotic influences).

The ability of the model to describe the chemical composition of phytoplankton across the different set of conditions addressed (both real and schematic) suggests that essential features of phytoplankton physiology have been adequately represented. In addition, another feature captured by this model is that it also reproduces the time course of changes in chemical composition and growth that occur when environmental conditions change. These aspects of model behavior were particularly evident in the Tagus application where the model was able to respond to different spatial and temporal sets of environmental conditions (e.g., shifts in C:Nut ratios). This capacity confers versatility to the model, increasing the potential simulation scenarios to apply the model as well as the magnitude of physical-biological interactions that can be studied.

Mohid.Life.1.0 model was designed to be a generic ecological model, meaning that the rates and variables had to be derived from the literature, estimated by calibration or, in some cases, assumed. While this unquestionably reduces the potential for using the model as a predictive tool in the Tagus application, the model exercise helped to address uncertainties in knowledge of the functioning of this particular system, but also to reinforce some assumptions made in other studies.

Finally, benchmarking or "beta testing" involving a wide number of users implementing the model will be a major step towards the dissemination and improvement of the model. Not only does this process will result in the identification of potential conceptual errors, but it will also provide guidance on how to modify the model so that it will meet users' needs more adequately. This will be the ultimate test on the model usefulness.

Bibliography

[1] H.W. Streeter and E.D. Phelps. A study of the pollution and natural purification of the ohio river, iii. factors concerning the phenomena of oxidation and reaeration. *U.S. Public Health Service, Pub. Health Bulletin*, 146, 1925.

[2] G. A. Riley. Factors controlling phytoplankton populations on georges bank. *Journal of Marine Research*, 6(1):54–73, 1946.

[3] G. A. Riley. A theoretical analysis of the zooplankton population of georges bank. *Journal of Marine Research*, 6(2):104–113, 1947.

[4] J. S. Wroblewski. Model of phytoplankton plume formation during variable oregon upwelling. *Journal of Marine Research*, 35(2):357–394, 1977.

[5] D. Prandle. Operational oceanography in coastal waters - introduction. *Coastal Engineering*, 41(1-3):3–12, 2000.

[6] W. G. Harrison. Regeneration of nutrients. In P. G. Falkowski and A. D. Woodhead, editors, *Primary productivity and biogeochemical cycles in the sea*, pages 385–407. Plenum Press, New York, 1992.

[7] E. Flather. Existing operational oceanography. *Coastal Engineering*, 41(1-3):13–40, 2000.

[8] M. J. R. Fasham. Modelling the marine biota. In M. Heimann, editor, *The global carbon cycle*, NATO ASI Series, pages 457–504. Springer Verlag, Heidelberg, 1993.

[9] Hans Burchard, Karsten Bolding, Wilfried Kühn, Andreas Meister, Thomas Neumann, and Lars Umlauf. Description of a flexible and extendable physical-biogeochemical model system for the water column. *Journal of Marine Systems*, 2004 (submitted).

[10] M. J. Behrenfeld and P. G. Falkowski. A consumer's guide to phytoplankton primary productivity models. *Limnology and Oceanography*, 42(7):1479–1491, 1997.

[11] M. E. Baird and S. M. Emsley. Towards a mechanistic model of plankton population dynamics. *Journal of Plankton Research*, 21(1):85–126, 1999.

[12] A. Huppert, B. Blasius, and L. Stone. A model of phytoplankton blooms. *American Naturalist*, 159(2):156–171, 2002.

[13] A. Huppert, R. Olinky, and L. Stone. Bottom-up excitable models of phytoplankton blooms. *Bulletin of Mathematical Biology*, 66(4):865–878, 2004.

[14] J. Huisman and B. Sommeijer. Population dynamics of sinking phytoplankton in light-limited environments: simulation techniques and critical parameters. *Journal of Sea Research*, 48(2):83–96, 2002.

[15] J. Huisman, M. Arrayas, U. Ebert, and B. Sommeijer. How do sinking phytoplankton species manage to persist? *American Naturalist*, 159(3):245–254, 2002.

[16] M. E. Baird, S. M. Emsley, and J. M. McGlade. Modelling the interacting effects of nutrient uptake, light capture and temperature on phytoplankton growth. *Journal of Plankton Research*, 23(8):829–840, 2001.

[17] K. Davidson. Modelling microbial food webs. *Marine Ecology-Progress Series*, 145(1-3):279–296, 1996.

[18] F. Azam, T. Fenchel, J. G. Field, J. S. Gray, L. A. Meyerreil, and F. Thingstad. The ecological role of water-column microbes in the sea. *Marine Ecology-Progress Series*, 10(3):257–263, 1983.

[19] T. F. Thingstad and R. Lignell. Theoretical models for the control of bacterial growth rate, abundance, diversity and carbon demand. *Aquatic Microbial Ecology*, 13(1):19–27, 1997.

[20] G. Bratbak and T. F. Thingstad. Phytoplankton-bacteria interactions - an apparent paradox - analysis of a model system with both competition and commensalism. *Marine Ecology-Progress Series*, 25(1):23–30, 1985.

[21] C. T. Codeco and J. P. Grover. Competition along a spatial gradient of resource supply: A microbial experimental model. *American Naturalist*, 157(3):300–315, 2001.

[22] T. Daufresne and M. Loreau. Ecological stoichiometry, primary producer-decomposer interactions, and ecosystem persistence. *Ecology*, 82(11):3069–3082, 2001.

[23] T. R. Anderson. Modeling the influence of food cn ratio, and respiration on growth and nitrogen-excretion in marine zooplankton and bacteria. *Journal of Plankton Research*, 14(12):1645–1671, 1992.

[24] J. P. Grover. The impact of variable stoichiometry on predator-prey interactions: A multinutrient approach. *American Naturalist*, 162(1):29–43, 2003.

[25] K. L. Cochrane, A. G. James, B. A. Mitchellinnes, G. C. Pitcher, H. M. Verheye, and D. R. Walker. Short-term variability during an anchor station study in the southern benguela upwelling system - a simulation-model. *Progress in Oceanography*, 28(1-2):121–152, 1991.

[26] J. W. Baretta, W. Ebenhoh, and P. Ruardij. The european-regional-seas-ecosystem-model, a complex marine ecosystem model. *Netherlands Journal of Sea Research*, 33(3-4):233–246, 1995.

[27] J. W. Baretta, J. G. Baretta-Bekker, and P. Ruardij. Data needs for ecosystem modelling. *Ices Journal of Marine Science*, 55(4):756–766, 1998.

[28] J. G. Baretta-Bekker, J. W. Baretta, and W. Ebenhoh. Microbial dynamics in the marine ecosystem model ersem ii with decoupled carbon assimilation and nutrient uptake. *Journal of Sea Research*, 38(3-4):195–211, 1997.

[29] J. G. Baretta-Bekker, J. W. Baretta, A. S. Hansen, and B. Riemann. An improved model of carbon and nutrient dynamics in the microbial food web in marine enclosures. *Aquatic Microbial Ecology*, 14(1):91–108, 1998.

[30] A. Moll and G. Radach. Review of three-dimensional ecological modelling related to the north sea shelf system - part 1: models and their results. *Progress in Oceanography*, 57(2):175–217, 2003.

[31] S. C. Doney, D. M. Glover, and R. G. Najjar. A new coupled, one-dimensional biological-physical model for the upper ocean: Applications to the jgofs bermuda atlantic time-series study (bats) site. *Deep-Sea Research Part Ii-Topical Studies in Oceanography*, 43(2-3):591–624, 1996.

[32] J. K. Moore, S. C. Doney, J. A. Kleypas, D. M. Glover, and I. Y. Fung. An intermediate complexity marine ecosystem model for the global domain. *Deep-Sea Research Part Ii-Topical Studies in Oceanography*, 49(1-3):403–462, 2002.

[33] J. I. Allen, J. Blackford, J. Holt, R. Proctor, M. Ashworth, and J. Siddorn. A highly spatially resolved ecosystem model for the north west european continental shelf. *Sarsia*, 86(6):423–440, 2001.

[34] R. Proctor and I. D. James. Nutrient fluxes and budgets for the north west european shelf from a three-dimensional model. *Science of the Total Environment*, 313-316:769–785, 2003.

[35] J. T. Holt, R. Proctor, J. C. Blackford, J. I. Allen, and M. Ashworth. Advective controls on primary production in the stratified western irish sea: An eddy-resolving model study. *Journal of Geophysical Research-Oceans*, 109(C5):–, 2004.

[36] E. Hofmann. Models for marine ecosystems. In S. Tuljapurkar and H. Caswell, editors, *Structured-population models in marine, terrestrial, and freshwater systems*, pages 409–432. International Thomson Publishing, 1997.

[37] Steven Chapra. *Surface water-quality modeling*. Civil Engineering Series. McGraw-Hill, New York, 1997.

[38] D. L. Kirchman. The uptake of inorganic nutrients by heterotrophic bacteria. *Microbial Ecology*, 28(2):255–271, 1994.

[39] I. D. James. Modelling pollution dispersion, the ecosystem and water quality in coastal waters: a review. *Environmental Modelling and Software*, 17(4):363–385, 2002.

[40] M. J. R. Fasham, H. W. Ducklow, and S. M. Mckelvie. A nitrogen-based model of plankton dynamics in the oceanic mixed layer. *Journal of Marine Research*, 48(3):591–639, 1990.

[41] R. J. Geider, H. L. MacIntyre, and T. M. Kana. A dynamic regulatory model of phytoplanktonic acclimation to light, nutrients, and temperature. *Limnology and Oceanography*, 43(4):679–694, 1998.

[42] E. A. Fulton, J. S. Parslow, A. D. M. Smith, and C. R. Johnson. Biogeochemical marine ecosystem models ii: the effect of physiological detail on model performance. *Ecological Modelling*, 173(4):371–406, 2004.

[43] O. Klepper, M. W. M. Vandertol, H. Scholten, and P. M. J. Herman. Smoes - a simulation-model for the oosterschelde ecosystem .1. description and uncertainty analysis. *Hydrobiologia*, 283:437–451, 1994.

[44] H. Scholten and M. W. M. Vandertol. Smoes - a simulation-model for the oosterschelde ecosystem .2. calibration and validation. *Hydrobiologia*, 283:453–474, 1994.

[45] R. J. Neves. *Étude experimentale et modélisation des circulations transitoire et résiduelle dans l'estuaire du Sado*. Ph.d. thesis, Univ. Liège, 1985.

[46] A. Santos. *Modelo hidrodinâmico tridimensional de circulação oceânica e estuarina*. Tese de doutoramento, Universidade Técnica de Lisboa, Instituto Superior Técnico, 1995.

[47] F. Martins. *Modelação matemática tridimensional de escoamentos costeiros e estuarinos usando uma abordagem de coordenada vertical genérica*. Tese de doutoramento, Universidade Técnica de Lisboa, Instituto Superior Técnico, 2000.

[48] H. Martins, A. Santos, E. F. Coelho, R. Neves, and T. Rosa. Numerical simulation of internal tides. *Proceedings of the Institution of Mechanical Engineers Part C-Journal of Mechanical Engineering Science*, 214(6):867–872, 2000.

[49] F. Martins, P. Leitao, A. Silva, and R. Neves. 3d modelling in the sado estuary using a new generic vertical discretization approach. *Oceanologica Acta*, 24:S51–S62, 2001.

[50] F. Martins, P. Leitao, and R. Neves. Simulating vertical water mixing in homogeneous estuaries: the sado estuary case. *Hydrobiologia*, 475(1):221–227, 2002.

[51] H. S. Coelho, R. J. Neves, P. C. Leitão, H. Martins, and Santos. A. The slope current along the western european margin: a numerical investigation. *Boletin del Instituto Español de Oceanografía*, 15:61–72, 1999.

[52] H. S. Coelho, R. J. Neves, M. White, P. C. Leitao, and A. J. Santos. A model for ocean circulation on the iberian coast. *Journal of Marine Systems*, 32(1-3):153–179, 2002.

[53] A. Santos, H. Martins, H. Coelho, P. Leitao, and R. Neves. A circulation model for the european ocean margin. *Applied Mathematical Modelling*, 26(5):563–582, 2002.

[54] P. C. Leitão. *Integração de escalas e de processos na modelação do ambiente marinho*. Tese de doutoramento, Universidade Técnica de Lisboa, Instituto Superior Técnico, 2002.

[55] L. I. Portela. *Mathematical modelling of hydrodynamic processes and water quality in Tagus estuary*. Ph.d. thesis, Universidade Técnica de Lisboa, Instituto Superior Técnico, 1996.

[56] EPA. Rates, constants, and kinetics formulations in surface water-quality modeling. Technical Report EPA/600/3-85/040, US Environmental Protection Agency, 1985.

[57] J. L. Martin. Application of a two-dimensional model of hydrodynamics and water quality ce-qual-w2 to degray lake, arkansas. Technical Report Technical Report E-87-1, US Army Engineer Waterways Experiment Station, 1987.

[58] J. L. Martin. Application of two-dimensional water-quality model. *Journal of Environmental Engineering-Asce*, 114(2):317–336, 1988.

[59] S. A. Wells. Theoretical basis for the ce-qual-w2 river basin model. Technical Report Technical Report EWR-6-97, Dept. of Civil Engineering, Portland State University, 1997.

[60] T. M. Cole and S. A. Wells. Ce-qual-w2: A two dimensional, laterally averaged, hydrodynamic and water quality model, version 3.1. Technical Report Instruction Report EL-02-1, US Army Corps of Engineers, Waterways Experiment Station, 2002.

[61] D. Prandle. Operational oceanography - a view ahead. *Coastal Engineering*, 41(1-3):353–359, 2000.

[62] R. O. Megard, D. W. Tonkyn, and W. H. Senft. Kinetics of oxygenic photosynthesis in planktonic algae. *Journal of Plankton Research*, 6(2):325–337, 1984.

[63] P. H. C. Eilers and J. C. H. Peeters. A model for the relationship between light-intensity and the rate of photosynthesis in phytoplankton. *Ecological Modelling*, 42(3-4):199–215, 1988.

[64] R. J. Geider, H. L. MacIntyre, and T. M. Kana. A dynamic model of photoadaptation in phytoplankton. *Limnology and Oceanography*, 41(1):1–15, 1996.

[65] R. J. Geider, H. L. MacIntyre, and T. M. Kana. Dynamic model of phytoplankton growth and acclimation: Responses of the balanced growth rate and the chlorophyll a:carbon ratio to light, nutrient-limitation and temperature. *Marine Ecology-Progress Series*, 148(1-3):187–200, 1997.

[66] A. Tsuda, S. Takeda, H. Saito, J. Nishioka, Y. Nojiri, I. Kudo, H. Kiyosawa, A. Shiomoto, K. Imai, T. Ono, A. Shimamoto, D. Tsumune, T. Yoshimura, T. Aono, A. Hinuma, M. Kinugasa, K. Suzuki, Y. Sohrin, Y. Noiri, H. Tani, Y. Deguchi, N. Tsurushima, H. Ogawa, K. Fukami, K. Kuma, and T. Saino. A mesoscale iron enrichment in the western subarctic pacific induces a large centric diatom bloom. *Science*, 300(5621):958–961, 2003.

[67] M. R. Droop. Nutrient status of algal cells in continuous culture. *Journal of the Marine Biological Association of the United Kingdom*, 54(4):825–855, 1974.

[68] K. J. Flynn, M. J. R. Fasham, and C. R. Hipkin. Modelling the interactions between ammonium and nitrate uptake in marine phytoplankton. *Philosophical Transactions of the Royal Society of London Series B-Biological Sciences*, 352(1361):1625–1645, 1997.

[69] T. Parsons, M. Takahashi, and G. Hargrave. *Biological Oceanographic Processes*. Pergamon Press, New York, 1984.

[70] C. Langdon. On the causes of interspecific differences in the growth irradiance relationship for phytoplankton .1. a comparative-study of the growth irradiance relationship of 3 marine-phytoplankton species - skeletonema-costatum, olisthodiscus-luteus and gonyaulax-tamarensis. *Journal of Plankton Research*, 9(3):459–482, 1987.

[71] R. A. Varela, A. Cruzado, and J. E. Gabaldon. Modeling primary production in the north-sea using the european-regional-seas-ecosystem-model. *Netherlands Journal of Sea Research*, 33(3-4):337–361, 1995.

[72] T. R. Anderson and P. J. L. Williams. Modelling the seasonal cycle of dissolved organic carbon at station e-1 in the english channel. *Estuarine Coastal and Shelf Science*, 46(1):93–109, 1998.

[73] J. A. Hellebust. Extracellular products. In W. D. P. Stewart, editor, *Algal physiology and biochemistry*, Botanical Monographs, pages 838–863. Blackwell scientific Publications, Oxford, 1974.

[74] U. H. Brockmann, K. Eberlein, H. D. Junge, E. Maierreimer, and D. Siebers. Development of a natural plankton population in an outdoor tank with nutrient-poor sea-water .2. changes in dissolved carbohydrates and amino-acids. *Marine Ecology-Progress Series*, 1(4):283–291, 1979.

[75] A. Penna, S. Berluti, N. Penna, and M. Magnani. Influence of nutrient ratios on the in vitro extracellular polysaccharide production by marine diatoms from the adriatic sea. *Journal of Plankton Research*, 21(9):1681–1690, 1999.

[76] U. Brockmann, V. Ittekkot, G. Kattner, K. Eberlein, and K. Hammer. Release of dissolved organic substances in the course of phytoplankton blooms. In J. Sündermann and W. Lenz, editors, *North Sea Dynamics*, pages 530–548. Springer-Verlag, New York, 1983.

[77] P. J. L. Williams and C. S. Yentsch. Examination of photosynthetic production, excretion of photosynthetic products, and heterotrophic utilization of dissolved organic-compounds with reference to results from a coastal subtropical sea. *Marine Biology*, 35(1):31–40, 1976.

[78] R. W. Sanders. Trophic strategies among heterotrophic flagellates. In D. J. Patterson and J. Larson, editors, *The Biology of Free-living Heterotrophic Flagellates*, pages 21–38. Clarendon Press, Oxford, 1991.

[79] J. A. Hall, D. P. Barrett, and M. R. James. The importance of phytoflagellate, heterotrophic flagellate and ciliate grazing on bacteria and picophytoplankton sized prey in a coastal marine-environment. *Journal of Plankton Research*, 15(9):1075–1086, 1993.

[80] A. L. Arenovski, E. L. Lim, and D. A. Caron. Mixotrophic nanoplankton in oligotrophic surface waters of the sargasso sea may employ phagotrophy to obtain major nutrients. *Journal of Plankton Research*, 17(4):801–820, 1995.

[81] R. W. Sanders, K. G. Porter, and D. A. Caron. Relationship between phototrophy and phagotrophy in the mixotrophic chrysophyte poterioochromonas-malhamensis. *Microbial Ecology*, 19(1):97–109, 1990.

[82] K. Nygaard and A. Tobiesen. Bacterivory in algae - a survival strategy during nutrient limitation. *Limnology and Oceanography*, 38(2):273–279, 1993.

[83] K. G. Porter. Phagotrophic phytoflagellates in microbial food webs. *Hydrobiologia*, 159(1):89–97, 1988.

[84] T. F. Thingstad, H. Havskum, K. Garde, and B. Riemann. On the strategy of "eating your competitor": A mathematical analysis of algal mixotrophy. *Ecology*, 77(7):2108–2118, 1996.

[85] M. T. Cottrell and C. A. Suttle. Dynamics of a lytic virus infecting the photosynthetic marine picoflagellate micromonas-pusilla. *Limnology and Oceanography*, 40(4):730–739, 1995.

[86] J. J. Cole. Interactions between bacteria and algae in aquatic ecosystems. *Annual Review of Ecology and Systematics*, 13:291–314, 1982.

[87] K. Nygaard and D. O. Hessen. Diatom kills by flagellates. *Nature*, 367(6463):520–520, 1994.

[88] S. L. Strom, R. Benner, S. Ziegler, and M. J. Dagg. Planktonic grazers are a potentially important source of marine dissolved organic carbon. *Limnology and Oceanography*, 42(6):1364–1374, 1997.

[89] C. P. D. Brussaard, R. Riegman, A. A. M. Noordeloos, G. C. Cadee, H. Witte, A. J. Kop, G. Nieuwland, F. C. Vanduyl, and R. P. M. Bak. Effects of grazing, sedimentation and phytoplankton cell-lysis on the structure of a coastal pelagic food-web. *Marine Ecology-Progress Series*, 123(1-3):259–271, 1995.

[90] J. A. Berges and P. G. Falkowski. Physiological stress and cell death in marine phytoplankton: Induction of proteases in response to nitrogen or light limitation. *Limnology and Oceanography*, 43(1):129–135, 1998.

[91] A. M. Waite, P. A. Thompson, and P. J. Harrison. Does energy control the sinking rates of marine diatoms. *Limnology and Oceanography*, 37(3):468–477, 1992.

[92] P. K. Bienfang, P. J. Harrison, and L. M. Quarmby. Sinking rate response to depletion of nitrate, phosphate and silicate in 4 marine diatoms. *Marine Biology*, 67(3):295–302, 1982.

[93] T. Kiorboe and J. L. S. Hansen. Phytoplankton aggregate formation - observations of patterns and mechanisms of cell sticking and the significance of exopolymeric material. *Journal of Plankton Research*, 15(9):993–1018, 1993.

[94] G. A. Jackson. A model of the formation of marine algal flocs by physical coagulation processes. *Deep-Sea Research Part a-Oceanographic Research Papers*, 37(8):1197–1211, 1990.

[95] A.C. Redfield, B.K. Ketchum, and F.A. Richards. The influence of organisms on the composition of sea-water. In M.N. Hill, editor, *The Sea*, volume 2, pages 26–77. Wiley, New York, 1963.

[96] S. Takeda. Influence of iron availability on nutrient consumption ratio of diatoms in oceanic waters. *Nature*, 393(6687):774–777, 1998.

[97] R. A. Armstrong. Stable model structures for representing biogeochemical diversity and size spectra in plankton communities. *Journal of Plankton Research*, 21(3):445–464, 1999.

[98] I. D. Lima, D. B. Olson, and S. C. Doney. Intrinsic dynamics and stability properties of size-structured pelagic ecosystem models. *Journal of Plankton Research*, 24(6):533–556, 2002.

[99] M. Heath, W. Robertson, J. Mardaljevic, and W. S. G. Gurney. Modelling the population dynamics of calanus in the fair isle current off northern scotland. *Journal of Sea Research*, 38(3-4):381–412, 1997.

[100] J. F. Dower, T. J. Miller, and W. C. Leggett. The role of microscale turbulence in the feeding ecology of larval fish. *Advances in Marine Biology, Vol 31*, 31:169–220, 1997.

[101] Susan M. Libes. *An introduction to marine biogeochemistry.* John Wiley and Sons, Inc., 1992.

[102] J. H. Steele and E. W. Henderson. The role of predation in plankton models. *Journal of Plankton Research*, 14(1):157–172, 1992.

[103] T. F. Thingstad. Utilization of n, p, and organic c by heterotrophic bacteria .1. outline of a chemostat theory with a consistent concept of maintenance metabolism. *Marine Ecology-Progress Series*, 35(1-2):99–109, 1987.

[104] R. M. W. Amon and R. Benner. Bacterial utilization of different size classes of dissolved organic matter. *Limnology and Oceanography*, 41(1):41–51, 1996.

[105] J. S. Covert and M. A. Moran. Molecular characterization of estuarine bacterial communities that use high- and low-molecular weight fractions of dissolved organic carbon. *Aquatic Microbial Ecology*, 25(2):127–139, 2001.

[106] D. L. Kirchman, Y. Suzuki, C. Garside, and H. W. Ducklow. High turnover rates of dissolved organic-carbon during a spring phytoplankton bloom. *Nature*, 352(6336):612–614, 1991.

[107] S. Suzuki, K. Kogure, and E. Tanoue. Immunochemical detection of dissolved proteins and their source bacteria in marine environments. *Marine Ecology-Progress Series*, 158:1–9, 1997.

[108] P. Carlsson and E. Granèli. Utilization of dissolved organic matter (dom) by phytoplankton, including harmful species. In D. M. Anderson, A. D. Cembella, and G. M. Hallegraeff, editors, *Physiological ecology of harmful algal blooms*, pages 509–524. Springer-Verlag, Berlin, 1998.

[109] L. J. Tranvik, E. B. Sherr, and B. F. Sherr. Uptake and utilization of colloidal dom by heterotrophic flagellates in seawater. *Marine Ecology-Progress Series*, 92(3):301–309, 1993.

[110] H. Ogawa, Y. Amagai, I. Koike, K. Kaiser, and R. Benner. Production of refractory dissolved organic matter by bacteria. *Science*, 292(5518):917–920, 2001.

[111] M. D. McCarthy, J. I. Hedges, and R. Benner. Major bacterial contribution to marine dissolved organic nitrogen. *Science*, 281(5374):231–234, 1998.

[112] J. P. Connolly and R. B. Coffin. Model of carbon cycling in planktonic food webs. *Journal of Environmental Engineering-Asce*, 121(10):682–690, 1995.

[113] J. Monod. *Recherches sur la croissance des cultures bactériennes*. Hermann, Paris, 1942.

[114] D. L. Kirchman, C. Lancelot, M. Fasham, L. Legendre, G. Radach, and M. Scott. Dissolved organic matter in biogeochemical models of the ocean. In G. T. Evans and M. J. R. Fasham, editors, *Towards a model of ocean biogeochemical processes*, pages 209–225. Springer-Verlag, Berlin, 1993.

[115] R. W. Eppley and E. H. Renger. Nitrogen assimilation of an oceanic diatom in nitrogen-limited continuous culture. *Journal of Phycology*, 10(1):15–23, 1974.

[116] M. J. Perry. Phosphate utilization by an oceanic diatom in phosphorus-limited chemostat culture and in oligotrophic waters of central north-pacific. *Limnology and Oceanography*, 21(1):88–107, 1976.

[117] R. W. Eppley, Coatswor.Jl, and Solorzan.L. Studies of nitrate reductase in marine phytoplankton. *Limnology and Oceanography*, 14(2):194–205, 1969.

[118] D. K. Button. Nutrient uptake by microorganisms according to kinetic parameters from theory as related to cytoarchitecture. *Microbiology and Molecular Biology Reviews*, 62(3):636–645, 1998.

[119] F. B. Bader. Kinetics of double-substrate limited growth. In M. J. Bazin, editor, *Microbial population dynamics*, pages 1–32. CRC Press, Boca Raton, FL, 1982.

[120] J. J. Vallino, C. S. Hopkinson, and J. E. Hobbie. Modeling bacterial utilization of dissolved organic matter: Optimization replaces monod growth kinetics. *Limnology and Oceanography*, 41(8):1591–1609, 1996.

[121] J. G. Barettabekker, B. Riemann, J. W. Baretta, and E. K. Rasmussen. Testing the microbial loop concept by comparing mesocosm data with results from a dynamical simulation-model. *Marine Ecology-Progress Series*, 106(1-2):187–198, 1994.

[122] F. Azam. Microbial control of oceanic carbon flux: The plot thickens. *Science*, 280(5364):694–696, 1998.

[123] J. J. Walsh, D. A. Dieterle, F. E. Muller-Karger, R. Bohrer, W. P. Bissett, R. J. Varela, R. Aparicio, R. Diaz, R. Thunell, G. T. Taylor, M. I. Scranton, K. A. Fanning, and E. T. Peltzer. Simulation of carbon-nitrogen cycling during spring upwelling in the cariaco basin. *Journal of Geophysical Research-Oceans*, 104(C4):7807–7825, 1999.

[124] J. J. Vallino. Improving marine ecosystem models: Use of data assimilation and mesocosm experiments. *Journal of Marine Research*, 58(1):117–164, 2000.

[125] R. J. Chróst. Microbial ectoenzymes in aquatic environments. In R. J. Chrost and J. Overbeck, editors, *Aquatic microbial ecology: biochemical and molecular approaches*, pages 47–78. Springer-Verlag, New York, 1990.

[126] C. Lancelot, G. Billen, C. Veth, S. Becquevort, and S. Mathot. Modeling carbon cycling through phytoplankton and microbes in the scotia-weddell sea area during sea ice retreat. *Marine Chemistry*, 35(1-4):305–324, 1991.

[127] R. M. W. Amon and R. Benner. Rapid-cycling of high-molecular-weight dissolved organic-matter in the ocean. *Nature*, 369(6481):549–552, 1994.

[128] P. E. Kepkay. Colloids and the ocean carbon cycle. In P. J. Wangersky, editor, *Marine Chemistry*, pages 35–56. Springer-Verlag, 2000.

[129] C. L. Moloney and J. G. Field. The size-based dynamics of plankton food webs .1. a simulation-model of carbon and nitrogen flows. *Journal of Plankton Research*, 13(5):1003–1038, 1991.

[130] T. Andersen and D. O. Hessen. Carbon, nitrogen, and phosphorus content of freshwater zooplankton. *Limnology and Oceanography*, 36(4):317–331, 1991.

[131] T. R. Anderson and D. O. Hessen. Carbon or nitrogen limitation in marine copepods. *Journal of Plankton Research*, 17(2):317–331, 1995.

[132] M. A. Brzezinski. The si-c-n ratio of marine diatoms - interspecific variability and the effect of some environmental variables. *Journal of Phycology*, 21(3):347–357, 1985.

[133] J. G. Barettabekker, J. W. Baretta, and E. K. Rasmussen. The microbial foodweb in the european-regional-seas-ecosystem-model. *Netherlands Journal of Sea Research*, 33(3-4):363–379, 1995.

[134] T. F. Thingstad, H. Havskum, H. Kaas, T. G. Nielsen, B. Riemann, D. Lefevre, and P. J. Williams. Bacteria-protist interactions and organic matter degradation under p-limited conditions: Analysis of an enclosure experiment using a simple model. *Limnology and Oceanography*, 44:62–79, 1999.

[135] J. A. Fuhrman, T. D. Sleeter, C. A. Carlson, and L. M. Proctor. Dominance of bacterial biomass in the sargasso sea and its ecological implications. *Marine Ecology-Progress Series*, 57(3):207–217, 1989.

[136] Boris Chubarenko, Vladimir Koutitonsky, Ramiro Neves, and Georg Umgiesser. Modeling concepts. In Ethem Gönenç and John Wolflin, editors, *Coastal lagoons: Ecosystem processes and modeling for sustainable use and development*, pages 231–306. CRC Press, 2005.

[137] P. Kohler and K. W. Wirtz. Linear understanding of a huge aquatic ecosystem model using a group-collecting sensitivity analysis. *Environmental Modelling and Software*, 17(7):613–625, 2002.

[138] J. E. Cloern. Our evolving conceptual model of the coastal eutrophication problem. *Marine Ecology-Progress Series*, 210:223–253, 2001.

[139] M. T. Cabrita, F. Catarino, and G. Slawyk. Interactions of light, temperature and inorganic nitrogen in controlling planktonic nitrogen utilisation in the tagus estuary. *Aquatic Ecology*, 33:251–261, 1999.

[140] H. Burchard and O. Petersen. Models of turbulence in the marine environment - a comparative study of two-equation turbulence models. *Journal of Marine Systems*, 21(1-4):29–53, 1999.

[141] E.J. Lessard and M.C. Murrell. Microzooplankton herbivory and phytoplankton growth in the northwestern sargasso sea. *Aquatic Microbial Ecology*, 16:173–188, 1998.

[142] INAG MARETEC. Water quality in portuguese estuaries: Tejo, sado and mondego. Technical report, INAG - MARETEC, 2002.

[143] Q. Dortch and T. E. Whitledge. Does nitrogen or silicon limit phytoplankton production in the mississippi river plume and nearby regions. *Continental Shelf Research*, 12(11):1293–1309, 1992.

[144] F. Braunschweig, F. Martins, P. Chambel, and R. Neves. A methodology to estimate renewal time scales in estuaries: the tagus estuary case. *Ocean Dynamics*, 53:137–145, 2003.

[145] R. T. Lemos and H. O. Pires. The upwelling regime off the west portuguese coast, 1941-2000. *International Journal of Climatology*, 24(4):511–524, 2004.

[146] P. Pina. *An Integrated Approach to Study The Tagus Estuary Water Quallity*. Dissertação para a obtenção do grau de mestre em ecologia, gestão e modelação dos recursos marinhos, Superior Técnico, Universidade Técnica de Lisboa, 2001.

[147] L. Cabeçadas, Brogueira, and G. Cabeçadas. Phytoplankton spring bloom in the tagus coastal waters: hydrological and chemical conditions. *Aquatic Ecology*, 33(243-250), 1999.

[148] A. Alvera-Azcarate, J. G. Ferreira, and J. P. Nunes. Modelling eutrophication in mesotidal and macrotidal estuaries. the role of intertidal seaweeds. *Estuarine Coastal and Shelf Science*, 57(4):715–724, 2003.

[149] W. V. Sobczak, J. E. Cloern, A. D. Jassby, and A. B. Muller-Solger. Bioavailability of organic matter in a highly disturbed estuary: The role of detrital and algal resources. *Proceedings of the National Academy of Sciences of the United States of America*, 99(12):8101–8105, 2002.

[150] J. E. Cloern. The relative importance of light and nutrient. *Aquatic Ecology*, 33:3–15, 1999.

[151] C. Gameiro, P. Cartaxana, M. T. Cabrita, and V. Brotas. Variability in chlorophyll and phytoplankton composition in an estuarine system. *Hydrobiologia*, 525(1-3):113–124, 2004.

[152] J. G. Ferreira. Development of an estuarine quality index based on key physical and biogeochemical features. *Ocean and Coastal Management*, 43(1):99–122, 2000.

[153] A. R. Trancoso, S. Saraiva, L. Fernandes, P. Pina, P. Leitao, and R. Neves. Modelling macroalgae using a 3d hydrodynamic-ecological model in a shallow, temperate estuary. *Ecological Modelling*, 187(2-3):232–246, 2005.

[154] M Vichi, S Masina, and A Navarra. An advanced model of pelagic biogeochemistry for the global ocean ecosystem. part ii: applications. *Journal of Marine Systems (submitted).*, 2005.

[155] J. T. Holt, J. I. Allen, R. Proctor, and F. Gilbert. Error quantification of a high-resolution coupled hydrodynamic-ecosystem coastal-ocean model: Part 1 model overview and assessment of the hydrodynamics. *Journal of Marine Systems*, 57(1-2):167–188, 2005.

[156] J. I. Allen, F. Gilbert, J. Holt, M. Holt, D. K. Mills, R. Proctor, and J. Siddorn. Eutrophication modelling of the southern north sea. mersea strand 1 - final report d5.3. Technical report, n/d.

[157] A. D. Jassby, J. E. Cloern, and B. E. Cole. Annual primary production: Patterns and mechanisms of change in a nutrient-rich tidal ecosystem. *Limnology and Oceanography*, 47(3):698–712, 2002.

[158] M. A. Cunha, M. A. Almeida, and F. Alcantara. Patterns of ectoenzymatic and heterotrophic bacterial activities along a salinity gradient in a shallow tidal estuary. *Marine Ecology-Progress Series*, 204:1–12, 2000.

[159] J. E. Cloern, C. Grenz, and L. Vidergar-Lucas. An empirical model of the phytoplankton chlorophyll : carbon ratio - the conversion factor between productivity and growth rate. *Limnology and Oceanography*, 40(7):1313–1321, 1995.

[160] H. W. Ducklow, D. L. Kirchman, H. L. Quinby, C. A. Carlson, and H. G. Dam. Stocks and dynamics of bacterioplankton carbon during the spring bloom in the eastern north-atlantic ocean. *Deep-Sea Research Part Ii-Topical Studies in Oceanography*, 40(1-2):245–263, 1993.

[161] P. M. Holligan, R. P. Harris, R. C. Newell, D. S. Harbour, R. N. Head, E. A. S. Linley, M. I. Lucas, P. R. G. Tranter, and C. M. Weekley. Vertical-distribution and partitioning of organic-carbon in mixed, frontal and stratified waters of the english-channel. *Marine Ecology-Progress Series*, 14(2-3):111–127, 1984.

[162] K. Y. Borsheim. Bacterial production rates and concentrations of organic carbon at the end of the growing season in the greenland sea. *Aquatic Microbial Ecology*, 21(2):115–123, 2000.

[163] R. M. W. Amon and R. Benner. Seasonal patterns of bacterial abundance and production in the mississippi river plume and their importance for the fate of enhanced primary production. *Microbial Ecology*, 35(3):289–300, 1998.

[164] E.P. Odum. *Fundamentals of ecology*. Saunders, Philadelphia„ 3d edition, 1971.

[165] W. K. W. Li, P. M. Dickie, W. G. Harrison, and B. D. Irwin. Biomass and production of bacteria and phytoplankton during the spring bloom in the western north-atlantic ocean. *Deep-Sea Research Part II-Topical Studies in Oceanography*, 40(1-2):307–327, 1993.

[166] K. R. Buck, F. P. Chavez, and L. Campbell. Basin-wide distributions of living carbon components and the inverted trophic pyramid of the central gyre of the north atlantic ocean, summer 1993. *Aquatic Microbial Ecology*, 10(3):283–298, 1996.

[167] W. K. W. Li and W. G. Harrison. Chlorophyll, bacteria and picophytoplankton in ecological provinces of the north atlantic. *Deep-Sea Research Part Ii-Topical Studies in Oceanography*, 48(10):2271–2293, 2001.

[168] J. J. Cole and M. L. Pace. Bacterial secondary production in oxic and anoxic freshwaters. *Limnology and Oceanography*, 40(6):1019–1027, 1995.

[169] J. M. Gasol, P. A. del Giorgio, and C. M. Duarte. Biomass distribution in marine planktonic communities. *Limnology and Oceanography*, 42(6):1353–1363, 1997.

[170] F. K. Shiah and H. W. Ducklow. Regulation of bacterial abundance and production by substrate supply and bacterivory - a mesocosm study. *Microbial Ecology*, 30(3):239–255, 1995.

[171] F. K. Shiah, K. K. Liu, and G. C. Gong. Temperature versus substrate limitation of heterotrophic bacterioplankton production across trophic and temperature gradients in the east china sea. *Aquatic Microbial Ecology*, 17(3):247–254, 1999.

[172] A. Hagstrom, J. Pinhassi, and U. L. Zweifel. Biogeographical diversity among marine bacterioplankton. *Aquatic Microbial Ecology*, 21(3):231–244, 2000.

[173] M. A. Cunha, J. M. Dias, M. A. Almeida, J. F. Lopes, and F. Alcantara. Fluxes of bacterioplankton between a tidal estuary and the sea: returning to the "outwelling hypothesys". *Aquatic Ecology*, 37:45–54, 2003.

[174] C. B. Officer and J. H. Ryther. The possible importance of silicon in marine eutrophication. *Marine Ecology-Progress Series*, 3(1):83–91, 1980.

[175] R. E. Turner and N. N. Rabalais. Coastal eutrophication near the mississippi river delta. *Nature*, 368(6472):619–621, 1994.

[176] C. Rocha, H. Galvao, and A. Barbosa. Role of transient silicon limitation in the development of cyanobacteria blooms in the guadiana estuary, south-western iberia. *Marine Ecology-Progress Series*, 228:35–45, 2002.

[177] B. Edvardsen. Toxicity of chrysochromulina species (prymnesiophyceae) to the brine shrimp, artemia salina. In T.J. Smayda and Y. Shimizu, editors, *Toxic Phytoplankton Bloom in the Sea*, pages 681–686. Elsevier Science Publisher, 1993.

[178] T. J. Tolhurst, B. Jesus, V. Brotas, and D. M. Paterson. Diatom migration and sediment armouring - an example from the tagus estuary, portugal. *Hydrobiologia*, 503:183–193, 2003.

[179] D. L. Strayer, N. F. Caraco, J. J. Cole, S. Findlay, and M. L. Pace. Transformation of freshwater ecosystems by bivalves - a case study of zebra mussels in the hudson river. *Bioscience*, 49(1):19–27, 1999.

[180] F. Chai, R. C. Dugdale, T. H. Peng, F. P. Wilkerson, and R. T. Barber. One-dimensional ecosystem model of the equatorial pacific upwelling system. part i: model development and silicon and nitrogen cycle. *Deep-Sea Research Part Ii-Topical Studies in Oceanography*, 49(13-14):2713–2745, 2002.

[181] G. H. Tilstone, B. M. Miguez, F. G. Figueiras, and E. G. Fermin. Diatom dynamics in a coastal ecosystem affected by upwelling: coupling between species succession, circulation and biogeochemical processes. *Marine Ecology-Progress Series*, 205:23–41, 2000.

[182] W. Ebenhoh, J. G. Baretta-Bekker, and J. W. Baretta. The primary production module in the marine ecosystem model ersem ii, with emphasis on the light forcing. *Journal of Sea Research*, 38(3-4):173–193, 1997.

[183] J. J. Cullen. The deep chlorophyll maximum - comparing vertical profiles of chlorophyll-a. *Canadian Journal of Fisheries and Aquatic Sciences*, 39(5):791–803, 1982.

[184] P. G. Falkowski and T. G. Owens. Light-shade adaptation - 2 strategies in marine-phytoplankton. *Plant Physiology*, 66(4):592–595, 1980.

[185] P. G. Falkowski, Z. Dubinsky, and K. Wyman. Growth-irradiance relationships in phytoplankton. *Limnology and Oceanography*, 30(2):311–321, 1985.

[186] P. G. Falkowski and J. Laroche. Acclimation to spectral irradiance in algae. *Journal of Phycology*, 27(1):8–14, 1991.

[187] W. Barkmann and J. D. Woods. On using a lagrangian model to calibrate primary production determined from in vitro incubation measurements. *Journal of Plankton Research*, 18:767–788, 1996.

[188] R. J. Geider. Light and temperature-dependence of the carbon to chlorophyll-a ratio in microalgae and cyanobacteria - implications for physiology and growth of phytoplankton. *New Phytologist*, 106(1):1–34, 1987.

[189] J. M. Sieburth, P. W. Johnson, and P. E. Hargraves. Ultrastructure and ecology of aureococcus - anophagefferens gen-et-sp-nov (chrysophyceae) - the dominant picoplankter during a bloom in narragansett bay, rhode-island, summer 1985. *Journal of Phycology*, 24(3):416–425, 1988.

[190] C. A. Suttle, A. M. Chan, and M. T. Cottrell. Use of ultrafiltration to isolate viruses from seawater which are pathogens of marine-phytoplankton. *Applied and Environmental Microbiology*, 57(3):721–726, 1991.

[191] C. J. Gobler, D. A. Hutchins, N. S. Fisher, E. M. Cosper, and S. A. Sanudo-Wilhelmy. Release and bioavailability of c, n, p, se, and fe following viral lysis of a marine chrysophyte. *Limnology and Oceanography*, 42(7):1492–1504, 1997.

[192] G. Bratbak, M. Heldal, S. Norland, and T. F. Thingstad. Viruses as partners in spring bloom microbial trophodynamics. *Applied and Environmental Microbiology*, 56(5):1400–1405, 1990.

[193] B. Biddanda, M. Ogdahl, and J. Cotner. Dominance of bacterial metabolism in oligotrophic relative to eutrophic waters. *Limnology and Oceanography*, 46(3):730–739, 2001.

[194] J. B. Cotner and B. A. Biddanda. Small players, large role: Microbial influence on biogeochemical processes in pelagic aquatic ecosystems. *Ecosystems*, 5(2):105–121, 2002.

Appendix A

Model comparison

A.1 Introduction

For many years the *MOHID* system relied upon the *WaterQuality* (*WQ*) model to simulate the ecologic dynamics and water quality of the system where the model was implemented. When this model was developed in the *MOHID* system, it captured the major trends of water column ecological models for marine systems at the time. Since then, the *WaterQuality* model has already been implemented in numerous studies, ranging from estuaries to coastal systems, focusing on a wide range of processes, from nutrient load impact assessment to primary production controlling mechanisms.

The *WaterQuality* model follows the general principle of NPZ models, having nitrogen as the only nutrient limiting phytoplankton growth[1]. Therefore, nitrogen is used as a currency between the components of the trophic structure (NPZ approach). The model does not account for the carbon content of phytoplankton and zooplankton. Nonetheless, model results for these groups are expressed in $\mathrm{mg}C\ \mathrm{l}^{-1}$, depending on the Redfield ratio for a conversion of nitrogen cell content to carbon biomass. Chlorophyll concentration is not explicitly accounted by the model, but is instead calculated from the phytoplankton carbon biomass by means of a fixed C:Chl*a* ratio. From the time it was implemented, the *WaterQuality* model has been upgraded and extended to include more nutrient cycles (P and Si) and new functional groups, bacteria and ciliates. Phytoplankton was also adapted to account for diatoms.

The recent trends in knowledge about the ecological dynamics of coastal and oceanic systems, as well as the recent developments in its mathematical modelling, has pushed the development of the *MOHID* system to keep in pace with the state-of-the-art. For that reasons, *mohid.Life.1.0* (*mL1.0*) was developed an implemented into the *MOHID* modelling tools. This imple-

[1] A full description of WaterQuality model can be downloaded at www.mohid.com after registration

Table A.1: Synthesis of the major characteristics of the marine ecological models in the MOHID system.

	WaterQuality	**Life**
Baseline philosophy	EPA (1985)	ERSEM I, II
Explicit cycles	N, P, Si	C, N, P, Si
C:Nut Stoichiometry	Fixed (Redfield ratio)	Variable (Droop nutrient kinetics)
Chlorophyll	Derived from carbon biomass using a fixed ratio	Synthesized, allowing variable C:Chl*a* ratios (photo adaptation)
Producers	Two predefined functional groups (silica and non-silica dependent)	Variable (1 or more) Silica-dependence as an option Functional group approach
Consumers	Two predefined functional groups	Variable (1 or more)
Decomposers	Present	Present
OM mineralization	Fixed rate and recycling by consumers	Recycling by consumers and decomposers (microbial loop)
Unit system	mg l^{-1}	Generic
Benthic model	In development	In development

mentation doesn't imply an abandon of the *WaterQuality* model. Keeping both models renders *MOHID* system greater versatility. As stated before, the nature of any particular study and the answers it is supposed to address may determine the degree of complexity needed in an ecological/water-quality model (a brief list of the major characteristics of each model is presented in table A.1). Also, the computing time demand can impose a choice on which model to use. Only after some reflections on the advantages and disadvantages of each model under any particular circumstances, a decision can be made on which one to use.

To better understand the major differences and similarities of both models behaviour, a simple comparison test is provided in this section. This test aims only at compare the output of the models under the same circumstances and to highlight the major features in the results. A tentative explanation on the results is offered whenever possible and relevant.

A.2 Methodology

A.2.1 Model runs

Both models were used under the same circumstances, i.e., the same running time and time step, the same meteorological forcing, the same loads

and flows for rivers and WWTP's discharges in the system, and with the same initial conditions for all variables. The same methodology was used for the coupled hydrodynamic model to ensure that differences in the output resulted only on the distinct structure and parameterization of each ecological model. *WQ* model setup consists on the nitrogen cycle, with mineral and organic forms, on dissolved oxygen evolution, and on phytoplankton and zooplankton dynamics. Parameter values adopted here where the same used in the studies mentioned before.

A.2.2 Compared variables

Only similar variables between the two models are compared for the last year of the simulation. Except for the intermediate form of nitrogen, nitrite, they correspond to the list of state variables addressed by the *WQ* model: ammonium, nitrate, oxygen, PON, labile DON, refractory DON, phytoplankton and zooplankton. Despite having different nomenclatures, the models address the same basic properties. Labile and semi-labile DON in *mL1.0* is compared with labile and refractory DON of model *WQ*, respectively. Because *mL1.0* current application has two producers groups and explicitly accounts for both groups, C biomass and Chl*a* content, both are compared against *WQ* results. While carbon biomass is a direct output of *WQ* and can be directly compared with *mL1.0* results, the same cannot be done to chlorophyll. *WQ* results for phytoplankton were converted to chlorophyll using two different C:Chl*a* ratios, 60 and 100, an then compared with *mL1.0* output. Carbon and chlorophyll values from *mL1.0* correspond to the total producers C and Chl*a* biomass (given by the sum of both groups).

A.2.3 Result analysis

A simple comparison of results is presented here, with plots of the output of the models for the shared variables. No statistical treatment or analysis was made to model results. As such, only a qualitative analysis is presented by means of simple plots for the same state variable in both models. Time series for the properties obtained at model stations (MS) were compared. To check model behaviour and ability to reproduce observed values, *in situ* data was plotted against model predictions. In addition, to evaluate model behaviour for the entire system, spatial fields for some properties were also compared whenever found helpful.

A.3 Results and discussion

A.3.1 Nutrients

Nitrate results show a striking similarity between the two models, both in the seasonal fluctuations and values range. Looking at figure A.1 it is possible to notice an agreement in model solution for all monitored stations. Both models capture the general tendency expressed by *in situ* data. The main difference between models regarding nitrate temporal evolution is that values are usually higher in *WQ* results. This occurrence tends to decrease towards the estuary mouth. Model results also agree in the spatial distribution of this property inside the estuary (figure A.3). Some discordance is found in summer months, with *mL1.0* results showing higher values in upper estuarine areas. Despite the differences between the two model results, the general pattern is very similar.

Ammonium concentrations (figure A.2), on the other hand, shows a rather different scenario. While *mL1.0* results show a clear seasonal pattern, ammonium concentrations remain almost constant (around $0.1\,\mathrm{mg}N\,\mathrm{l}^{-1}$) throughout the simulated period in *WQ* results. Despite missing the seasonal regime, *WQ* results have a good agreement with measured values. In general, *mL1.0* seems to overestimate ammonium concentrations in the system while *WQ* seems to underestimate it.

Ammonium results in *mL1.0* can be five times higher than ammonium concentrations in *WQ*. The difference is particularly notice in upper estuarine areas and during winter months. Because ammonium is a by-product of biological activity, the main reason of this discrepancy in results must be attributed to the influence of biological groups. As an example, the lack of a marked seasonal regime in the biological groups (discussed below) accounts for the steady conditions of ammonium concentrations in *WQ*. Bacterial activity mineralizing OM and the lack of uptake by producers in winter months can account for the high concentrations of this nutrient in *mL1.0*.

A.4 Oxygen

Predictions for oxygen concentrations shows a good agreement between models. In figure A.4 it is possible to see that except for MS4, all others have a similar oxygen concentration the entire year. The same agreement can be seen in the spatial distribution inside the estuary (figure A.5).

A.5 Biological groups

Both models have an output for phytoplankton carbon biomass and so this state variable was used to compare producer's abundance. Estimates for

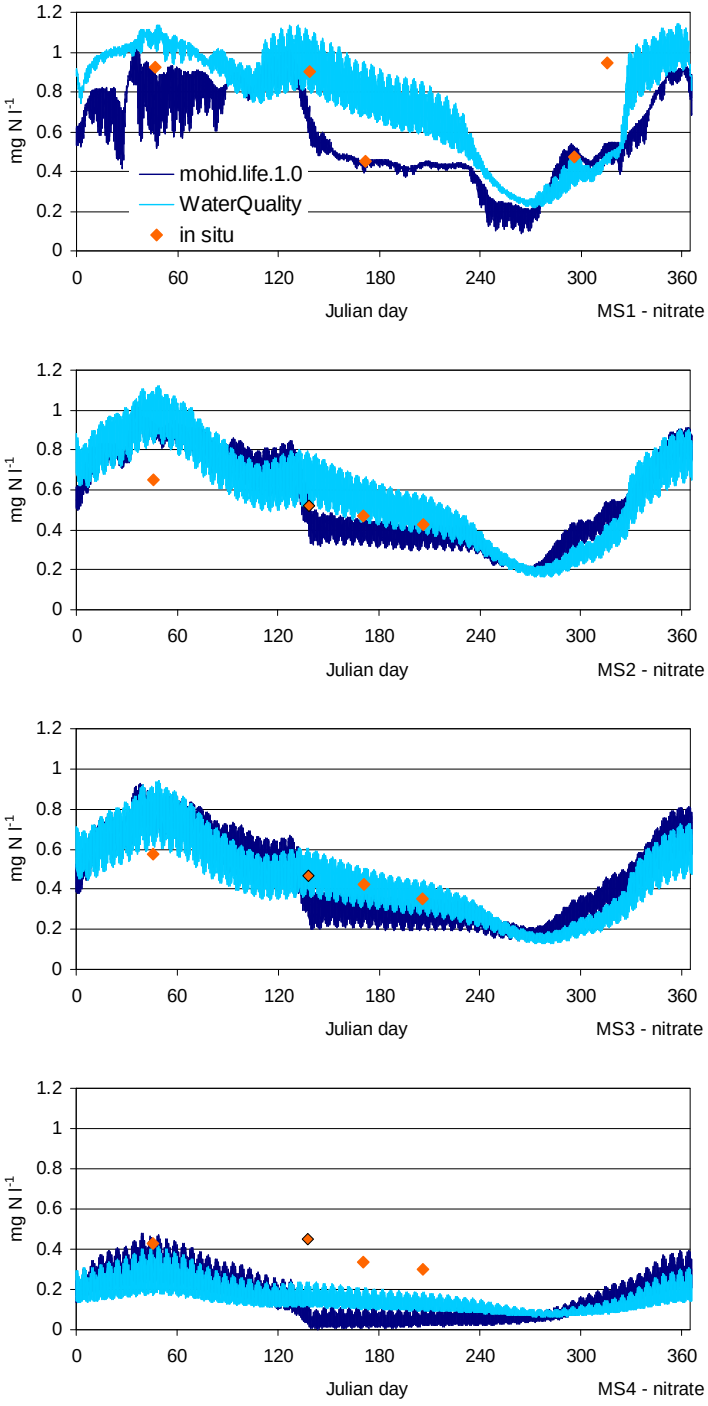

Figure A.1: Results for nitrate ($mgNl^{-1}$) observed at the monitored stations.

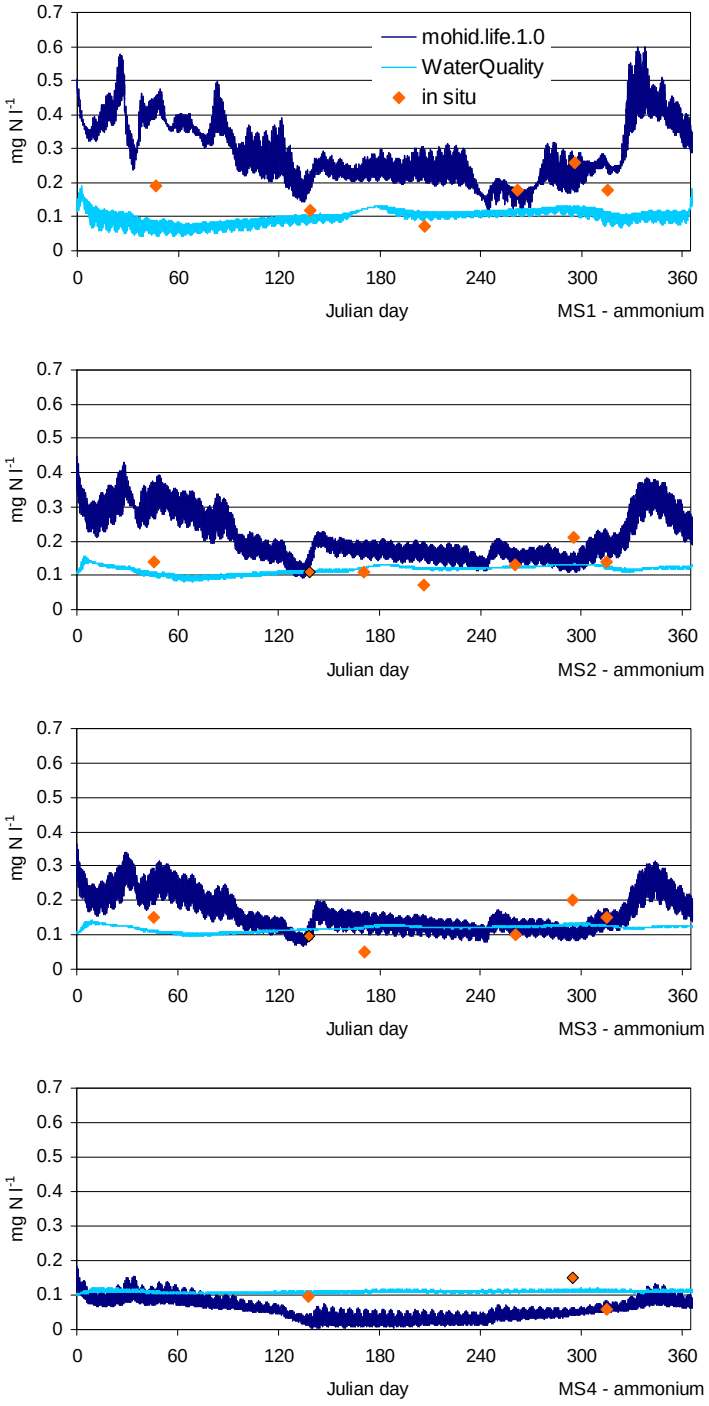

Figure A.2: Results for ammonium ($mgNl^{-1}$) observed at the monitored stations.

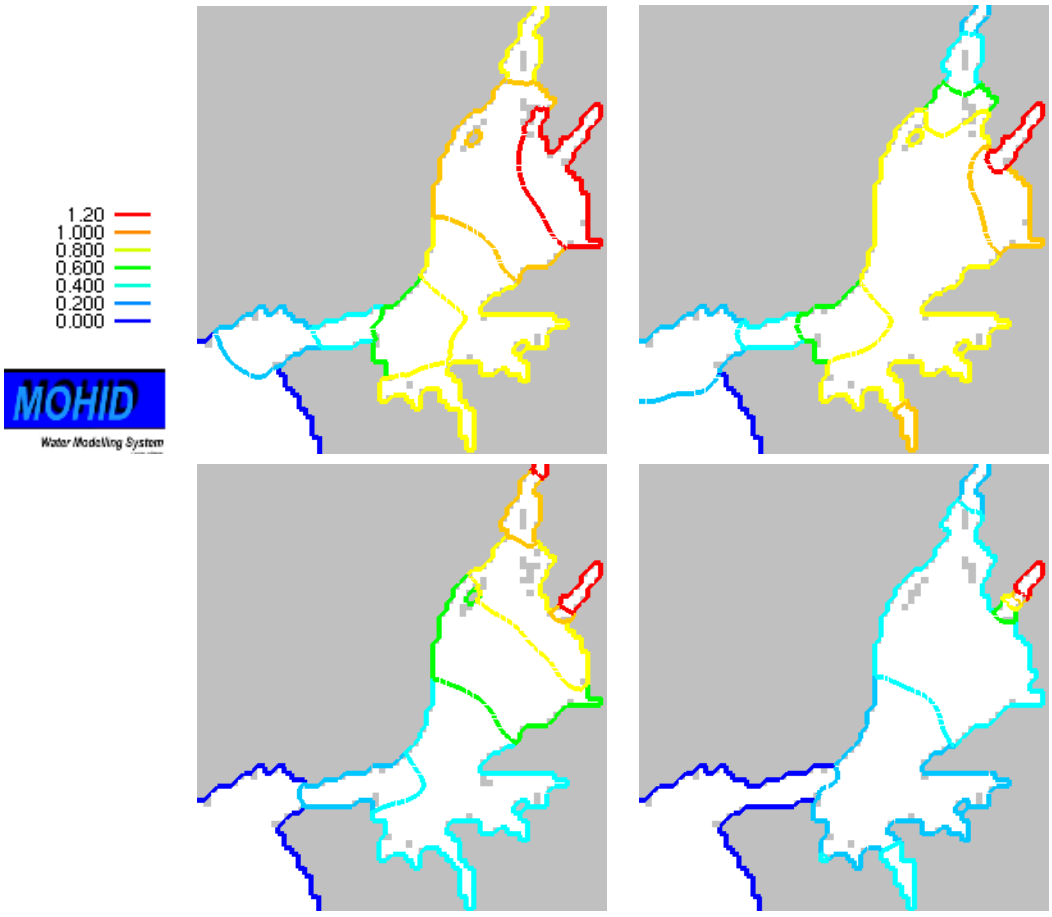

Figure A.3: Model results for nitrate horizontal distribution inside the estuary. First row shows *WQ* results and second column *mL1.0* results. Model predictions for Julian day 43 and 177 for winter (top row) and summer (bottom row) results, respectively. Values in $mgCl^{-1}$.

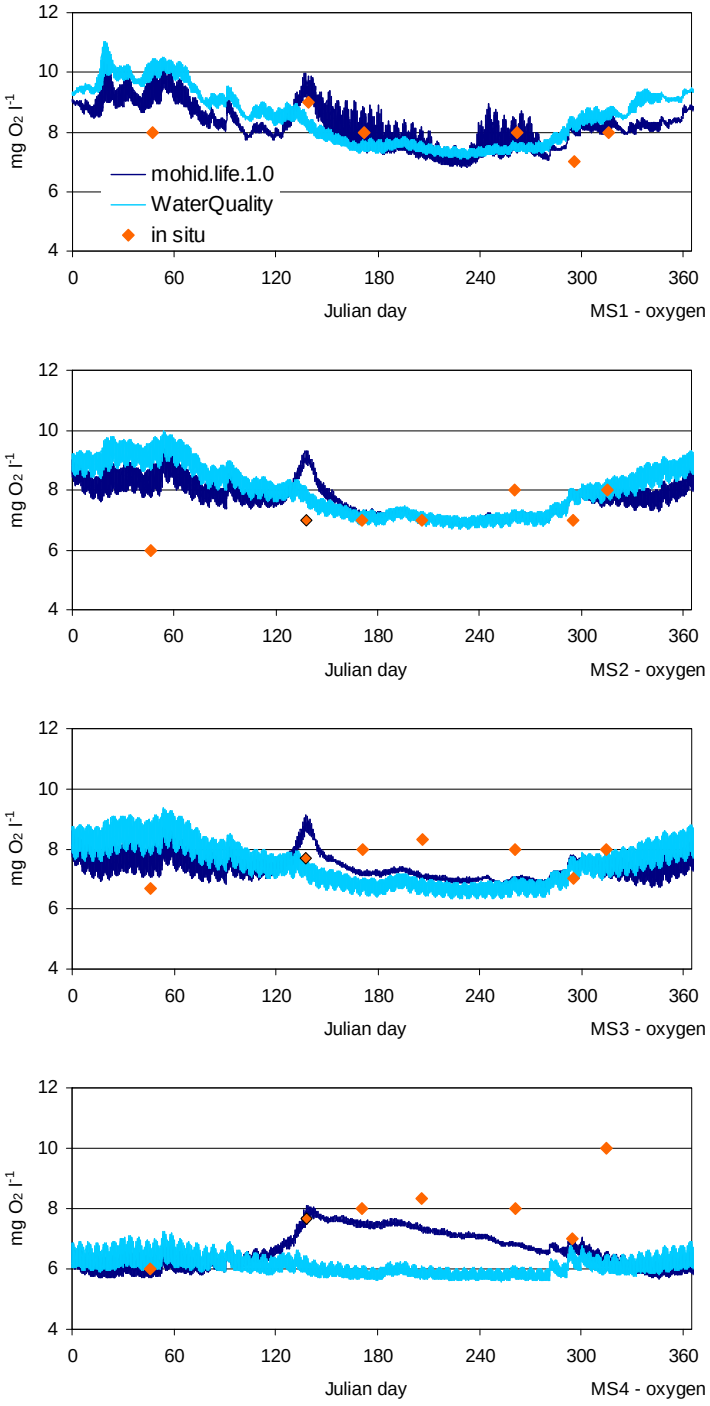

Figure A.4: Results for oxygen (mgO_2l^{-1}) observed at the monitored stations.

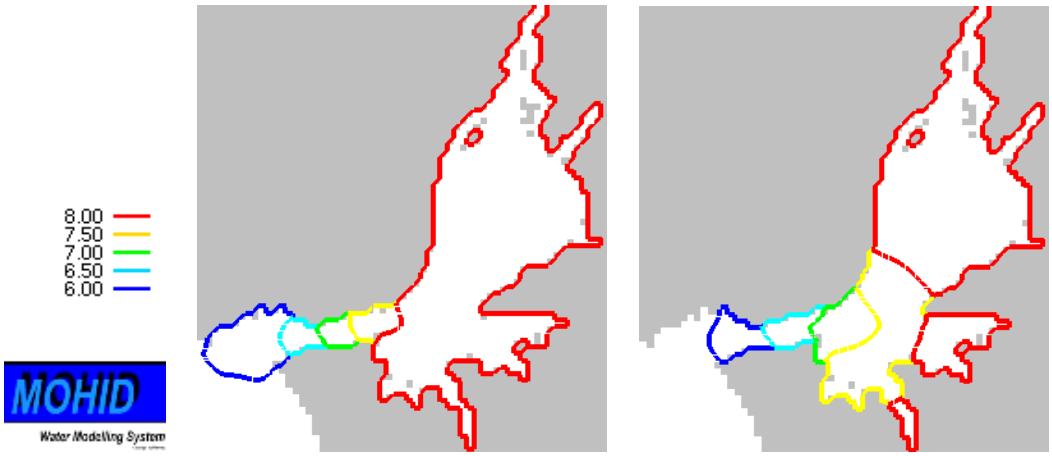

Figure A.5: Model results for dissolved oxygen horizontal distribution inside the estuary. First row shows *WQ* results and second column *mL1.0* results. Model predictions for Julian day 43 for winter results. Values in mgO_2l^{-1}.

phytoplankton evolution, illustrated in figure A.6, show different results between the two models. Probably the most striking difference is the obvious mismatch between results regarding to the spring bloom formation. In addition, *WQ* results are characterized by higher values in winter and lower values in summer, when compared to *mL1.0* results. *WQ* results retain a seasonal trend but only a mild bloom is observable in late-summer.

Because *WQ* does not account for chlorophyll cell content, a fixed ratio is used to derive this property from carbon biomass. Usually the C:Chl*a* ratio is chose to best fit observations whenever available, whereas *mL1.0* explicitly account for chlorophyll cell content, with the C:Chl*a* determined by ambient light conditions and nitrogen uptake. Despite the difference between models, chlorophyll concentration results from *mL1.0* were compared with *WQ* estimations using two different C:Chl*a* ratios, 60 and 100. Results from the different assumptions can be seen in figures A.7 and A.8. More than providing a comparison between the two models, this analysis highlights the limitation of using a fixed ratio to determine chlorophyll from carbon biomass. It is difficult to determine which C:Chl*a* ratio is the most appropriate ratio to convert from carbon biomass to chlorophyll concentrations. The fact that *WQ* model misses the bloom formation is late spring compromises any conclusion.

The clear seasonal regime in the light regime forcing functions determines a fluctuation in the C:Chl*a* ratio of natural assemblages. As such, a fixed ratio may suit better results in a particular period of the year (e.g., C:Chl*a* of 60 in summer), but may prove inappropriate on other occasions. Even achieving a good seasonal regime in phytoplankton production, the *WQ* is constrained by a fixed C:Chl*a* ratio in the estimation of chlorophyll.

Ultimately, the choice of any C:Chl*a* will impair the outcome because it may provide a good fit to data in some occasions, but will eventually give an overestimate or underestimate on others.

Zooplankton grazing on phytoplankton can be ruled out as a possible explanation for the lack of a bloom in late-spring and the low concentrations during summer. Zooplankton biomass remains relatively constant in *WQ* during the entire simulated period (figure A.9), even showing a mild depression during summer.

Given the lack of a top-down (grazing) or bottom-up (nutrients) control on primary production, *WQ* results suggest that phytoplankton growth is being slowed possible by the adopted parameter values. The different parameterization of phytoplankton's light response between models can also account for the observed difference in results.

A.6 Organic matter

All compared forms of organic nitrogen show the same seasonal and spatial trend, failing sometimes a match in values range, especially during summer. PON outcome from the models show a reasonable agreement in the predictions for winter months (an example can be found in figure A.10), but there is a clear difference in all monitored stations during the rest of the year, as noticed in figure A.11. Results in *mL1.0* have systematically higher concentrations. Because both models were forced with the same set of conditions, this occurrence can only be explained as a result of biological activity.

Of all compared organic forms, labile DON show less agreement between the two models (figure A.12). Here, despite some agreement on concentration evolution in time, *WQ* results are usually higher. The main difference between models regarding DON dynamics are related with the mineralization kinetics. While *WQ* has a fixed mineralization rate, the same process is explicitly handled in *mL1.0* by bacteria consumption and recycling. As a consequence, labile DON concentrations are kept low because they are used by bacteria as N substrate. With river influence at a minimum during summer, all labile organic matter forms are generated internally and so they are entirely consumed by bacteria.

Finally, semi-labile DON results in *mL1.0* show a fairly good agreement with refractory DON of *WQ*. Again, the major differences are found during summer months with *mL1.0* values systematically higher (figure A.13). Because it is not considered as refractory, semi-labile organic matter in *mL1.0* is more rapidly available for use, but also released as a fraction of all excreted and mortality products. This means that especially at high biological activity episodes like blooms, its concentrations have a marked increase followed by a decrease when the activity starts to slow down. Both models deal with this component of DON in different ways, a fact that helps to explain the

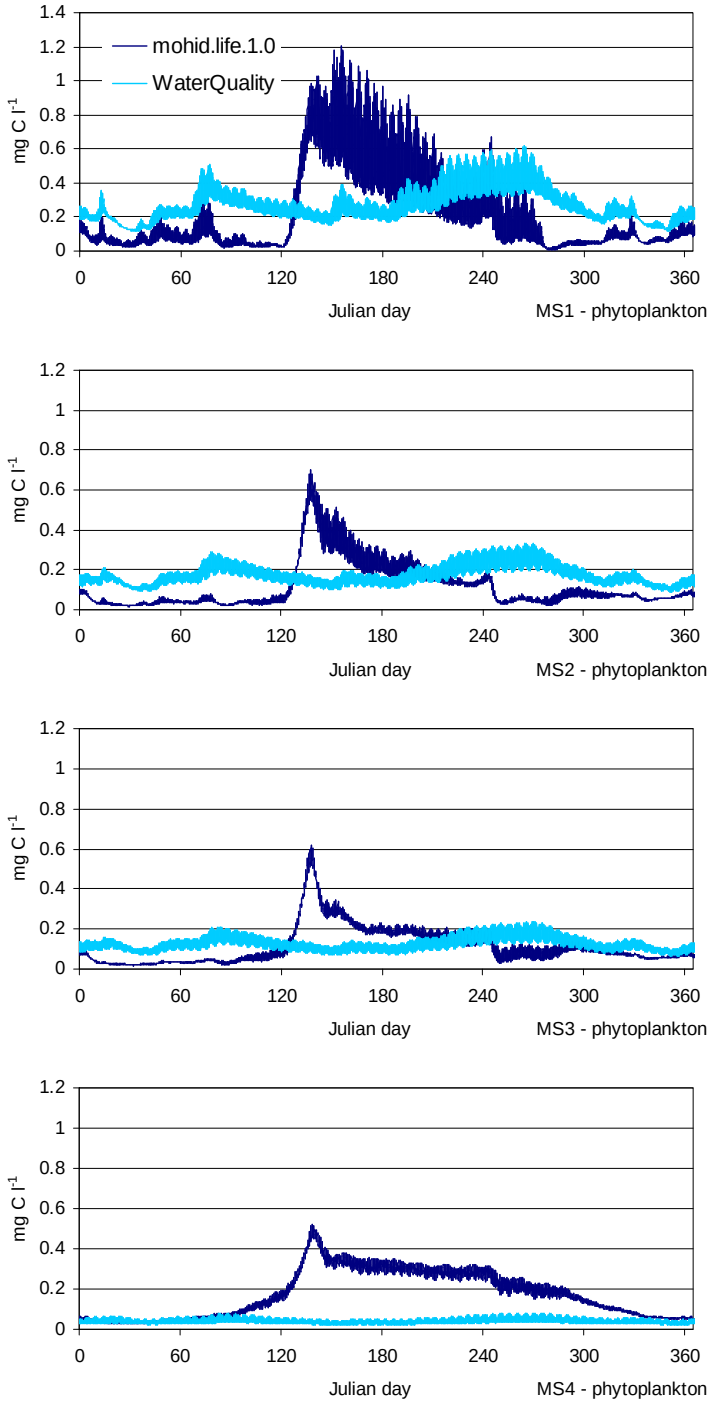

Figure A.6: Results for phytoplankton carbon biomass ($mgCl^{-1}$) observed at the monitored stations.

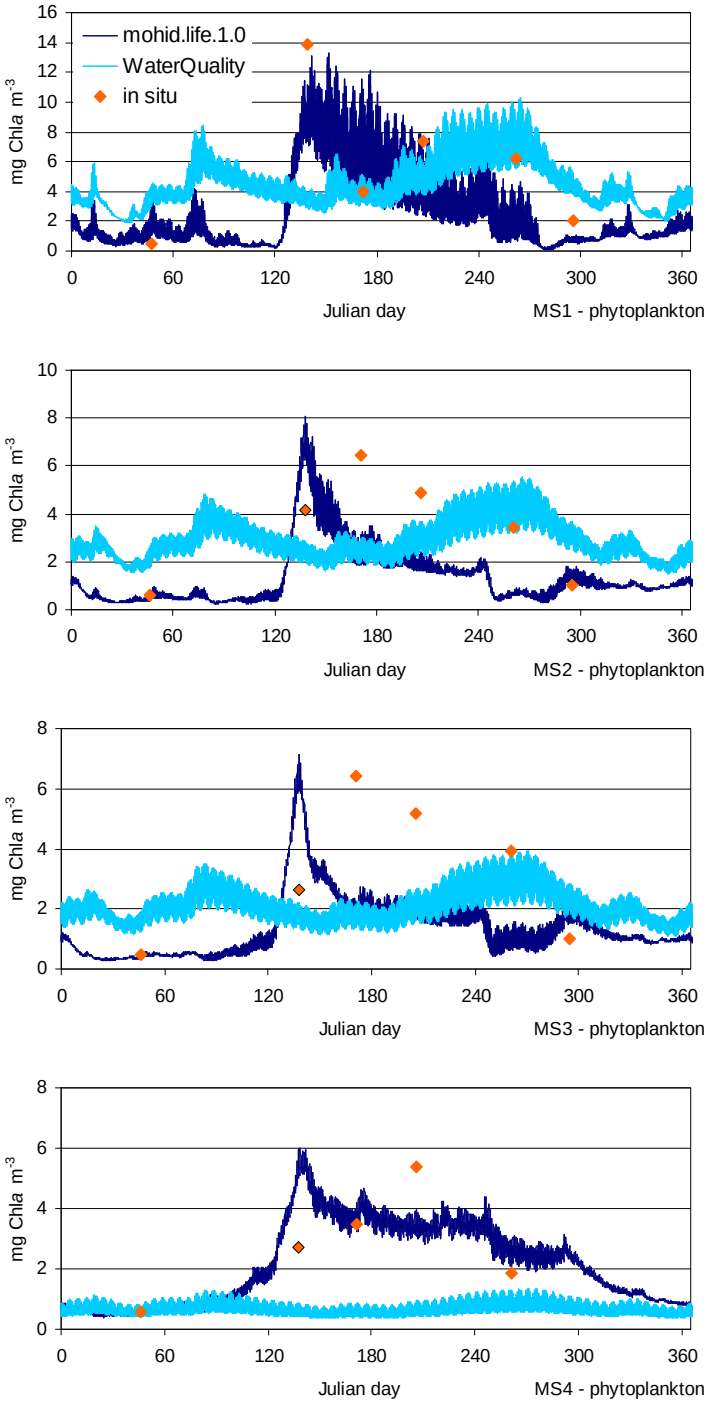

Figure A.7: Results for phytoplankton chlorophyll concentration ($mgChlam^{-3}$) observed at the monitored stations. *WQ* results calculated with a C:Chl*a* ratio of 60.

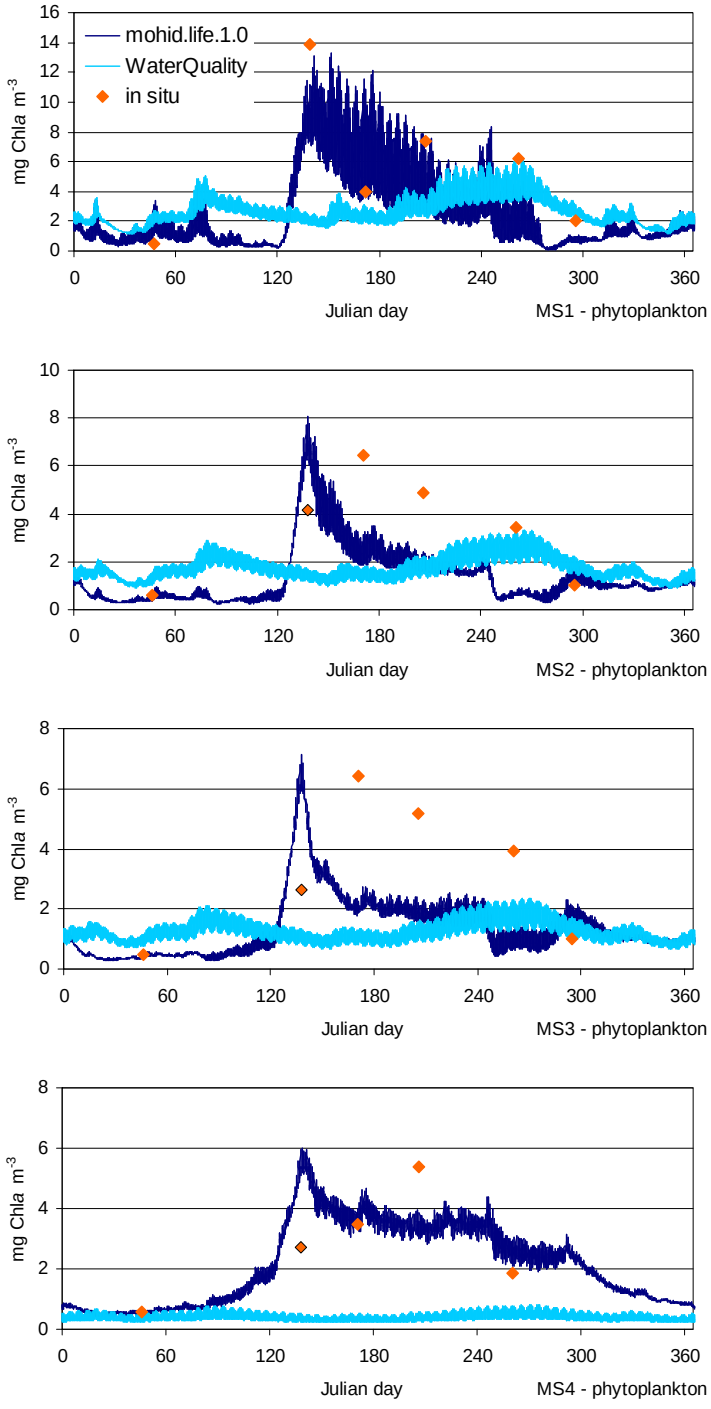

Figure A.8: Results for phytoplankton chlorophyll concentration ($mgChlam^{-3}$) observed at the monitored stations. *WQ* results calculated with a C:Chl*a* ratio of 100.

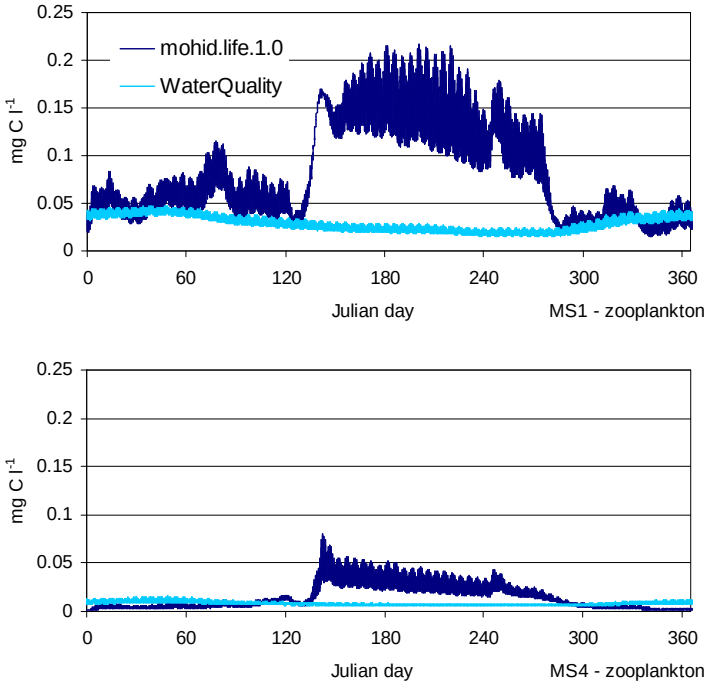

Figure A.9: Results for zooplankton carbon biomass ($mgCl^{-1}$) observed at the monitored stations.

observed discrepancy in summer months.

A.7 Conclusions

A fairly reasonable agreement was observed between the two models output, with the exception of biological groups, phytoplankton and zooplankton; *mL1.0* has a marked seasonal fluctuation in all compared variables, while *WQ* results shows a smaller variation during the entire year.

While resulting from a distinct producer's dynamics parameterization between the two models, this discrepancy does not reflect a limitation in *WQ* phytoplankton parameterization. Rather than being attributed to the *WQ* model philosophy, the absence of a phytoplankton response in summer can result from the adopted parameter values.

Both models can address the same issues and capture the dynamic of the system, but the level of detail is different. As an example, nutrient and light limitation in production can only be inferred in *WQ*, while in *mL1.0* they can be estimated by model output (by nutrient cell quota by and C:Chla ratio evolution). But *mL1.0* has a downside when compared with WQ; it takes about 1.5 times more computational time to simulate the same scenario (particular relevant in long time simulations), and the results are fare more time-consuming to analyze.

Ultimately, the choice to use one of the models will rely on the study requirements. *WQ* can be suited to study major characteristics of a particular system, specially water quality evolution in time and the response of the system to different nutrient and OM loads scenarios. Despite the same can be done using *mL1.0*, the application will have a higher computational time-demand, compromising its applicability if numerous successive runs are required. If a detailed study of the ecologic dynamics of a system is required, then *mL1.0* becomes the only feasible choice, especially if carbon cycle is the currency between model components (e.g., microbial loop in marine systems).

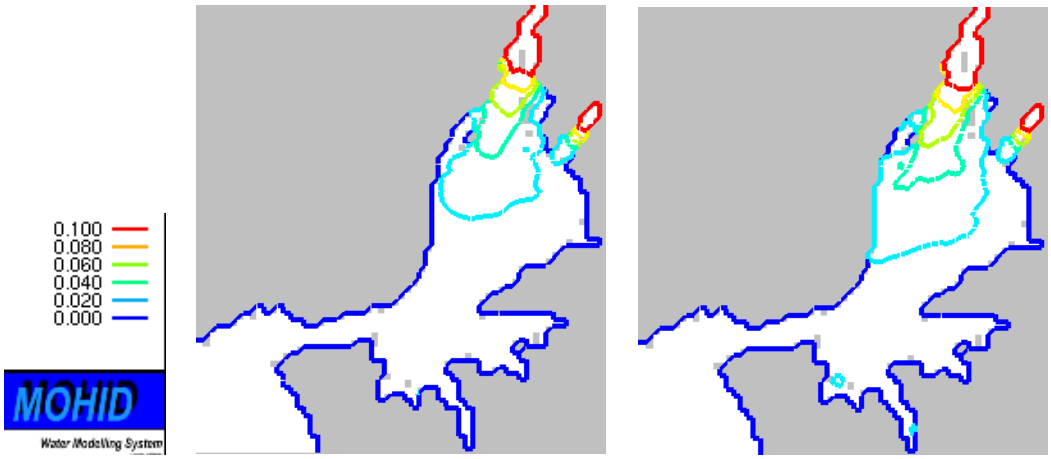

Figure A.10: Model results for PON horizontal distribution inside the estuary. First row shows *WQ* results and second column *mL1.0* results. Model predictions for Julian day 43 (winter). Values in $mgNl^{-1}$.

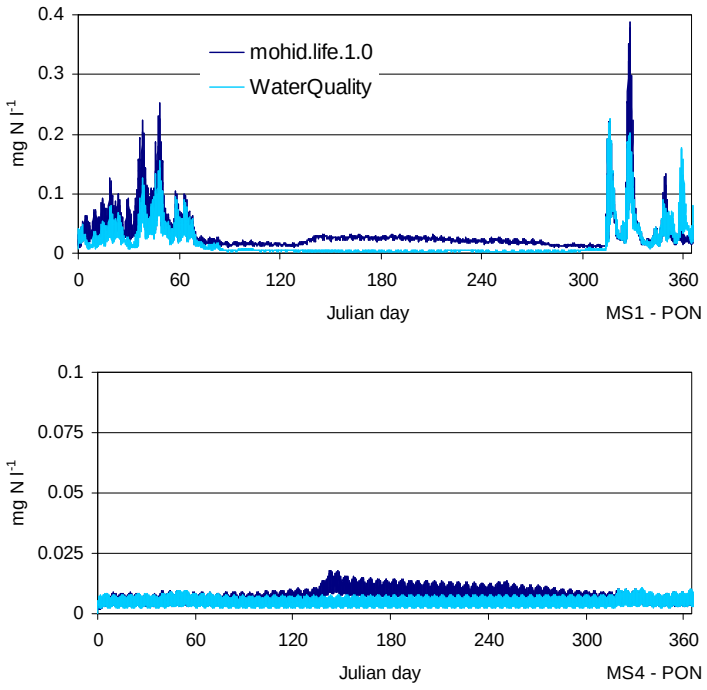

Figure A.11: Results for PON ($mgNl^{-1}$) observed at the monitored stations.

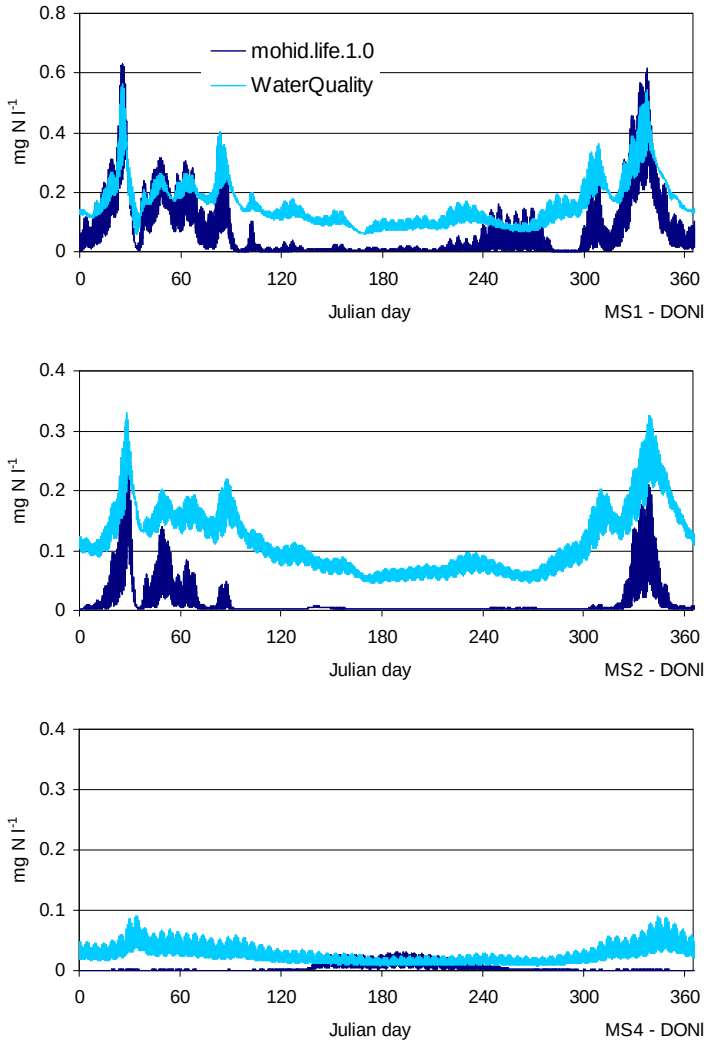

Figure A.12: Results for labile DON ($mgNl^{-1}$) observed at the monitored stations.

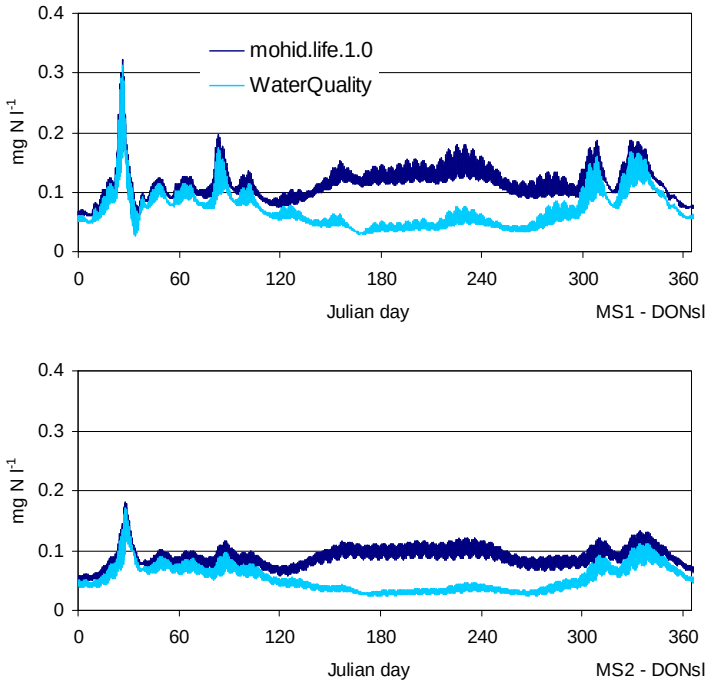

Figure A.13: Results for semi-labile/refractory DON ($mgNl^{-1}$) observed at the monitored stations.